Trinity College Dublin
Coláiste na Tríonóide, Baile Átha Cliath
The University of Dublin

Investigating the Role of Altered Energy Metabolism in the Therapeutic Response of Rectal Cancer

Croí Ellyn Buckley (B.Sc. M.Sc.)

Ph.D. Thesis (Volume 1)

Submitted to Trinity College Dublin for the degree of

Doctor of Philosophy

September 2022

Department of Surgery, Trinity St. James's Cancer Institute, Trinity Translational Medicine Institute, Trinity College Dublin and St. James' Hospital

Thesis supervisors: Dr Niamh Lynam-Lennon (Primary Supervisor)

Prof. Jacintha O'Sullivan (Secondary Supervisor)

Declaration

I declare that this thesis has not been submitted as an exercise for a degree at this or any other university and it is entirely my own work. I agree to deposit this thesis in the University's open access institutional repository or allow the Library to do so on my behalf, subject to Irish Copyright Legislation and Trinity College Library conditions of use and acknowledgement. I consent to the examiner retaining a copy of the thesis beyond the examining period, should they so wish (EU GDPR May 2018).

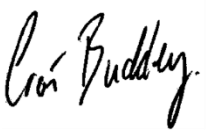

Croí Buckley

30th September 2022

Date

Thesis Abstract

Colorectal cancer (CRC) is the 3rd most commonly diagnosed cancer world-wide, accounting for an estimated 10% of all cancers diagnosed annually globally. One in three CRCs occur in the rectum. The standard of care for locally-advanced rectal cancer (LARC) treatment is neoadjuvant chemoradiation therapy (neoCRT), followed by surgery. Unfortunately, resistance to neoCRT is a significant clinical problem in the management of rectal cancer, with only an estimated 15-30% of rectal cancer patients achieving a complete pathological response (pCR). Therefore, there is an urgent unmet need to identify underlying mechanisms of treatment resistance and novel treatment strategies to improve response in rectal cancer. In recent years, altered tumour energy metabolism has been demonstrated to be associated with radioresistance in cancer, but its role in rectal cancer is incompletely understood. In this thesis, the role of altered tumour energy metabolism in rectal adenocarcinoma and the potential of metformin, a clinically-approved anti-diabetic drug and metabolic modulator, as a novel radiosensitiser was investigated in rectal cancer.

SW837 rectal cancer cells and HCT116 colon cancer cells were identified as an *in vitro* model of inherent radioresistance/radiosensitivity. SW837 cells were significantly more resistant to fluorouracil (5-FU) cytotoxicity, when compared to HCT116 cells. To identify potential underlying mechanisms of radioresistance in this model, HCT116 and SW837 cells were characterised in terms of multiple parameters frequently implicated in radioresistance. Radiosensitive HCT116 cells displayed significantly elevated proliferative rates, a more radiosensitive basal cell cycle distribution and induced G2/M arrest earlier following irradiation with clinically-relevant doses of X-ray radiation, when compared to radioresistant SW837 cells. In addition, radioresistant SW837 cells displayed more efficient repair of radiation-induced DNA damage, and a reduced reliance on glycolysis, when compared to HCT116 cells. Transcriptomic profiling of HCT116 and SW837 cells demonstrated a significantly altered transcriptome in SW837 cells, when compared to HCT116 cells. In addition, ingenuity pathway analysis (IPA) of transcriptomic data demonstrated significant alterations in pathways commonly associated with radioresponse, in SW837 cells including cell cycle, DNA damage repair, oxidative stress and metabolism, including significant upregulation of oxidative phosphorylation related genes.

As hypoxia is a common feature of solid malignancies, and contributes to the development of radioresistance, the inherent model of radioresistant and radiosensitive CRC was characterised under hypoxic (0.5% O_2) conditions. SW837 cells remained significantly more radioresistant, when compared to HCT116 cells under hypoxia (0.5% O_2). Enhanced radiation-induced apoptosis was demonstrated in HCT116 cells under hypoxia (0.5% O_2). Hypoxic exposure was demonstrated to significantly alter cell cycle distribution and phenotype in both HCT116 and SW837 cells. Radiation-induced DNA damage was efficiently repaired under hypoxic conditions in both cell lines. Hypoxia was demonstrated to decrease oxidative phosphorylation and increase glycolysis in both HCT116 and SW837 cells.

The effect of inhibition of metabolism on radioresponse was assessed in HCT116 and SW837 cells. A novel drug, Pyrazinib (P3), which was previously demonstrated to act as an anti-metabolic radiosensitiser in oesophageal cancer was demonstrated to significantly inhibit oxidative phosphorylation and glycolysis, and induce mitochondrial dysfunction in SW837 cells. However, P3 did not radiosensitise HCT116 or SW837 cells under normoxic or hypoxic conditions. Metformin, a clinically approved drug in the management of diabetes, and an inhibitor of complex I of the electron transport chain, was demonstrated to significantly inhibit oxidative phosphorylation in HCT116 and SW837 cells, and induce mitochondrial dysfunction. Metformin treatment was demonstrated to significantly radiosensitise HCT116 and SW837 cells to clinically-relevant doses of 1.8 Gy radiation, and was superior to 5-FU, which is the current standard of care.

The potential mechanisms of metformin-induced radiosensitisation were subsequently assessed. Metformin was demonstrated to affect cell cycle distribution and progression following radiation in HCT116 and SW837 cells. Metformin treatment induced DNA damage, inhibited DNA damage repair, induced cell death and increased glutathione levels in CRC cells. Metformin significantly altered the transcriptome of SW837 cells, altering pathways related to metabolism, DNA damage repair and oxidative stress. Metformin treatment significantly inhibited oxidative phosphorylation and glycolysis in pre-treatment rectal cancer biopsies, but did not alter metabolism in non-cancer rectal tissue. Metformin also induced the secretion of inflammatory proteins from rectal cancer and non-cancer rectal tissue.

Metabolomic profiling of pre-treatment rectal cancer sera identified 16 metabolites significantly associated with pathological response to neoCRT (tumour regression score) (TRS).

Metabolomic profiling of pre-treatment rectal cancer biopsies and tumour conditioned media (TCM) demonstrated significant correlations with clinicopathological features, including TRS. Transcriptomic profiling of pre-treatment rectal tumour biopsies demonstrated significant alterations in gene expression between patients with a good response (TRS 0) and poor response (TRS 2) to treatment and in patients with a pathological tumour (T) stage of T3/4, when compared to those with a pathological T stage T0. IPA analysis of transcriptomic data also demonstrated significant alterations to metabolic pathways in patients with a pathological T stage of T3/4, when compared to those with T0. Real-time metabolic phenotyping of rectal tumour and non-cancer rectal tissue demonstrated significantly elevated oxidative phosphorylation levels, when compared to glycolysis. Metabolomic profiling of non-cancer rectal tissue and rectal cancer tissue demonstrated 23 metabolites, primarily phosphatidylcholines, significantly altered in rectal cancer tissue, and four metabolites significantly altered in TCM, when compared to non-cancer conditioned media (NCM). The protein secretome of rectal cancer was significantly altered, when compared to non-cancer tissue, as assessed by multi-plex ELISA. Transcriptomic profiling demonstrated significant alterations to the metabolome of rectal cancer, when compared to non-cancer rectal tissue, including alterations to metabolic pathways. Hierarchical clustering analysis demonstrated accurate clustering into cancer and non-cancer cohorts using combined metabolomic and transcriptomic data.

Together this thesis demonstrates altered energy metabolism in the development and therapeutic response of rectal cancer, highlighting the potential role of metabolic markers as predictive biomarkers of treatment response in rectal cancer. Importantly, the potential utility of metformin, as a novel anti-metabolic radiosensitiser in rectal cancer, to boost patient response to treatment, is also demonstrated.

Acknowledgements

First and foremost, I would like to thank my supervisor, Dr Niamh Lynam-Lennon. Thank you for all of your support and mentorship over the last few years. Your attention to detail is second to none and has been a huge help to me in writing this thesis, and no doubt will benefit me for years to come. Your unwavering patience and support have been greatly appreciated. Thank you for encouraging me, challenging me and teaching me how to become a better researcher. It was great to work with you.

I would also like to extend my thanks to my secondary supervisor, Prof. Jacintha O'Sullivan. Thank you for your support and encouragement since the start of this project. You are an incredible mentor, and a constant source of enthusiasm and encouragement.

I would like to thank all of the members of the Department of Surgery who have helped with the completion of this project. Thank you to the past and present members of the Lower GI Biobank, Rebecca O'Brien, Dr Aisling Heeran and Niamh Clarke. In particular, thanks to Dr Tim Nugent and Dr Noel Donlon for your hard work recruiting patients to this study and obtaining clinical data. Thank you to Dr Cara Dunne, Mr John Larkin, Mr Paul McCormick, Mr Brian Mehigan, Mr Michael Kelly, Mr Robert Hannon and Mr Diarmuid O'Ríordáin in St. James's Hospital and the Beacon Hospital Dublin for recruiting patients for this study.

I would also like to extend my sincere gratitude to the patients who so kindly and selflessly donated their samples to this research. Without you, this research would have been impossible.

Thank you to Prof. Kathrin Røe Redalen and Dr Sebastian Meltzer for providing pre-treatment sera for this study. Thank you to Prof. Lorraine Brennan and Dr Xiaofei Yin for performing metabolomic profiling in this study. Thank you, Dr Elaine Kenny, for your help with transcriptomic profiling.

I would also like to extend my gratitude to everyone in the Department of Surgery who helped with the completion of this research. Dr Simone Marcone, thank you for your help with IPA. Fiona O'Connell, thank you for your help with running MSD analysis and generating correlation plots. Laura Kane, thank you also for performing hierarchical clustering analysis for this study.

Thank you to all members of the Department of Surgery, past and present, for your support over the years. Stephen and Joanne, thank you for all of your help and feedback.

Andrew, Jason, Maria, Noel, Christina, Cliona, Amy, Aisling, Fiona, Eimear, Laura, Christine and Marina, thank you for everything over the last few years, it was wonderful working with you all. Dr Aoife Cannon, thank you for being an incredible mentor and friend. Your pep talks were such a source of encouragement for me. A special thanks to Rebecca O'Brien, for being the best bench buddy and lab sister I could ask for. Thank you for all of your help with sample collection, but also for being an incredible friend.

Thank you to all of my friends for being a constant source of encouragement, and providing a welcome distraction just when I needed it most. A special thank you to Rosie, for tolerating me ranting about science and lab-life, and for being my go-to holiday/hiking/cinema/everything friend.

I'd also like to thank my sister, Aoife, and my soon to be brother-in-law Graeme, for all of your endless support and encouragement. Thank you for allowing me to take the dogs whenever I needed a pick me up, and for always believing in me. Thank you to my wonderful aunt Lucy. You have always been my biggest cheerleader, and I have never met anyone with a bigger heart.

Finally, the biggest thank you of all goes to my extraordinary parents, Tim and Ger. My entire life you have supported me in whatever I chose to do, and always believed in me and my abilities. I won the lottery by having you as my parents, and I would not have been able to do any of this without you by my side.

Ph.D. Outputs

Co-Author Publications

Laura E. Kane, Gregory S. Mellotte, Eimear Mylod, Rebecca M. O'Brien, Fiona O'Connell, **Croí E. Buckley**, Jennifer Arlow, Khanh Nguyen, David Mockler, Aidan Meade, Barbara Ryan, Stephen Maher

Diagnostic accuracy of blood-based biomarkers for pancreatic cancer: A systematic review and meta-analysis. Cancer. Res. Commun. 2022 Sept 12; 0190

Maria Davern, Marie-Claire Fitzgerald, **Croí E. Buckley**, Aisling B Heeran, Noel E Donlon, Jason McGrath, Fiona O' Connell, Malvika R. Deshpande, Conall Hayes, Jamie MacDonald, Andrew D. Sheppard, John V. Reynolds, Stephen G. Maher, Niamh Lynam-Lennon, Brona Murphy, Joanne Lysaght

PD-1 and TIGIT blockade differentially affect tumour cell survival under hypoxia and glucose deprived conditions in oesophageal adenocarcinoma; implications for overcoming resistance to PD-1 blockade in hypoxic tumours. Transl. Oncol. 2022 Mar 1;19:101381

Maria Davern, Rebecca M. O' Brien, Jason McGrath, Noel E Donlon, Ashanty M Melo, **Croí E. Buckley**, Andrew D. Sheppard, John V. Reynolds, Niamh Lynam-Lennon, Stephen G. Maher, Joanne Lysaght

PD-1 blockade enhances chemotherapy toxicity in oesophageal adenocarcinoma. Sci. Rep. 2022 Feb 28;12(1):3259

Aisling B. Heeran, Helen P. Berrigan, **Croí E. Buckley**, Heelena Moni Bottu, Orla Prendiville, Amy M. Buckley, Niamh Clarke, Noel E. Donlon, Timothy Nugent, Michael Durand, Cara Dunne, John O. Larkin, Brian Mehigan, Paul McCormick, Lorraine Brennan, Niamh Lynam-Lennon, Jacintha O'Sullivan.

Radiation Induced Bystander Effect (RIBE) alters mitochondrial metabolism using a human rectal cancer ex vivo explant model. Transl Oncol. 2021 Jan;14(1):100882.

Aisling B. Heeran, Margaret R. Dunne, Maria Morrissey, **Croí E. Buckley**, Niamh Clarke, Aoife Cannon, Noel E. Donlon, Timothy Nugent, Michael Durand, Cara Dunne, John O. Larkin, Brian Mehigan, Paul McCormick, Niamh Lynam-Lennon, Jacintha O'Sullivan.
The Protein Secretome is Altered in Rectal Cancer Tissue Compared to Normal Rectal Tissue, and Alterations in the Secretome Induce Enhanced Innate Immune Responses. Cancers (Basel). 2021 Feb 2;13(3):571.

First Author Publications (in preparation)

Croí E. Buckley, Xiaofei Yin, Sebastian Meltzer, Anne Hansen Ree, Kathrine Røe Redalen, Lorraine Brennan, Jacintha O'Sullivan, Niamh Lynam-Lennon
Energy Metabolism is altered in Radioresistant Rectal Cancer

Croí E. Buckley, Rebecca O'Brien, Aisling Heeran, Timothy Nugent, Noel Donlon, Adnan Hafeez, Diarmuid S. O'Ríordáin, Robert A. Hannon, Brian Mehigan, Paul McCormick, Cara Dunne, John Larkin, Lorraine Brennan, Jacintha O'Sullivan, Niamh Lynam-Lennon
Metformin as an anti-metabolic radiosensitiser in rectal cancer

Croí E. Buckley, Rebecca O'Brien, Aisling Heeran, Xiaofei Yin, Timothy Nugent, Noel Donlon, Sebastian Meltzer, Anne Hansen Ree, Adnan Hafeez, Diarmuid S. O'Ríordáin, Robert A. Hannon, Brian Mehigan, Paul McCormick, Cara Dunne, John Larkin, Kathrine Røe Redalen, Lorraine Brennan, Jacintha O'Sullivan, Niamh Lynam-Lennon
Multi-omic profiling of rectal tumour and sera samples from rectal cancer patients demonstrates metabolomic alterations associated with cancer development and therapy response.

Croí E. Buckley, Jacintha O'Sullivan, Niamh Lynam-Lennon
Review paper: Altered metabolism and therapeutic resistance of gastrointestinal cancers

Conference Presentations

Oral Presentations

Irish Radiation Research Society (IRRS) annual meeting 2021. Online, 16th-17th September 2021. Title: Targeting energy metabolism to enhance treatment response in rectal cancer

Association for Radiation Research (ARR) Annual conference 2021. Online 12th-14th July 2021. Title: Targeting energy metabolism to enhance treatment response in rectal cancer

FEBS ALC 2019: Oncometabolism: from Conceptual Knowledge to Clinical Applications, Luso, Portugal, 1-6th December 2019. Title: Investigating the Anti-Metabolic Effects of a Novel Small-Molecule Compound on Radioresistant Rectal Cancer

Irish Association for Cancer Research (IACR) Annual Meeting, Belfast, February 20th February 2019. Title: Energy Metabolism in Treatment-Resistant Bowel Cancer (Lay abstract presentation)

TTMI Precision Medicine Cancer Symposium, Dublin, 15th February 2019

Title: Energy Metabolism in Treatment-Resistant Bowel Cancer (Lay abstract presentation)

Poster Presentations

International (presenting author)

British Association of Cancer Research (BACR) Response and Resistance in Cancer Therapy, 6-8th September 2021. Title: Targeting Energy Metabolism to Enhance Radioresponse in Rectal Cancer

EACR Virtual Congress: Innovative Cancer Science, 9th-12th June 2021. Title Targeting Energy Metabolism to Improve Therapeutic Response in Rectal Cancer

IACR Virtual Conference, 24th-26th March 2021. Title: Targeting Energy Metabolism to Overcome Therapeutic Resistance in Rectal Cancer

International Congress on Radiation Research (ICRR) 2019, Manchester, UK, 25-29th August 2019.Title: Investigating the Anti-Metabolic Effects of a Novel Small-Molecule Compound on Radioresistant Rectal Cancer

FEBS ALC 2019: Oncometabolism: from Conceptual Knowledge to Clinical Applications, Portugal, 1-6th December 2019. Title: Investigating the Anti-Metabolic Effects of a Novel Small-Molecule Compound on Radioresistant Rectal Cancer

Mechanisms to Therapies: Innovations in Cancer Metabolism, European Association of Cancer Research (EACR), Bilbao, Spain, 9-11th October 2018. Title: MERiT: Targeting Metabolism for individualised Rectal Cancer Treatment

National (presenting author)

Irish Association of Cancer Research Annual Meeting, Cork, 30th March-1st April 2022. Title: Targeting energy metabolism to enhance treatment response in rectal cancer.

Irish Association of Cancer Research Annual Meeting, Cork, 30th March-1st April 2022

Multi-omic profiling of rectal tumour and sera samples from rectal cancer patients demonstrates metabolomic alterations associated with cancer development and therapy response

Irish Association of Cancer Research Annual Meeting, Galway, 26-28th February 2020. Title: Investigating the Anti-Metabolic Effects of a Novel Small-Molecule Compound on Radioresistant Rectal Cancer

11th International Trinity St. James's Cancer Institute International Cancer Conference, 24-25th September 2019. Title: Investigating the Anti-Metabolic Effects of a Novel Small-Molecule Compound on Radioresistant Rectal Cancer

Irish Association of Cancer Research Annual Meeting, Belfast, 20-22nd February 2019. Title: Investigating the Anti-Metabolic Effects of a Novel Small-Molecule Compound on Radioresistant Rectal Cancer

Young Cancer Researchers Network (YCRN), Cork, 21-22nd June, 2018. Title**:** MERiT: Targeting Metabolism for individualised Rectal Cancer Treatment

Irish Association of Cancer Research Annual Meeting, Dublin, 21-23rd February 2018

Title**:** Investigation of the role of the complement system in the radioresistance of rectal cancer.

Virtual Conference/Seminar Attendance

New York Academy of Sciences (NYAS) Rising Stars of Cancer Metabolism and Signalling, April 23rd 2021

13th Annual Symposium on Translational Research in Oncology, 4th December 2020

EACR Virtual Conference on Cancer Metabolism, 2nd September 2020

Precision Oncology Ireland/TTMI Colorectal Cancer Research Seminar, 7th July 2020

EACR 2020 Virtual Congress, 18-19th June 2020

Abcam Cancer and Metabolism, 15th June 2020

EACR DNA Damage Responses and Cancer, 20th May 2020

Training Courses and Taught Modules

Workshops Attended

PPI Workshop for Cancer Researchers, Irish Cancer Society 10TH December 2019.

Development Workshop for Researchers, Irish Cancer Society, 15th November 2019.

Health Research Board (HRB) Ones2Watch, 10th October 2019.

Prof. Patrick Johnson IACR Award for Excellence in Cancer Research Outreach Finalist Workshop, 4th February 2019.

Agilent Cell Analysis Workshop (Seahorse), Trinity Biomedical Sciences Institute (TBSI), 4th October 2018.

TrAnslational Radiobiology Group Trinity (TARGeT) Workshop, Trinity Translational Medicine Institute (TTMI), 3rd May 2018.

Wellcome Trust-HRB Clinical Research Facility (CRF) Annual Scientific Meeting, St. James's Hospital, 13th December 2017.

Cancer Theranostics Workshop, TTMI, 20th November 2017.

Health and safety courses completed

Biological Safety Training, 24th October 2018

Chemical Safety Training, 26th April 2018

Radiological Protection Training, 11th January 2018

TTMI Safety Induction, 28th November 2017 and 18th November 2019

Cryogenics Safety Briefing, 16th November 2017

An Introduction to Good Clinical Practice (GCP) IHC E6, for Investigators and Site-staff, 10th November 2017 and renewed 13th November 2019

Fire Safety Training, 24th October 2017

Modules completed

Research Integrity Training, Epigeum (online)

Drug Discovery and Development (CRDI) – February-March 2019 (online) (2.5ECTS)

Key Skills for Biomedical Research – February 2019 (5 ECTS)

Generic Skills for PhD Students; January – March 2018 (5 ECTS)

Techniques and Strategies in Molecular Medicine (Clinical Research and Development Ireland) (CRDI), 4-5th December 2018 (5 ECTS)

Applied Biomedical Imaging Workshop, RCSI, 10-11th May 2018 (2.5 ECTS)

Public and patient outreach and awards

Prof. Patrick Johnson IACR Award for Excellence in Cancer Research Outreach Finalist Workshop, 4th February 2019.

Human Health and Disease Alumni Careers Event, 2017 and 2018.

Trinity Access Programme (TAP) TTMI Primary School Outreach Event, 11th April 2018 and May 1st 2019

TTMI Transition Year Outreach Programme, 27th February 2018

Table of Contents

List of Figures

List of Tables

Abbreviations

2-DG	2-deoxyglucose
5-FU	5-Fluorouracil
AJCC	American Joint Committee on Cancer
AMPK	AMP-activated protein kinase
ANOVA	Analysis of variance
APC	Adenomatous polyposis coli
APE-1	Apurinic endonuclease
ATP	Adenosine triphosphate
Bax	Bcl-2 associated X
Bcl-2	B cell lymphoma
BER	Base excision repair
BrdU	5-Bromo-2'-deoxyuridine
CAD	Caspase activated DNAse
CDK	Cyclin-dependent kinase
CEA	Carcinoembryonic antigen
CIMP	CpG island methylator phenotype
CIN	Chromosome instability
CMS	Consensus molecular subtypes
COX	Cyclooxygenase
CRC	Colorectal cancer
CT	Computed tomography
DCA	Dichloroacetate
DCF	Dichlorofluorescein
DDR	DNA damage response
DISC	Death-inducing signalling complex
DMSO	Dimethylsulfoxide
DNA	Deoxyribonucleic acid
DNA-PKcs	DNA-dependent protein kinase catalytic subunit
dNTP	Deoxyribose nucleotide triphosphate

DRE	Digital rectal examination
DSB	Double-strand break
DSS	Disease specific survival
ECACC	European Collection of Cell Culture
ECAR	Extracellular acidification rate
EDTA	Ethylene-diamine tetra-acetic acid
ELISA	Enzyme linked immunosorbent assay
EMT	Epithelial mesenchymal transition
ERUS	Endoscopic rectal ultrasound
ETC	Electron transport chain
FADD	Fas-associated death domain
FADH	Flavin adenine dinucleotide
FAP	Familial adenomatous polyposis
Fas	Fatty acid synthetase
FBS	Foetal Bovine Serum
FCCP	Carbonyl cyanide 4-(trifluoromethoxy) phenylhydrazone
FdUMP	Fluorodeoxyuridine
FIT	Faecal immunohistochemistry test
FOBT	Faecal occult blood test
FOLFIRINOX	Leucovorin, fluorouracil, irinotecan, oxaliplatin
FUTP	Fluorouridine triphosphate
GLP-1	Glucagon-like peptide 1
GLUT-1	Glucose transporter 1
GPX	Glutathione peroxidase
GSH	Glutathione
GSSG	Oxidised glutathione
GST	Glutathione-s-transferase
Gy	Gray
H2AX	H2A histone family member 2 X
HCC	Hepatocellular carcinoma
HCRT	Hyperthermo chemoradiotherapy

HDI	Human Development Index
HIF	Hypoxia inducible factor
HK	Hexokinase
HNPCC	Hereditary nonpolyposis colorectal cancer
HR	Homologous recombination
IAP	Inhibitor of apoptosis
ICD-O	International Classification of Diseases for Oncology
IDH	Isocitrate dehydrogenase
IPA	Ingenuity Pathway Analysis
IR	Ionising radiation
L-15	Leibovitz'-15
LARC	Locally-advanced rectal cancer
LCRT	Long-course radiation therapy
LDH	Lactate dehydrogenase
MAP	Molecule Activity Predictor
mCRC	Metastatic colorectal cancer
mDCF	Modified docetaxel, 5-FU and cisplatin
miR	MicroRNA
MnSOD	Manganese superoxide dismutase
MRI	Magnetic resonance imaging
MS	Mass spectrometry
MSI	Microsatellite instability
MtDNA	Mitochondrial DNA
mTOR	Mammalian target of rapamycin
NADH	Nicotinamide adenine dinucleotide
NADPH	Reduced nicotinamide adenine dinucleotide phosphate
NeoCRT	Neoadjuvant CRT
NeoRT	Neoadjuvant radiation therapy
NER	Nucleotide excision repair
NGS	Next generation sequencing
NHEJ	Non-homologous end joining

NMR	Nuclear magnetic resonance
OAC	Oesophageal adenocarcinoma
OCR	Oxygen consumption rate
OCT-1	Organic cation transporter 1
OS	Overall survival
P3	Pyrazinib
PARP	Poly-ADP-ribose polymerase
PBS	Phosphate buffered saline
PCA	Principal component analysis
pCR	Complete pathological response
PDAC	Pancreatic ductal adenocarcinoma
PE	Plating efficiency
PFA	Paraformaldehyde
PFS	Progression free survival
PI	Propidium iodide
PPP	Pentose phosphate pathway
RFS	Relapse free survival
RNA	Ribonucleic acid
RNA-Seq	RNA sequencing
ROS	Reactive oxygen species
RPMI-1640	Roswell Park Memorial Institute-1640
RT	Radiation therapy
RT°	Room temperature
SCRT	Short-course radiation therapy
SEM	Standard error of the mean
SF	Surviving fraction
SOD	Superoxide dismutase
SRC	Spare respiratory capacity
SSB	Single-strand break
SSBR	Single-strand break repair
T2DM	Type II diabetes mellitus

TCA	Tricarboxylic acid cycle
TEM	Transanal endoscopic microsurgery
TIGAR	TP53 induced glycolysis and apoptosis regulator
TME	Total mesorectal excision
TNF	Tumour necrosis factor
TNM	Tumour node metastasis
TRS	Tumour regression score
TS	Thymidylate synthase
UICC	Union for International Cancer Control
UV	Ultraviolet
VDAC	Voltage dependant anion selective channel protein
WT	Wild type
XIAP	X-linked inhibitor of apoptosis
XLF	XRCC4-like factor
XRCC	X-ray cross-complementing

Chapter 1: General Introduction

1.1. Colorectal Cancer

1.1.1. *Epidemiology and incidence*

Colorectal cancer (CRC) is the 3rd most commonly diagnosed invasive cancer worldwide, with an estimated 1.8 million cases of CRC diagnosed annually (1). In 2020, CRC accounted for 10% of all newly diagnosed cancers globally (**Fig. 1.1**). In Ireland, approximately 3,000 cases of CRC are diagnosed annually (2), with CRC being the 2nd most common cancer in men and the 3rd most common cancer in women, accounting for 12.4% and 10.2% of cancer cases, respectively (2). Furthermore, current data demonstrates that 1 in 24 people in Ireland will be diagnosed with CRC by the age of 75 (2). The global burden of CRC cancer is projected to increase, with incidence rates predicted to rise by 60% by the year 2030 (3) and a further projected 3.2 million cases in the year 2040 (4).

Following lung cancer only, CRC accounts for 9.4% of all cancer-related deaths, and therefore has the 2nd highest cancer-related mortality rate (1). Alarmingly, this equated to an estimated 935,000 lives lost to CRC in the year 2020, globally (1). In Ireland, an estimated 1,010 deaths are attributed to CRC annually (2). CRC is the 2nd most common cause of cancer related death in males, contributing to 12.5%, and the 3rd most common cause of cancer related death in females, accounting for 9.7% (2). In addition, by the year 2030, CRC is predicted to contribute to 1.1 million deaths worldwide, demonstrating the growing burden of CRC globally (3).

Reports on CRC incidence and mortality combine data from cancers of the colon, rectum and often anus, as defined as C18-C21 by the International Classification of Diseases for Oncology (ICD-O) guidelines (5) (**Fig. 1.2**) . Rectal cancer, defined as tumours occurring in the distal 15 cm from the anal margin, accounts for an estimated 35% of CRC cases in the European Union (6). In 2020, globally, approximately 3.8% of all newly diagnosed cancers, or over 730,000 cases were rectal cancers (1). In Ireland, incidence rates of rectal cancer are projected to rise by 92% in females, and 97% in males by the year 2045, with the number of new rectal cancer diagnoses annually projected to rise from 923 in 2015 to an estimated 1,793 new cases in 2045 (7). Rectal cancers are responsible for 3.4% of cancer-related deaths worldwide, with an estimated 330,000 lives lost to rectal cancer in the year 2020 (1). In addition, incidence and mortality rates of rectal cancer are believed to be underestimated, as they are often misclassified as colon cancers in reports.

CRC is commonly associated with higher income countries and socio-economic development, with elevated incidence rates demonstrated in North America, Western Europe and Australasia, and the lowest incidence rates demonstrated in Africa and Central America (1, 8). These incidence rates are believed to reflect the poor dietary and lifestyle factors demonstrated in regions with a higher Human Development Index (HDI). Incidence rates are steadily increasing in formerly low-HDI and poor socio-economic countries, including regions of Eastern Europe, in tandem with the Westernisation of lifestyles and diets in these regions (1).

While global incidence rates of CRC are projected to rise in the coming years, recent evidence from Europe and North America have suggested a gradual decline to both incidence and mortality rates in older populations (>50 years), believed to be attributable to the introduction of national screening programmes which allow for identification of pre-cancerous and early disease (9). Alarmingly, the opposite trend is emerging in the younger age demographic in many high HDI countries, including Ireland, with incidence rates rising among young adults (<50 years) (10-12). A recent meta-analysis conducted by Saad El Din *et al.*, examining 40 studies spanning 12 countries, further demonstrated increasing incidence of young CRC (<50 years), indicated to be driven mainly by increased rectal cancer incidence in this younger demographic (13). Alarmingly, these young CRC cases, are often more aggressive, poorly differentiated and have a worse prognosis (14, 15). Furthermore, these CRCs in younger age demographics seem to present at a late stage, believed to be due, in part, to the lack of routine screening for younger populations (12, 14, 16, 17).

The incidence of rectal cancer, in particular, is significantly increasing in the younger age demographic in high HDI countries including the U.K, Australia and Canada (4, 10, 14). Importantly, almost one-third of all rectal cancer diagnoses in the United States occur in those under 55 years of age, indicating the growing burden of rectal cancer in younger cohorts (18). While the precise cause of this increasing burden of rectal cancer amongst the young is not known, evidence suggest that the increasing obesity rates in young adults, a sedentary lifestyle, and elevated alcohol and smoking rates in this demographic may play a role (11). These data warrant further investigation into the risk factors associated with the growing rectal cancer incidence in younger populations.

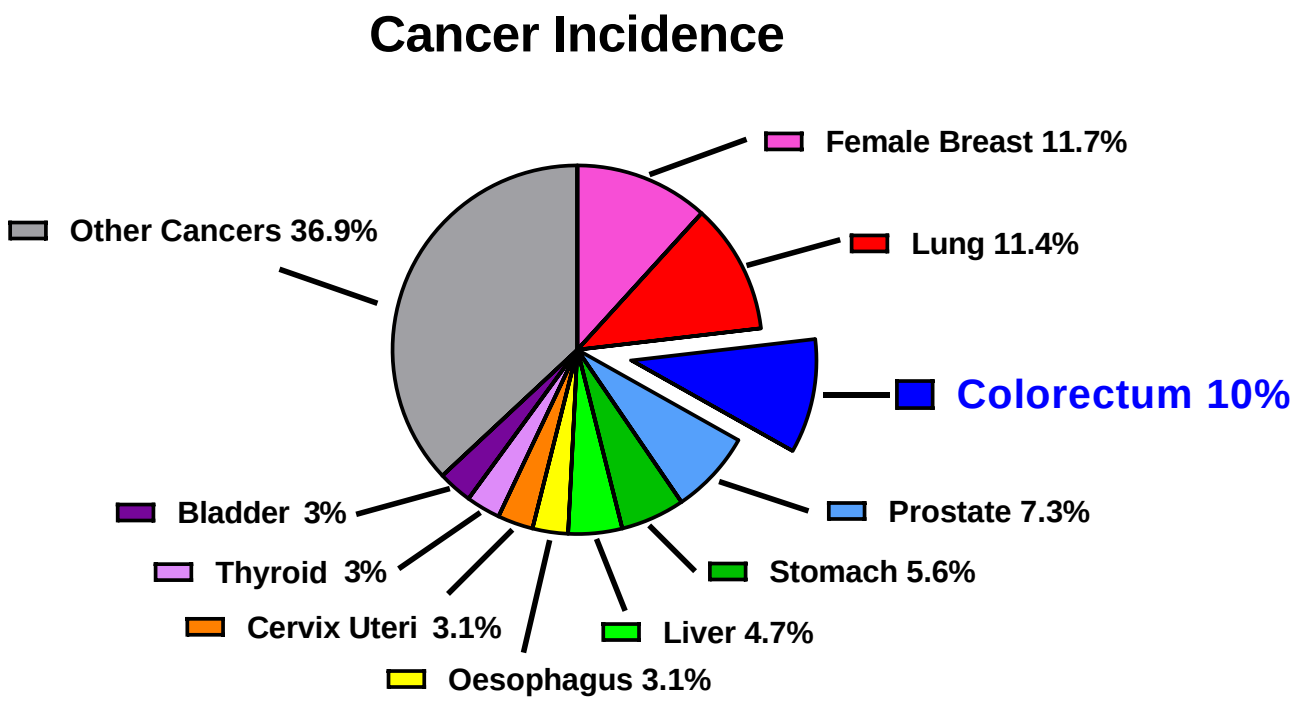

***Fig. 1.1*: Global cancer incidence rates.** CRC is the 3rd most commonly diagnosed invasive cancer (excluding non-melanoma skin cancer) and has the 2nd highest mortality rate across sexes. Data and figure adapted from Sung *et al.* (1).

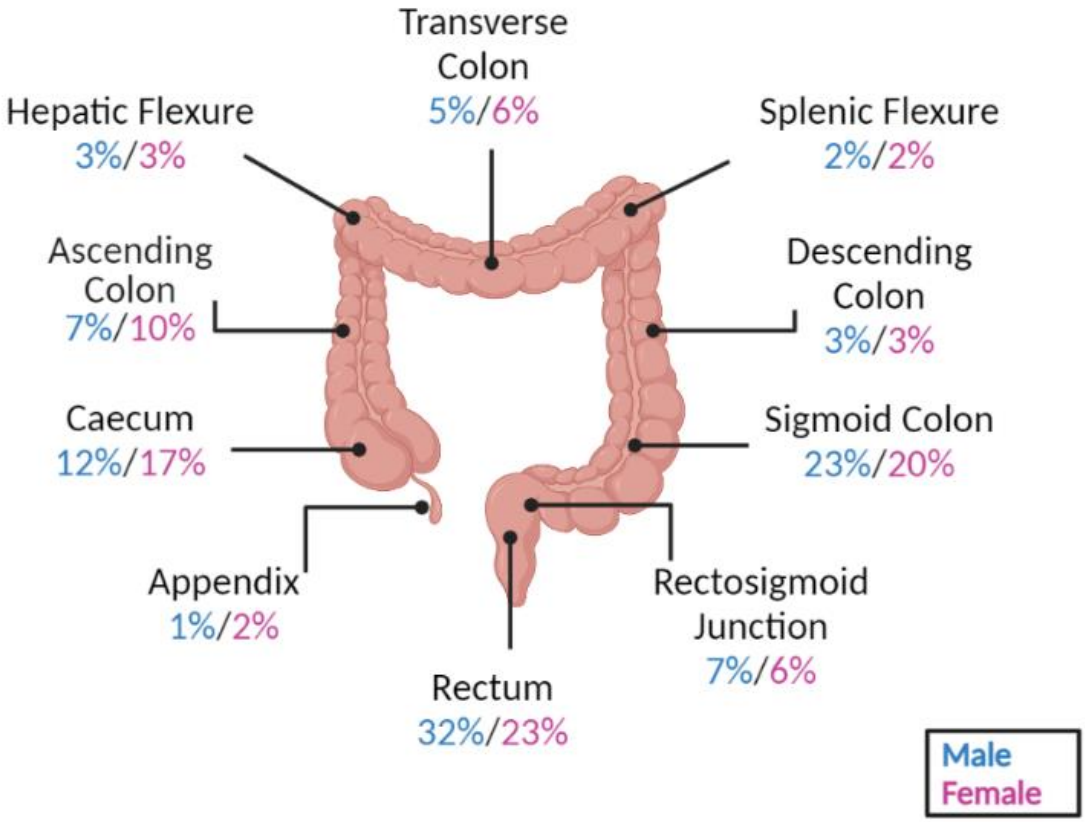

Fig. 1.2: **Distribution of colorectal cancer cases diagnosed by anatomical site.** Data taken from Cancer Research UK, based on CRC incidence rates in the UK between 2010 – 2012. Incidence rates in males presented in blue. Incidence rates in females presented in pink. Image created using Biorender.com.

1.1.2. *Aetiology and Risk Factors*

CRC is typically a slow growing disease, which often develops in a step-wise manner from normal colorectal epithelium to adenoma development to cancerous lesion (19). Different molecular pathways and features contribute to the initiation and development of pre-cancerous polyps and subsequent carcinomas, including chromosomal instability (CIN), microsatellite instability (MSI) and CpG island methylator phenotype (CIMP) (20). Most CRCs are driven by the CIN pathway, occurring in an estimated 65-70% of sporadic CRC tumours (21). CRCs driven by the CIN pathway are typically very slow growing, often developing over decades (21).

In recent years, the well-established model of polyp to carcinoma development in CRC has been challenged, with new theories of CRC tumourigenesis being proposed (22). One such model is the 'Big Bang' tumour evolution model, proposed by Sottoriva *et al.*, which challenges the traditional viewpoint of slow CRC development, and proposes that once all driver mutations are acquired in adenomas, tumours subsequently grow from a single expansion of a diverse population of tumour cells (23). This model proposes that this early diverse expansion contributes to the wide intratumour heterogeneity often observed in tumours, and not later subclonal expansion, as is currently accepted.

Family history is one of the main risk factors for the development of CRC, with an estimated 20-25% of CRCs occurring in patients with family members with a history of CRC (20). Familial adenomatous polyposis (FAP) is an inherited disorder which contributes to an estimated 1-2% of CRC patients (20). Another hereditary condition which contributes to the development of CRC is Lynch Syndrome, also referred to as hereditary nonpolyposis colorectal cancer (HNPCC), which is believed to account for 5-10% of CRC cases, and comes with a lifetime risk of 80% for developing CRC (24). Although hereditary factors are known risk factors for CRC development, they are more strongly associated with the development of colon cancers than rectal cancers (6).

Other risk factors for the development of CRC include age, with the majority of CRCs occurring in those over 70, and gender, with CRC mortality rates are higher in males than in females (23.2/13.1 deaths per 100,000 annually in Ireland, respectively) (2, 6). The distribution of CRCs varies within genders however, with right-sided tumours occurring more frequently than left in females, and left-sided tumours more commonly diagnosed in males (8). Other lifestyle and dietary factors are also considered risk factors for the development of CRC, with

healthy lifestyle factors including healthy weight, physical activity, non-smoking, limited alcohol consumption and a healthy diet being associated with lower CRC risk (25).

1.1.3. *Diagnosis and staging of rectal cancer*

Screening programmes, including at-home stool testing (faecal occult blood tests (FOBT) or faecal immunohistochemistry tests (FITs)) and routine colonoscopies have been introduced in most high HDI countries, for those aged over 50 years of age. In Ireland, a free BowelScreen programme is available for those aged between 60 and 69 (26). In this screening service, an initial FIT test is performed, and if a positive test result is obtained, patients are then invited for a follow-up colonoscopy (26). These screening programmes have permitted the detection of early-stage cancers and pre-cancerous polyps, contributing to reduced incidence and mortality rates in these demographics (27). However, only an estimated 65% of adults in the United States comply with recommended screening (28). In addition, in 2013, only 40.2% of the eligible population participated in the BowelScreen programme in Ireland (26) Unfortunately, this lack of adherence to national screening recommendations and limited access of routine screening for younger demographics (< 50 years), in which CRC rates are steadily increasing, means that despite this opportunity for secondary prevention of CRC, many CRCs are diagnosed at a late stage (27). For example, in Ireland, 1 in 2 cases of CRC were diagnosed at late stage (stage III/IV) between 2014 to 2016 (29). Another factor which contributes to late diagnosis is the set of common symptoms of CRC, which are either often mistakenly considered harmless or do not present until late stage, with the development of a large tumour mass, including cramping, pain or bleeding with bowel movements (27).

Diagnosis with CRC, following symptomatic indication, or during routine screening, requires endoscopic examination, including histological confirmation from biopsies (**Fig.1.3**) (6). In rectal cancers specifically, digital rectal examination (DRE) to palpate rectal tumours is often conducted prior to endoscopy (6). For clinical pre-treatment staging of rectal cancer, physical examination including DRE, full blood count, liver and renal functional testing, quantification of serum carcinoembryonic antigen (CEA) and a computed tomography (CT) scan of the thorax and abdomen are recommended to identify metastases and aid with staging (**Fig. 1.3**) (6). Most commonly, endoscopic examination for rectal cancer is conducted by rigid rectoscopy or colonoscopy to the caecum are used to exclude synchronous colonic tumours. For stage II, III or IV rectal cancer, pre-surgical chest, abdomen and pelvic contrast-enhanced CT is recommended in Ireland (30).

Endoscopic rectal ultrasound (ERUS) can be used for staging of only very early-stage rectal cancers, and aids to identify candidates for whom transanal endoscopic microsurgery (TEM), may be used in management (6). Magnetic resonance imaging (MRI) is the most accurate method for clinical locoregional staging classification (TNM staging), and to aid with pre-surgical planning, and is recommended in rectal cancer patients (6, 30). In patients with rectal cancer with colonic obstruction, in which the tumour cannot be endoscopically passed, a pre-surgical CT colonography should be performed (30).

Together, these methods are employed to categorise rectal cancers into staging, as classified by the Union for International Cancer Control (UICC) TNM staging UICC guidelines, and described in (**Table 1.1**) (31). The TNM, staging is based on the depth of the primary tumour invasion (T), the involvement of lymph nodes (N) and the presence or absence of metastatic disease (M). These factors permit the classification of cancers into stages (I-IV), which are crucial in determining optimal therapeutic strategies.

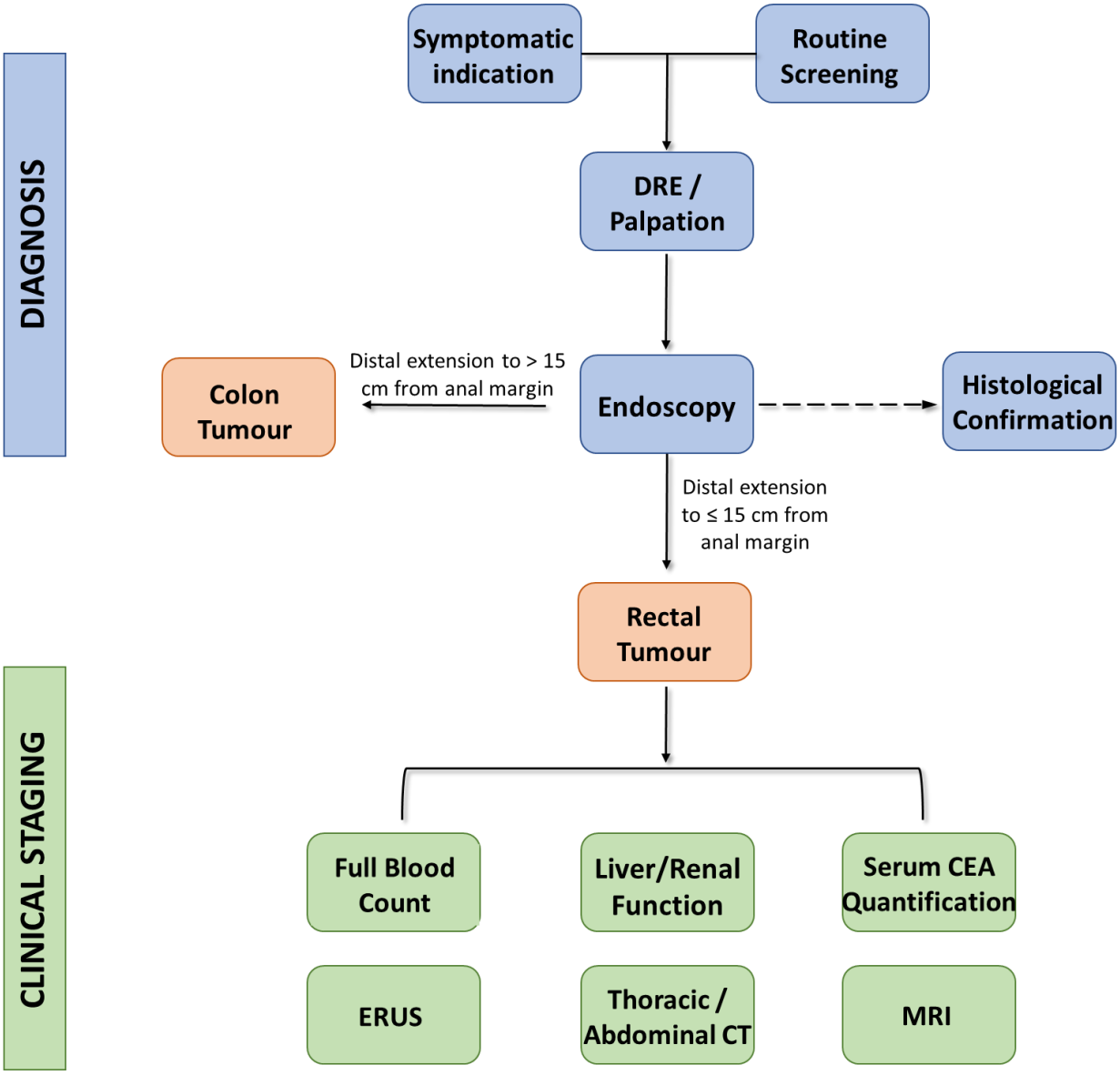

Fig. 1.3: **Schematic of diagnostic and staging pathway of rectal cancer.** Illustration of major steps in the diagnosis and staging of rectal cancer. Patients undergoing routine screening or with symptomatic indication of rectal tumours are assessed initially by palpation and diagnostic biopsies are taken by endoscope for histological confirmation of cancer. Tumours located > 15 cm from the anal margin are classified as colon cancers, while those located ≤ 15 cm from the anal margin are deemed rectal cancers. Subsequent pre-treatment clinical staging of rectal cancer is assessed by endoscopy/pathology in addition to blood counts, sera CEA quantification, liver/renal function and imaging (CT/MR/ERUS, as appropriate). Abbreviations; DRE, digital rectal examination; CEA, carcinoembryonic antigen; ERUS, endorectal ultrasound, CT computed tomography, MRI magnetic resonance imaging. Data adapted from (6, 30).

***Table 1.1*: UICC TNM clinical staging guidelines for colon and rectal cancer.** Data taken from (31).

T- Primary Tumour	
TX	Primary tumour cannot be assessed
T0	No evidence of primary tumour
Tis	Carcinoma *in situ:* invasion of lamina propria
T1	Tumour invades submucosa
T2	Tumour invades muscularis propria
T3	Tumour invades subserosa or into non-peritonealised pericolic or perirectal tissues
T4	Tumour directly invades other organs or structures and/or perforates visceral peritoneum
T4a	Tumour perforates visceral peritoneum
T4b	Tumour directly invades other organs or structures
N- Regional lymph nodes	
NX	Regional lymph nodes cannot be assessed
N0	No regional lymph node metastasis
N1	Metastasis in 1-3 regional lymph nodes
N1a	Metastasis in 1 regional lymph nodes
N1b	Metastasis in 2-3 regional lymph nodes
N1c	Tumour deposit(s) in the subserosa, or in non-peritonealised pericolic or perirectal soft tissue without regional lymph node metastasis
N2	Metastasis in 4 of more regional lymph nodes
N2a	Metastasis in 4-6 regional lymph nodes
N2b	Metastasis in 7 or more regional lymph nodes
M- distant metastasis	
M0	No distant metastasis
M1	Distant metastasis
M1a	Metastasis confined to one organ without peritoneal metastases
M1b	Metastasis in more than one organ
M1c	Metastasis to the peritoneum with or without other organ involvement

1.1.4. *Colon cancer vs. rectal cancer*

As the colon and rectum are in close anatomical proximity, colonic and rectal cancers are often misclassified as the same disease. As previously mentioned, data on CRC incidence and mortality often do not divide colon and rectal cancers into separate categories. However, rectal and colon cancers are distinct conditions, not only anatomically, but have also been demonstrated to display distinct underlying molecular mechanisms, immunological phenotypes and therapeutic implications (32-34). Furthermore, not only are rectal cancers often misclassified in epidemiological data, but the use of *in vitro* models derived from primary rectal cancer are severely underutilised, with colon cancer cell lines commonly utilised instead (35, 36).

The underlying molecular and genetic pathways contributing to oncogenesis of colon and rectal cancer have been proposed to be distinct. In an important study by Guinney *et al.*, CRCs were subclassified according to consensus molecular subtypes (CMS) into 4 main subgroups (CMS 1-4) (37). Importantly, this study highlighted major molecular differences between right sided (proximal colon) cancers and left-sided (distal colon and rectal) cancers. Further evidence has demonstrated that underlying oncogenesis mechanisms differ between rectal and colon cancers, with CIN being a common feature of rectal cancers, while MSI and CIMP being most common in colon cancers (38, 39). Furthermore, while KRAS mutations are most common in colon cancers (39), p53 expression is demonstrated to be elevated in rectal cancers, when compared to colon cancers, and associated with worse disease-free survival in rectal cancer (40). Furthermore, rectal cancers have been proposed to be more reliant on the adenomatous polyposis coli (APC)/β-catenin pathway than colon cancers (40).

The most distinct difference between colon and rectal cancers is worse prognosis of rectal cancers, when compared to colon cancers (41). Multiple studies have demonstrated that rectal cancers display enhanced propensity to recur and metastasise (41). One major difference between colon and rectal cancers are the anatomical location of metastases (42). While the liver is a common site of metastases in colon and rectal cancers, lung/thoracic metastases are almost two times more common in rectal cancers, than in colon cancers (38, 42). Furthermore, bone marrow recurrence following treatment occurs in 2.1% of rectal cancer recurrences yet is an extremely rare site of recurrence in primary colon cancers (38). In addition, surgical management of rectal cancer is more challenging, and requires more technical expertise than that of colon cancers, due to the heightened risk of damage to

surrounding structures, including possible major bleeding or induction of incontinence (38). These factors together determine the different therapeutic regimes used in the management of rectal and colon cancers, with radiation therapy being an added modality in rectal cancer treatment.

Together, these data indicate the importance of specifically classing CRCs as either rectal or colon cancers, to aid with research and management of these cancers.

1.1.5. *Treatment of rectal cancer*

The treatment strategy for rectal cancer is determined by staging (6, 30). As mentioned, in very early-stage rectal cancers, cT1 with negative nodal status and favourable histopathological features, local excision, or TEM would be utilised (6, 30). Following surgery, serial clinical and radiological surveillance should be employed to identify recurrence. In early-stage rectal cancers, not suitable for local excision, including cT1 with unfavourable histopathology, or cT2/cT3a/cT3b, radical total mesorectal excision (TME) is the standard of care for surgery (6, 30). TME also involves removing all mesorectal fat and lymph nodes, to mitigate the higher risk of lymph node involvement and recurrence in these tumour stages (6).

For intermediate tumours (cT3a/b, cN1/2), TME is the standard of care, however, the addition of neoadjuvant treatment is not often recommended for these tumours, as there is a low risk of recurrence with quality TME surgery (6). For locally-advanced rectal cancer (LARC) (> cT3b, with extra-mural vascular invasion), the standard of care is radical TME surgery with neoadjuvant chemoradiation therapy (neoCRT) (6). The addition of neoadjuvant treatment aims to reduce the risk of recurrence, and to target any micrometastasis.

Neoadjuvant treatment for locally-advanced disease involves two options of radiotherapy treatment. One strategy is the use of short course radiotherapy (SCRT), which consists of 5 fractions of 5 Gray (Gy) radiation over one week (total 25 Gy), followed by surgery at least 10 days post radiation treatment. The other more commonly utilised option is long course radiation therapy (LCRT), which consists of a total 45-50.4 Gy in 25-28 fractions (6). In neoCRT treatment, radiation therapy is combined with either fluorouracil (5-FU) or oral capecitabine.

1.1.6. *The tumour response to neoCRT in rectal cancer*

Therapeutic response to neoCRT in rectal cancer is assessed using the modified Ryan tumour regression score (TRS) (30). This system is a four-point scale, as recommended by American

Joint Committee on Cancer (AJCC) guidelines, based on a modification to the three-point scale by Ryan *et al.* (43). This scale is applied when any form of preoperative therapy is employed and assesses surgical specimens for the presence/absence of tumour cells and fibrosis (**Table 1.2**). TRS 0 represents a complete response and is characterised by no viable tumour cells following treatment. TRS 1 is characterised by single or rare small groups of remaining cancer cells and is representative of a near complete response to treatment. TRS 2 represents evidence of residual cancer, with tumour regression, characterising a partial response. TRS 3 represents a poor or no response to treatment, characterised by extensive residual cancer, with no evidence of tumour regression. Resistance to neoCRT is a major clinical problem in the management of rectal cancer, with a conservative estimate of 15-30% of patients achieving a complete pathological response (pCR), which is associated with favourable prognosis in rectal cancer (44-47).

Novel neoadjuvant treatment strategies are also currently under investigation for their potential use in rectal cancer, to boost the therapeutic efficacy of the current standard of care. Total neoadjuvant therapy (TNT), which combines both systemic chemotherapy and neoCRT prior to surgery, has recently been demonstrated to result in enhanced patient outcomes in LARC patients (48). A recent meta-analysis of eight phase II/III randomised control trials, demonstrated enhanced complete pathological response (pCR) rates, improved disease-free survival (DFS) and overall survival (OS) outcomes, in LARC patients receiving TNT, when compared to standard neoCRT (48).

***Table 1.2*: Modified Ryan tumour regression score used in Ireland** (30).

TRS	Description
0	No viable tumour cells (complete response)
1	Single cells or rare small groups of cancer cells (near-complete response)
2	Residual cancer with evident tumour regression, but more than single cells or rare groups of cancer cells (partial response)
3	Extensive residual cancer with no evident tumour regression (poor or no response)

Abbreviations; TRS, Tumour regression score.

1.1.6.1. *Radiation therapy*

Radiation therapy is a mainstay of cancer treatment, with an estimated 50% of all cancer patients receiving radiation therapy as part of their treatment (49). Radiation therapy involves the use of ionising radiation (IR) principally in the form of X-rays or γ-rays, to damage DNA of cancer cells. While IR damages both cancer and normal cells, the aim of radiation therapy is to maximise cancer-specific damage, while minimising exposure to IR in normal cells (49). Radiation therapy is most commonly delivered by external beam radiation, in fractionated doses.

The purpose of a fractionated radiation strategy is to spare normal tissue damage, while concurrently enhancing tumour-specific damage, by exploiting the 4 R's of radiation therapy (50). The 4 R's of radiotherapy, first described in a seminal paper by Withers in 1975, highlight four factors which influence the efficacy of radiation therapy, and include repair, reoxygenation, redistribution and regeneration (50). Repair refers to how fractionation of radiation therapy permits the repair of damage to normal tissue, between fractions. Furthermore, DNA damage repair mechanisms are often impaired in cancer cells while normal cell repair pathways remains in-tact, aiding the anti-neoplastic effects of radiation therapy. Reoxygenation is a crucial parameter in the efficacy of fractionated radiation therapy, as hypoxia is a critical mediator of radioresistance in solid tumours, due to the importance of oxygen radiolysis in the indirect induction of IR-induced DNA damage. Redistribution refers to how fractionation permits the progression of cells through the cell cycle between radiation delivery. This cell cycle redistribution is a crucial factor of the efficacy of radiation, as each phase of the cell cycle display differing radiosensitivity, with cells in the S phase being the most resistant to radiation, and cells in the G2/M phase being most radiosensitive (51, 52). Regeneration refers to the repopulation of both normal and cancer cells between radiation fractions, which is a crucial parameter in determining therapeutic response (53).

Radiotherapy is an effective therapeutic strategy in the management of solid cancers, contributing to an estimated 40% of curative treatment (49). However, as with many anti-neoplastic treatments, its use is often accompanied by therapeutic toxicity and side effects (54). Radiation therapy associated toxicity may be acute, and occur within two weeks post radiation exposure, and include inflammatory effects such as dermatitis, mucositis and nausea, depending on the anatomical location of radiation. Late effects of radiation therapy may only arise months following treatment, and can include fibrosis and the development of

secondary cancers (54). In rectal cancer specifically, the common side effects include late anal toxicity, loss of faecal continence and impaired sexual function (54-56). These side effects are worst in low-lying rectal tumours (54-56).

1.1.6.2. *Radiation-induced damage*

The primary target of radiation therapy is DNA. IR induces various DNA aberrations including single base damage, single-strand breaks (SSBs) and double-strand-breaks (DSBs). DSBs are the most critical form of IR-induced DNA damage for its anti-neoplastic effects (57).

IR-induces cellular DNA damage via both direct and indirect manners. Direct damage, induced by physical damage of DNA accounts for an estimated 35% of IR-induced DNA lesions. The majority of IR-induced DNA damage is mediated by indirect actions, via the interaction of IR and H_2O (49, 58). Radiolysis of H_2O produces reactive oxygen species (ROS), including free radicals, H_2O_2 and superoxide (58). The unpaired electron of these free radicals is highly reactive and interacts with DNA molecules to induce molecular structural damage.

DNA damage induced by either direct or indirect mechanisms of radiation therapy can accumulate, and if it cannot be repaired, the cell will ultimately lose reproductive integrity. Cell death following radiation exposure can occur hours to weeks, and is complex (49). Radiation-induced cell death can be achieved by various pathways, including mitotic catastrophe, necrosis, apoptosis, senescence or autophagy (59, 60).

1.1.6.3. *5-FU*

5-FU is an anti-metabolite chemotherapeutic agent, and has been the primary chemotherapeutic agent in the management of colorectal cancer for more than 50 years (61). 5-FU is a fluoropyrimidine, a uracil analogue, which enters cells by utilising the same transport mechanism as uracil. Once in a cell, 5-FU is converted to active metabolites, fluorodeoxyuridine triphosphate (FdUMP) and fluorouridine triphosphate (FUTP), which disrupt the synthesis of RNA and inhibit the nucleotide synthetic enzyme thymidylate synthase (TS) (61). This disruption to normal RNA synthesis and TS function induces cellular cytotoxicity.

5-FU is commonly utilised in tandem with radiation treatment in the management of rectal cancer. 5-FU treatment in a neoadjuvant setting can contribute to reducing tumour bulk and downstage tumours prior to surgical resection, aiding in the delineation of surgical margins, improving survival and local control rates (62). Furthermore, 5-FU is utilised as a clinical radiosensitising drug, when treatment occurs prior to or during radiation exposure (62, 63). The exact mechanisms of 5-FU induced radiosensitisation are incompletely understood,

however, the scheduling and delivery mechanism of 5-FU is demonstrated to affect radiosensitisation efficacy (63). 5-FU is typically delivered by constant intravenous infusion in rectal cancer (6). Capecitabine, a pro-drug which is converted to 5-FU within the body in a multistep process mediated by the enzyme thymidine phosphorylase (63). Capecitabine is delivered orally, and was designed to mimic continuous infusion of 5-FU without the complications associated with intravenous drug administration (62). Oral capecitabine is commonly utilised in neoCRT treatment of rectal cancer, in place of intravenous 5-FU (6, 30). Continuous 5-FU levels throughout fractionated radiation treatment is demonstrated to contribute to enhanced radiosensitisation (63). Mechanisms underlying 5-FU-mediated radiosensitisation include alteration to basal cell cycle distribution and progression prior to radiation exposure, including S phase specific killing (62, 64). In addition, in an *in vitro* model of colorectal cancer, 5-FU treatment was demonstrated to inhibit expression of ERCC1, indicating a potential role of reduced DNA repair efficiency in 5-FU mediated radiosensitisation (65).

1.2. Mechanisms of radiation resistance in rectal cancer

Despite being the standard of care for LARC, response rates to neoCRT remain low, with pCR rates 15-30% (44-47). This means that the majority of patients are subject to therapy-associated toxicities with minimal to no therapeutic benefit. There are currently no markers used routinely in the clinic that can predict prior to treatment those patients who are likely to respond to neoCRT and conversely, those patients who are likely to be resistant to the standard of care.

Subsequently, there is an urgent unmet need to identify biomarkers predictive of response to neoCRT to enable improved stratification of patients, and also to identify novel therapeutic targets that may boost response to treatment in the neoadjuvant setting. Intrinsic tumour factors including tumour size, location and vascular invasion are known to contribute to inherent radioresistance of tumours (66). In addition to these physical factors, cellular and genetic factors, including DNA damage repair mechanisms, cell cycle, cell death, hypoxia, oxidative stress and metabolism also mediate radioresponse in cells (**Fig. 1.4**).

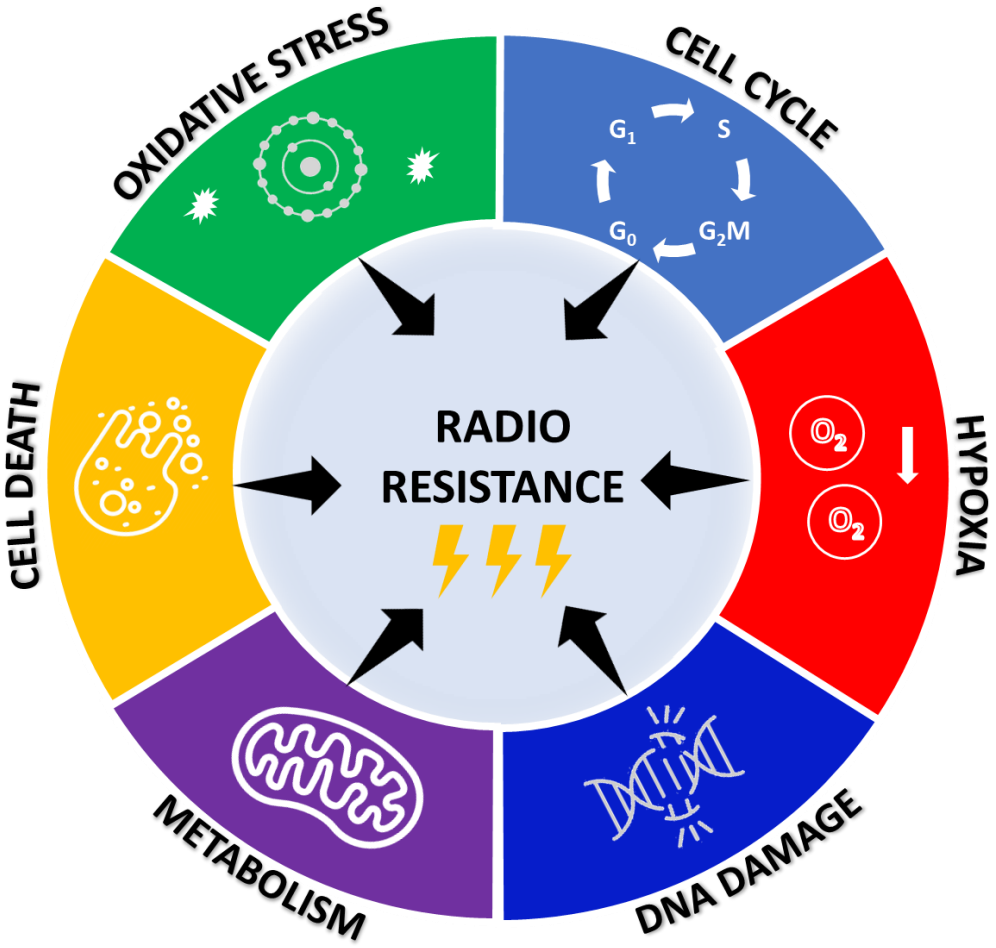

Fig. 1.4: **Overview of the major mechanisms contributing to radioresistance in cancer cells.** The radiosensitivity of cells is affected by molecular mechanisms including cell cycle phase and progression, hypoxia, altered DNA damage repair, altered tumour metabolism, evasion of cell death and enhanced oxidative stress.

1.2.1. *DNA damage response and radioresistance*

The induction of DNA damage is the primary mechanism of the anti-cancer effects of radiation therapy (67). Consequently, DNA damage repair is the most comprehensively studied factor affecting cellular radioresponse, and is also commonly considered to be the most influential (68).

Exposure to radiation induces a variety of DNA lesions, including single base damage, SSBs and DSBs (67). The DNA damage response (DDR) consists of a complex network of pathways to co-ordinate DNA damage repair and halt cell cycle progression to mitigate spread of DNA damage to daughter cells. Due to the wide variety of DNA lesions which can occur, multiple different pathways to repair these lesions make up the DDR.

Oxidative damage induced by IR can result in damaged bases, which are repaired by the base excision repair (BER) pathway (69). In BER, damaged bases are cleaved by DNA glycosylases, leaving apurinic sites, which are subsequently cleaved by apurinic endonuclease 1 (APE-1) leaving SSBs (67, 69). These SSBs, and SSBs induced by IR are repaired by part of the BER, called single strand break repair (SSBR), which is either short-patch or long-patch SSBR. The SSBs are initially detected for repair by poly-ADP-ribose polymerase (PARP-1 or PARP-2) for recruitment of BER enzymes, including APE-1 and X-ray cross-complementing-1 (XRCC1). While the majority of oxidative base damage from IR is repaired by BER, under hypoxic conditions, nucleotide excision repair (NER) is also involved (70).

Alterations to BER have been implicated in radioresistance in cancer, and have been identified as targets for radiosensitising drugs (71). Overexpression of components of BER have been demonstrated as poor prognostic markers in rectal cancer patients, including APE-1, ERCC-1 (72, 73). In a stage Ib clinical trial (**NCT01589419**), Veliparib, a PARP inhibitor has been demonstrated to have an acceptable safety profile in combination treatment with neoadjuvant capecitabine and radiation treatment in LARC patients (74). In addition, preliminary anti-tumour effects including tumour downstaging in 71% of patients, and pCR in 29% of patients was observed, highlighting the potential utility of PARP inhibition with neoCRT in rectal cancer (74). However, this drug combination was investigated in a Phase II clinical trial, with preliminary reports indicating no benefit of this regime over the standard of care (75, 76).

DSBs are the most lethal type of radiation-induced damage in cells. There are two major pathways involved in the repair of DSBs, homologous recombination (HR) and non-homologous end joining (NHEJ) (67). NHEJ is the predominant form of DSB repair employed by cancer cells in response to IR-induced damage. NHEJ is initiated by the binding of Ku70/80 proteins to DSBs, which recruits DNA-dependent protein kinase catalytic subunit (DNA-PKcs) and the nuclease Artemis to process the broken strand ends, and remove overhangs (77). Polymerases are recruited to repair DSBs by adding nucleotides. Finally, a ligase IV complex consisting of XRCC4 and XRCC4-like factor (XLF) is recruited to the site to ligate the repaired DNA ends. Importantly, the NHEJ pathway does not use a template to repair the DNA sequence and subsequently frequently results in deletions at the repair break site, and error prone repair (67). The NHEJ is active at all stages of the cell cycle.

Alterations to NHEJ have been demonstrated to play a role in cancer and radioresistance (78). A deficiency in any NHEJ proteins results in radiosensitivity and deficient DSB repair (79). In pre-radiation rectal tumour biopsies, increased nuclear Ku-70 expression, assessed by immunohistochemistry, has been demonstrated to be associated with poor DFS and radioresistance in rectal cancer patients (80). Upregulation of DNA-PK results in enhanced radioresistance (81), and inhibition inducing radiosensitisation (82, 83). Furthermore, XRCC4 silencing induces radiosensitisation in cancer cells (84).

The second pathway utilised by cells in response to DSB is HR. HR uses a sister chromatid as a reference for repairing damage, and so is active at G2 and S phases of the cell cycle, when the sister chromatid is available (85). Due to the presence of the sister chromatid, HR results in very accurate DNA repair, with little error. The HR pathway begins with degradation by nucleases (Mre11-Rad50-Xrs2) at the DSB in the 5' to 3' direction, leaving 3' single stranded overhang tails (85). Replication protein A (RPA) then binds the overhangs and Rad51 is recruited with the assembly of the nucleoprotein filament scaffold. This filament then initiates the homology search, by forming the displacement or D-loop and strand invasion, with Rad 54 and Rad 51 coupling. In this manner, the homologous undamaged molecule acts as a template for repairing bases at the DSB.

Rad 51 inhibition has been demonstrated to sensitise cancer cells to radiation therapy (86). The expression of XRCC2, involved in HR, has been demonstrated to be overexpressed in colorectal cancer tissue and *in vitro* (87, 88). A study by Qin *et al.*, demonstrated an association with XRCC2 expression and radioresistance in LARC patients, and identified XRCC2 as a

predictive marker of response to preoperative radiotherapy in these patients (89). In addition, *in vitro* knockdown of XRCC2 results in DNA damage repair following radiation, and cell death via G2/M arrest in colorectal cancer SW480 cells (89).

1.2.2. *Cell cycle and radioresistance*

The cell cycle consists of four phases, the Gap (G)1, Synthesis (S), G2, Mitosis (M) phases and one extra-cyclical phase, the G0 phase. The two G phases separate the S phase and M phase, to allow cells to prepare for chromosome segregation and cell division (90). Both the basal position of cells within cell cycle phase, and cell cycle progression and checkpoint activation are critical determinants of cellular radioresponse (66).

The basal position of cells within the cell cycle contributes to the inherent radiosensitivity of cells. Cells in the G2 and M phases are the most radiosensitive, while cells in G1 are more resistant, and S phase cells are the most resistant to IR (51, 52, 68). The inherent resistance of S phase cells is believed to be in part due to enhanced DNA synthesis and repair enzymes in this phase, and enhanced levels of glutathione (68). The enhanced radiosensitivity of cells in the G2/M phase is in part due to a larger physical DNA target for direct IR-induced damage, but mostly as there is little time for DNA repair prior to chromosome segregation (68).

Progression through the cell cycle is regulated by multiple checkpoints, which are induced upon DNA damage, including following radiation exposure (66, 91). The purpose of these checkpoints is to maintain genetic integrity and permit the repair of DNA damage prior to chromosome replication or cell division. IR induces checkpoints and cell cycle arrest in the G1, S and G2 phases of the cell cycle (**Fig. 1.5**) (91).

The G1 checkpoint is activated to permit repair of DNA damage prior to replication of damaged DNA in the S phase. The induction of cell cycle arrest in G1 phase can be induced by multiple pathways, with each utilising the ATM/ATR and CHK1/CHK2 kinases as mediators (92). Following DNA damage induction, ATM and ATR are activated and phosphorylate kinases CHK1 and CHK2. These effector kinases induce degradation of Cdc25A downstream, which locks the CDK (cyclin-dependent kinase) 2-Cyclin E kinase complex, inhibiting progression to S phase. A second pathway of the G1 checkpoint, DNA damage induces activation of ATM/ATR, which phosphorylate and stabilise tumour suppressor protein p53, inducing its transcriptional activity (92). One of the key genes activated by p53 activation is p21, a CDK inhibitor, which blocks progression to the S phase of cell cycle by binding and inhibiting the CDK2-Cyclin E

complex (66). This dual G1 checkpoint does not directly facilitate DNA damage repair, however it is believed to preserve genomic integrity by forcing cells to be eliminated by apoptosis, mediated by p53 (93).

The intra-S phase cell cycle checkpoint induces a relatively short delay to cell cycle progression and occurs to prevent progression of cells with DNA damage acquired while in the S phase (92). The pathway of activation of the intra-S phase checkpoint is similar to that of the G1 phase, in which IR-mediated DNA damage induces activation of ATM/ATR, which in turn phosphorylate downstream mediators including CHK1/2. These CHK1/2 kinases subsequently phosphorylate and degrade Cdc25A, leading to inhibition of progression in the S phase of the cell cycle by CDK2-Cyclin A inhibition (94).

There are two main G2 checkpoints, which prevent cells with DNA damage from entering mitosis, and permit damage repair. The main mediator of the G2 checkpoint is inhibition of CDK1 kinase, the activation of which is critical for the normal progression from G2 to M phase (92). In the G2 checkpoint, ATM is phosphorylated and activates CHK2. Subsequently, Cdc25C is inhibited, culminating in the inhibition of the CDK1-Cyclin B complex, and arrest to progression to M phase. This ATM-dependent pathway results in an 'early' G2/M block which occurs early following radiation exposure and represents the failure of cells that were in G2 phase at time of irradiation from entering mitosis (95). A second G2/M checkpoint occurs hours post radiation exposure, and is ATM independent, and represents the accumulation of cells which had been irradiated at earlier points of the cell cycle and is dependent on ATR.

The relationship between cell cycle checkpoints and radioresistance is a growing area of research in the field of radiosensitising drugs (94). One of the most attractive targets for the development of radiosensitising drugs is the G2/M checkpoint, as the G1 checkpoint is intact in normal cells, while cancer cells are often deficient in this checkpoint (94, 96, 97). By combining radiation with a G2/M inhibitor, normal cells can compensate for the loss of this G2/M by cell cycle arrest in the G1 phase. However, cancer cells, deficient in p53 and subsequently lacking G1 checkpoint function, can no longer stall cell cycle for DNA damage repair following radiation exposure, and succumb to cell death. Two of the primary targets within the G2/M checkpoint proposed as potential drug targets to enhance radiosensitivity are ATR and CHK1, which are currently under investigation in clinical trials (98).

The contribution of cell cycle to radioresistance in CRC has been supported in the literature. A recent paper by Lin *et al.* demonstrated differences to cell cycle gene expression in two *in vitro* models of radioresistant colorectal cancer (99). Furthermore, a recent study by Lee *et al.* demonstrated alterations to cell cycle gene expression between radioresistant and radiosensitive organoids from LARC patients (100). Furthermore, multiple studies have demonstrated G2/M arrest as a common feature of radiosensitisation in CRC (101-103).

1.2.3. *Apoptosis and radioresistance*

If damage induced by radiation cannot be repaired, cell death will occur, via a variety of cellular death pathways (60, 66).

Dysfunctional cell cycle checkpoints in cancer cells can permit the radiation-damaged cells to enter mitosis with damaged DNA, leading to mitotic catastrophe (60). Despite common misconceptions, mitotic catastrophe is not a type of cell death, rather it can result in the induction of cell death pathways. Cells in which mitotic catastrophe occurs lose replicative integrity and induce mitotic cell death, most often intrinsic apoptosis (60, 104).

The role of apoptosis, or programmed cell death, in response to radiation exposure has been highlighted in recent years. Apoptosis is now being considered the primary mode of cell death following radiation exposure (105). Apoptosis is characterised by morphological differences, including membrane blebbing, chromatin condensation and cell shrinkage (106). There are two main apoptotic pathways, the intrinsic and extrinsic pathways, both of which are p53 dependent and mediated by caspase activation. The intrinsic pathway, also referred to as mitochondrial apoptosis, involves the fine balance of pro and anti-apoptotic proteins, caspase activation and cytochrome-c release (106). Damage-induced loss of mitochondrial membrane potential and enhanced mitochondrial permeability results in the release of pro-apoptotic proteins into the cytosol, including cytochrome-c and Smac/DIABLO. Cytochrome *c* activates Apaf-1 and procaspase-9, which form the apoptosome, culminating in caspase-9 activation (107). This subsequently activates caspase-3 and the downstream execution pathway leading to cell death. These steps of intrinsic apoptosis are regulated by the Bcl-2 family of pro- and anti-apoptotic proteins, especially the release of cytochrome-*c* from the mitochondria (108).

The extrinsic pathway involves the activation of death receptors. These receptors are from the tumour necrosis factor (TNF) family, primarily fatty acid synthetase (Fas) receptor and TNFR-1. Upon binding to their ligands, adaptor proteins Fas-associated death domain

(FADD) and TNF receptor-associated death domain (TRADD) are recruited and associate with pro-caspase-8 (109, 110). These steps culminate in the formation of the death-inducing signalling complex (DISC) and activation of pro-caspase-8 to activated caspase-8. Caspase-8 then triggers caspase-3 activation and the induction of the execution phase of apoptotic cell death (106, 111).

Both the intrinsic and extrinsic apoptosis pathways merge upon the induction of the execution pathway, via the activation of the executor caspases (caspase-3, caspase-6 and caspase-7) (106). This culminates in the activation and release of endonuclease caspase activated DNAse (CAD), which triggers chromatin condensation. Cytoskeletal reorganisation and membrane blebbing result in the formation of apoptotic bodies, which are finally phagocytosed.

Apoptosis has been demonstrated to be associated with radioresponse in many cancers (112). The expression of B cell lymphoma 2 (Bcl-2) family of pro- and anti- apoptotic proteins have been demonstrated to be dysregulated in CRC and have been proposed as therapeutic targets (113). In rectal cancer patients, Bcl-2/Bcl-2 associated X (Bax) ratio has been demonstrated to act as a predictive marker of response to radiation therapy (RT) (114). Furthermore, Bax expression alone has been associated with tumour regression and enhanced response to CRT in rectal cancer patients with Bax expression significantly higher in those achieving a pCR, when compared to those achieving a partial response (54% vs. 29%) (115). Survivin, a member of the inhibitor of apoptosis (IAP) protein family, has been demonstrated to correlate with poor prognosis and worse patient survival in CRC (116). Furthermore, a role for survivin in radioresistance of rectal cancer has been supported in an *ex vivo* study (117). Other IAPs have been proposed as modulators of radioresistance in rectal cancer, with inhibition of X-linked IAP (XIAP) rescuing cellular radiosensitivity *in vitro* and the ratio of DIABLO and XIAP being associated with therapeutic response in rectal cancer patients (118). XIAP alone has also been proposed as an indicator of resistance to neoCRT in rectal cancer (119). A mimetic of smac/DIABLO, JP-1201, has been demonstrated to enhance radiosensitivity of colorectal cancer both *in vitro* and *ex vivo* (120). In addition, alterations to the extrinsic apoptotic pathway has also been demonstrated in rectal cancer, with levels of serum soluble Fas demonstrated to be altered in rectal cancer patients, when compared to healthy controls, and being associated with response rates to CRT (121).

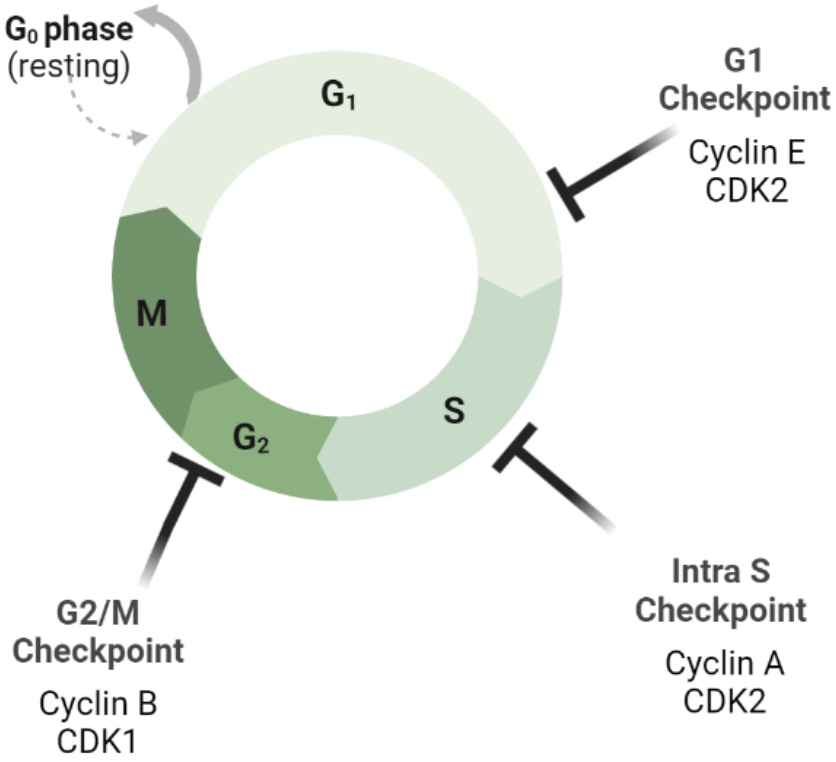

Fig. 1.5: **The cell cycle and checkpoints.** Upon DNA damage induction, cell cycle checkpoints are activated at G1, S and G2 phase. The checkpoints regulate the progression of cells through the cell cycle, to permit DNA damage repair, and to stop the replication of cells with damaged DNA. Figure made using Biorender.com.

1.2.4. *Oxidative stress and radioresistance*

The majority of radiation-induced DNA damage is mediated by indirect actions, via the interaction of IR and H_2O (49, 58). Radiolysis of H_2O produces reactive oxygen species (ROS), including free radicals, H_2O_2 and superoxide which damage DNA and other cellular components (58). One mechanism utilised by cells to counteract this IR-induced ROS damage is the upregulation of cellular antioxidants.

Antioxidant enzymes, including superoxide dismutase (SOD), catalase, glutathione peroxidase (GPX) neutralise ROS and have been demonstrated to be upregulated in many cancer types (122). SOD has been demonstrated to be upregulated in radioresistant cancers including glioblastoma (123). Manganese SOD (MnSOD/SOD2) has been demonstrated to be elevated in radioresistant nasopharyngeal cancer, with inhibition of SOD2 inducing radiosensitisation in this model (124). In addition, MnSOD overexpression has been demonstrated to enhance radioresistance in oral squamous cell carcinoma and alter cell cycle distribution (125). Levels of another antioxidant enzyme, catalase, are significantly associated with radioresistance (123, 126). Furthermore, mitochondrial targeted overexpression of catalase has been demonstrated to enhance radioresistance *in vitro* and *in vivo* (127).

Glutathione (GSH) and glutathione-dependent enzymes, including GPX and glutathione-s-transferase (GST) also play a crucial role in the detoxification of ROS. Glutathione can be made *de novo* with cysteine acting as a rate-limiting factor. In addition, if GSH, the reduced form of glutathione, is depleted in times of cellular stress, recycling of oxidised GSH (GSSG) can occur to replenish the availability of cysteine for GSH synthesis (128). GSH-mediated ROS detoxification is dependent on enzymes including GPX and GST (129). Elevated GSH is demonstrated in rectal (130) and colon (131) cancer, and correlated with poor clinical responses (132). Increased GSH has also been associated with radioresistance (133, 134). In addition, GPX levels are elevated in radioresistant glioblastoma cells (123).

1.2.5. *Hypoxia and radioresistance*

Hypoxia is a common feature of solid malignancies and is one of the major determinants of cellular radioresistance. Studies demonstrate that hypoxic tumour cells display an estimated 2.5-3 fold enhanced resistance to radiation, when compared to normoxic cells (135). The key regulator of hypoxia is hypoxia inducible factor-1 (HIF-1). HIF-1 is a heterodimer which consists of the rate limiting HIF-1α and the constitutively expressed HIF-1β. Upon hypoxic exposure, HIF-1α is stabilised and translocated to the nucleus for gene regulation (136).

HIF-1α displays a progressive increase in expression during disease progression in many cancers, including CRC (137-144), gastric and oesophageal cancers (145). In addition, elevated HIF-1α expression is associated with poor clinical outcomes in cancers, such as CRC (143, 146), oesophageal (147, 148) and gastric cancers (145). Overexpression of HIF-1α is also associated with poorer survival in oesophageal squamous cell carcinoma patients receiving adjuvant chemotherapy (148).

In a study conducted by Shioya *et al.*, HIF-1α expression was predictive of response to hyperthermo-chemoradiotherapy (HCRT) in a cohort of 50 rectal cancer patients with advanced disease (149). Importantly, relapse free survival (RFS) was reported as 82.8% in the HIF-1α negative group, compared to 47.8% in those with positive HIF-1α expression, suggesting strong prognostic potential in rectal cancer (149). The evidence highlighting a potential link between hypoxia and poor outcomes in cancer patients are supported by mechanistic *in vitro* studies investigating hypoxia and therapeutic response. HIF-1α expression has been demonstrated to enhance chemotherapy-induced apoptosis in colon cancer cells (150).

In interrogating the mechanism mediating hypoxia-induced therapeutic resistance, one of the most obvious associations is the requirement of oxygen to fix indirect radiation-induced DNA damage, caused by free radicals and oxidative stress, the main mediator of IR-mediated damage. Consequently, a hypoxic tumour microenvironment permits the repair of IR-induced damage, resulting in resistance to radiation treatment (151).

1.3. Metabolism

1.3.1. *Overview of major energy metabolism pathways in cancer*

1.3.1.1. *Glycolysis and oxidative phosphorylation*

Survival and proliferation are inherent characteristics of tumour cells and importantly, has been highlighted as a hallmark of cancer (152, 153). A major mechanism through which cancer cells adapt to challenging conditions, such as nutrient deprivation or hypoxia and continue to proliferate is via alteration of their metabolic phenotype (154-157).

The major precursor for energy (adenosine triphosphate) (ATP) generation is glucose, which is catabolised for energy production via two main processes, depending on oxygen availability (154, 156, 157).

Glycolysis occurs in the cytosol and involves a series of enzymatic reactions to convert one molecule of glucose to two molecules of pyruvate, generating 2 ATP molecules (**Fig. 1.6**)

(158). This pyruvate subsequently undergoes further processing by the tricarboxylic acid (TCA) cycle, in the inner mitochondrial membrane. The TCA cycle is a cyclical chain of enzymatic reactions, with generates nicotinamide adenine dinucleotide (NADH) and flavin adenine dinucleotide 2 (FADH2). Pyruvate is converted to acetyl coenzyme A (acetyl Co-A), which is subsequently condensed to form citrate with oxaloacetate. Citrate is then processed to isocitrate by isocitrate dehydrogenase (IDH), which is further processed to form α-ketoglutarate. This is then processed into succinyl-CoA, to succinate. Fumarate is then produced from succinate, and is further processed to malate. Finally, malate is oxidised to oxaloacetate, and the cycle begins again (154). The NADH and FADH2 generated by the TCA cycle is then utilised by the oxidative phosphorylation pathway for the generation of ATP. Electrons from NADH/FADH2 are passed through Complexes I-IV of the electron transport chain (ETC) to O_2. This generates a proton gradient across the inner mitochondrial membrane, which is utilised by complex IV, ATP synthase, for the generation of ATP.

In the presence of oxygen, this pathway is utilised, where glucose is metabolised by glycolysis and TCA for a total generation of 36 moles of ATP per mole of glucose (154). Alternatively, under anoxic conditions, glucose may be metabolised via glycolysis to lactate, in a process called fermentation or anaerobic respiration, producing 2 moles of ATP per mole of glucose. Often, cells seem to favour one process of energy production, with the majority of normal cells under oxygenated conditions favouring oxidative ATP production, due to the increased ATP yield obtained in this process. However, in order to fulfil the increased biosynthetic and bioenergetic demands of a growing tumour, cancer cells are forced to alter their metabolic phenotype (156). This was first reported by Otto Warburg in 1956, where the Warburg Effect, or 'aerobic glycolysis' was initially described in cancer cells (159, 160), in which cancer cells enhance glycolytic flux and lactate production, irrespective of the oxygen availability status of a cell. Despite the glycolytic pathway ultimately producing a marked reduction in the quantity of ATP, when compared to oxidative phosphorylation, cancer cells often rely on this glycolytic phenotype as it ultimately produces ATP at a faster rate, and generates metabolic intermediates utilised for biosynthesis of cellular components. This dramatically altered metabolism of tumours, when compared to normal tissues has been repeatedly supported across cancer types and triggered a growing area of research into cancer energy metabolism (154-157, 161, 162).

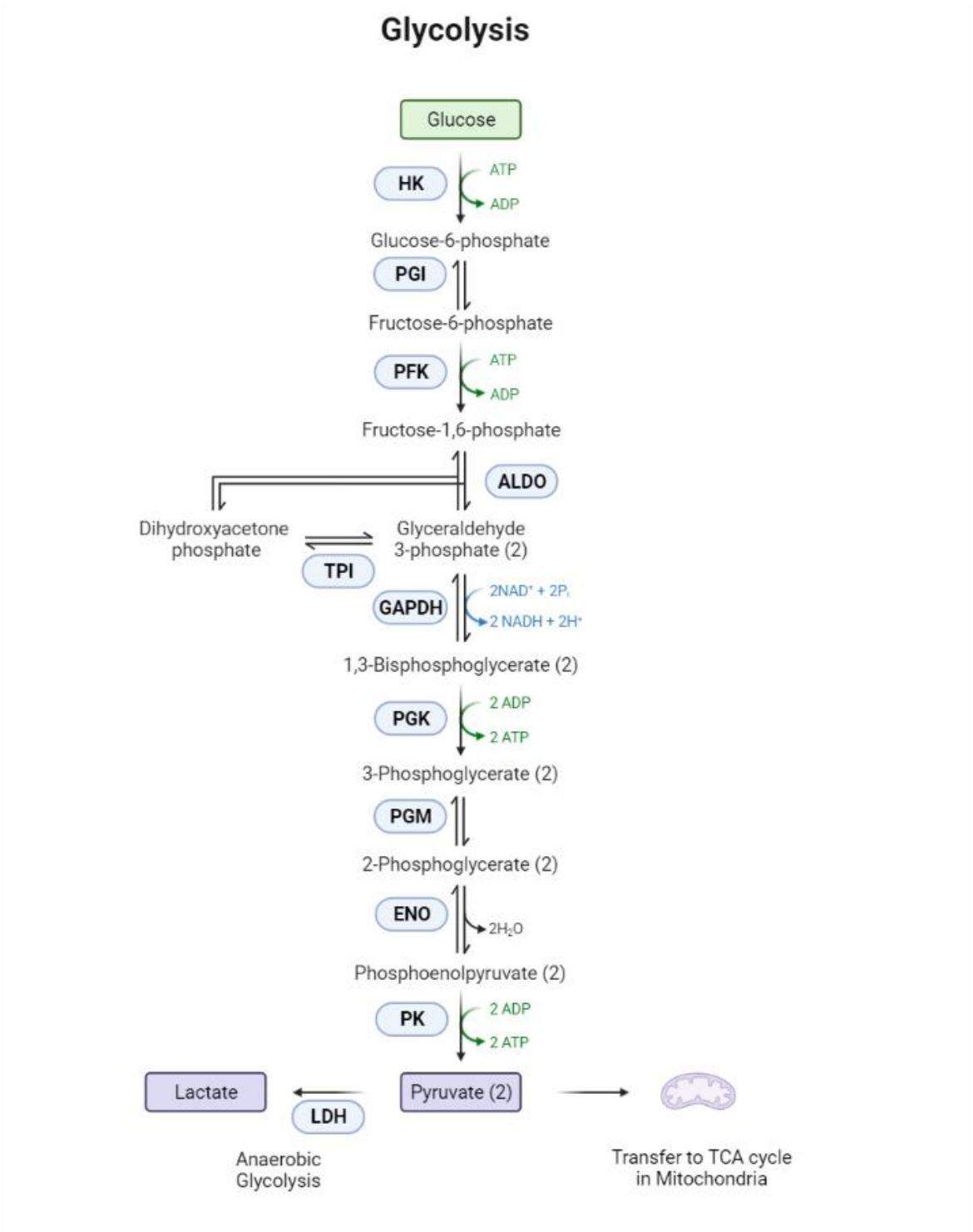

Fig. 1.6: **Overview of glycolysis pathway.** The major enzymes and metabolites of the glycolytic cascade are illustrated. Glucose is taken into the cell, and processed by a series of metabolic enzymes for the ultimate production of ATP and pyruvate. Pyruvate is then transported to the mitochondria for further processing by the TCA cycle, or is converted to lactate under anaerobic conditions. HK hexokinase; PGI phosphoglucose isomerase; PFK phosphofructokinase, ALDO aldolase, TPI triosephosphate isomerase, GAPDH glyceraldehyde-3-phosphate dehydrogenase; PGK phosphoglycerate kinase; PGM phosphoglyceromutase; ENO enolase, PK pyruvate kinase; LDH lactate dehydrogenase. Figure adapted from Biorender.com.

1.3.2. *Altered metabolism in cancer development and progression*

The Warburg effect is characterised by decreased glucose levels, due to the enhanced glucose uptake required for enhanced glycolytic flux, and subsequently elevated lactate production. Glucose has been demonstrated to be consistently reduced in colorectal tumours, when compared to normal adjacent tissue (163-167). In addition, lactate has consistently been demonstrated to be the most commonly upregulated metabolite across cancers; including colorectal (163-167), rectal (130), oesophageal (168-170) and gastric cancers (171, 172).

In addition, intermediates of the TCA cycle (such as malate, succinate) have been demonstrated to be altered in CRC. Malate has been demonstrated to be decreased in colorectal tumours, when compared to normal tissues, perhaps reflecting a reduction in TCA cycle flux in these tumours (164). In contrast, succinate, another intermediate of the TCA cycle has been demonstrated to be significantly increased in rectal cancer tissues, when compared to normal adjacent tissue with increasing concentration found along progression of the disease (130).

Metabolic reprogramming is also involved in the progression of human malignancies (173). A recent study conducted by Graziano *et al.* in CRC demonstrated that glycolysis-related genes including hexokinase-1 (HK1) lactate dehydrogenase A (LDHA), pyruvate kinase (PKM2), glucose-transporter-1 (GLUT-1) and voltage-dependant anion-selective channel protein-1 (VDAC1) display significantly-higher expression in both primary tumour and lung metastases, when compared to normal colorectal mucosa (174). Interestingly, this panel of glycolytic genes displayed a trend towards increased expression in lung metastases, when compared to primary tumour samples, but only LDHA expression was significantly increased (174). Furthermore, a high glycolytic profile in metastatic CRC (mCRC) tumours with either KRAS or NRAS mutations was associated with poor prognosis. In addition, this study proposed that RAS mutations may regulate cellular energy metabolism in CRC cells by promoting glucose uptake. These findings suggest that altered glucose metabolism is implicated in the progression of CRC, and the development of metastasis. A major step in the initiation of tumour cell metastasis is epithelial-mesenchymal transition (EMT), a process where tumour epithelial cells adopt a migratory mesenchymal-like phenotype. The link between EMT and metabolism is well established, with enhanced energy production required for the induction of proliferation, motility, invasiveness and extravasation of tumour cells (175). Many EMT-related genes and pathways, including SNAIL, have been associated with altered tumour metabolism. It has been

demonstrated that when undergoing EMT, cancer cells, including pancreatic cancer cell lines, undergo a shift from aerobic glycolysis to oxidative phosphorylation (176).

In addition, multiple classification systems of CRC have highlighted the importance of metabolic phenotype in subgroups of CRCs. The consensus molecular subtype (CMS) classification system identified four distinct groups of CRCs with distinguishing features, based on comprehensive gene expression profiles of over 4,000 patient samples (37). One of these subtypes, CMS3, was identified as the metabolic CRC subtype, accounting for an estimated 13% of CRCs. CMS3 tumours had an overrepresentation of KRAS mutations, and corresponding enrichment for metabolic pathway signatures, including glucose, fructose, glutamine and fatty acid metabolism (37).

1.3.3. *Altered metabolism and therapeutic response*

Altered tumour energy metabolism has been associated with therapeutic response in many cancers (177-181). An increase in glucose uptake, along with subsequent increased lactate production, characteristic of an enhanced glycolytic phenotype has been demonstrated to be associated with chemoresistance, in an *in vitro* model of chemoresistant gastric cancer (182). In addition, isogenic *in vitro* models of gemcitabine-resistant pancreatic cancer demonstrate enhanced glucose uptake, lactate production and glycolytic enzyme gene expression in resistant cells compared to sensitive parental cells (183). Elevated glucose uptake, lactate production and low pyruvate production, reflecting elevated glycolysis, has also been demonstrated in doxorubicin-resistant HT29 CRC cells (184). Cellular glucose transporters, particularly GLUT-1, have an important rate-limiting function in controlling cellular glycolytic rates. The overexpression of GLUT-1, the primary glucose transporter, is a common feature of malignancy (185). Research now suggests that this overexpression is not only associated with advanced disease stage but may also act as a predictor of treatment response.

A meta-analysis of 41 studies of various cancer types, demonstrated that high GLUT-1 expression is associated with poorer prognosis, including shorter disease-free survival (DFS), progression-free survival (PFS) and disease-specific survival (DSS) (185). The role of GLUT-1 in the response to treatment of rectal cancer is somewhat controversial, with a number of studies demonstrating that negative or low GLUT-1 levels is associated with an enhanced patient response to neoCRT (186, 187), whilst, high expression levels correlate with poor patient prognosis (188). A role for GLUT-1 in resistance to CRT is also implicated in oesophageal cancer. In a panel of OSCC cell lines, inhibition of GLUT-1 was demonstrated to

enhance response to cisplatin (189), whilst high GLUT-1 expression in pre-treatment biopsies was demonstrated to be predictive of poor response to mDCF (modified docetaxel, 5-FU and cisplatin) chemotherapy, tumour stage and histological response grade in patients with OSCC (189). Elevated GLUT-1 expression was also demonstrated to be associated with tumour and nodal stage, response to neoadjuvant CRT and poor RFS in oesophageal adenocarcinoma (OAC) patients (190).

HK2 is a rate-limiting enzyme in the glycolytic cascade. Several studies have provided evidence implicating HK2 in the chemoresistance of CRC. HK2 elevated expression has been observed in a model of oxaliplatin-resistant CRC (191). In CRC cell lines, HK2 inhibition by 2-deoxyglucose (2-DG) treatment has been demonstrated to reverse resistance to 5-FU and oxaliplatin (192). In addition, B7H3, an immune checkpoint molecule, has recently been demonstrated to enhance aerobic glycolysis and resistance to oxaliplatin and 5-FU in CRC by regulation of HK2 (192). Research suggests that B7H3 antagonises DNA damage induced by these chemotherapies, promoting resistance via upregulation of glycolysis. Furthermore, the microRNA miR125b, which inhibits HK2 activity, was demonstrated to re-sensitise 5-FU resistant cells via downregulation of glycolysis in hepatocellular carcinoma (HCC) (193).

Two of the primary isomers of pyruvate kinase, PKM1 and PKM2, a key regulatory enzyme of the glycolytic cascade, have also been implicated in the response of cancers to treatment (194). Overexpression of PKM1 has been observed in 5-FU and oxaliplatin resistant CRC cell lines (195, 196) and a paclitaxel-resistant gastric cancer cell line (197). Elevated PKM2 expression has also been implicated in the resistance to various chemotherapeutic agents in functional studies of pancreatic cancer (198), CRC (199), OSCC (200) and gastric cancer (201). In addition, the microRNA miR-122, which inhibits PKM2, is downregulated in chemoresistant lines of CRC (199) and HCC (202), with chemoresistance associated with enhanced glycolysis. Supporting these findings, a recent meta-analysis including data from over 12,000 patients with various cancer types demonstrated that elevations in key glycolytic enzymes were predictive of shorter OS in oesophageal, gastric, hepatocellular, gallbladder, colorectal and pancreatic cancer (203). Together, these findings suggest that alterations in the expression of key glycolytic enzymes may play an important role in the resistance of cancer cells to therapy.

Alterations to mitochondrial metabolism have also been implicated in therapeutic resistance of cancers. Mitochondrial dysfunction is common in cancer cells, with mitochondrial DNA (mtDNA) mutations being a common feature of many cancers, including

gastric cancer, CRC and HCC (204) and often associated with poor prognosis or a more aggressive phenotype (205-207). Interestingly, cervical cells with induced impaired mitochondria, and therefore more reliant on glycolysis, have displayed higher sensitivity to radiation, when compared to wild-type (WT) cells which utilise both glycolysis and oxidative phosphorylation for energy production (208). Additionally, pancreatic cancer cells with mutated mtDNA were more resistant to apoptosis-inducing agents, and 5-FU and cisplatin treatment than WT cells both *in vitro* and *in vivo* (209). These findings suggest a potential role for mtDNA mutations in treatment resistance (reviewed in (206, 210, 211)). Furthermore, as chemotherapy and radiation therapy induce DNA damage, this may suggest that therapy-induced mtDNA damage can result in metabolic alterations associated with the development of acquired radio/chemoresistance.

Supporting a role for oxidative phosphorylation in radioresistance, our group has previously demonstrated that increased oxidative phosphorylation is associated with a radioresistant phenotype in OAC, both *in vitro* and in patient samples (212, 213). Furthermore, treatment with a novel small molecule inhibitor, Pyrazinib, significantly inhibited both oxidative phosphorylation and glycolysis, and sensitised an isogenic model of radioresistant OAC to radiation, supporting altered metabolism and specifically enhanced oxidative phosphorylation, as an underlying mechanism of radioresistance in OAC (212). This is also supported in colon cancer, where it was demonstrated that HCT116 cells switch from glycolysis to oxidative phosphorylation in response to radiation, displaying metabolic adaptation, while inhibition of oxidative phosphorylation reduced clonogenic survival (214). Furthermore, the use of metformin, a drug routinely used for management of diabetes, and also an inhibitor of Complex I of the ETC, has been reviewed for its potential use as a radiosensitiser in various cancers (215-218).

A role for oxidative phosphorylation has also been implicated in chemoresistance. Mitochondrial dysfunction, enhanced ATP production, and elevated oxygen consumption rate (OCR), indicative of enhanced oxidative phosphorylation rates, have been demonstrated in an oxaliplatin-resistant CRC cell line, indicating a distinct metabolic switch to oxidative phosphorylation associated with the development of chemoresistance in CRC (191). In cell-line models of 5-FU resistant colon cancer, elevated OCR, OCR-linked ATP turnover, and maintenance of spare respiratory capacity has also been demonstrated (196). Furthermore, this study demonstrated that combined treatment with 5-FU and Complex I inhibition with

metformin resulted in enhanced anti-tumour effects and proposed potential utility of such anti-metabolic combination approaches in the treatment of chemotherapeutic-resistant colon cancer. These 5-FU resistant lines were also demonstrated to display oxidative phosphorylation-addiction. This is also supported in oesophageal cancer, in which our group recently demonstrated that oxidative phosphorylation is elevated in cisplatin-resistant OAC cells (219). In addition, reduced expression of mitochondrial respiratory chain cyclooxygenase (COX) subunits in pre-treatment biopsies of OAC were demonstrated to be associated with enhanced response to cisplatin therapy (220). Also in this study, knockdown of COX *in vitro* resulted in chemosensitivity to cisplatin. This study suggests that OAC cells with intact oxidative phosphorylation display a higher tolerance for cisplatin-induced cell death. In pancreatic cancer, a recent Phase 1 study of CPI-613, a novel inhibitor of pyruvate dehydrogenase and α-ketoglutarate dehydrogenase, improved response rates to FOLFIRINOX (leucovorin, fluorouracil, irinotecan, oxaliplatin), when compared to previous studies of chemotherapy alone in metastatic pancreatic ductal adenocarcinoma (PDAC) (221, 222), demonstrating the potential utility of mitochondrial metabolism inhibitors in enhancing response to treatment in this therapy-resistant cancer. However, in an isogenic model of gemcitabine-resistant pancreatic cancer, OCR was demonstrated to be reduced, and extracellular acidification rate (ECAR) increased, when compared to sensitive cells (183), potentially suggesting that the metabolic alterations observed in chemoresistance may be chemotherapeutic agent-specific.

1.3.4. *Potential mechanisms of therapeutic resistance associated with altered metabolism*

1.3.4.1. *Altered metabolism and hypoxia*

Reduced oxygen availability and upregulation of HIF-1α are inherently linked to the regulation of metabolic pathways (223-225).

In regions of low oxygen availability, cells adapt to conserve oxygen, by downregulating oxidative respiration and oxygen-linked ATP production. This is primarily mediated by the inhibition of complex IV of the electron transport chain, via the activation of the HIF-1 transcription factor (226). In addition to the inhibition of mitochondrial oxidative respiration, cancer cells are forced to upregulate glycolysis for energy production via the activation of HIF-1α (226). HIF-1α has been demonstrated to upregulate the transcription of most glycolytic genes, including GLUT-1, the major glucose transporter and glycolytic enzymes (157, 223, 227). In addition, HIF-1α induces the upregulation of genes involved in the pentose phosphate

pathway, increasing the generation of anabolic intermediates required for cell growth and antioxidant capacity (223). Furthermore, lactate and pyruvate generated as a result of increased glycolytic flux promote the accumulation of HIF-1α, regardless of oxygen availability status, to create a feed-forward mechanism between glycolytic and HIF-1 signalling (225, 228, 229).

Many cancers utilise glutamine as an energy source, by supporting the TCA cycle, and also to maintain cellular biosynthesis, including that of antioxidants. A recent study demonstrated that GLS1, which metabolises mitochondrial glutamine, is hypoxia-regulated in CRC patients (230). Furthermore, in this study GLS1 was demonstrated to be significantly upregulated, along with elevated glutamine uptake and glutamate production, under hypoxia (1% O_2), compared to normoxic conditions (20% O_2) in CRC cell lines. In this way, cancer cells hijack the inherent metabolic response of cells to hypoxia in order to proliferate, demonstrating the impact of hypoxia on tumour cell metabolism.

Interestingly, the radiosensitising treatment of mitochondrial complex I inhibitor metformin is hypothesised to be due, at least in part, to the enhanced oxygen availability which results from oxidative phosphorylation inhibition (217, 231). In a study of CRC cell lines and an *in vivo* model, treatment with metformin and phenformin were demonstrated to overcome radiation resistance induced by hypoxia exposure, by blocking oxygen consumption (232).

These data demonstrate the link between tumour metabolism and hypoxia in cancers and highlight the potential role of this relationship in radiation resistance.

1.3.4.2. *Altered metabolism and oxidative stress*

Energy metabolism has been demonstrated to play a key role in redox balance maintenance, suggesting a potential mechanism by which altered tumour metabolism impacts on treatment response.

Enhanced glucose metabolism induces the production and availability of antioxidants (233), which prevent fixation of DNA damage induced by ionising radiation, contributing to radioresistance. GSH is a primary thiol antioxidant, the production of which has been demonstrated to be enhanced by an increased glycolytic flux (233). Increased GSH production has been identified in metabolomic studies of rectal (130) and colon (131) cancer. Interestingly, increased GSH was associated with poor clinical outcomes in a CRC cohort (132). In addition, the oxidative phase of the pentose phosphate pathway (PPP), which branches off

from glycolysis, plays a crucial role in the maintenance of a GSH antioxidant pool, via the production of reduced nicotinamide adenine dinucleotide phosphate (NADPH) (234). ROS detoxification, via enhanced glycolysis and PPP has been proposed as a potential mechanism of chemoresistance in multiple cancers, including oesophageal cancer (200). Interestingly, a reduction in NADPH production following treatment with hydroxethyldisulfide in glucose-deprived colon cancer cell lines resulted in enhanced sensitivity to radiation-induced oxidative stress in colon cancer cell lines (235). Inhibition of glycolysis with 2-DG treatment has been demonstrated to induce radiosensitisation in cervical cancer both *in vitro* and *in vivo*, accompanied by enhanced GSSG levels (236).

Another mechanism of increased GSH production is mediated by pyruvate, produced during glycolysis. Pyruvate is known to contribute to the maintenance of the glutathione pool. Pyruvate production has been demonstrated to be increased in many cancers including gastric (172) and oesophageal (237) cancer. Another metabolite which has been demonstrated to act as an antioxidant is lactate (238). Increased glycolytic flux results in the enhanced production of lactate in many cancers including colorectal (130, 163-167), oesophageal (168-170) and gastric cancer (171, 172, 239). The accumulation of these anti-oxidative metabolites in many cancers may be one of the mechanisms underlying impaired efficacy of radiation therapy. Inhibition of lactate has also been demonstrated to reduce levels of taurine and glutathione, which act as antioxidants in a model of glioma (240). Importantly, this lactate inhibition was also demonstrated to enhance radiosensitivity in this model.

These studies indicate a potential role for antioxidants, induced by altered tumour metabolism, in the resistance of cancers to radiation therapy.

1.3.4.3. *Altered metabolism and apoptosis*

Apoptosis requires large energy reserves to fuel pathways. Importantly, mtDNA is demonstrated to be necessary for many forms of cell death (241, 242).

The most obvious parallel to draw between apoptosis and metabolism revolves around the intrinsic pathway of apoptosis, also known as the mitochondrial apoptotic pathway. Disruption to mitochondrial metabolism can impair this intrinsic apoptotic pathway. Investigations into metabolic stress-induced apoptosis have demonstrated that following glucose deprivation, expression of Bcl-2 and Bcl-XL are protective against apoptosis in various cell types (162). Interestingly, upregulation of Bcl-XL protein, an anti-apoptotic member of the Bcl-2 family has been demonstrated in CRC, and associated with tumourigenesis (243).

Furthermore, TP53-induced glycolysis and apoptosis regulator (TIGAR), an enzyme involved in glycolytic regulation and associated with protection from apoptosis, displays enhanced expression in CRC cell lines and tissue samples, when compared to normal tissue, further demonstrating the intrinsic link between these two processes in cancers (244).

Furthermore, oxidative phosphorylation is essential for Bax and Bak activation (245). Conversely, Bcl-2, which prevents Bax and Bak activation, inhibit mitochondrial respiration and activity of complex I of the electron transport chain (246, 247). It has thus been proposed that inhibition of oxidative phosphorylation may be one mechanism by which Bcl-2 inhibits Bax and Bak activation.

Therapeutic inhibition of glycolysis has been demonstrated to impair apoptosis in cancers. In an *in vitro* model of CRC, inhibition of HK2 was demonstrated to enhance mitochondrial-apoptosis in these cells (248). Furthermore, inhibition of PKM2 in CRC, and subsequent glycolytic inhibition resulted in promotion of apoptosis and inhibition of proliferation, migration and invasion (249). This is also supported by evidence of dichloroacetate (DCA), a glycolytic inhibitor, inducing apoptosis in CRC cell lines (250). In addition, glycolytic inhibition has been demonstrated to induce mitochondrial-apoptosis in a cell-line model of gastric cancer (251). In an *in vivo* model of gastric cancer, glycolytic inhibition resulted in upregulated expression of pro-apoptotic proteins Bax, cytochrome c and cleaved caspase-3 and downregulation of anti-apoptotic Bcl-2 and survivin proteins, culminating in enhanced mitochondrial apoptosis as a result of glycolytic inhibition (252).

1.3.4.4. *Altered metabolism and cell cycle*

Cell division and the progression of the cell cycle is an energetically demanding process, and thus metabolic status and cell cycle are intrinsically linked. The availability of nutrients and the metabolic capacity of cancer cells can determine whether cells can initiate cell division (253, 254).

Nutrient availability is a crucial determinant of the progression of cells through each phase of the cell cycle. The presence/absence of growth factors determine whether cells progress to the G1 phase or exit the cell cycle and enter the G0 phase, a metabolically conserved phase outside of the cell cycle in which cells display decreased gene expression and lowered biosynthetic pathway activation (254). A growth-factor dependent restriction site regulates early G1 phase of the cell cycle, with D-type cyclins, key mediators of G1 cell cycle phase being metabolically modulated (255). In mid to late G1, the progression of cells to the

S phase is regulated by a nutrient-sensitive cell cycle checkpoint which enables the progression of cells only when adequate nutrients are available (253, 255). In addition, cells committed to mitosis have been demonstrated to increase expression of 6-phosphofructo-2-kinase/fructose-2,6-bisphosphatase-3 (PFKFB3), which regulates glycolytic progression (256, 257). Inhibition of glycolysis has been demonstrated to impair progression through this early G1 restriction point (256, 257). Treatment with the glycolytic inhibitor 2-DG has been demonstrated to inhibit cell cycle progression, at G0/G1 and G2/M phases in various cancer cell lines (258, 259). Furthermore, 2-DG treatment was demonstrated to induce G0/G1 phase arrest and apoptosis in CRC cells *in vitro* (260). These inhibitory effects of 2-DG treatment on cell cycle progression are believed to be in part due to enhanced cyclin expression, including cyclin B1 and D1, and are proposed to contribute to the radiosensitising effects of 2-DG in cancer cells (261).

Importantly, not only does metabolism impact cell cycle regulators and progression, but mediators of cell cycle can also impact metabolic pathways (254). Overexpression of cyclin D1 has been demonstrated to supress both glycolytic activity and mitochondrial function (262). Cyclin B1/CDK1, involved in the G2/M cell cycle checkpoint, have been demonstrated to regulate mitochondrial metabolism (263). CDK1 is well established as a regulator of mitochondrial dynamics, mitochondrial bioenergetics and mitochondrial apoptosis. Cyclin B1/CDK1 acts as a regulator of complex I of the electron transport chain, and subsequently is proposed as a regulator of ATP output and oxidative phosphorylation (263). Furthermore, during G2/M phase progression, CDK1 enhances oxidative phosphorylation rates to fuel mitosis.

1.3.4.5. *Altered metabolism and DNA damage*

Metabolism and DNA damage are intrinsically linked, with DNA damage repair having a large biosynthetic and energetic cellular demand.

One of the key requirements for DNA damage repair is the availability of nucleotides for single and double strand repair. Glutamine and aspartate are required for *de novo* synthesis of nucleotides and maintenance of the deoxyribose nucleotide triphosphate (dNTP) pools (264, 265). Glucose and the pentose phosphate pathway are necessary for the generation of metabolic intermediates for nucleotide, protein and NADPH synthesis, all of which are of crucial importance in the DDR. An important step in the repair of damage is the unfolding of DNA to permit the recruitment of DDR proteins. Metabolites and metabolic

intermediates, including methyl and acetyl groups are required for this DNA and chromatin restructuring, and further demonstrates the link between metabolism and DDR (264).

Enhanced glycolytic rates have been demonstrated to facilitate repair of IR-induced DNA damage by activating DSB repair pathways NHEJ and HR (266). Inhibition of glycolysis with 2-DG treatment is demonstrated to inhibit DNA damage repair and enhance micronuclei formation *in vitro*, which is proposed as a mechanism of 2-DG mediated radiosensitisation (267). This association between enhanced glycolysis and radioresistance in cancer cells is mediated in part through the activation of AKT, a kinase with an important role in cellular proliferation and metabolism (268). In addition, inhibition of LDHA, a major enzyme in the glycolytic cascade, has been demonstrated to sensitise cancer cells to radiation treatment by promoting the generation of DSBs and reducing DDR capacity (269).

Mitochondrial metabolism also influences DNA damage induction and repair, potentially playing a role in the cellular response to DNA-damaging agents. One of the primary mechanisms linking mitochondria and DNA damage is through response to oxidative stress and ROS damage as discussed. In addition, mitochondrial dysfunction is associated with DSB and phosphorylation of H2A histone family member 2 X (H2AX) in mtDNA (270). ATM is a crucial component of the induction of the DDR following radiation treatment. Interestingly, recent data demonstrate that inhibition of ATM kinase, eliminates nuclear DNA damage recognition and mitochondrial radiation responses, reducing oxidative phosphorylation levels (271).

PARP inhibition has been proposed as a potential therapeutic option to enhance response to radiation in cancer cells. Inhibition of PARP has been demonstrated to enhance oxidative metabolism, through the modulation of SIRT1 activation (272). In addition, PARP inhibition has been demonstrated to inhibit glycolysis (273).

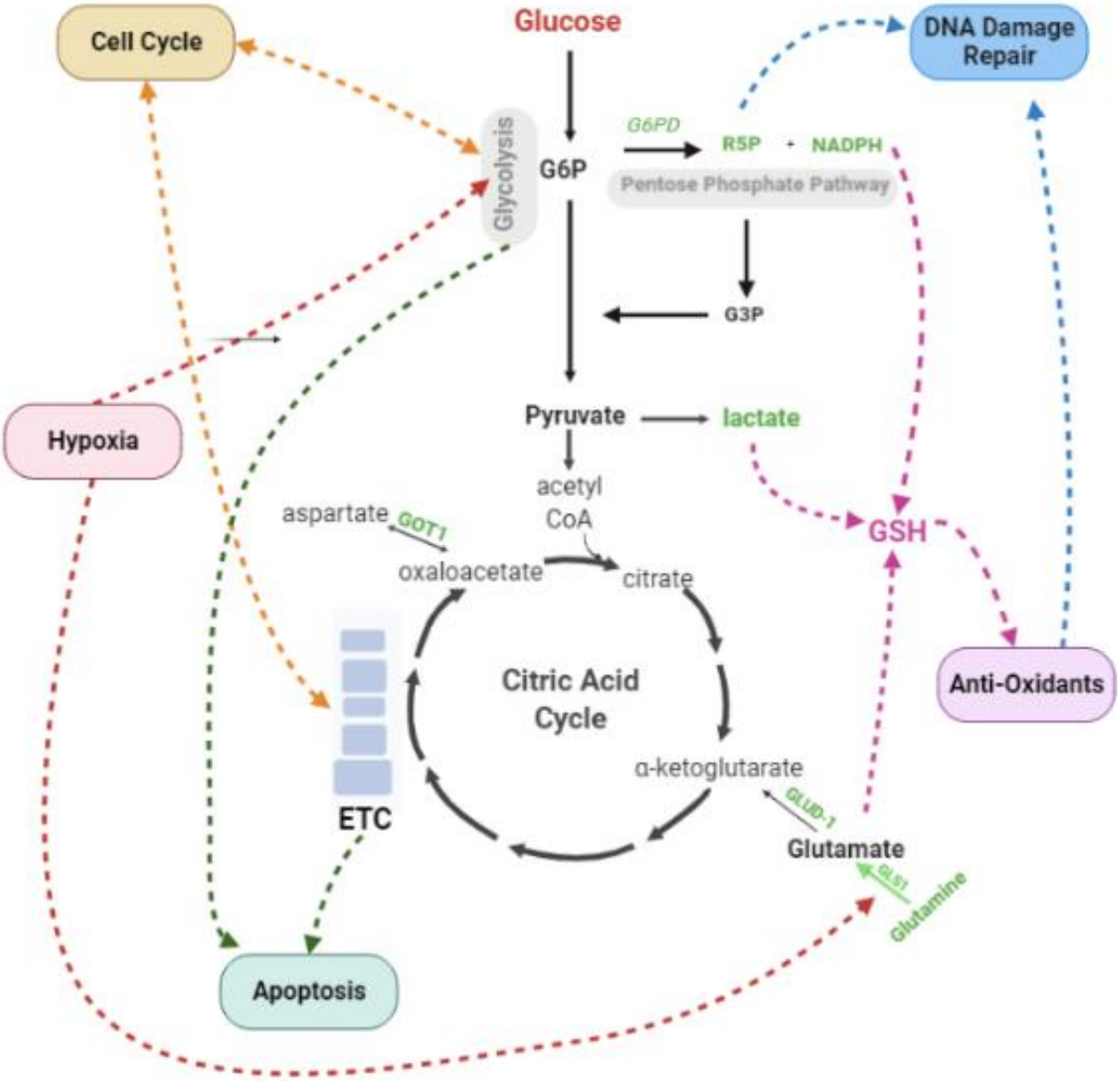

Fig. 1.7: **Overview of the interplay between energy metabolism and major mechanisms of radioresistance in cancer.** Energy metabolism is intrinsically linked to various mechanisms of radioresistance, including cell cycle, DNA damage repair, oxidative stress, apoptosis and hypoxia. Figure generated using BioRender.com.

1.4. Targeting metabolism: metformin

1.4.1. *Overview*

Metformin hydrochloride (metformin) is a biguanide drug used in the management of type II diabetes mellitus (T2DM) (274). Metformin was derived from guanidine, compounds found in the French lilac, which are demonstrated to lower blood glucose levels (275). The first of the biguanide family of drugs to be utilised for the management of T2DM was phenformin, which while being effective, was demonstrated to have significant side effects, including lactic acidosis (276). Subsequently, metformin was approved for use in Europe in 1957, and in the United States of America in 1995 for the management of T2DM (275). Metformin is a safe, cheap and easily accessible drug, and in recent years its clinical application has extended from use in T2DM, to management of gestational diabetes, polycystic ovary syndrome and metabolic syndrome (277). In recent years, metformin has been proposed to have clinical utility in the prevention and treatment of various cancers (275). For example, since 2005 it has been reported that metformin treatment reduces the risk of cancer by up to 23% world-wide (278).

1.4.2. *Mechanisms of action of metformin*

Despite being approved for use clinically for more than 60 years, the precise mechanisms of action of metformin are yet to be completely elucidated. Metformin has been documented to have pleiotropic effects, affecting many physiological and biochemical pathways.

The best studied effect of metformin is its antihyperglycemic action, wherein treatment lowers blood glucose levels and improves insulin sensitivity (279). Metformin acts on the liver, intestine and skeletal muscle to lower blood glucose levels (279). The liver is believed to be the main site of action for these effects of metformin, and is known to express high levels of metformin transporter organic cation transporter 1 (OCT1) (275). In the liver, metformin enhances glucose uptake by increasing translocation of GLUT-1, and subsequently enhances the insulin-mediated suppression of gluconeogenesis (275, 280). In addition, metformin enhances glucagon-like peptide 1 (GLP-1) and reduces glycogen synthesis (275).

While the physiologic effects of metformin treatment are well established, the precise molecular and biochemical effects are still incompletely understood, and under investigation. The main molecular target of metformin is the mitochondrion, where metformin is demonstrated to act as a potent inhibitor of Complex I of the electron transport chain. Complex I is the entry point for reduced NADH into the ETC. Metformin inhibition of Complex

I results in a shift to the cellular balance of NAD/NADH, which reduces the activity of depending enzymes, including those of the TCA cycle (274). In addition, diminished flow of electrons through the ETC as a result of metformin treatment ultimately results in diminished Complex V activity, reduced oxygen consumption and ATP synthesis. Low ATP levels trigger activation of AMP-activated protein kinase (AMPK), which induces potent inhibitory effects on lipogenesis, gene transcription, cell cycle and mammalian target of rapamycin (mTOR) signalling (274).

1.4.3. *Metformin and cancer incidence and progression*

In recent years, evidence has emerged highlighting a potential role of metformin in cancer. People with diabetes have been demonstrated to have an enhanced risk of cancer incidence (281). In an observational study by Evans *et al*., it first emerged that patients with diabetes who were on metformin treatment had lower cancer incidence rates, when compared to those on other diabetic drugs (282). These findings prompted a new field of research into the potential utility of metformin in cancer, with 384 individual clinical trials having been registered investigating metformin treatment for prevention or treatment of various cancer types.

Metformin intervention has been associated with reduced risk of developing various cancers in diabetic patients including gastric (283), breast (284) and hepatic (285) cancer. Furthermore, multiple recent meta-analyses have demonstrated survival benefit in diabetic patients on metformin with cancer in various cancer types including pancreatic (286), lung (287), liver (288) and breast (289). Many observational studies have demonstrated a reduced risk of CRC with metformin treatment (290-292). The risk of developing CRC has been reported to be reduced by 17% (293) to 25% (294) in diabetic patients on metformin. In addition, in CRC patients with T2DM on metformin, enhanced survival outcomes are also observed, with one study reporting a reduction by 44% to all-cause mortality, and 34% to CRC-specific mortality (295). This association between metformin use and CRC is believed to be contributed in part by the impact on metformin on polyp development (296, 297). These findings were supported in a recent phase III double-blind randomised study in non-diabetic patients, where metformin use was demonstrated to reduce the occurrence of total polyps to 38%, and of adenomas to 30.6%, when compared to those on placebo (56.5% and 51.6% respectively) (298). Most studies investigating metformin use in cancer patients are retrospective and in patients with

T2DM, and so there is a need for more investigation into the role of metformin in non-diabetic cancer patients.

1.4.4. *Metformin and therapeutic response in cancer*

Metformin treatment is commonly associated with enhanced survival outcomes in many cancer types (296). One potential reason for this may be the enhanced therapeutic response often demonstrated in cancer patients treated with metformin (216, 299-302)

Metformin treatment has been demonstrated to enhance pCR rates in combination with chemotherapy/radiation therapy treatment in cancer (303). In a recent study in rectal cancer patients by Skinner *et al.,* pCR rates were demonstrated to be significantly enhanced in diabetic patients using metformin (35%), when compared to both non-diabetics not on metformin (16.6%) and diabetics not on metformin (7.5%), following neoadjuvant and adjuvant chemotherapy (300). In a recent small phase I/II clinical trial of metformin treatment with neoCRT in non-diabetic rectal cancer, evidence supported enhanced pCR rates in metformin treatment, however this was a pilot study with small sample size, and warrants further investigation in a larger cohort (304). In CRC, metformin has been demonstrated to act as a radiosensitising drug, highlighting its potential utility in this cancer (231, 305).

The mechanisms by which metformin treatment can impact on therapeutic efficacy are incompletely understood, however multiple mechanisms have been proposed. Metformin treatment has been demonstrated to impair DNA damage repair in *in vitro* and *in vivo* cancer models (305-307). In addition, metformin has been demonstrated to induce cell cycle arrest and cell death in cancer cells (299, 308-310). Furthermore, metformin is demonstrated to enhance oxidative stress in cancer, another proposed mechanism of metformin-induced therapeutic sensitisation (296, 311-313).

1.5. Predictive biomarkers of therapeutic response

1.5.1. *Introduction to predictive biomarkers*

A major clinical challenge in the management of rectal cancer is the poor response to the standard of care, neoCRT, with only an estimated 15-30% achieving a pCR (44-47). There is an urgent need to identify predictive signatures of patient response, to enhance patient stratification to optimised therapeutic strategies and to reduce the proportion of patients exposed to harsh therapeutic toxicities, while deriving limited clinical benefit.

Biomarkers, or biological markers, are distinct measurable biological traits, which indicate an altered medical state. Cancer biomarkers are clinically utilised not only as a

diagnostic and screening tool, but also for other applications including prognostic indicators, treatment stratification and as predictive signatures of therapeutic response (314). Biomarkers can take many forms, but are primarily RNA, DNA, protein or peptide markers (315). In addition, many biological samples have been utilised for the development of biomarkers in cancer, including tissue samples, urine, saliva and sera. In recent years, omics, including genomic, proteomic, transcriptomic and metabolomic data, are commonly being utilised for the identification of biomarkers in cancer (316).

1.5.2. *Transcriptomic profiling in biomarker identification*

Transcriptomic analysis is the study of the expression of all genes in a cell or organism, and allows further investigation of genetic pathways than traditional genomic assessment of mutation status or copy number variant (317). Whole transcriptome analysis captures both coding and non-coding RNA, and allows for more comprehensive understanding of the functional role of genes than DNA sequencing permits (318). Transcriptomic analysis produces molecular fingerprints of diseases to identify altered pathway activation and highlight potential therapeutic targets. In recent years the accelerated technological development of next generation sequencing (NGS) has permitted the growth and accessibility of transcriptomic analysis platforms (318).

Transcriptomic analysis by RNA-Sequencing (RNA-Seq) was utilised in a recent study to identify differentially expressed genes in CRC patients with good/poor response to adjuvant chemotherapy. In this study PNN and KCNQ1OT1 were identified as potential predictive biomarkers of chemoresponse (319). In a recent study by Canto *et al.*, transcriptomic-based secretome analysis was used in an *in silico* approach to predict patient response in LARC patients, and identified markers were validated in a small patient cohort (320). In a small study, transcriptomic analysis revealed differentially expressed genes in responders and non-responders (n=15) to neoCRT in rectal cancer patients, identifying FN1 and COL3A1 as potential predictive biomarkers of response (321). While there are many studies such as these attempting to utilise transcriptome analysis to predict response to chemotherapy or radiotherapy in CRC, these studies do have limitations. The majority of these studies use small cohort sizes and training sets (<100) and are often reported without external validation (322). A recent review of transcriptomic analysis for the generation of predictive signatures in rectal cancer concluded that an optimal gene signature of prediction of response to CRT in rectal

cancer has not been met, and that little gene overlap has emerged from reported studies (323).

1.5.3. *Metabolomic profiling in biomarker identification*

Metabolomic profiling is the quantitative measurement of endogenous small metabolites within a biological system (324). Metabolomics assesses thousands of metabolites and is utilised as an output of enzyme and pathway functionality (325).

Metabolomics is often referred to as the end-point omic, as it reflects the genetic, epigenetic and proteomic profiles of disease. The most commonly utilised metabolomic profiling techniques are nuclear magnetic resonance (NMR) spectroscopy and mass spectrometry (MS), which are high-resolution and permit the identification of a wide range of metabolites in a biological sample. NMR can detect 50-200 metabolites, depending on sample type (326). In contrast, MS has a much lower detection limit (pM) than NMR (µM). MS is coupled to either liquid or gas chromatography, to allow the separation of metabolites (326).

Metabolomics has now widely been utilised for the identification of diagnostic, prognostic or predictive biomarkers in cancer (327). In CRC, Qui *et al*. performed metabolomic profiling on four CRC cohorts, and identified a signature to predict disease recurrence and survival following surgery and chemotherapy (328). In addition, Chan *et al.* demonstrated that metabolomic profiling could discriminate between normal and malignant mucosa, but could also distinguish pathological characteristics, which related to prognosis (329). A recent meta-analysis of metabolomic profiling in CRC demonstrated that while in some cases single metabolites could act as biomarkers of disease, a panel of metabolites could strengthen its applicability (330).

1.5.4. *Use of multi-omic profiling for predictive biomarker identification*

While omic profiling such as transcriptomics and metabolomics have become more widespread in recent years, few reliable biomarkers are emerging. Many researchers now believe that a multi-omics analytical approach would be best to integrate data from these applications (317).

Data has shown that while there are many proposed biomarkers emerging from single-omic profiling of cancers, even within cancer types there is very little overlap in indicated biomarkers. By combining upstream omics, such a genomic or transcriptomic profiling with downstream measurements of pathway activity such as metabolomic profiling, a more comprehensive understanding of biological systems can be identified (331). Combination of

multiple omic techniques allows for the generation of biological networks, to reduce the complexity of data outputs from any single omic, to a more streamlined, and functionally-relevant picture of the condition under assessment (331).

In a recent study of gastric cancer, multi-omic profiling, combining genomic copy number variation and transcriptomic data, followed by functional enrichment analysis to characterise networks between the omics, identified key driver genes of gastric cancer that may have a key role in the regulation of cell death (332). In addition, a study utilising omics data from the TCGA database successfully identified biomarkers of prognosis and recurrence in prostate adenocarcinoma (333). Furthermore, multi-omic profiling (transcriptomic and proteomic) of models of bladder cancer, recently identified altered genes and pathways associated with resistance to gemcitabine and cisplatin, including DDR (334).

This suggests that combination of multi-omic platforms is an effective and robust method to identify potential predictive biomarker signatures of response in cancer.

1.6. Aims and Hypothesis

1.6.1. *Overall Hypothesis*

Rectal cancer displays an altered metabolic phenotype, which is associated with therapy response. Targeting energy metabolism will boost response to radiation treatment in rectal cancer.

1.6.2. *Overall aim*

The overall aim of the thesis was to profile energy metabolism in rectal cancer, and investigate its relationship with development of disease, treatment response and other clinicopathological factors to determine the potential clinical utility of a metabolic biomarkers signature in rectal cancer. This study also aimed to determine the potential utility of a metabolic inhibitor to enhance radiosensitivity in rectal cancer.

1.6.3. *Specific Aims of thesis*

- Characterise an *in vitro* model of radioresistant and radiosensitive CRC in terms of radio and chemosensitivity, cell cycle, cell death, DNA damage repair, mitochondrial function, metabolism and gene expression.
- Characterise an *in vitro* model of radioresistant and radiosensitive CRC in terms of radio and chemosensitivity, cell cycle, cell death, DNA damage repair, mitochondrial function, metabolism and gene expression under hypoxic conditions.
- Evaluate the potential use of novel small molecule drug P3, and established drug metformin as metabolic modulators and radiosensitising drugs in an *in vitro* model of radioresistant and radiosensitive CRC and investigate the effects of metformin on the metabolism of non-cancer and cancer rectal biopsies *ex vivo*.
- Assess the underlying mechanisms of metformin-mediated radiosensitisation in an *in vitro* model of radioresistant and radiosensitive CRC.
- Profile the metabolome and transcriptome of pre-treatment tissue biopsies from rectal cancer and non-cancer rectal tissue and assess alterations between cancer and non-cancer rectal tissue metabolome and transcriptome.
- Assess and compare the secreted metabolome from tumour conditioned media and non-cancer rectal tissue conditioned media, to further investigate the altered metabolome of rectal cancer.

- Characterise the metabolome of pre-treatment sera samples from rectal cancer patients, and its correlation with clinicopathological factors, including tumour staging, differentiation, and therapeutic response. Further assess the potential utility of metabolomic and transcriptomic data from rectal cancer tissue as biomarkers of therapeutic response and other clinicopathological factors.

Chapter 2: Identification and basal characterisation of an *in vitro* model of inherent radioresistance in rectal cancer

2.1. Introduction

CRC is the 3rd most commonly diagnosed cancer worldwide, accounting for an estimated 10% of cancers (1). Furthermore, CRC has the 2nd highest rate of cancer-related mortality, resulting in an estimated 9.4% of cancer-related deaths (1). One third of all CRCs occur in the lower bowel, or the rectum, and it is predicted that in Ireland, incidence rates of rectal cancer are projected to rise by 93-97% by the year 2045 (7). The standard of care for locally-advanced rectal cancer is neoCRT followed by surgery (335). Typically, patients receive long-course radiotherapy (45-50 Gy in 1.8 Gy fractions over 5-6 weeks), combined with a 5-FU or capecitabine based chemotherapy regime, prior to TME (6).

Response to neoCRT is assessed pathologically. A pCR, which is characterised by no viable tumour cells, is a known predictor of overall and disease-free survival (44). Unfortunately, pCR rates remain low at <30% (44). Radiation plays a central role in the treatment of rectal cancer, however, resistance to treatment is a major clinical challenge for the management of rectal cancer (336). Consequently, there is an urgent unmet need to identify mechanisms underlying therapeutic resistance to identify biomarkers predicting response for improved patient stratification and novel therapeutic targets to enhance patient response to the standard of care, to improve treatment and survival for rectal cancer patients.

The mechanisms underlying radioresistance in rectal cancer are still poorly understood. One limitation of studies in this area is the lack of radioresistant model systems. Most of the research investigating radioresistance in rectal cancer has utilised colon cancer cell lines (35, 36). In recent years, research has demonstrated that not only are right-sided colon and left-sided CRCs anatomically distinct diseases, but also that there are different molecular, immunological and therapeutic implications between these two anatomically distinct sites (32-34). For example, rectal cancers have been demonstrated to display elevated p53 expression and enhanced reliance on the APC/β-catenin signalling pathway, when compared to colon cancers (40). Furthermore, distinct therapeutic strategies are employed in the management of colon and rectal cancer, especially regarding the inclusion of neoadjuvant radiation therapy for locally-advanced rectal cancer, and not colon cancer (337). Despite radiation therapy not being commonly utilised for the management of colon cancer, the vast majority of research investigating mechanism of radiation resistance in rectal cancer utilise cell lines originally derived from primary colon cancers. The use of *in vitro* models derived from primary rectal cancer are severely underutilised as an experimental tool and is a

limitation to rectal cancer research (35, 36). Therefore, the characterisation and identification of rectal cancer cell line models of inherent radioresistance are vital for research into treatment resistance in this cancer subtype.

Another useful research model are isogenic models of radioresistance, which are generated from the same cell of origin, but display different radiosensitivity and therefore, enable the investigation of underlying mechanisms of radioresistance without the potential interference of baseline genetic variation (338). A number of approaches have been used to generate isogenic models of radioresistance across different cancer types including chronic exposure to x-ray radiation (339, 340), and therefore, represent *in vitro* models of acquired radioresistance. This method has been utilised previously to generate isogenic models of radioresistant CRC (341, 342). However, many studies have used high bolus doses of irradiation to generate these models , which do not reflect the doses that a patient receives (343). The identification and development of *in vitro* models of both inherent radioresistance and acquired radioresistance is important to further our understanding of the mechanisms underlying radioresistance in rectal cancer.

It has long been established that intrinsic tumour factors, such as tumour volume, stage and hypoxia contribute to patient response to radiation therapy, however these factors alone do not determine radioresponse suggesting that, altered molecular mechanisms and pathways also contribute to radioresistance (66). The exact mechanisms contributing to radioresistance are poorly understood (344). Many factors are believed to contribute to a radioresistant phenotype in cancer including but not limited to DNA damage induction and repair (67), cell cycle distribution and progression (66), oxidative stress and altered tumour metabolism (177).

The anti-tumour effects of radiation are mediated via the induction of critical DNA damage, inhibiting cell survival. Ionising radiation (IR) directly and indirectly induces a plethora of DNA aberrations, including single base damage, SSBs and DSBs. DSBs are the most critical form of IR-induced DNA damage for its anti-neoplastic effects (57). DNA damage induced by radiation, if not repaired, subsequently leads to cell death. As such, alterations in both basal induction and susceptibility to DNA damage and DNA damage repair mechanisms are commonly involved in in cellular radioresistance (67).

DNA is the target of radiation therapy, however only 35% of DNA damage is induced directly, with the majority of DNA damage induced as a result of indirect oxygen radical-

dependent mechanisms. ROS and antioxidant capacity is believed to be a major underlying mechanism of radioresistance (345, 346). GSH is the most abundant non-protein thiol, and has long been proposed to contribute to therapeutic resistance in cancer (347). GSH production has been demonstrated to be significantly increased in rectal and colon cancer (130, 131).

One major parameter often implicated in the radioresponse is the cell cycle. It has long been established that the radioresistance of a cell can be determined by the cell cycle phase position of the cell, and this has been supported by many studies which synchronise cell cycle phase distribution (51, 52). Cells in the S phase of the cell cycle are the most resistant to radiation-induced DNA damage, whilst cells in the G2/M phases are the most radiosensitive (52). Furthermore, in addition to the basal cell cycle position determining cellular radioresponse, cell cycle progression is also implicated (66). DNA damage response and cell cycle are intrinsically linked, with cell cycle progression being monitored and controlled by cell cycle checkpoints, which are activated upon DNA damage induction. These cell cycle checkpoints allow for cell cycle arrest to permit repair of radiation-induced DNA damage, and avoiding the replication of damaged DNA, or mitosis. Cell cycle checkpoint regulation has been proposed as a mechanism of radioresistance in rectal cancer (344).

If radiation-induced DNA damage cannot be repaired, the cell will ultimately undergo cell death, primarily by mitotic catastrophe, necrosis, apoptosis or autophagy (60). While apoptosis is not traditionally recognised as a major mechanism of radiation-induced cell death, in recent years, evidence has suggested that programmed cell death may play an important role (59). Furthermore, the apoptotic index of tumour cells has been proposed to contribute to underlying cellular radioresponse. There are two major apoptotic pathways, the intrinsic mitochondrial apoptotic pathway, and the extrinsic pathway. Intrinsic apoptosis is linked to DNA damage repair, and is often utilised by cells undergoing mitotic catastrophe. Extrinsic apoptosis, which is dependent on death receptor signalling, has also been demonstrated to be activated following irradiation (60).

A potential role for altered tumour energy metabolism in the therapeutic response has recently been proposed (177, 208, 348). Oxidative phosphorylation, a mitochondrial energy metabolism pathway, has been associated with a radioresistant phenotype *in vitro* and *ex vivo* in oesophageal adenocarcinoma by our department (212, 213). Furthermore, mitochondrial dysfunction, including mtDNA mutations have been associated with therapeutic resistance in

a number of cancer types (206, 210). There are many proposed mechanisms for altered metabolism affecting therapeutic response including DNA damage repair (266), hypoxia (225) and oxidative stress (233).

To investigate the potential mechanisms underlying radioresistance in rectal cancer, this chapter identified an *in vitro* model of radiosensitive and radioresistant CRC and characterised this model in terms of parameters frequently implicated in radioresistance.

2.2. Overall Objective and Specific Aims of Chapter 2

In this chapter, the inherent radiosensitivity of a panel of CRC cell lines was profiled to identify an *in vitro* model of inherent radioresistance in rectal cancer. The generation of a novel isogenic radioresistance model was also attempted. An *in vitro* model of radioresistant rectal cancer was then characterised in terms of common mechanisms implicated in radioresistance, including DNA damage induction and repair, oxidative stress, cell cycle, cell death and altered metabolism to investigate mechanism(s) underlying the inherent radioresistance of this *in vitro* rectal cancer model. Transcriptomic profiling was also performed to further characterise this *in vitro* model.

Specific objectives of chapter:

- Identify model of inherent radioresistant and radiosensitive CRC cell lines
- Generate isogenic model of radioresistant rectal cancer
- Characterise cell lines for potential mechanisms contributing to radioresistance including:
    - Proliferation
    - Cell Cycle basally and following irradiation
    - DNA damage following irradiation
    - Apoptosis basally and following irradiation
    - Glutathione production
    - Mitochondrial Function
    - ATP production
    - Metabolic profiling by Seahorse technology
- Profile the transcriptome of HCT116 and SW837 cells to interrogate potential underlying mechanisms of radioresistance.

2.3. Materials and Methods

2.3.1. *Reagents and materials*

Laboratory chemicals and reagents were stored according to the manufacturer's instructions. All cell culture reagents were purchased from Gibco, unless otherwise stated. All plastic materials were purchased from Sarstedt (Numbrecht, Germany) unless otherwise stated.

2.3.2. *Cell culture*

All cell culture was performed utilising aseptic technique, in a grade III laminar flow-cabinet. The hood, and everything used within the unit, were swabbed with 70% (v/v) ethanol before and after use. A clean Howie lab coat used only in the cell culture facility, and sterile disposable latex gloves were worn at all times to prevent contamination. The hood was routinely sterilised with ultraviolet (UV) lights, and the airflow turned on 10 min prior to use to ensure adequate air flow.

2.3.2.1. *Human colorectal adenocarcinoma cell lines*

The SW837, SW1463 and HRA-19 rectal cancer cell lines, and the HCT116 colon cancer cell line were used throughout this study. All cell lines were obtained from the European Collection of Cell Culture (ECACC) (**Table 2.1**). The SW837 rectal cancer cell line was originally established from a stage IV, Dukes Type C rectal adenocarcinoma from a 53-year-old Caucasian male. The HRA-19 cell line was established from a Dukes Type B rectal adenocarcinoma from a 66-year-old male. The SW1463 cell line originated from a Dukes Type C rectal adenocarcinoma from a 66-year-old Caucasian female. The HCT116 colon cancer cell line was originally obtained from an adult male colon adenocarcinoma.

Human rectal cancer cell lines SW837 and SW1463 were maintained in Leibovitz's (L-15) culture media (Lonza, Basel, Switzerland), supplemented with penicillin-streptomycin (1%) (v/v) (Lonza), foetal bovine serum (FBS) (10%) (v/v) (Gibco, Waltham, MA, USA), and L-Glutamine (Lonza) (1%) (v/v) (Complete medium), in non-vented flasks. HRA-19 rectal cancer and HCT116 colon cancer cells were maintained in Roswell Park Memorial Institute (RPMI)-1460 medium (Gibco), supplemented with penicillin-streptomycin (1%) (v/v), and FBS (10%) (v/v) (complete medium), in vented flasks. Cell lines were cultured at 37°C, in 5% CO_2/ 95% atmospheric air. Cell lines cultured in L-15 medium were grown in non-vented flasks, as this medium is required to be maintained in the absence of CO_2, due to a phosphate-based buffering system.

***Table 2.1*: Colon and rectal cancer cell lines utilised**

Cell Line	Origin	Derived from	Stage/Grade of Tumour	Mutations
SW837	53 y, Caucasian male	Primary rectal adenocarcinoma	Stage IV, Dukes Type C	APC mut, p53 point mut, KRAS mut
HRA-19	66 y, male	Primary rectal adenocarcinoma	Dukes Type B	p53 point mut
SW1463	66 y, Caucasian female	Primary rectal adenocarcinoma	Dukes Type C	KRAS mut
HCT116	Adult male	Primary colon adenocarcinoma	Dukes Type A	APC wt, p53 wt KRAS mut

Abbreviations: wt, wild type; mut, mutation; y, years; N/A, not available. Data obtained from ECACC and (349, 350).

2.3.2.2. *Cell line subculturing*

Cells were monitored daily using an inverted phase contrast light microscope (Nikon Corporation, Tokyo Japan) to determine their confluency and health. Cells were sub-cultured at 70-80% confluency. Growth medium was removed to waste, and the cells were gently washed with 2-3 mL phosphate-buffered saline (PBS) (Gibco) to remove residual FBS. PBS wash was removed to waste and a volume of 1-3 mL trypsin ethylene-diamine tetra-acetic acid (EDTA) (0.05% (w/v) trypsin, 0.02% (w/v) EDTA) (Lonza) was added to the cells to lift the adherent cells from the base of the flask. The cells were incubated at 37°C, for 2-10 min to allow the trypsin to efficiently cleave the cells from the base of the flask. The rectal cancer cell lines (SW837, SW1463 and HRA-19) were the most resistant to trypsinisation, and therefore required a higher volume of trypsin, and a longer incubation time for dissociation. Trypsin was neutralised by adding appropriate complete medium of at least an equal volume of trypsin used. The required volume of cell suspension was added to 12 mL of fresh media in a new 75 cm^2 cell culture flask. SW837 and HCT116 cell lines were normally split in a 1:8 or 1:10 split ratio, while SW1463 and HRA-19 cells were split in a 1:3 or 1:4 ratio.

2.3.2.3. *Preparation of frozen cell stocks*

Confluent cells were routinely frozen down in order to maintain frozen stocks. Cells which had reached 70-80% confluency, therefore in the log growth phase, were trypsinised and the suspension neutralised with complete medium as previously described in **Section 2.3.2.2**. The cell suspension was transferred to a 15 mL tube and centrifuged for at 1,300 rpm for 3 min at

room temperature (RT°). The supernatant was discarded to waste, and the cell pellet disrupted by manual agitation. The cells were then resuspended in freezing solution (10% (v/v) dimethylsulfoxide (DMSO) (Sigma Aldrich), 90% (v/v) appropriate culture medium) in a dropwise manner with gentle agitation. For a confluent 75 cm^2 flask, approximately 3 vials of frozen cell stocks were prepared, with 1 mL of freezing solution and cells suspension added to each labelled cryovial. Vials were then placed in ethanol overnight at -80 °C, to slow down freezing and prevent the formation of intracellular crystals. Cells were subsequently transferred to liquid nitrogen for long-term storage.

2.3.2.4. *Reconstitution of frozen stocks*

Frozen cell vials were thawed via agitation in a water bath, at 37°C. Once fully defrosted, the cell suspension was transferred into 12 mL of warmed complete medium appropriate for that cell line. The suspension was centrifuged at 1,300 rpm, for 3 min at RT°. The supernatant was discarded to waste and the cell pellet resuspended in 1 mL of medium. A volume of 4 mL of appropriate culture medium was added to a 25 cm^2 flask, and the 1 mL cell suspension transferred into this flask. Flasks were labelled with cell line, passage number, date and initials. Once cells reach 70-80% confluency, they were transferred into 75 cm^2 flasks.

2.3.2.5. *Cell counting*

Confluent cells were trypsinised as previously described (**Section 2.3.2.2**), and the neutralised cell suspension was transferred to a 15 mL tube. The cell suspension was pelleted by centrifugation at 1,300 rpm for 3 min, at RT°. The supernatant was discarded to waste, and the cell pellet resuspended in 1 mL medium. A volume of 20 µL cell suspension was added to 180 µL trypan blue (Lonza), in a well of a 96-well plate (1:10 dilution). A volume of 20 µL cell/trypan blue suspension was added to a glass haemocytometer (Neubauer glass haemocytometer (0.01 mM depth)) (Marienfeld Superior, Lauda-Königshofen, Germany). Live cells were counted using a light microscope, according to the following protocol. The trypan blue allows for distinguishing live/dead cells as dead cells take up trypan blue dye due to their disrupted cell membrane and appear blue under magnification. In contrast, live cells appear clear and rounded, as they exclude the dye. The haemocytometer has an inbuilt 3 x 3 grid, within which each corner grid contains a smaller 4 x 4 grid (**Fig. 2.1**).

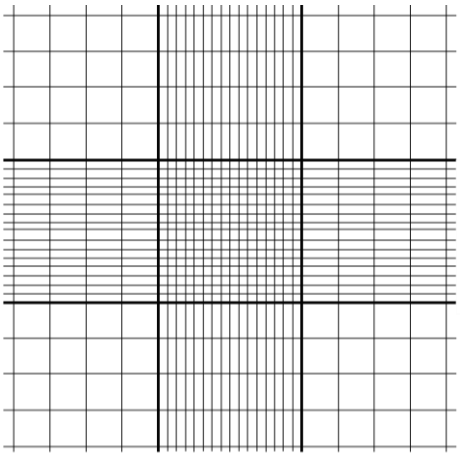

Fig. 2.1: **Grid outline of haemocytometer for cell counting.**

Live cells within the 4 outer corner grids were counted, with cells crossing the top and left border of each grid being counted, while those crossing the bottom and left borders being excluded from the count. The concentration of cells in the 1 mL cell/media suspension was determined using the following calculation:

$$No.of\ cells\ per\ mL = \frac{N}{4}\ x\ 10\ x\ 10^4$$

Where:
N = total number of live cells counted (number in each grid counted added together)
4 = number of grids counted (the 4 corner grids)
10 = the dilution factor (i.e. 20 µL cell suspension in 180 µL trypan blue)
10^4 = constant

In order to determine the volume of cell suspension required to obtain a desired number of cells, the following formula was utilised:

$$X = \frac{No.cells\ required\ for\ experiment}{No.of\ cells\ counted\ per\ mL}\ x\ 1000$$

Where:
X = volume (µL) of cell suspension required to give desired number of cells
1000 = Volume (µL) in which cells are suspended

The determined volume of cell suspension needed was then diluted in an appropriate volume of medium to obtain the desired concentration for seeding.

2.3.2.6. *Mycoplasma testing (luminescent assay)*

All cell lines were routinely tested for mycoplasma infection. The supernatant from cells was tested using the MycoAlert™ Mycoplasma detection kit (Lonza), which is a luminescent assay based on the activity of mycoplasmal enzymes. Viable mycoplasma in sample will react with the MycoAlert™ substrate, to convert ADP to ATP, while there will be no conversion in samples free of infection. Therefore, the ratio of ATP measured prior to addition of the substrate to post substrate-addition, measured via luciferase-mediated luminescence, indicates the presence or absence of mycoplasmal infection in a sample.

A volume of 500 µL supernatant from confluent flasks was removed and centrifuged at 1,300 rpm, for 3 min at RT°, to pellet any cell debris. A volume of 100 µL supernatant from each sample was then added to a white-walled 96-well plate. The MycoAlert™ Reagent was used as a negative control, while the MycoAlert™ positive control was used as a positive control. A volume of 100 µL reconstituted MycoAlert™ Reagent was added to each sample and allowed to equilibrate for 5 min at RT°. A baseline reading of the plate was taken using the GloMax Explorer™ luminescent spectrophotometer (ProMega, Madison, WI, USA), taking a 1 s luminescence reading (Reading A). A volume of 100 µL MycoAlert™ Substrate was then added to each sample and control and incubated for 5 min at RT°. Luminescence was measured as before (Reading B). The ratio of Reading B to Reading A was then calculated, with a positive reading of mycoplasma infection being indicated by a ratio > 1.2, a negative reading being indicated by a ratio of <0.9 and a borderline report being reported as 0.9-1.2. Any borderline samples were subsequently re-tested, and any cell-lines positive for infection discarded.

2.3.3. *X-ray irradiation*

All irradiations were performed using an X-Strahl cabinet X-ray irradiator (RS225) (X-Strahl, Suwanee, GA, USA), at a dose rate of 1.74 Gray (Gy)/min. The uniform delivery of ionising radiation to cells plated on cell culture dishes, or in flasks, was ensured with the generation of a broad radiation beam (12.5 cm x 12.5 cm). Cells were irradiated at the centre of the beam, at a distance of 40 cm with a beam produced by 195 kV and 15 mA. The dosimetry was performed by a qualified medical physicist, using ionisation chambers and thermoluminescent dosimeters. Mock-irradiated controls were handled identically to irradiated samples but not exposed to radiation.

2.3.4. *Clonogenic assay for assessment of radiosensitivity*

The sensitivity of cell lines to radiation was determined using the clonogenic assay, which is the gold-standard method for measuring cellular cytotoxicity (351). Adherent cells in the exponential growth phase were harvested by trypsinisation (**Section 2.3.2.2**), counted (**Section 2.3.2.5**) and seeded from a single-cell suspension into 6-well plates at optimised seeding densities (**Table 2.2**). Cells were allowed to adhere overnight in 5% CO_2/95% atmospheric air at 37°C. Cells were then irradiated, while control plates were mock-irradiated (**Section 2.3.3**), and incubated for 7-14 days at 37°C, 5% CO_2/95% atmospheric air, until at least 50 colonies had formed but had not merged.

Table 2.2: **Optimised clonogenic seeding densities per X-ray dose for each CRC cell line.**

Cell Line	Optimised cell seeding density (cells/well) (6-well plate)					
	0 Gy or DMSO/5-FU treatment	**1.8 Gy**	**2 Gy**	**4 Gy**	**5 Gy**	**6 Gy**
HCT116	0.5×10^3	1×10^3	1×10^3	2×10^3	3×10^3	4×10^3
SW837	3×10^3	5×10^3	6×10^3	8×10^3	9×10^3	1×10^4
HRA-19	3×10^3	4×10^3	4×10^3	5×10^3	6×10^3	6×10^3
SW1463	4×10^3	8×10^3	8×10^3	1×10^4	1.2×10^4	1.2×10^4

2.3.4.1. *Clonogenic assessment of chemosensitivity*

To investigate the sensitivity of HCT116 and SW837 cells to 5-FU chemotherapy, the gold-standard clonogenic assay was performed. Cells were harvested by trypsinisation (**Section 2.3.2.2**), counted (**Section 2.3.2.5**) and seeded from a single-cell suspension into 6-well plates at optimised seeding densities (**Table 2.2**). Cells were allowed to adhere to the plates overnight in 5% CO_2/95% atmospheric air, at 37°C. Following 24 h or 42 h, cells were treated with a range of doses of 5-FU (5 µM, 10 µM, 15 µM or 20 µM) or DMSO vehicle control (0.001%), and incubated in 5% CO_2/95% atmospheric air, at 37°C. At 72 h post seeding (48 h or 30 h post drug treatment), drug treatments were removed, and replaced with 1.5 mL RPMI.

2.3.4.2. *Fixation and staining of colonies*

Once colonies had formed but had not yet merged, the medium was removed to waste. A volume of 500 µL fixing/staining solution (0.05% (w/v) crystal violet (Sigma), 25% (v/v) Methanol (Honeywell) in PBS) was added to each well and incubated for 30 min, at RT°. For

the HCT116 cell line, these cells did not fix with methanol and so an optimised fixing/staining protocol was determined. Once medium was removed, a volume of 500 µL 4% paraformaldehyde (PFA) (4°C) (ChemCruz) was added to the well of HCT116 cells and incubated for 10 min at RT°. PFA was removed to waste, and the colonies stained with crystal violet solution (0.05% (w/v)) for 30 min at RT°. The stain was removed to waste, and the wells gently washed with water. Plates were then left to air-dry overnight before being counted. All crystal violet waste was neutralised with NaOH prior to disposal.

2.3.4.3. *Clonogenic colony counting*

Colonies were counted using a PC-software operated colony counter (Gelcount™, Oxford Optronix Ltd). Plating efficiencies (PE), based on control colony counts, were calculated using the following formula: PE = no. colonies / no. cells seeded. The surviving fraction (SF) was calculated using the following formula: SF = No. colonies / (No. cells seeded x PE). The SF reflects the number of colonies produced following treatment, in respect to the PE. Survival curves were then constructed by plotting the SF on the Y-axis and the treatment on the X-axis.

2.3.5. *Generation of isogenic radioresistant model*

The protocol for generation of a radioresistant line was followed as previously optimised and described by our lab (339, 340). SW837 or HCT116 cells were grown to 70% confluency in 75 cm^2 flasks and exposed to clinically-relevant 1.8 Gy x-rays as previously described (**Section 2.3**) Age and passage-matched parental cells were handled identically and mock-irradiated. Cells were trypsinised and sub-cultured once they reached 90% confluency (**Section 2.2.3.2**). Radiosensitivity was assessed via the gold-standard clonogenic assay (**Section 2.5.3**), beginning at R10/P10.

Two alternative protocols were also utilised in a bid to generate radioresistant lines. In one, a similar protocol to that outlined above was utilised, except cells were exposed to 5 Gy doses of X-ray irradiation, allowed to recover, sub-cultured and irradiated again until a total of 25 Gy was delivered over a period of 5 weeks, reflecting a short-course radiotherapy regime. Another attempt to generate a radioresistant line exposed cells to 5 Gy irradiation every day for 5 days.

2.3.6. *Seahorse XF cell Mito stress test*

Cells were seeded at optimised seeding densities (10,000 cells per well for HCT116, 30,000 cells per well for SW837, 15,000 cells per well for HRA-19 cells, 30,000 cells per well for SW1463) in a 24-well cell culture XFe24 microplate (Agilent Technologies, Santa Clara, CA,

USA) at a volume of 100 µL and allowed to adhere at 37°C, 5% CO_2/95% atmospheric air. Following 5 h post seeding, an additional 150 µL complete media was added to each well. After 24 h, cells were treated with either RPMI, vehicle control (0.2% DMSO) or a series of concentrations of P3 (1 µM, 5 µM, 10 µM, 12.5 µM, 15 µM, 20 µM) and incubated overnight at 37°C, 5% CO_2/95% atmospheric air. Following 24 h, treatment was removed and cells were washed with unbuffered Seahorse XF Base DMEM (Agilent*)* (supplemented with 10 mM glucose (Sigma), 10 mM sodium pyruvate (Sigma) and L-glutamine) and placed in a non-CO_2 incubator for 1 h at 37°C. OCR and ECAR were measured using the Seahorse XFe24 Extracellular Flux Analyser. Three baseline measurements of OCR and ECAR were taken over 24 min, consisting of 2 repetitions of mix (3 min)/ wait (2 min)/ measurement (3 min), to establish basal respiration. These steps were repeated following the injection of a series of mitochondrial inhibitors (oligomycin (Sigma), carbonyl cyanide 4-(trifluoromethoxy) phenylhydrazone (FCCP) (Sigma) and antimycin-A (Sigma). The injection of these inhibitors permitted the further investigation of the metabolic phenotype of the cells being tested, as described in detail later. All OCR/ECAR readings were normalised using the crystal violet assay (**Section 2.3.9**).

2.3.7. *Analysis of mitochondrial function*

Three surrogate markers of mitochondrial function, reactive oxygen species (ROS), mitochondrial membrane potential and mitochondrial mass were assessed using a series of fluorescent probes (2,7 dichlorofluorescein (DCF)(5 µM), Rhodamine-123 (5 µM) and MitoTracker Green^{FM} (0.3 µM)), as previously described (212). HCT116 cells (10,000 cells per well), HRA-19 cells (15,000 cells per well), and SW837 cells (30,000 cells per well) were seeded in triplicate in a 96-well plate, and allowed to adhere overnight in 5% CO_2/95% atmospheric air 37°C. Following 24 h, the media was removed and cells were incubated with 50 µL of fluorescent probe (in PBS (Mg^{2+}) (Sigma)) for 30 min, in the dark at 37°C, 5% CO_2/95% atmospheric air. The probe was removed, fresh PBS was added and the fluorescence was immediately read using a FLx800 Fluorescence microplate reader (Mason Technology, Dublin, Ireland). Fluorescence values were subsequently normalised to cell number using the crystal violet assay (**Section 2.3.9**).

2.3.8. *ATPlite analysis*

ATP levels were measured using the ATPLite Luminescence ATP Detection Assay System (Perkin Elmer). This assay system is based on the production of light from the reaction of ATP with luciferin and D-luciferin, with the emitted light being proportional to ATP concentration. Cells were seeded in triplicate in a white-walled 96-well plate (Perkin Elmer). Cells were also seeded into a standard 96-well plate, for later normalisation. Following 24 h, 50 µL of Mammalian Cell Lysis Solution (Perkin Elmer) was added to each well of the white-walled 96-well plate, and incubated on an orbital shaker, for 5 min at 700 rpm at RT°. A volume of 50 µL Substrate Solution (Perkin Elmer, Waltham, MA, USA) was added to each well of the white-walled plate, and incubated for 5 min at 700 rpm, at RT°. The plate was subsequently dark-adapted for 10 min at RT°. The luminescence was measured for 1 s on a GloMax Explorer luminescent plate reader (Promega). Luminescence was normalised using the crystal violet assay (**Section 2.3.9**) performed on the corresponding standard 96-well plate.

2.3.9. *Crystal violet assay*

The crystal violet assay was utilised as a means of normalisation of mitochondrial function assays, ATPlite assay and Seahorse assays. Medium was removed from cells following completion of the experiment, and cells were fixed via the addition of 50 µL 1% glutaraldehyde ((v/v) in PBS), per well (96-well plate, or 24-well Seahorse plate) for 15 min, at RT°. HCT116 cells were fixed with cold 4% PFA (v/v) for 10 min, at RT°. The fixative was removed to waste and cells were washed with 50 µL PBS. The wash was removed and cells were stained with 0.1% crystal violet (w/v) (in dH_2O) for 30 min at RT°. The crystal violet was removed to waste and the wells gently washed with 50 µL water. The water was removed and the plate allowed to dry overnight. The crystal violet dye was then eluted via the addition of 50 µL 1% Triton-X100 (in PBS) on an orbital shaker for ~ 1 h, or until the dye fully eluted, at RT°. The absorbance was read at 595 nm on a VersaMax microplate reader (Molecular Devices, Sunnyvale, CA USA).

2.3.10. *Annexin-V/propidium iodide (PI) analysis of apoptosis by flow cytometry*

Apoptosis was measured using the standard annexin V-FITC (Biolegend, San Diego, CA, USA) and PI (Invitrogen, Waltham MA, USA)) assay, which was assessed by flow cytometry. Annexin-V can detect apoptotic cells through binding of phosphatidyl serine, which, due to disruption of the phospholipid bilayer in early apoptosis, is exposed on the outer membrane of dead and dying cells. Annexin-V antibody is bound to FITC to allow for detection of fluorescence in flow cytometry. PI cannot enter live cells, as their plasma membrane is intact, and excludes the

dye, but it can enter necrotic and dead cells, and bind to their DNA due to their permeabilised cell membrane. Utilising these properties and binding affinities of these two dyes enables distinguishing of live cells (AV- PI-), early apoptotic cells (AV+ PI-) and late apoptotic/necrotic cells (AV+PI+).

Confluent cells in the exponential growth phase were harvested, counted and seeded, as described (HCT116: 400,000 cells per well, SW837 500,000 cells per well/ HRA-19 400,000 cells per well) in 6-well plates, and allowed to adhere overnight, at 37°C, 5% CO_2/95% humidified air. After 24 h, cells were irradiated with 1.8 Gy or 5 Gy X-ray radiation, while controls were mock-irradiated (**Section 2.4**). At 24 h and 48 h post-irradiation, supernatants, containing non-adherent cells and dead cells, were collected in labelled 5 mL falcon tubes (BD Sciences). Cells were washed with 500 µL PBS, and harvested by trypsinisation, as previously described (**Section 2.3.2.2**). Cell suspensions were transferred and combined with the corresponding supernatant previously removed from that well. Cells were pelleted via centrifugation at 1,300 rpm for 3 min, at RT°. The supernatant was discarded and the cell pellet washed via the addition of 500 µL PBS, gentle vortexing, and then pelleted by centrifugation at 1,300 rpm, for 3 min at RT°. The supernatant was discarded to waste, and the cells resuspended in 500 µL Annexin-V Binding Buffer (1X) (diluted from 10X stock) (0.1 M HEPES, 1.4 M NaCl, 25 Mm $CaCl_2$ in dH_2O). Samples were vortexed and cells pelleted via centrifugation at 1,300 rpm for 3 min at RT°. The supernatant was discarded and a volume of 100 µL Annexin-V-FITC staining solution (Annexin-V-FITC (1:100), in Annexin-V binding buffer (1X)) added to each tube, except for appropriate controls. Cells were vortexed and incubated in the dark for 15 min, at 4°C.

A volume of 1 mL binding buffer (1X) was added to each tube, vortexed and cells pelleted by centrifugation at 1,300 rpm, for 3 min at RT°. Supernatants were discarded and the cells were resuspended in 250 µL of binding buffer (1X). Immediately prior to acquisition, 250 µL of diluted PI (in binding buffer) (1:4000) was added to appropriate tubes (now 1:8000 dilution of PI in tube). Tubes were vortexed and samples acquired using a FACS Canto II flow cytometer (BD Biosciences), acquiring 40,000 events per tube. Positive controls for compensation were generated by incubating cells in 2 mL DMSO for 5 min at RT°, prior to staining with antibodies. These cells were then mixed with live cells to allow for identification of distinct positive and negative peaks of apoptotic cells. A list of controls used is detailed below in **Table 2.3**. Data was analysed using FlowJo™ version 10.6.2 software.

Table 2.3: **Experimental controls required for Annexin-V/PI analysis**

	AV-FITC Antibody added	**PI added**
Unstained	No (buffer only)	No (buffer only)
AV single stain	Yes	No (buffer only)
PI single stain	No (buffer only)	Yes
AV^+ Dead cells	Yes	No (buffer only)
PI^+ Dead cells	No (buffer only)	Yes

2.3.11. *Assessment of cell cycle and DNA damage by flow cytometry*

Cell cycle analysis was performed with PI staining analysed by flow cytometry. PI is a fluorescent dye which can bind intracellular DNA. The intensity of PI fluorescent staining, measured by flow cytometry, reflects the DNA content of cell. This permits the identification and quantification of cells in each cell cycle phase in a sample, as each phase has a distinct DNA content. Cells in the G0/G1 phase have a DNA content of 2n, while those in G2/M phase have twice this, at 4n, reflecting the doubled DNA content prior to cell division. The S phase has a DNA content greater than 2n, but less than 4n, and so is displayed graphically between the G0/G1 phase and G2/M phase on a linear histogram plot on flow cytometry.

DNA damage, namely DSBs, in response to cytotoxic treatment can be measured using the surrogate marker phosphorylated H2AX (γH2AX). The levels of γH2AX in a cell was measured using a γH2AX antibody conjugated to the fluorescent marker, AlexaFluor 488 (Biolegend).

Confluent cells in the exponential growth phase, were harvested by trypsinisation, counted and seeded into 12-well plates (HCT116: 200,000 cell/well, SW837 250,000 cell/well, HRA-19 250,000 cell/well). Cells were allowed to adhere overnight at 5% CO_2/95% atmospheric air, at 37°C. Cells were exposed to clinically-relevant doses of X-ray irradiation (1.8 Gy or 5 Gy) or mock-irradiated (0 Gy), as previously described (**Section 2.3.3**). At 20 min, 6 h, 10 h and 24 h post irradiation, cells were collected into 5 mL falcon tubes (BD Biosciences, Franklin Lakes, NJ, USA) and pelleted by centrifugation at 1,300 rpm, for 3 min, at RT°. Supernatant was discarded, cells were resuspended in 1 mL PBS, and fixed via the addition of 2.5 mL ethanol (90% v/v in PBS), in a dropwise manner while vortexing, to prevent aggregation and clumping of the cells. The addition of ethanol permits fixation of the cells, and aids

permeabilization, to allow PI to enter the cell upon staining. Cells were incubated in this fixing solution for 30 min, at RT°. Cells were pelleted by centrifugation at 1,300, for 3 min at RT°. Supernatant was discarded and a volume of 1 mL PBS was added to each sample and stored at 4°C until day of staining.

To stain, cells were pelleted via centrifugation. Supernatant was discarded and cells washed with 1 mL FBS (2% v/v)/PBS, vortexing and pelleted by centrifugation at 1,300 rpm, for 3 min at RT°. Supernatant was discarded and cells were stained for γH2AX via the addition of 100 µL γH2AX staining solution (PBS/FBS (2%) (v/v)/Triton-X100 (0.1%) (v/v)/γH2AX antibody (1:100)), except for appropriate controls. Cells were incubated in γH2AX staining solution in the dark, for 2 h at RT°. A volume of 1 mL PBS/FBS (2%) was added to each sample, vortexed and centrifuged as above. Supernatant was discarded and samples washed with 1 mL PBS/FBS (2%), centrifuged and supernatant was discarded. Samples were then resuspended in 500 µL PI staining solution (PI (0.025 mg/mL)/ RNAse A (0.1 mg/mL)/Triton-X100 (0.1%)/PBS), except for appropriate controls. Samples were vortexed and incubated in the dark, for 30 min at 37°C. Samples were acquired, with a minimum of 10,000 events collected, excluding doublets, using the FACSCanto II flow cytometer (BD Biosciences). A positive control for γH2AX, for laser compensation was generated utilising cells fixed 20 min post exposure to 10 Gy X-ray irradiation, mixed with unirradiated cells. A list of controls utilised is described below in **Table 2.4**. γH2AX-AlexaFluor-488 was measured on the FITC channel, while PI was measured on the PerCP-Cy5 channel. Data were analysed using FlowJo™ Version 10.6.2.

***Table 2.4*: Experimental controls for cell cycle and DNA damage analysis.**

Control	γH2AX Antibody Added	PI Added
Unstained (for data analysis/gating)	No	No
PI only (for compensation/gating)	No	Yes
γH2AX only (0 Gy) (for data analysis/gating)	Yes	No
γH2AX only (5 Gy) (for data analysis/gating)	Yes	No
γH2AX only (for compensation) (10 Gy, 20 min)	Yes	No

2.3.12. *5-Bromo-2'-deoxyuridine (BrdU) enzyme-linked immunosorbent assay (ELISA)*

To assess the basal proliferative rates of CRC cells, the Cell Proliferation BrdU colorimetric ELISA (Roche, Basel, Switzerland) was utilised.

HCT116 and SW837 CRC cells were seeded in triplicate in a 96-well plate (10,000 cells per well) in 100 µL RPMI and allowed to adhere overnight at 37°C, at 5% CO_2/95% atmospheric air. After 24 h, 10 µL BrdU labelling solution was added to each sample, except for appropriate controls. The cells were allowed to incubate and incorporate the BrdU label for 6 h at 37°C at 5% CO_2/ 95% atmospheric air. The labelling medium was then removed to waste, and the cells were dried at 37°C. A volume of 200 µL FixDenat was added to cells and allowed to incubate for 30 min at 37°C. FixDenat was removed to waste by pipetting and tapping. Anti-BrdU-peroxidase (POD) antibody conjugate was added to cells (100 µL per well), except for appropriate controls, and cells were incubated for 90 min at 37°C at 5% CO_2/95% atmospheric air. The anti-BrdU-POD was removed to waste by pipetting and tapping, and cells were rinsed by the addition of 200 µL washing solution (PBS). The wash was removed by tapping, and the washing step repeated two more times. The final wash was removed to waste, and substrate solution (100 µL per well) was added and incubated until sufficient colour development (10 min), and absorbance measured at 370 nm (reference wavelength 492 nm) using the VersaMax microplate reader (Molecular Devices).

2.3.13. *GSH/GSSG Glo™ assay*

GSH and GSSG levels were assessed in HCT116 and SW837 cells using the GSH/GSSG-Glo™ luminescent assay (Promega) according to the manufacturer's instructions.

HCT116 and SW837 cells were seeded in RPMI in white-walled 96-well plates (Promega) at 15,000 cells per well. Cells were cultured at 37°C at 5% CO_2/95% atmospheric air. Following 24 h, medium was removed to waste, and cells were lysed with either Total or Oxidised Glutathione Reagent, which was prepared in advance, at 50 µL per well. The plate was then agitated by shaking on a plate mixer for 5 min at RT°. Luciferin Generation Reagent was added to each well at 50 µL per well. The plate was briefly agitated using a plate shaker briefly and allowed to incubate for 30 min at RT°. A volume of 100 µL Luciferin Detection Reagent was added to each well, the plate shaken briefly, and incubated at RT° for 15 min. Luminescence was measured at 1 s integration time using the Explorer Luminometer (Promega). An identical plate of cells was set up and treated as with the experimental plate and was used for normalisation of assay results by crystal violet assay (**Section 2.3.9**).

2.3.14. *RNA isolation*

To isolate RNA from HCT116 and SW837 CRC cells, the miRNeasy® Mini Kit (Qiagen, Hilden, Germany) was used. This kit allows for the purification of total RNA from cells, including small RNA such as microRNA (miRNA). This kit utilises phenol/guanidine-based lysis of samples and silica-membrane-based purification of total RNA.

HCT116 and SW837 cells were seeded in 6-well plates (250,000 cell/well) and were allowed to adhere at 37°C at 5% CO_2/95% atmospheric air. After 48 h, medium was removed to waste and confluent cells were washed with PBS (500 µL per well). PBS was removed to waste, and 500 µL trypsin was added to each well, and cells incubated for 5 min at 37°C, in 5% CO_2/95% atmospheric air. Once cells were trypsinised, a volume of 500 µL RPMI was added to each well, and cells were transferred to 1.5 mL tubes (Eppendorf, Hamburg, Germany). Samples were centrifuged at 3000 rpm, for 3 min at 4°C. The supernatant was discarded and the cell pellets were washed and resuspended in 700 µL cold PBS. Samples were centrifuged at 3000 rpm, for 3 min at 4°C. The supernatant was discarded and cell pellets were stored at -80 °C until required for RNA isolation.

To isolate RNA, the MiRNeasy Mini Kit (Qiagen) was used according to the manufacturer's instructions. A volume of 700 µL QIAzol lysis reagent was added to the cell pellet, and thoroughly mixed by pipetting. The suspension was vortexed briefly. The homogenate was incubated at RT° for 5 min, before a volume of 140 µL 1-bromo-3-chloropropane (BCP) was added and the tube was shaken vigorously for 15 s. The homogenate was allowed to rest for 1 min at RT°, before being centrifuged at 12,000 x g for 15 min at 4°C, to allow for phase separation. The upper aqueous phase was transferred to a new 1.5 mL collection tube, and 525 µL of ethanol (Sigma) was added to each tube and mixed by pipetting. A volume of 700 µL of each sample was transferred to a RNeasy Mini spin column in a 2 mL collection tube. The samples were then centrifuged at 10,000 x g for 15 s at RT°. The flow-through was discarded and any remaining sample was added to each spin column and centrifuged as the step previous. A volume of 700 µL RWT buffer was added to each spin column, and samples were centrifuged at 10,000 x g for 15 s at RT°. Buffer RPE (500 µL) was added to each spin columns and centrifuged at 10,000 x g for 15 s at RT°. This step was repeated, but the sample centrifuged for 2 min to dry the membrane. The spin column was transferred to another collection tube and centrifuged for 1 min at full speed. The spin column

was transferred to a new 1.5 mL collection tube, and 30 µL RNase-free water was added to each sample. Samples were centrifuged at 8000 x g for 1 min to elute the RNA.

2.3.15. *RNA quantification*

RNA was quantified using a Nanodrop 1000 spectrophotometer (version 3.1, Nanodrop technology). Initially, 1 µL RNase-free water was loaded to each probe to blank the instrument. The water was gently wiped away, and 1 µL of each sample of isolated RNA was loaded to each probe on the instrument and concentration measured in ng/µL. To assess RNA quality, the 260:280 and the 260:230 ratios were also recorded.

2.3.16. *Transcriptomic analysis*

Transcriptomic profiling was conducted utilising mRNA sequencing using the Lexogen QuantSeq 3' mRNA-Seq.

RNA samples were prepared for sequencing using the QuantSeq™ 3' mRNA-Seq Library prep kit (Lexogen), according to the manufacturer instructions. Briefly, 50 ng of isolated RNA was mixed in a volume of 5 µL, with 5 µL First Strand cDNA Synthesis Mix 1 reagent in a polymerase chain reaction (PCR) plate. The plate was sealed and centrifuged to pool samples at the bottom of each well. The plate was heated to 85°C for 3 min, and then cooled to 42°C using a thermocycler to denature the RNA solution. A volume of 10 µL of a mastermix (9.5 µL First Strand cDNA Synthesis Mix 2 and 0.5 µL Enzyme Mix 1 reagent per reaction) (pre-warmed to 42°C) was added to each denatured RNA sample in the PCR plate and mixed by pipetting. The plate was sealed, briefly centrifuged to pool samples, and incubated at 42°C for 15 min.

The RNA template was then degraded, to ensure efficient second strand synthesis. A volume of 5 µL RNA Removal Solution was added directly to the first strand cDNA synthesis reaction, mixed by pipetting and the plate was resealed. The plate was centrifuged to pool samples, incubated at 95°C for 10 min and cooled to 25°C. The plate was centrifuged to pool samples, prior to second strand synthesis initiation, in which the library is converted to double strand DNA (dsDNA), initiated by a random primer

A volume of 10 µL Second Strand Synthesis Mix 1 was added to each reaction well and mixed by pipetting. The plate was sealed and centrifuged to pool samples. The plate was incubated at 98°C for 1 min, and cooled down to 25°C, using a slow ramp speed of 0.5°C/second. The reaction plate was incubated at 25°C for 30 min, centrifuged and the seal removed. A volume of 5 µL of a master mix containing 4 µL Second Strand Synthesis Mix 2,

and 1 µL Enzyme Mix 2 per reaction was added to each sample and mixed well by pipetting. Reactions were incubated at 25°C for 15 min and centrifuged to pool samples.

The dsDNA library was then purified using magnetic beads, which remove all reaction components. Purification beads (16 µL) were added to each reaction, mixed by pipetting and incubated for 5 min at RT°. The plate was placed on a magnet, for 2-5 min until the supernatant was clear. The supernatant was removed to waste, the plate removed from the magnet and the beads resuspended in 40 µL of Elution Buffer. Samples were incubated for 2 min at RT°. A volume of 56 µL of purification solution was added to the bead mixture, to precipitate the library. Samples were mixed by pipetting, and incubated for 5 min at RT°. The plate was placed on the magnet for 2-5 min, until the supernatant was clear. Supernatant was removed to waste, while the plate remained in contact with the magnet. A volume of 120 µL EtOH (80%) was added to each sample well, and incubated for 30 s at RT°. Supernatant was removed to waste, with the plate remaining in contact with the magnet. The washing step was repeated two more times with EtOH, and supernatant removed. Beads were allowed to air-dry for 5-10 min while the plate remained on the magnet. The plate was removed from the magnet, and the beads incubated in 20 µL of Elution Buffer per well, for 2 min at RT°. The plate was replaced on the magnet for 2-5 min, until the supernatant was clear. A volume of 17 µL of the clear supernatant was transferred to a new PCR plate.

The library was then amplified by PCR to provide sufficient material for quality control and sequencing, and add adapter sequences. A volume of 8 µL PCR mastermix (7 µL PCR Mix and 1 µL Enzyme Mix) was added to each reaction and mixed by pipetting. The plate was centrifuged to pool the reaction mixture. A volume of 5 µL of respective i7 index was added to each sample, and thoroughly mixed by pipetting. The PCR plate was sealed, and centrifuged. 15 cycles of PCR were performed according to the following sequence; denaturation at 98°C for 30 s followed by 15 cycles of 98°C for 10 s/ 65°C for 20 s/ 72°C for 30 s, with a final extension at 72 °C for 1 min, hold at 10°C.

The library was then purified of PCR components. A volume of 30 µL Purification Beads was added to each reaction, and incubated at RT° for 5 min. The plate was placed onto a magnet, and the beads were collected for 2-5 min, until the supernatant was clear. The supernatant was discarded, without removing the plate from the magnet. A volume of 30 µL Elution Buffer was added to each reaction, and incubated at RT° for 2 min. A volume of 30 µL Purification Solution was added to the bead/buffer mixture to precipitate the library. Samples

were incubated at RT° for 5 min, before being placed on a magnet until the supernatant ran clear. Supernatant was discarded, and a volume of 120 µL EtOH (80%) was added to the reaction and incubated for 30 s. The washing step was removed, and the beads allowed to air-dry. A volume of 20 µL Elution Buffer was added to each well, and reactions incubated at RT° for 2 min. The beads were allowed to collect on a magnet until the supernatant was clear. A volume of 15 µL supernatant was transferred to a new PCR plate, ready for sequencing.

An equal molar amount was pooled for sequencing, with a loading concentration of 320pM loaded onto the NovaSeq flowcell. Sequencing was performed using the NovaSeq 6000 (Illumina), and an SP v1.5 sequencing kit (Illumina) with 1 x 100bp reads.

2.3.17. *Transcriptomic data analysis*

Raw files from transcriptomic profiling were assessed using the BlueBee™ Bioinformatics platform (Lexogen, Vienna, Austria). Raw reads were trimmed and aligned for automated gene counting. Once gene reads and counts were complete, differential expression analysis was performed using the DESeq2 R script extension within BlueBee software, which compares gene expression counts between samples and performs the Wald test, with Benjamini-Hochberg correction. Genes were considered differentially expressed with an adjusted *p* value ($p$adj) < 0.05.

Differential expression data was subsequently assessed by bioinformatics software, Ingenuity Pathway Analysis (IPA) (Qiagen), to cluster differentially expressed genes and assess pathway activation and inhibition within samples.

2.3.18. *IPA analysis*

Significantly differentially expressed genes, and corresponding Log_2 Fold Change values were imported to IPA bioinformatics software. Core analysis in IPA was performed, which utilises the Qiagen Knowledge Base, to identify networks and predict specific biological function and pathway involvement in the uploaded experimental transcriptomic dataset.

Downstream Effects Analysis in IPA was utilised to predict alterations to downstream biological functions in uploaded experimental datasets. A networking algorithm utilises information about gene relationships and activation pathways from the literature and the Qiagen Knowledge Base to predict biological function alterations in experimental data. The overlap between genes in the dataset, and those known to be involved in each biological function is used to predict alterations to biological functions. As each biological function is comprised of multiple functional pathways, significance is represented as *p*-value range.

Canonical Pathway Analysis in IPA, utilising the Qiagen Knowledge Base, was utilised to predict involvement and activation or inhibition of specific biological pathways in the experimental dataset. The *p*-value denotes the significance between the overlap of input experimental data and the Ingenuity Knowledge Base, indicating confidence in pathway involvement. The Z-score refers to software prediction of the activation or inhibition of each affected canonical pathway, with a Z-score ≥ 2, or ≤ -2 indicating significant activation or inhibition of each pathway, respectively.

2.3.19. *Statistical analysis*

Statistical analysis and graphing were performed using Graphpad Prism v9 software. Data is presented as mean ± standard error of the mean (SEM), unless otherwise stated. Statistical comparisons were carried out using analysis of variance (ANOVA) testing, post-hoc Tukey's multiple comparisons testing, or *t*-testing, depending on the experimental set up, as described in figure legends. For transcriptomic data analysis, BlueBee, DESeq2 R extension and IPA software were utilised for statistical analysis. DESq2 utilised Wald testing, while IPA utilised Fisher's Exact Test, as stated in figure/table legends. Results were considered significant where probability (p) ≤ 0.05.

2.4. Results

2.4.1. *Characterisation of the inherent radiosensitivity of a panel of colorectal cancer cell lines*

To characterise the basal radiosensitivity and to identify a model of inherently radiosensitive and radioresistant CRC cells, the inherent radiosensitivity of the HCT116, SW837, HRA-19 and SW1463 CRC cells at 0 Gy, 2 Gy, 4 Gy and 6 Gy X-ray radiation was assessed using the gold-standard clonogenic assay.

Following irradiation with a clinically-relevant dose of 2 Gy X-ray radiation, HCT116 colon cancer cells were demonstrated to be significantly more radiosensitive, when compared to all rectal cancer cell lines; SW837 (p = 0.0090), HRA-19 (p = 0.0010) and SW1463 (p = 0.0068) (Mean surviving fraction (SF) (%) at 2 Gy ± SEM; HCT116 29.83 ± 0.7, SW837 64.23 ± 7.01, HRA-19 71.03 ± 5.09, SW1463 64.7 ± 6.77) (**Fig. 2.2**). Similarly, HCT116 cells were demonstrated to be significantly more radiosensitive to 4 Gy X-ray radiation, when compared to all rectal cancer cell lines; SW837 (p = 0.0038), HRA-19 (p = 0.0002) and SW1463 (p = 0.0041) (mean SF (%) at 4Gy ± SEM; HCT116 4.09 ± 0.43, SW837 42.18 ± 6.3, HRA-19 45.58 ± 3.7, SW1463 31.81 ± 4.67) (**Fig. 2.2**). In addition, HCT116 were demonstrated to be significantly more radiosensitive following irradiation with 6 Gy, when compared to SW837 (p = 0.0103), HRA-19 (p = 0.0015) and SW1463 (p = 0.0020) (Mean SF (%) at 6 Gy ± SEM; HCT116 0.31 ± 0.06, SW837 19.3 ± 4.01, HRA-19 30.57 ± 4.06, SW1463 14.86 ± 2.04) (**Fig. 2.2**).

There were no statistically significant differences demonstrated between rectal cancer cell lines (SW837, HRA-19, SW1463) at 2 Gy or 4 Gy irradiation, indicating that these cell lines have similar radiosensitivity at these doses of X-ray radiation. Following 6 Gy irradiation, the surviving fraction of HRA-19 was significantly higher than SW1463 (p = 0.0275) (Mean SF (%) at 6 Gy ± SEM; HRA-19 30.57 ± 4.06 vs. SW1463 14.86 ± 2.04). There were no significant differences to radiosensitivity observed between SW837 and HRA-19 rectal cancer cells at 6 Gy (p = 0.096) (**Fig. 2.2**).

These data demonstrate that the colon cancer cell line HCT116 is the most inherently radiosensitive colorectal cell line, when compared to the inherently radioresistant SW837, HRA-19 and SW1463 rectal cancer cell lines. The SW837 rectal cancer and HCT116 colon cancer cell lines were selected for future experiments, as an *in vitro* model of inherent radioresistance/radiosensitivity.

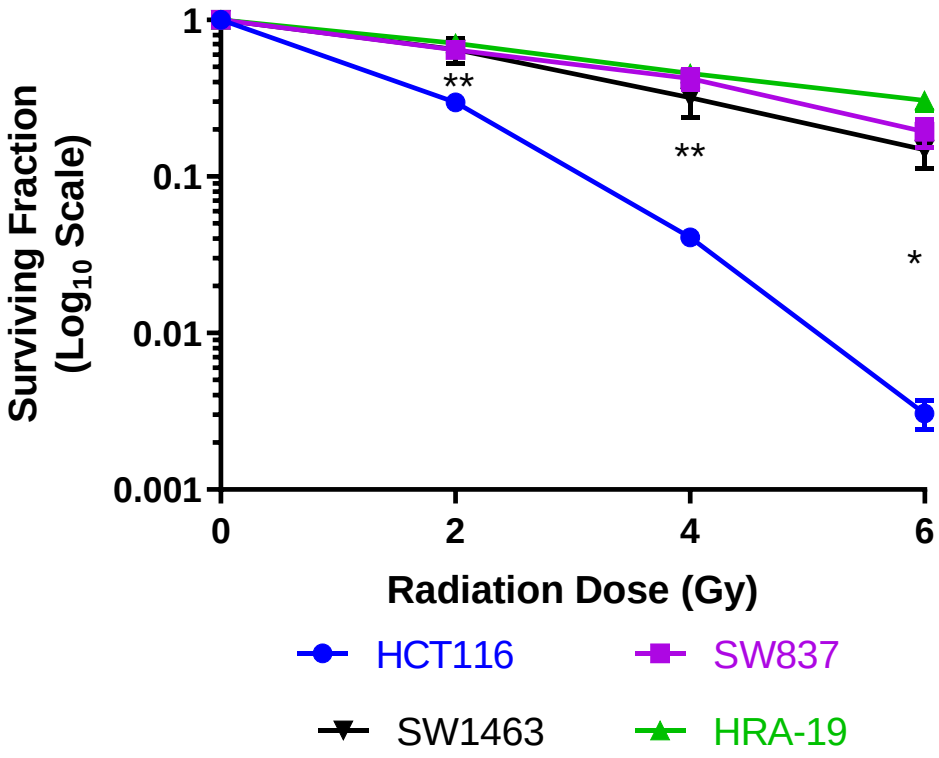

Fig. 2.2: **Rectal cancer cells, SW837, SW1463 and HRA-19 are significantly more radioresistant than HCT116 colon cancer cells.** Radiosensitivity of HCT116, SW837, HRA-19 and SW1463 cells treated with 0 Gy, 2 Gy, 4 Gy and 6 Gy X-ray radiation was assessed by clonogenic assay. Data is presented as mean ± SEM for 4 independent experiments. Statistical analysis was performed by 2-way ANOVA and multiple comparisons testing. *$p < 0.05$, **$p < 0.01$.

2.4.2. *Generation of an isogenic model of radioresistance in rectal cancer.*

Previously in our laboratory, chronic irradiation with fractionated doses of clinically relevant X-ray radiation (2 Gy) resulted in the successful generation of a novel radioresistant oesophageal adenocarcinoma cell line (OE33R) (339).

The generation of novel isogenic models of radioresistant CRC was attempted by chronic exposure of HCT116 and SW837 cells to clinically-relevant doses of 1.8 Gy, with a passage and recovery period (~1 week) between irradiations. Parental cells were handled identically but were mock-irradiated.

Following 53 irradiation exposure and recovery cycles in SW837 cells (**Fig. 2.3A**) and 42 irradiation exposure and recovery cycles in HCT116 cells (**Fig. 2.3B**), no significant alterations in radiosensitivity were demonstrated in either cell line by clonogenic assay. In addition, the cumulative dose (95.4 Gy in SW837 cells, and 75.6 Gy) given to cells was also higher than a patient would receive, reducing the clinical relevance.

In a second attempt to generate an isogenic model of radioresistance, HCT116 and SW837 cells were exposed to 5 doses of 5 Gy radiation, with cells allowed to recover in between radiation doses. The rationale behind this strategy was to reflect the doses of radiation delivered in the clinic to rectal cancer patients undergoing short-course radiation therapy (5 fractions of 5 Gy over 5 weeks). No significant alterations in radiosensitivity were demonstrated in either cell line by clonogenic assay. (**Fig. 2.3C** and **D**).

In a third attempt, both HCT116 and SW837 cells were exposed to 5 fractions of 5 Gy, with no recovery period in between. However, this approach resulted in cell death and inhibited replicative capacity in radiosensitive HCT116 cells. SW837 cells exposed to this irradiation strategy survived initially, but stopped proliferating following one sub-culture.

All three irradiation strategies utilised failed to generate a radioresistant subline in HCT116 or SW837 cells.

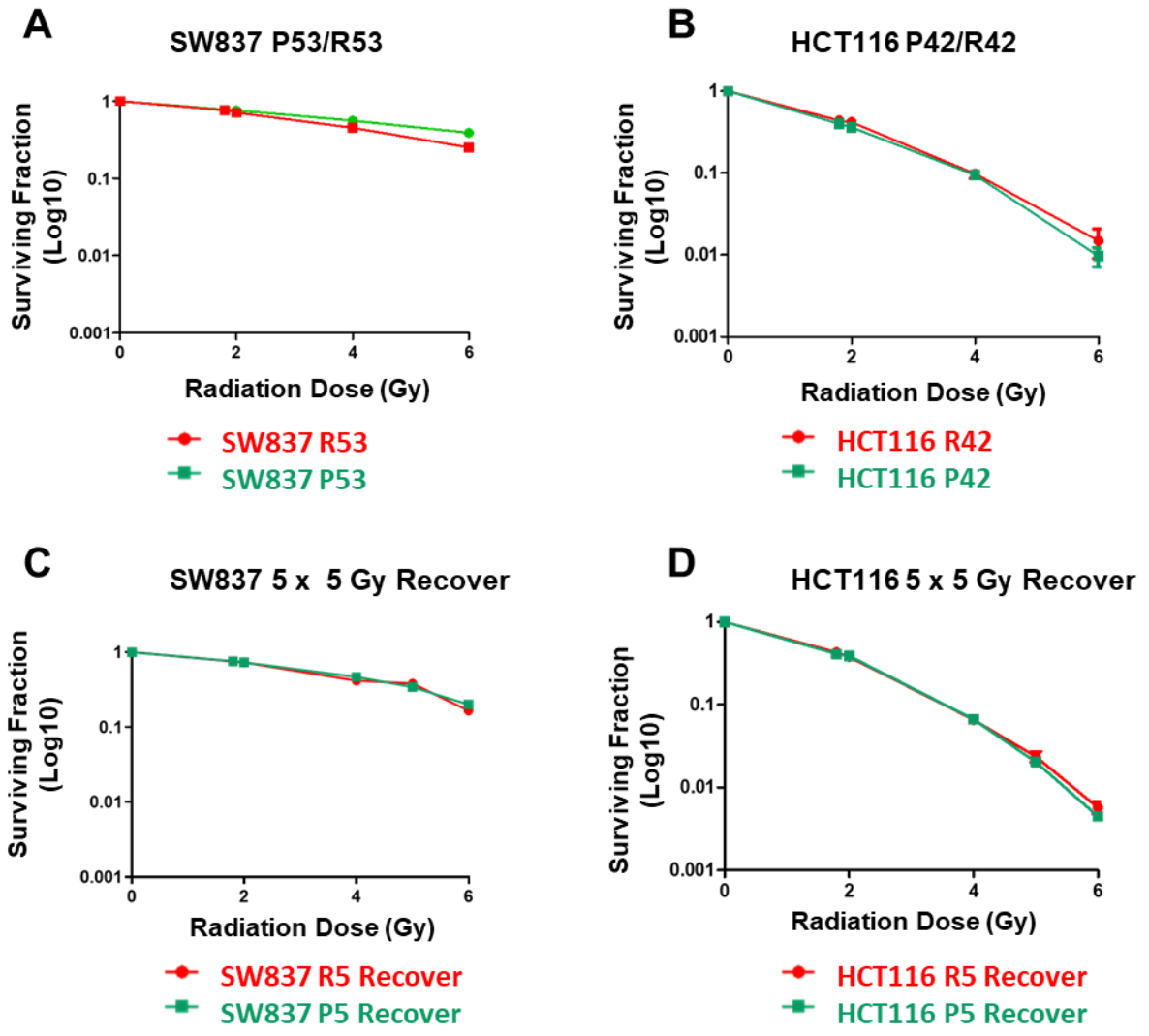

Fig. 2.3: **Clonogenic assessment of radiosensitivities of attempted isogenic models of HCT116 and SW837.** The survival of each isogenic/parental model of HCT116 and SW837 to X-ray radiation was assessed by clonogenic assay. **A**) The survival of SW837 R53 cells which had received 53 cycles of 1.8 Gy radiation (cumulative dose 95.4 Gy) and matching parental SW837 P53 cells. Survival of SW837 R53 and SW837 P53 was similar following exposure to 1.8 Gy, 2 Gy, 4 Gy and 6 Gy bolus dose. **B)** The survival of HCT116 R42, which had received 42 cycles of 1.8 Gy radiation (cumulative dose 75.6 Gy) and matching parental HCT116 P42 cells. Survival of HCT116 R42 is similar to that of HCT116 P42 at 1.8 Gy, 2 Gy, 4 Gy and 6 Gy bolus dose. **C)** The survival of SW837 R5 Recover cells, which had received 5 cycles of 5 Gy radiation, with recovery between each cycle (cumulative dose 25 Gy) and matching parental SW837 P5 Recover cells. Survival of SW837 R5 Recover cells was similar to that of SW837 P5 parental cells at 1.8 Gy, 2 Gy, 4 Gy and 6 Gy radiation. **D)** Survival of HCT116 R5 Recover cells, which had received 5 cycles of 5 Gy radiation, with recovery between each cycle (cumulative dose 25 Gy) and matching parental HCT116 P5 Recover cells. Survival of HCT116 R5 Recover cells was similar to that of HCT116 P5 Recover cells at 1.8 Gy, 2 Gy, 4 Gy and 6 Gy. Data is presented as mean ± SEM for 3 independent experiments. Statistical analysis was performed by paired *t*-tests.

2.4.3. *SW837 cells are more resistant to 5-FU chemotherapy than HCT116 cells*

Having identified SW837 rectal cancer cells and HCT116 colon cells as a model of inherent radiosensitivity/radioresistance (**Section 2.4.1, Fig. 2.2**), the inherent sensitivity of both cell lines to 5-FU was investigated by clonogenic assay.

SW837 radioresistant rectal cancer cells were demonstrated to be significantly more resistant to 30 h exposure to 5-FU, when compared to HCT116 colon cancer cells at 10 μM (p = 0.033), 15 μM (p = 0.016) and 20 μM (p = 0.0136) (mean SF (%) ± SEM; HCT116 10 μM (90.98 ± 1.47), 15 μM (88.73 ± 0.695), 20 μM (72.56 ± 3.04), SW837 10 μM (96.02 ± 0.588), 15 μM (99.83 ± 2.70), 20 μM (93.02 ± 3.797)) (**Fig. 2.4A**).

Furthermore, longer exposure to 5-FU (48 h), was demonstrated to further increase cytotoxicity in sensitive HCT116 cells, when compared to HCT116 colon cancer cells following 10 μM (p = 0.006), 15 μM (p = 0.0028) and 20 μM (p = 0.0216) (mean SF (%) ± SEM; HCT116 10 μM (75.48 ± 2.43). 15 μM (54.47 ± 6.44), 20 μM (38.78 ± 7.43), SW837 10 μM (93.48 ± 2.86), 15 μM (91.645 ± 3.55), 20 μM (80.65 ± 9.37)) (**Fig. 2.4B**).

These data demonstrate that radioresistant SW837 cells are more resistant to 5-FU-based chemotherapy, when compared to HCT116 cells.

2.4.4. *HCT116 cells display elevated proliferative rates, when compared to SW837 rectal cancer cells*

To determine whether altered proliferative rates may contribute to the radioresistance of SW837 rectal cancer cells, the BrdU assay was utilised (**Section 2.3.12**).

Radiosensitive HCT116 cells were demonstrated to display a significantly increased proliferative capacity (p = 0.0304), when compared to radioresistant SW837 cells (Mean BrdU absorbance ± SEM; HCT116 (1.306 ± 0.039), SW837 (0.9531 ± 0.099) (**Fig. 2.5**).

These data indicate a potential contribution of reduced proliferation in the radioresistance of SW837 cells.

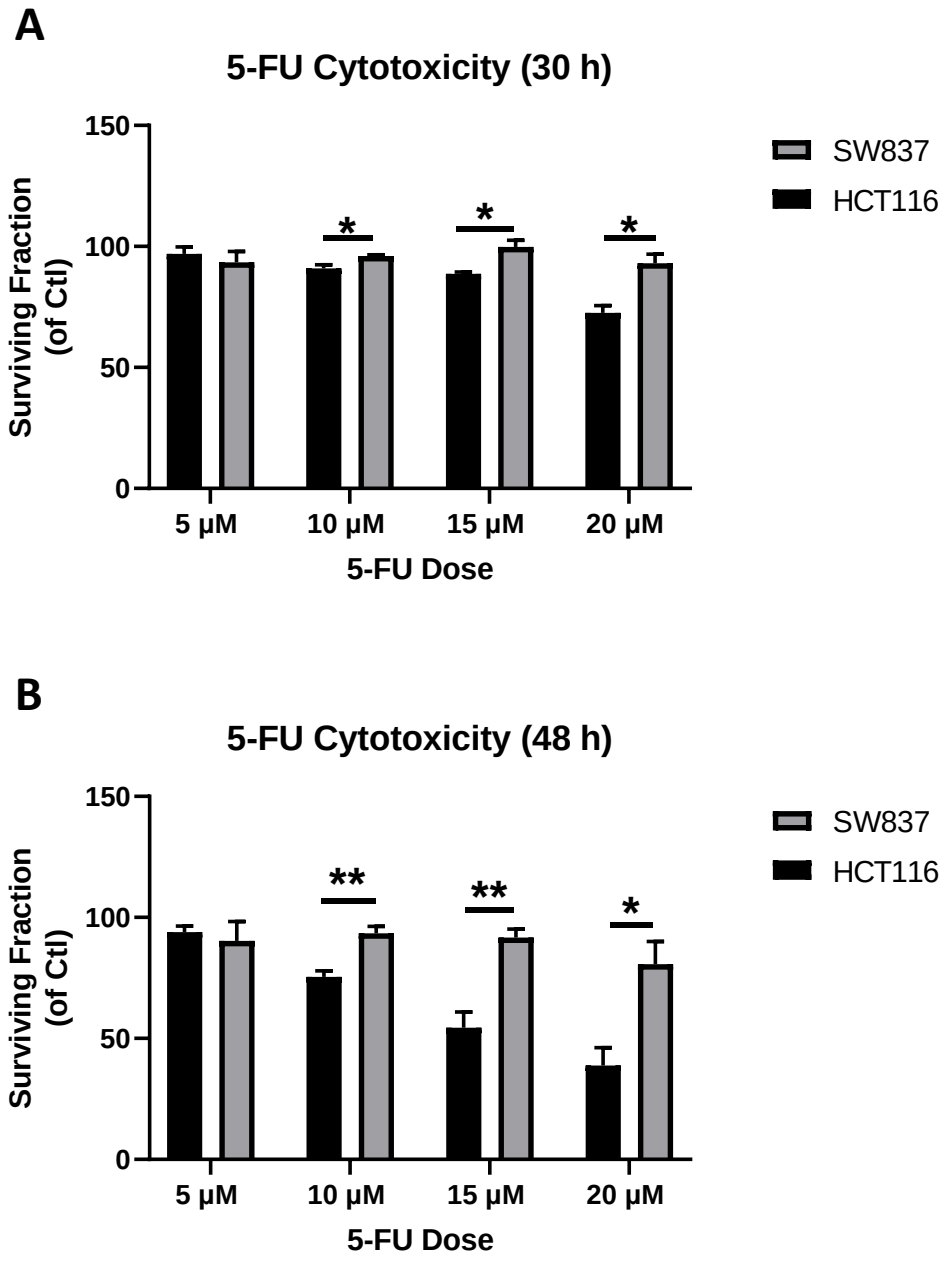

Fig. 2.4: **SW837 cells are more resistant to 5-FU-induced cytotoxicity, than HCT116 cells.** Chemosensitivity was assessed by the gold-standard clonogenic assay. Cells were treated for 30 h or 48 h with varying doses of 5-FU, controls were treated with DMSO vehicle control. **A)** Surviving Fractions of SW837 and HCT116 cells following treatment with DMSO, or a series of concentrations of 5-FU for 30 h**. B**) Surviving Fractions of SW837 and HCT116 cells following treatment with DMSO, or a series of concentrations of 5-FU for 48 h. Data is presented as mean ± SEM for 3, or 4 independent experiments. Statistical analysis was performed using a series of unpaired t-tests. *$p < 0.05$, **$p < 0.01$.

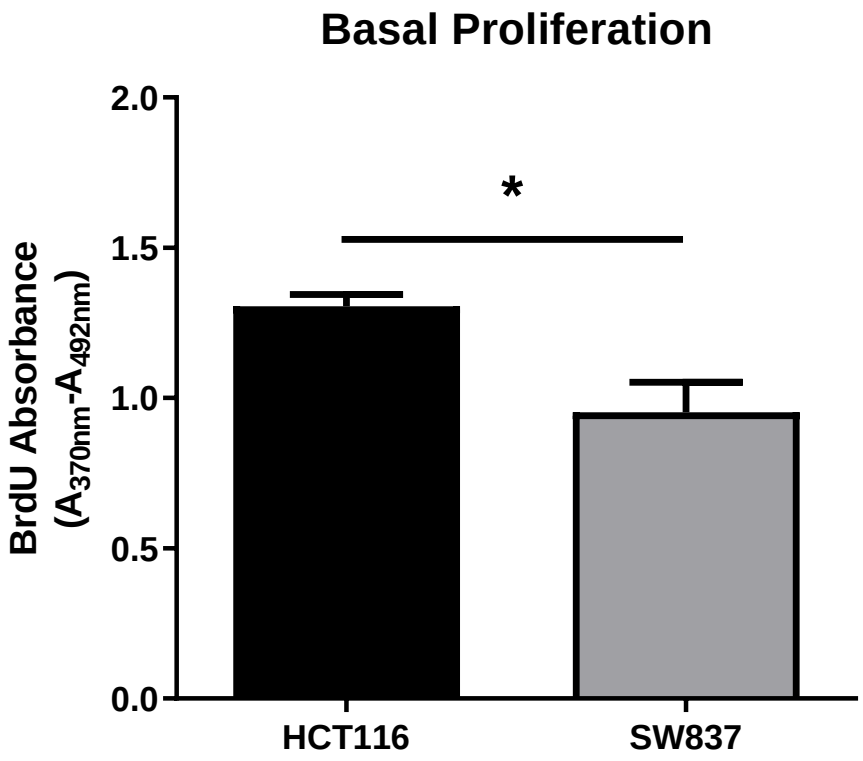

Fig. 2.5: **Radiosensitive HCT116 cells display increased basal proliferation, when compared to radioresistant SW837.** Basal cellular proliferation was assessed by BrdU ELISA. HCT116 cells display increased BrdU absorbance, when compared to SW837 cells. Data is presented as mean ± SEM from 3 independent experiments. Statistical analysis was performed using a series of unpaired *t*-tests. *$p < 0.05$.

2.4.5. *Radiation-induced apoptosis in HCT116 and SW837 cells*

To assess whether basal levels of apoptosis differ between radiosensitive HCT116 and radioresistant SW837 cells, and whether radiation-induced apoptosis contributes to the radioresistance of SW837 cells, apoptosis was assessed by PI and AV-FITC staining and flow cytometry at 24 h and 48 h following irradiation with 1.8 Gy and 5 Gy.

Unirradiated controls were utilised to assess basal levels of cell death between HCT116 and SW837 cells. Basally, there were no statistically significant alterations in the proportion of live cells (AV-PI-), between HCT116 and SW837 unirradiated controls, at either timepoint (**Fig. 2.6A, 2.7A**). In addition, no significant alterations in the proportion of cells in early apoptosis (AV+PI-), late apoptosis (AV+PI+) or necrosis (AV-PI+) was demonstrated between unirradiated controls of HCT116 and SW837 at either timepoint (**Fig. 2.6 B-D, 2.7B-D**). These data demonstrate that basal levels of cell death are similar between HCT116 and SW837 cells.

To assess the effect of radiation on HCT116 and SW837 cells, cell death was measured at 24 h and 48 h following exposure to 1.8 Gy or 5 Gy X-ray radiation. No significant differences in the proportion of live cells were demonstrated in either HCT116 or SW837 cells at 24 h or 48 h post exposure to 1.8 Gy or 5 Gy doses of radiation, when compared to unirradiated controls (**Fig. 2.6A, 2.7B**). While a trend towards an increased proportion of HCT116 cells undergoing early apoptosis (AV+PI-) was demonstrated at 48 h post 1.8 Gy radiation ($p = 0.0545$) (**Fig. 2.7B**), no significant alterations in the level of early apoptosis was demonstrated in either HCT116 or SW837 cells at either timepoint (**Fig. 2.6B, 2.7B**). In HCT116, at 24 h post radiation, a significant increase in the proportion of cells undergoing late apoptosis (AV+PI+) was demonstrated following 5 Gy radiation, when compared to unirradiated control ($p = 0.046$) (Mean % AV+PI+ cells ± SEM; HCT116 24 h 0 Gy 1.26 ± 0.64 vs HCT116 24 h 5 Gy 2.62 ± 0.87) (**Fig. 2.6C**). Furthermore, no significant alterations to the proportion of necrotic cells were demonstrated in HCT116 or SW837 cells at either timepoint, following exposure to radiation (**Fig. 2.6D, 2.7D**).

These data demonstrate no significant alterations to basal cell death between HCT116 and SW837 cells. Furthermore, while slight alterations in cell death were observed following radiation exposure in HCT116 cells only, these data suggest that alterations in apoptosis may not be a major contributor to the radioresistance of rectal cancer cells.

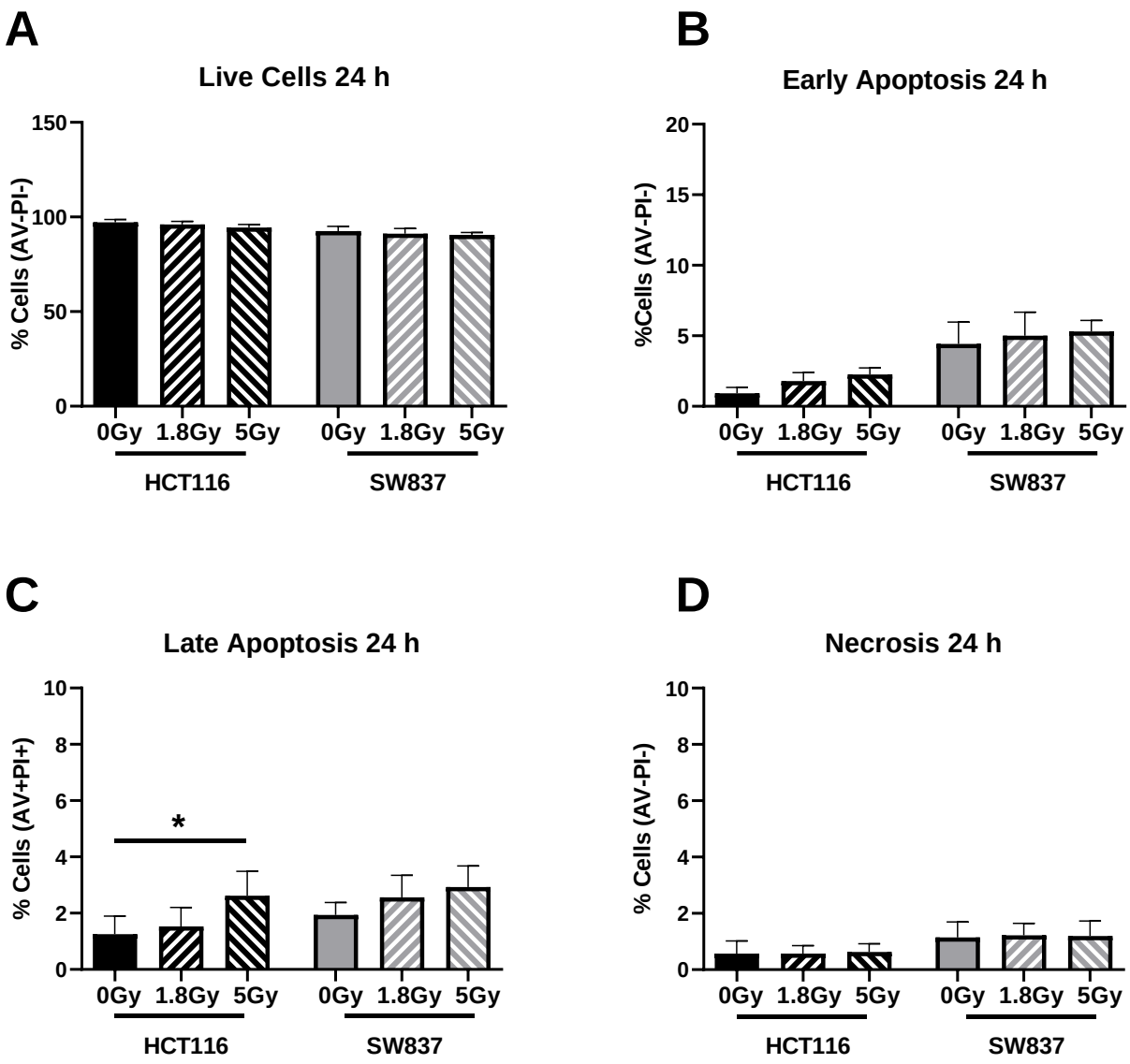

Fig. 2.6: **Cell death basally and 24 h following exposure to radiation in radiosensitive HCT116 and radioresistant SW837 cells.** Apoptosis was assessed by PI and Annexin V -FITC staining and flow cytometry. **A)** Proportion of live cells (AV-PI-) in HCT116 and SW837 cells basally and 24 h following exposure to 1.8 Gy or 5 Gy radiation. **B)** Proportion of early apoptotic cells (AV+PI-) in HCT116 and SW837 cells basally and 24 h following exposure to 1.8 Gy or 5 Gy radiation. **C)** Proportion of late apoptotic cells (AV+PI+) in HCT116 and SW837 cells basally and 24 h following exposure to 1.8 Gy or 5 Gy radiation. **D)** Proportion of necrotic cells (AV-PI+) in HCT116 and SW837 cells basally and 24 h following exposure to 1.8 Gy or 5 Gy radiation. Data is presented as mean ± SEM for 3 independent experiments. Statistical analysis was performed using a series of unpaired t-tests. *$p < 0.05$.

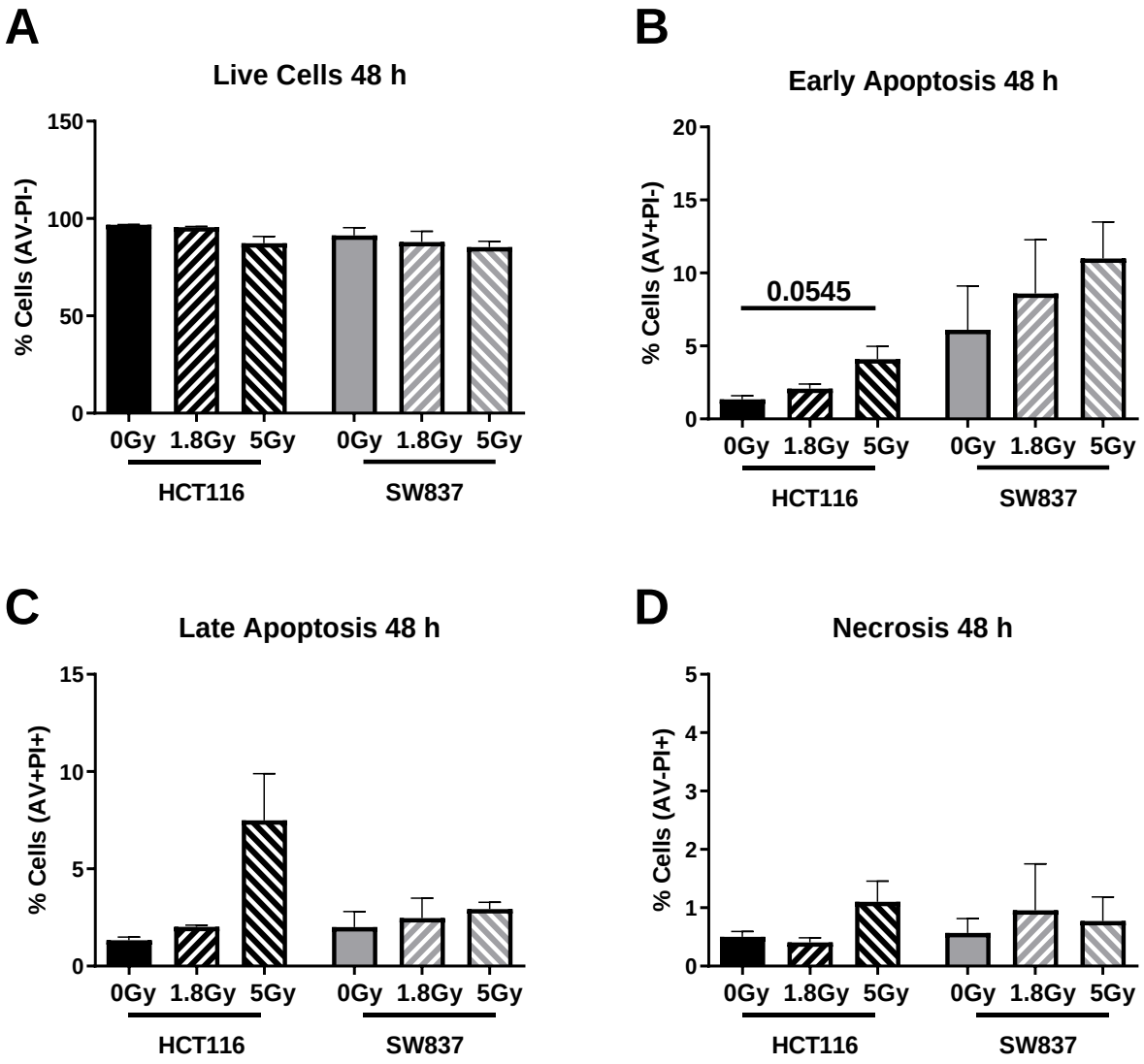

Fig. 2.7: **Cell death basally and 48 h following exposure to irradiation in radiosensitive HCT116 and radioresistant SW837 cells.** Apoptosis was assessed by PI and Annexin V -FITC staining and flow cytometry. **A)** Proportion of live cells (AV-PI-) in HCT116 and SW837 cells basally and 48 h following exposure to 1.8 Gy or 5 Gy radiation. **B)** Proportion of early apoptotic cells (AV+PI-) in HCT116 and SW837 cells basally and 48 h following exposure to 1.8 Gy or 5 Gy radiation. **C)** Proportion of late apoptotic cells (AV+PI+) in HCT116 and SW837 cells basally and 48 h following exposure to 1.8 Gy or 5 Gy radiation. **D)** Proportion of necrotic cells (AV-PI+) in HCT116 and SW837 cells basally and 48 h following exposure to 1.8 Gy or 5 Gy radiation. Data is presented as mean ± SEM for 3 independent experiments. Statistical analysis was performed using a series of unpaired t-tests.

2.4.6. *Basal cell cycle distribution is altered between HCT116 and SW837 cells*

Cell cycle distribution has long been associated with radioresistance, with cells in the G2/M phase being the most sensitive to irradiation, and cells S phase being most radioresistant. Cell cycle distribution was assessed by PI staining and flow cytometry to investigate the potential role of altered cell cycle phase distribution in the radioresistance of the SW837 cell line.

Radioresistant SW837 rectal cancer cells were demonstrated to have a significantly higher fraction of cells in the G0/G1 phase, when compared to HCT116 colon cancer cells (p = 0.0156) (mean % G0/G1 phase ± SEM; HCT116 (25.51 ± 5.82) vs SW837 (50.10 ± 4.5)) (**Fig. 2.8).** Furthermore, the proportion of SW837 cells in the radioresistant S phase was significantly higher, when compared to HCT116 radiosensitive cells (p = 0.0263) (mean % S phase ± SEM; HCT116 14.98 ± 1.18) vs. SW837 (18.83 ± 0.58)). In addition, SW837 rectal cancer cells demonstrated significantly fewer cells in the radiosensitive G2/M phase, when compared to HCT116 cells (p = 0.0044) (mean % G2/M phase ± SEM; HCT116 (36.99 ± 2.18) vs SW837 (21.58 ± 2.7)) (**Fig. 2.8**).

These data demonstrate that the inherently radioresistant SW837 rectal cancer cells, display a more radioresistant basal cell cycle distribution, when compared to radiosensitive HCT116 cells. These differences in cell cycle distribution may contribute to the differences in radiosensitivity in these cell lines.

2.4.7. *Radiation alters cell cycle progression in HCT116 and SW837 cells*

Progression through the cell cycle phases following irradiation can be an indicator of radioresponse. To assess the potential contribution of cell cycle progression in the radioresistance of SW837 cells, cell cycle phase distribution was assessed at 20 min, 6 h, 10 h and 24 h following exposure to clinically-relevant doses of 1.8 Gy or 5 Gy X-ray radiation in HCT116 and SW837 cancer cell lines by PI staining and flow cytometry.

No alterations in cell cycle phase distribution were observed in HCT116 or SW837 cells at 20 min or 6 hour following radiation exposure, when compared to unirradiated controls (**Fig. 2.9A-D**)**.**

At 10 h post radiation, no alterations in cell cycle phase distribution were observed in radioresistant SW837 rectal cancer cells (**Fig. 2.9F**). However, in the radiosensitive HCT116 colon cancer cell line, an increase in cells in the G2/M phases was demonstrated following 1.8 Gy and 5 Gy radiation, when compared to unirradiated controls (p = 0.0089, p = 0.0221) (mean % G2/M cells ± SEM; 0 Gy 36.5 ± 4.7, 1.8 Gy 54.23 ± 4.51, 5 Gy 58.43 ± 7.15) (**Fig. 2.9**). In

addition, at 10 h post irradiation with 1.8 Gy and 5 Gy, HCT116 cells demonstrated a decreased in the proportion of cells in the G0/G1 (p = 0.0084, p = 0.0292) and S phases (p = 0.0073, p = 0.0148) (mean % G0/G1 phase cells ± SEM; 0 Gy 29.15 ± 6.06, 1.8 Gy 13.93 ± 3.77, 5 Gy 8.97 ± 1.26) (mean % S phase ± SEM; 0 Gy 12.94 ± 1.42, 1.8 Gy 8.51 ± 1.76, 5 Gy 8.068 ± 1.54). These data are indicative of G2/M arrest, a typical damage response to radiation exposure and indicates an inhibition to cell cycle progression and activation of cell cycle regulation checkpoints.

At 24 h following radiation exposure, similar cell cycle alterations were demonstrated in radiosensitive HCT116 cells, with radiation increasing the proportion of cells in the G2/M phase following 1.8 Gy and 5 Gy radiation (p = 0.0291, p = 0.0066) (mean % cells in G2/M phase ± SEM; 0 Gy 34.33 ± 2.56, 1.8 Gy 40.68 ± 2.25, 5 Gy 64.45 ± 2.62) (**Fig. 2.9G**). Exposure to 5 Gy radiation also decreased the proportion of HCT116 cells in G0/G1 (p = 0.0495) and S phases (p = 0.0186) (mean % cells in G0/G1 ± SEM; 0 Gy 24.48 ± 9.62, 5 Gy 14.71 ± 4.99) (mean % cells in S phase ± SEM; 0 Gy 10.93 ± 1.24, 5 Gy 3.56 ± 0.82).

In radioresistant SW837 rectal cancer cells, moderate radiation-induced cell cycle alterations were demonstrated 24 h post radiation, with the induction of G2/M arrest following 5 Gy (p = 0.0447) (mean % G2/M cells ± SEM; 0 Gy 19.6 ± 1.16, 5 Gy 38.73 ± 4.83) (**Fig. 2.9H**). A trend towards decreased proportion of SW837 cells in the G0/G1 phase was observed at 24 h, although this did not reach statistical significance (p = 0.0506).

These data demonstrate induction of G2/M arrest following radiation exposure in HCT116 and SW837 cells. This inhibition of cell cycle progression following radiation exposure is enhanced in radiosensitive HCT116 cells, when compared to radioresistant SW837 cells. These data suggest a potential role for altered cell cycle checkpoints in the radioresistance of SW837 cells.

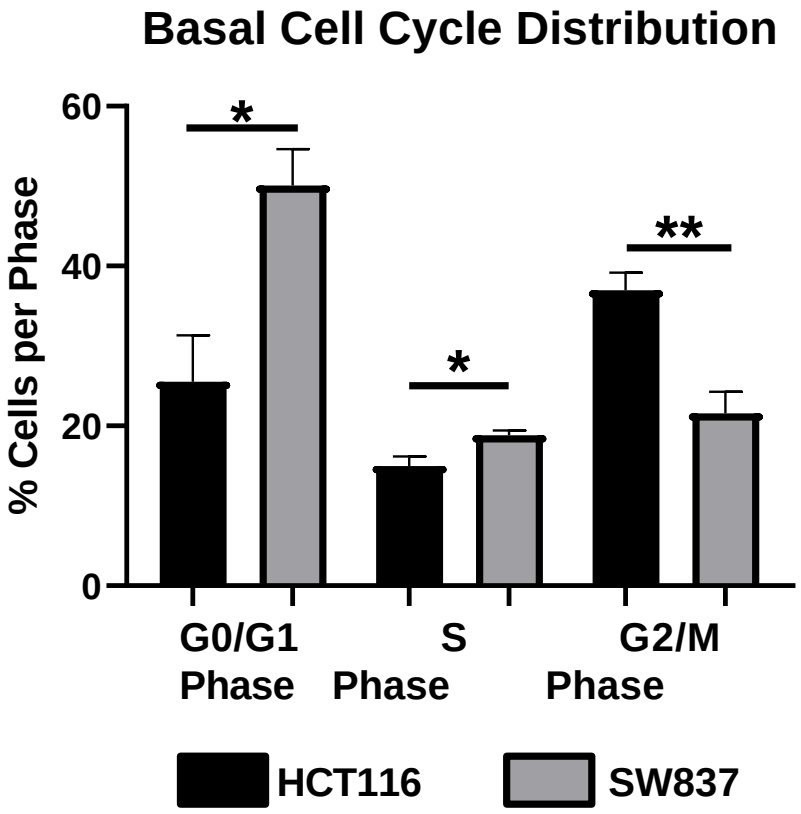

Fig. 2.8: **Basal cell cycle distribution is significantly altered between radiosensitive HCT116 and radioresistant SW837 cells.** Cell cycle distribution was assessed by PI staining and flow cytometry in HCT116 and SW837 cells. Data is presented as mean ± SEM for 3 independent experiments. Statistical analysis was performed by unpaired *t*-test. *$p < 0.05$, ** $p < 0.01$.

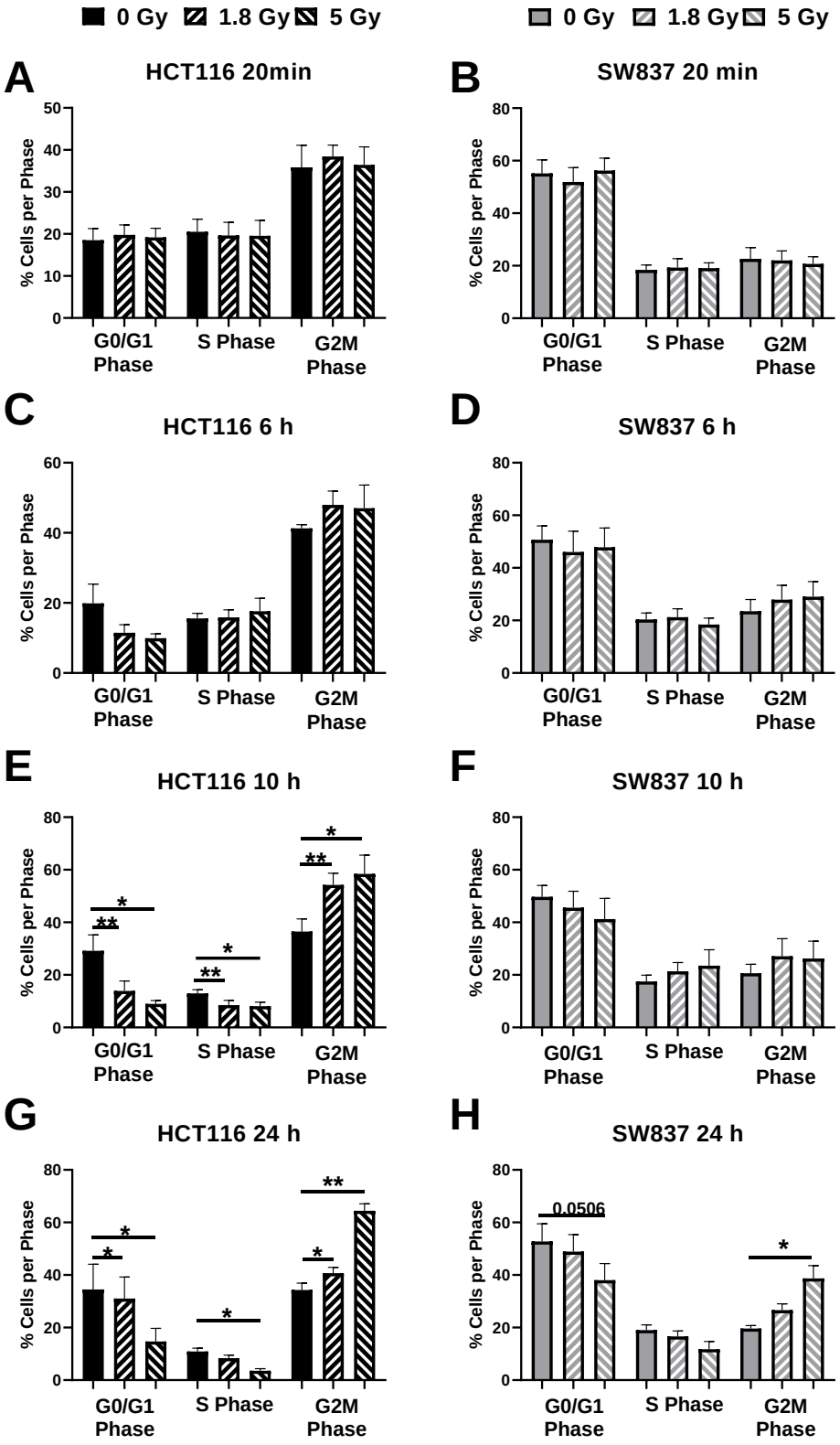

Fig. 2.9: **Effect of radiation exposure on cell cycle progression in radiosensitive HCT116 and radioresistant SW837 cells.** Cell cycle phase distribution was assessed by PI staining and flow cytometry in HCT116 and SW837 cells at (**A-B**) 20 min**,** (**C-D**) 6 h**,** (**E-F**) 10 h and (**G-H**) 24 h post exposure to 0 Gy, 1.8 Gy or 5 Gy radiation. Data is presented as mean ± SEM for 3 independent experiments. Statistical analysis was performed by paired t-testing. **p* < 0.05, ***p* < 0.01.

2.4.8. *SW837 cells display enhanced DNA damage repair*

To investigate whether alterations in DNA damage induction and repair contribute to the differing radiosensitivities of HCT116 and SW837 cancer cells, DNA damage was assessed by γH2AX-AlexaFluor-488 staining and flow cytometry (**Section 2.3.11**). H2AX is rapidly phosphorylated to γH2AX at the sites of DNA DSB's , and can be used as a surrogate marker of DNA damage (352). In addition, the loss of γH2AX foci at sites of DNA DSB is consistent with their repair, allowing investigation of the kinetics of DNA repair following radiation-induced DSB.

In radiosensitive HCT116 cells, a significant increase in γH2AX fluorescence was observed at 20 min post 1.8 Gy and 5 Gy radiation, when compared to unirradiated controls (p = 0.0013, p = 0.0275, respectively) (Mean MFI ± SEM; 0 Gy 466.5 ± 102.3, 1.8 Gy 561 ± 104.8, 5 Gy 707 ± 118.3) (**Fig. 2.10A**)**.** At 6 h post irradiation, DNA damage persisted following 1.8 Gy irradiation (p = 0.0023), with a trend towards increased DNA damage following 5 Gy (p = 0.0732) (mean MFI ± SEM; 0 Gy 464.5 ± 104.5, 1.8 Gy 535.5 ± 110.2, 5 Gy 546.3 ± 94.73). This DNA damage following 5 Gy radiation was not resolved by 10 h, or 24 h, when compared to control in this radiosensitive HCT116 cell line (p = 0.0228, p = 0.0324) (mean MFI ± SEM; 10h 0 Gy 384.5 ± 88.02, 10 h 5 Gy 496.8 ± 84.18, 24 h 0 Gy 372.1 ± 109.7, 24 h 5 Gy 471.3 ± 88.57) (**Fig. 2.10A**).

In radioresistant SW837 rectal cancer cells, DNA damage induction was observed following 1.8 Gy and 5 Gy irradiation at 20 min post irradiation, when compared to unirradiated control (p = 0.0468, p = 0.0299) (mean MFI ± SEM; 0 Gy 240.3 ± 42.26, 1.8 Gy 341.3 ± 26.81, 5 Gy 512.3 ± 66.64) (**Fig. 2.10B**)**.** DNA damage following 1.8 Gy was resolved by 6 h post irradiation (p = 0.205), while γH2AX fluorescence following 5 Gy persisted at 6 h, when compared to control (p = 0.0229) (mean MFI ± SEM; 0 Gy 225.3 ± 19.15, 5 Gy 418 ± 30.35). By 10 h post irradiation, all irradiation-induced DNA damage was resolved in SW837 cells, with no difference in γH2AX fluorescence at 10 h or 24 h post irradiation, when compared to unirradiated control (**Fig. 2.10B**).

These data demonstrate a significant induction of γH2AX immediately following radiation exposure in both HCT116 and SW837 cells, indicating similar levels of IR-induced DNA damage in both cell lines. Importantly, these data also demonstrate that in radiosensitive HCT116 cells, repair of IR-induced DNA damage is impaired, with γH2AX foci persisting at 24 h following radiation exposure, while in the radioresistant model, SW837, radiation-induced

DNA damage was repaired by 10 h post radiation. These data indicate that enhanced DNA damage repair may contribute to the radioresistance of SW837 cells.

2.4.9. *SW837 cells are less reliant on glycolysis than HCT116 cells*

Recent evidence supports a potential role for altered tumour metabolism as a contributor to therapeutic resistance, including radioresistance. To investigate the potential contribution of altered energy metabolism in the radioresistance of SW837 cells, basal energy metabolism was assessed in both HCT116 and SW837 cell lines, using the Seahorse^{TM} XFe24 analyser. This permits the assessment of two major metabolic pathways; oxidative phosphorylation, represented by OCR and glycolysis, represented by ECAR in live cells in real time.

Basally, HCT116 and SW837 cell lines displayed similar OCR levels (**Fig. 2.11A)** (Mean OCR ±. SEM; HCT116 343.3 ± 83.84, SW837 232 ± 32.6, HRA-19 177.6 ± 43.01, SW1463 350.7 ± 59.39). Basal ECAR levels were significantly lower in radioresistant SW837 rectal cancer cells, when compared to radiosensitive HCT116 colon cancer cells (p = 0.045) **(Fig. 2.11B)** (ECAR ± SEM; HCT116 48.38 ± 9.408, SW837 22.77 ± 2.16).

In order to accurately examine the basal metabolic reliance of each cell line, the OCR:ECAR ratio was calculated by dividing the basal OCR values by the basal ECAR values of each cell line (353). Interestingly, radioresistant SW837 cells were demonstrated to have a significantly higher reliance on oxidative metabolism than glycolytic metabolism, when compared to radiosensitive HCT116 cells (p = 0.014) (OCR:ECAR ± SEM; HCT116 6.67 ± 0.65 (OxPhos) : 1 (Glycolysis), SW837 9.94 ± 0.75 (OxPhos) : 1 (Glycolysis)) (**Fig. 2.11C**).

Together, these data demonstrate that radioresistant SW837 cells are less reliant on glycolysis, while radiosensitive HCT116 cells are reliant on both glycolysis and oxidative metabolism.

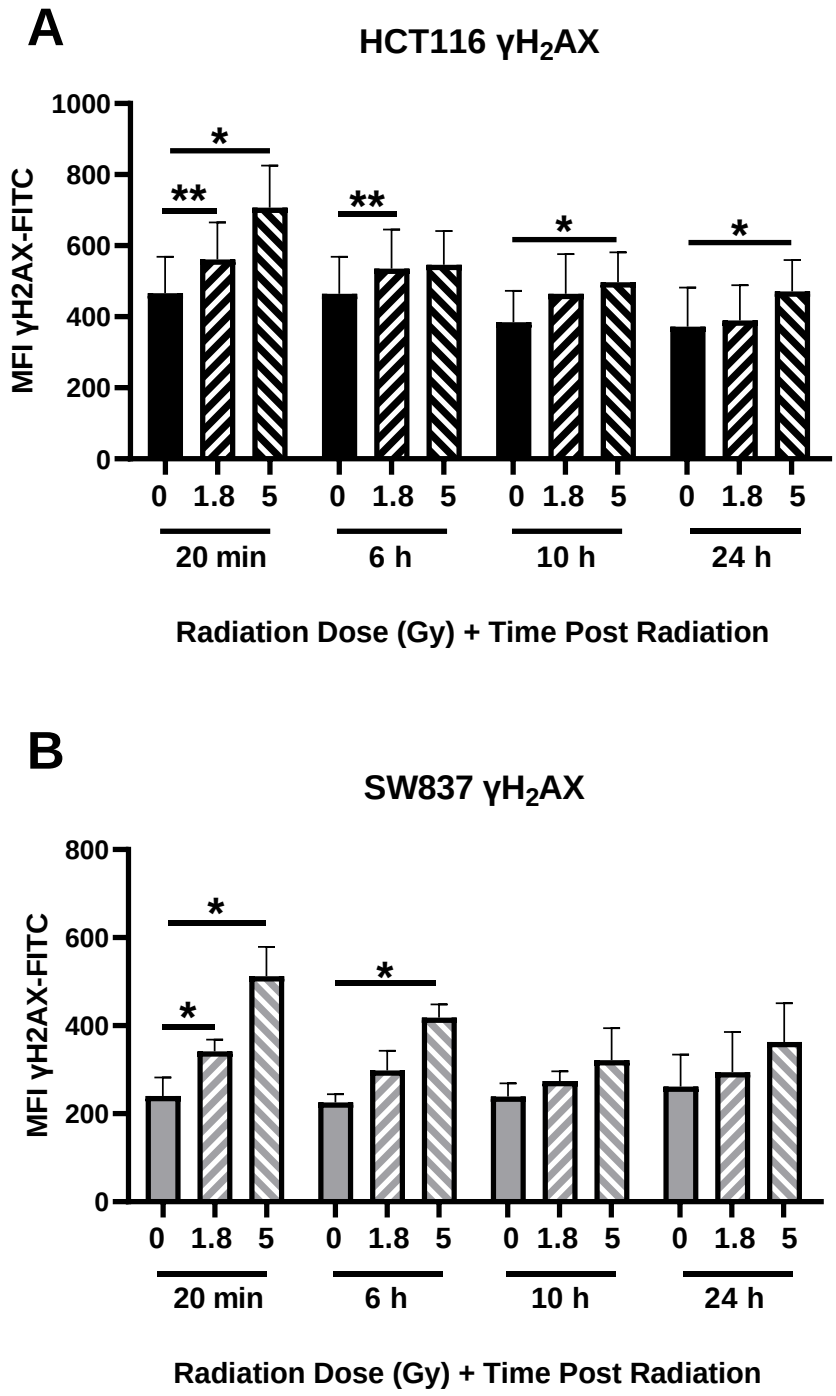

Fig. 2.10: **Radioresistant SW837 cells display enhanced repair of IR-induced DNA damage, compared to radiosensitive HCT116 cells.** DNA damage was assessed by γH2AX-FITC staining and flow cytometry in **(A)** HCT116 and **(B)** SW837 cells at 20 min, 6 h, 10 h and 24 h post exposure to 0 Gy, 1.8 Gy or 5 Gy radiation. Data is presented as mean ± SEM for 4 independent experiments. Statistical analysis was performed by paired ANOVA and post-hoc multiple comparisons testing. *$p < 0.05$, **$p < 0.01$.

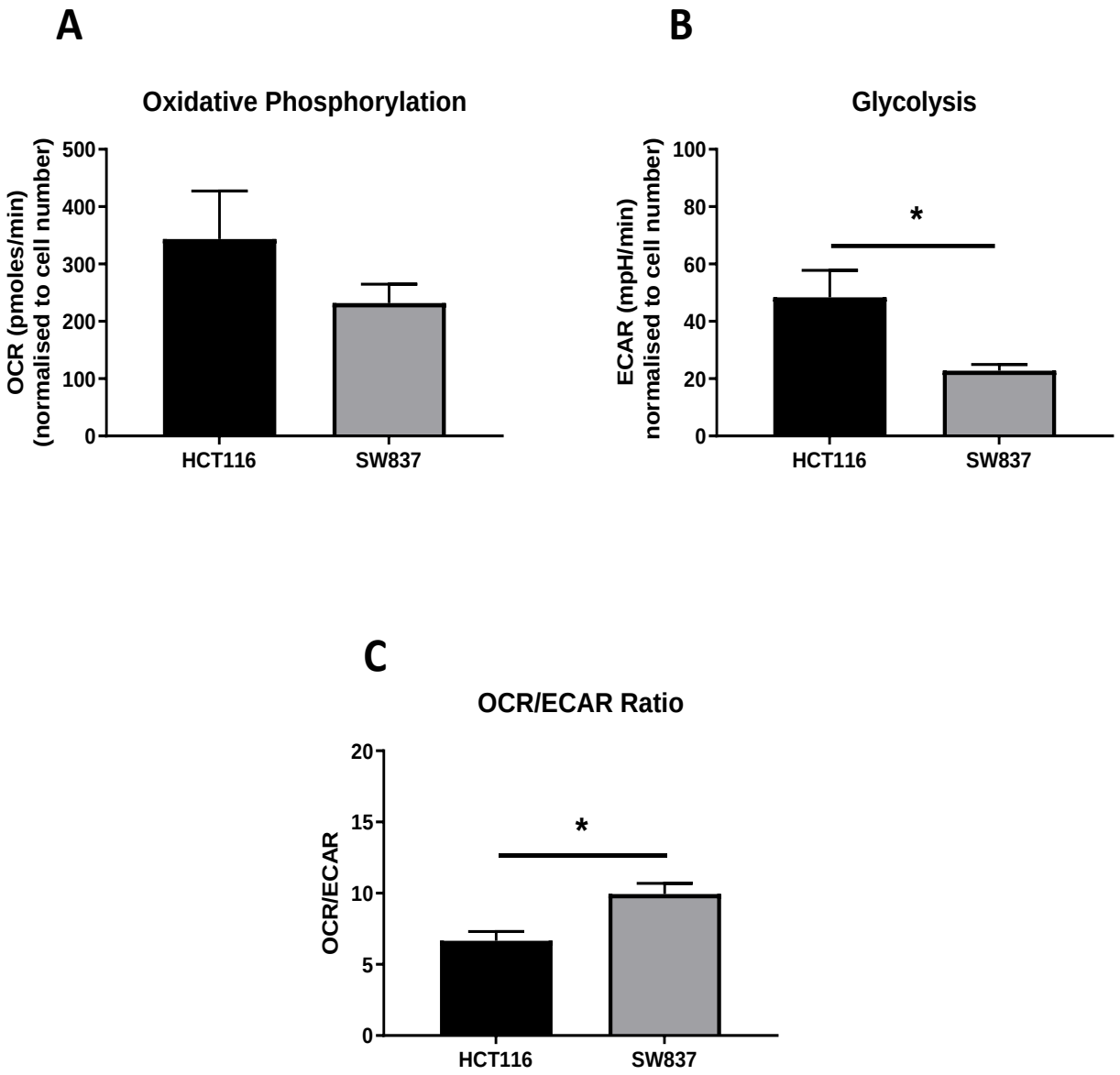

Fig. 2.11: **Radioresistant SW837 cells demonstrate significantly lower reliance on glycolysis, when compared to radiosensitive HCT116 cells.** The OCR and ECAR rates of HCT116 colon and SW837 rectal cancer cell lines were assessed using the Seahorse XFe24 analyser. **A)** Basal OCR (oxidative phosphorylation) of HCT116 and SW837 cell lines. **B)** Basal ECAR (glycolysis) of HCT116 and SW837 cells. **C)** OCR:ECAR Ratio of HCT116 and SW837 cells. Data is presented as mean ± SEM for 11 independent experiments. Statistical analysis was performed by unpaired *t*-testing. **p* < 0.05.

2.4.10. SW837 cells display elevated spare respiratory capacity compared to HCT116 cells

To further investigate the metabolic reliance of HCT116 and SW837 cell lines, a series of mitochondrial inhibitors were injected using the Seahorse XFe24 live-cell metabolic assay, and their effects on OCR measured in real-time.

Non-mitochondrial oxygen consumption levels were similar between HCT116 and SW837 cell lines (**Fig. 2.12A**). No differences were demonstrated between basal respiration rates, or maximal respiratory capacity of HCT116 and SW837 cells (**Fig. 2.12B-C**). Interestingly, radioresistant SW837 cells were demonstrated to have a significantly higher spare respiratory capacity (SRC) (as a %), which reflects the ability of a cell to adapt and respond to an energy demand, when compared to HCT116 cells (p = 0.0096) (Mean SRC as % ± SEM; HCT116 108.4 ± 5.51, SW837 177.9 ± 10.99) **(Fig. 2.12D**). No significant differences were demonstrated in oxygen-linked ATP turnover (**Fig. 2.12E**), proton leak (**Fig. 2.12F**) or coupling efficiency (**Fig. 2.12G**).

These data suggest that SW837 cells may demonstrate enhanced metabolic plasticity as demonstrated by a significantly higher spare respiratory capacity, when compared to radiosensitive HCT116 cells.

2.4.11. *Glycolytic parameters are similar in HCT116 and SW837 cells*

To further interrogate metabolic phenotypes of HCT116 and SW837 cell lines, glycolytic parameters were assessed (354).

A trend toward higher total glycolytic capacity, which reflects the ECAR rate following mitochondrial metabolism inhibition by oligomycin A injection, was demonstrated in radiosensitive HCT116 cells, when compared to radioresistant SW837 cells, although this did not reach statistical significance (p = 0.075) (mean total glycolytic capacity ± SEM; HCT116 102.5 ± 19.43, SW837 56.81 ± 5.79) **(Fig. 2.13A)**. Glycolytic reserve capacity, which reflects the potential glycolytic capacity reserved for use under stress per cell line, was demonstrated to be similar in HCT116 and SW837 cells **(Fig. 2.13B)**.

These data demonstrate similar glycolytic parameters between HCT116 and SW837 cells.

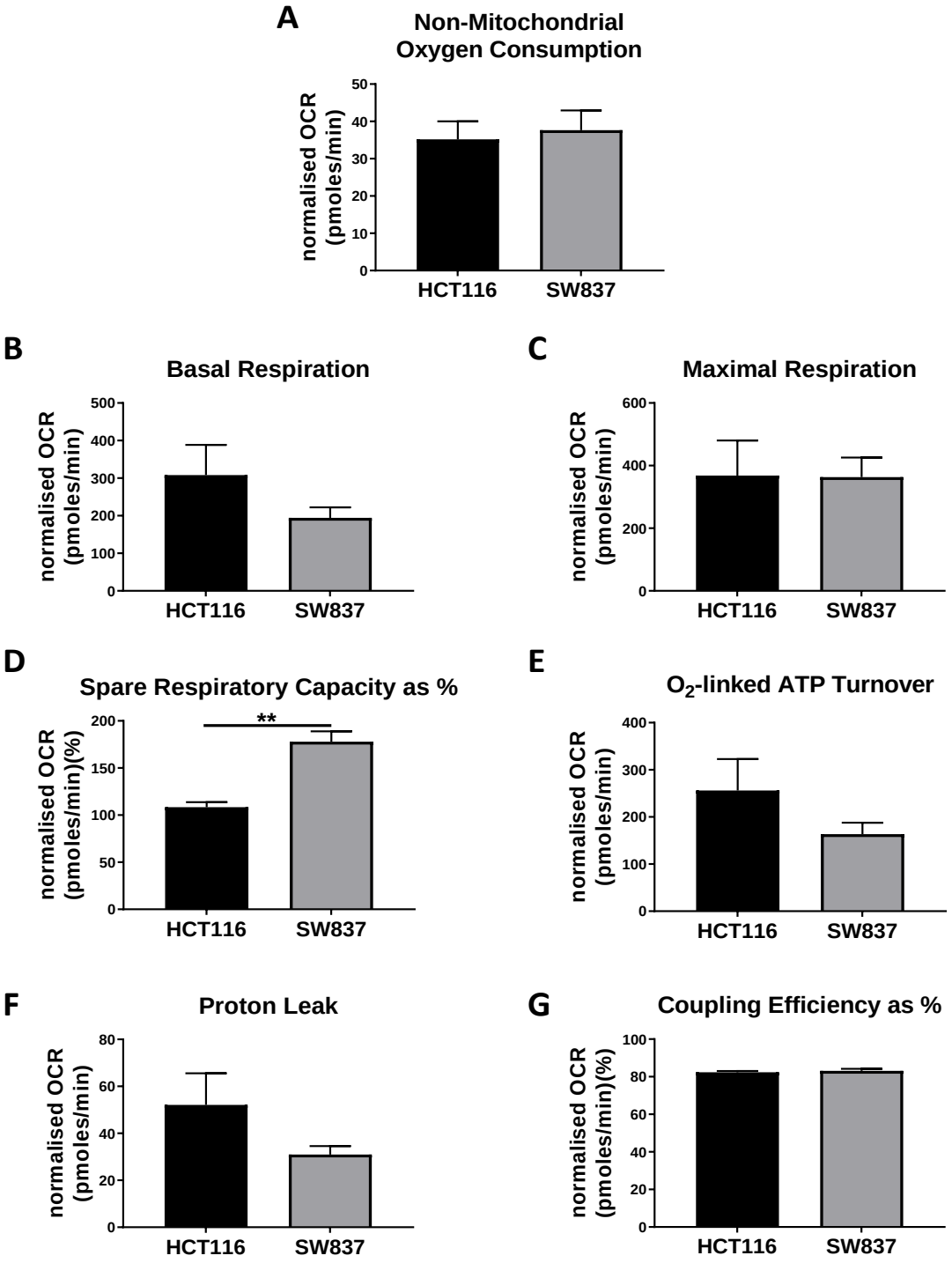

Fig. 2.12: **Spare respiratory capacity is increased in radioresistant SW837 cells, when compared to radiosensitive HCT116 cells.** Metabolic parameters were assessed using Seahorse™ XFe24 analyser and a series of mitochondrial inhibitors. **A)** Non-mitochondrial oxygen consumption. **B)** Basal respiration. **C)** Maximal respiration. **D)** Proton leak. **E)** O_2-linked ATP production. **F)** Spare-respiratory capacity as %. **G)** Coupling Efficiency. Data is presented as mean ± SEM for 11 independent experiments. Statistical analysis was performed using unpaired *t*-testing. $^{**}p < 0.01$.

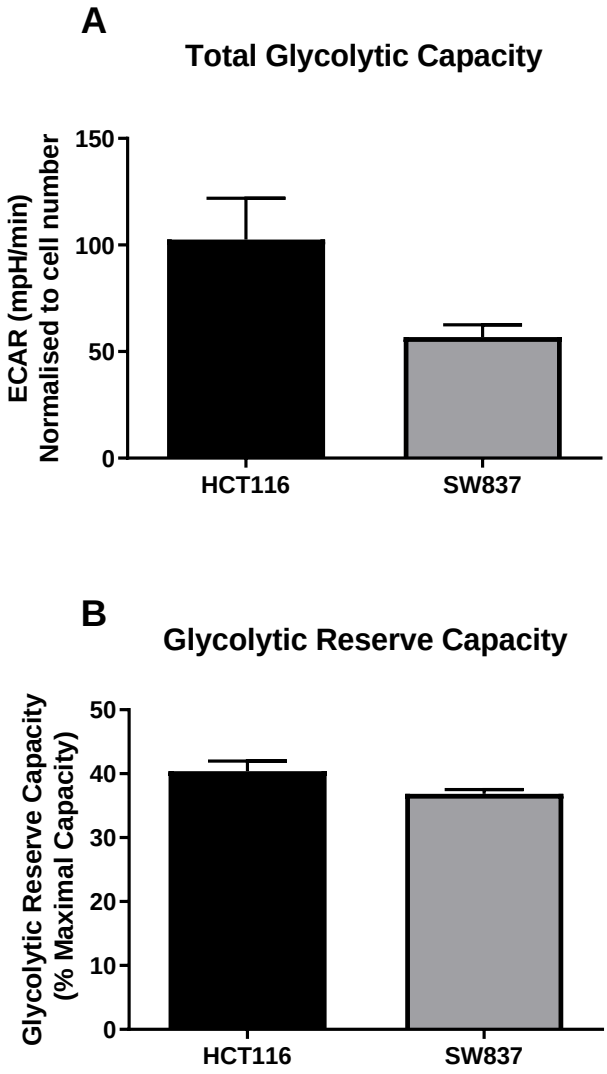

Fig. 2.13: **HCT116 and SW837 cells display similar glycolytic parameters.** Glycolytic parameters were assessed using Seahorse™ XFe24 analyser and oligomycin A treatment in HCT116 and SW837 CRC cell lines. **A)** Total glycolytic capacity, the mean value of ECAR measurements following oligomycin injection. **B)** Glycolytic reserve capacity, the % difference between total glycolytic capacity and basal ECAR. Data is presented as mean ± SEM for 10 independent Statistical analysis was performed using unpaired *t*-testing.

2.4.12. HCT116 and SW837 cells produce similar ATP levels

Having demonstrated altered reliance on glycolysis and oxidative phosphorylation between the SW837 and HCT116 cells (**Section 2.4.9-2.4.11**), alterations in ATP production was assessed using the ATPlite™ luminescence ATP detection assay system.

No significant differences in quantitative ATP levels were demonstrated between HCT116 and SW837 CRC cell lines (**Fig. 2.14**).

2.4.13. HCT116 and SW837 cells display similar mitochondrial function

Having profiled energy metabolism in HCT116 and SW837 cells, basal mitochondrial function was assessed in each cell line using three surrogate markers of mitochondrial function (mitochondrial membrane potential, mitochondrial mass and ROS production).

Mitochondrial mass was similar in both cell lines (Mean normalised MitoTracker fluorescence ± SEM; HCT116 2.26 ± 0.12, SW837 1.32 ± 0.35) (**Fig. 2.15A**). Basal ROS production was similar in both cell lines (Mean normalised DCF-DA fluorescence ± SEM; HCT116 2.45 ± 0.57, SW837 1.07 ± 0.16) (**Fig. 2.15B**). No alterations in mitochondrial membrane potential were demonstrated between the cell lines (Mean normalised rhodamine fluorescence ± SEM; HCT116 146.9 ± 46.35, SW837 118.9 ± 37.43) (**Fig. 2.15C**).

These data suggest that alterations in in mitochondrial function, as measured by mitochondrial mass, ROS production and mitochondrial membrane potential, do not contribute to the radioresistance of SW837 cells.

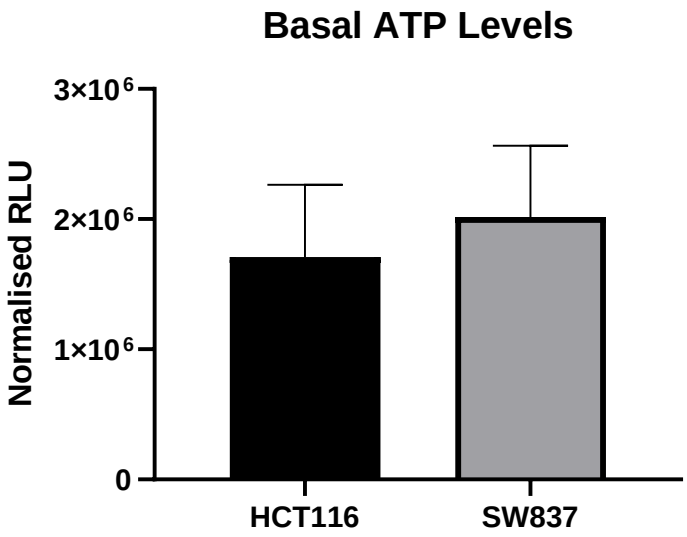

Fig. 2.14: **HCT116 and SW837 cells display similar levels of ATP.** ATP production was assessed by ATPlite luminescent assay. No significant differences were demonstrated between HCT116 and SW837 cell lines. Data is presented as mean ± SEM of 3 independent experiments. Statistical analysis was performed by unpaired *t*-testing.

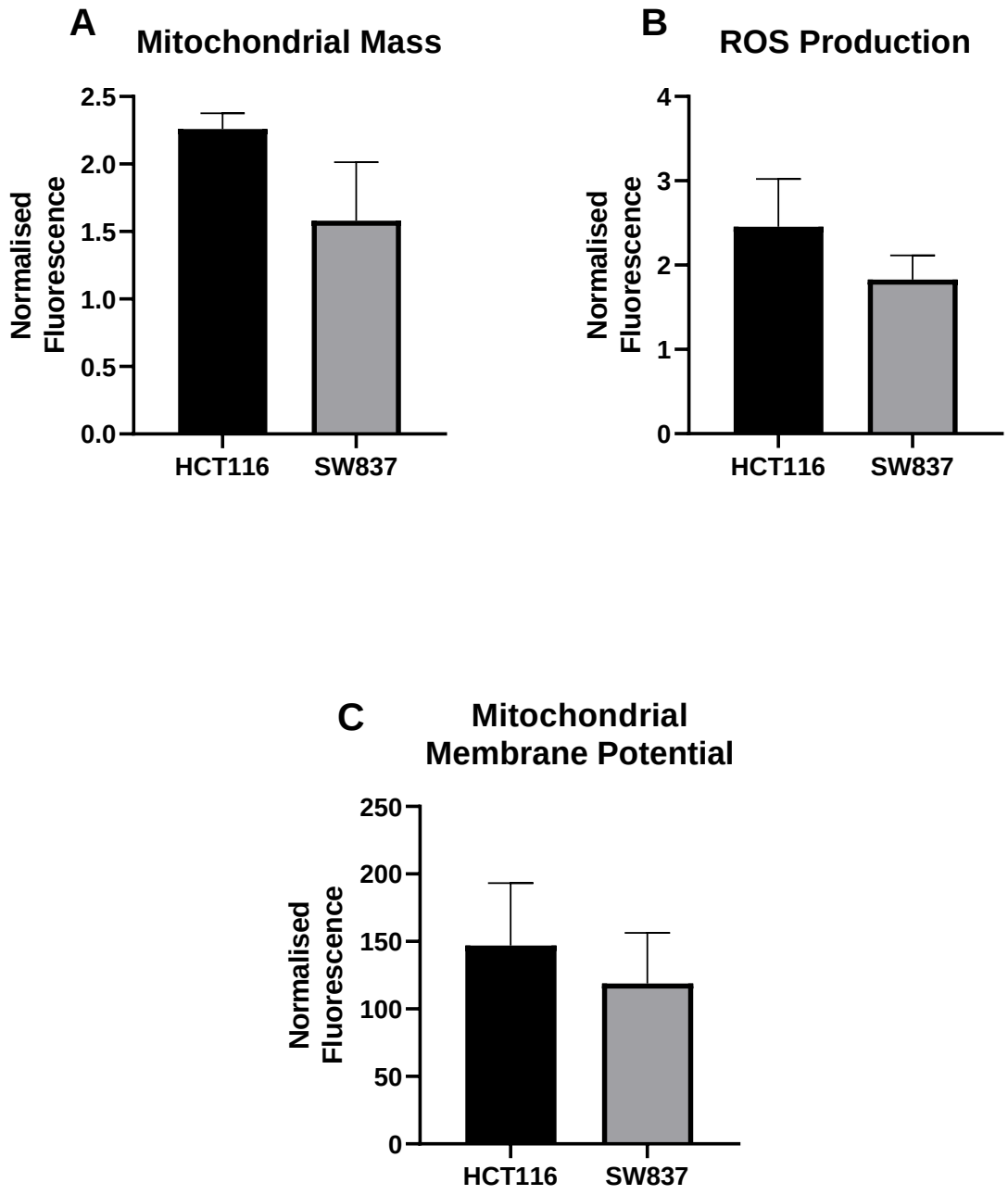

Fig. 2.15: **Mitochondrial function is similar in HCT116 and SW837 cells.** Mitochondrial function was assessed using a series of fluorescent probes in the HCT116 and SW837 cells. **A)** Mitochondrial mass was assessed using MitoTracker Green FM. **B)** ROS production was assessed using 2,7 DCF-DA. **C)** Mitochondrial membrane potential was assessed using Rhodamine-123. Data is presented as mean ± SEM of 7 (HCT116) or 8 (SW837) independent experiments. Statistical analysis was performed by unpaired *t*-testing.

2.4.14. *HCT116 and SW837 cells display similar total and oxidised glutathione levels*

Oxidative stress and antioxidant capacity is often indicated as a mechanism of radiation resistance. In order to characterise this in the inherent model of radioresistant (SW837) and radiosensitive (HCT116) CRC cell lines, the GSH:GSSH Glo™ assay was utilised.

No significant differences in total GSH or GSSG were demonstrated basally between HCT116 and SW837 cells (**Fig. 2.16A-B**). Furthermore, basal GSH:GSSG ratio, indicative of oxidative stress levels was similar between the two cell lines characterised (**Fig. 2.16C**).

These data indicate that glutathione-mediated antioxidant capacity is not a major mechanism underlying the enhanced radioresistance of SW837 cells.

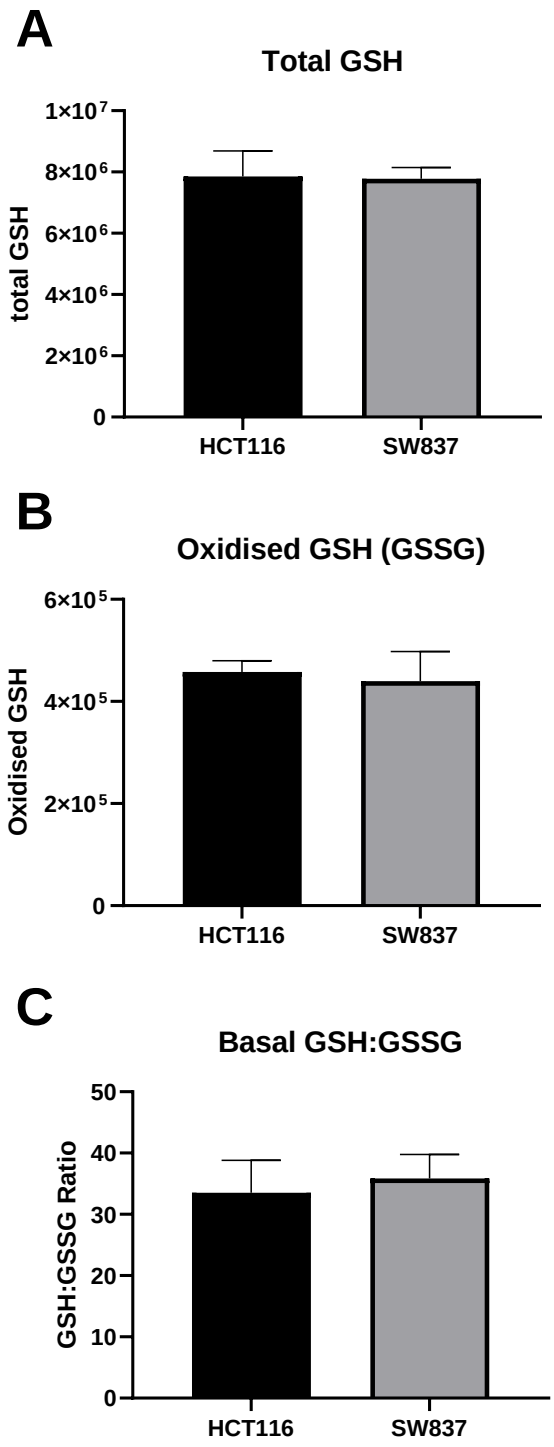

Fig. 2.16: **Basal GSH production in radiosensitive HCT116 and radioresistant SW837 cells.** GSH was assessed using the Promega GSH:GSSG Glo™ luminescent assay. **A)** Total GSH. **B)** GSSG **C)** GSH:GSSG ratio. Data is presented as mean ± SEM for 4 independent experiments. Statistical analysis was performed by unpaired *t*-test.

2.4.15. *Radioresistant SW837 cells display a significantly altered basal transcriptome*

To further characterise HCT116 and SW837 cells, and the potential mechanisms underlying their differing radiosensitivities, basal transcriptomic profiling was performed using the Lexogen QuantSeq 3' mRNA FWD sequencing kit. Differential expression analysis was performed using Bluebee™ software, utilising the DESeq2 R script extension.

A total of 24,359 genes were expressed across the two cell lines. The principal component analysis (PCA) plot demonstrates the first two components of the PCA of the normalised counts, demonstrating clear separation between replicates of HCT116 and SW837 cells (**Fig. 2.17).** PC1 described the most variation within the data, accounting for 76%, while PC2 accounted for 12% (**Fig. 2.17**). Differential expression analysis revealed a total of 2,641 genes were significantly altered between HCT116 and SW837 cells, based on adjusted *p*-value (*p*-adj) < 0.05 (**Fig. 2.18A**).

In total, 1,173 genes were significantly downregulated, and 1,468 genes significantly upregulated in SW837 cells, when compared to HCT116 cells (**Fig. 2.18A**), suggesting that alterations in the transcriptome may contribute to the radioresistance of SW837 cells. Of the significantly altered genes, the top 25 downregulated and upregulated genes in SW837 cells are demonstrated in **Fig. 2.18B-C.** DPYSL5 (dihydropyrimidinase-related protein-5), which is involved in signal transduction was the most downregulated gene (as determined by fold change, Log2 Fold Change = -4.96) in SW837 cells, when compared to HCT116 cells. RNF212 (Ring-finger protein 212), which functions as a ubiquitin ligase, was the most upregulated gene (Log2 Fold Change = 5.12), in SW837 cells, when compared to HCT116 cells.

The top 30 genes most significantly disparate between HCT116 and SW837 cells are displayed in **Table 2.5**. NECTIN3 (Nectin cell adhesion molecule 3), which is involved in cell-cell junctions was the most significantly downregulated gene (as determined by *p*-adj, *p*adj = 3.07×10^{-25}) in SW837 cells, when compared to HCT116 cells. TGFBI (transforming growth factor beta (β) induced), which is involved in cellular adhesion and movement, was the most significantly upregulated gene (*p*-adj = 2.56×10^{-34}) in SW837 cells, when compared to HCT116 (**Table 2.5**).

These data demonstrate extensive significant differences between the basal transcriptome of SW837 and HCT116 cells, suggesting that alterations in the transcriptome contribute to the radioresistance of SW837 cells.

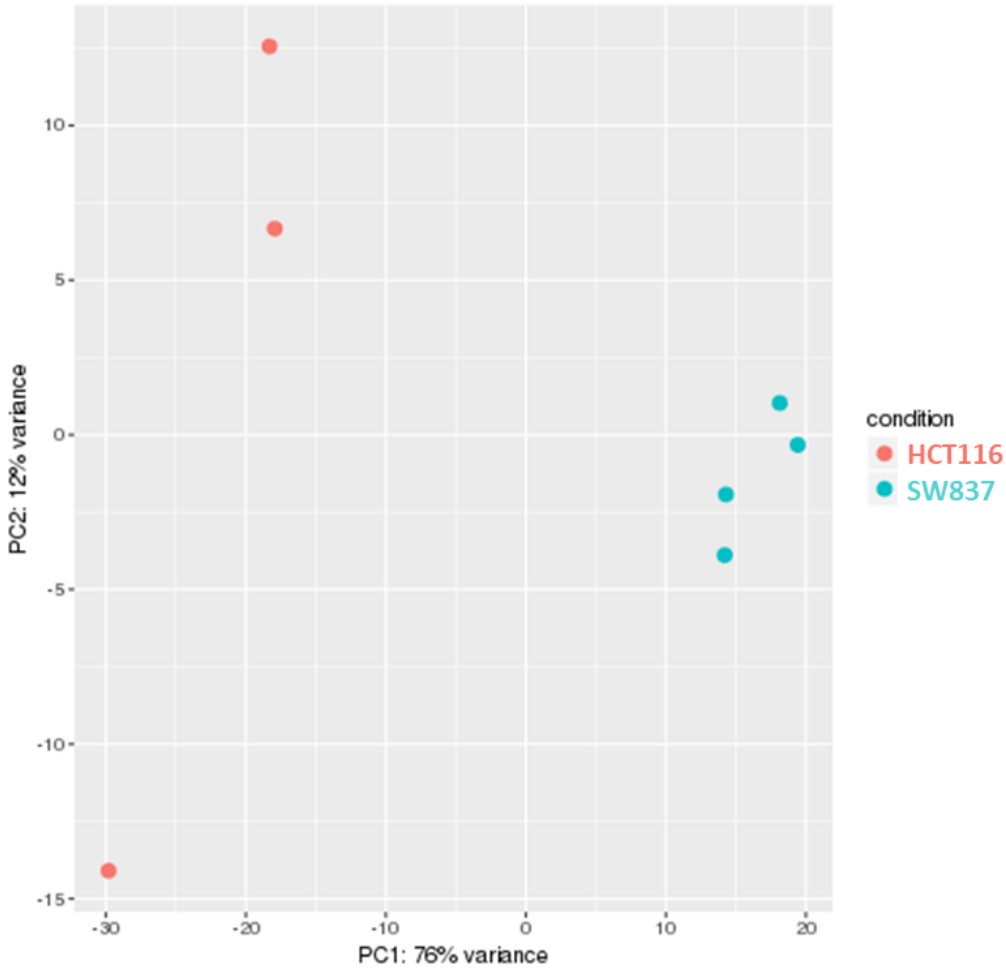

Fig. 2.17: **Principal component analysis demonstrates clear separation between HCT116 and SW837 replicates.** PCA was performed on normalised read counts from HCT116 and SW837 replicates utilised for transcriptomic profiling were assessed using BlueBee software, to assess clustering of replicates. PC1 (x-axis) accounts for 76% of variation between samples, while PC2 (y-axis) accounts for 12% of variance.

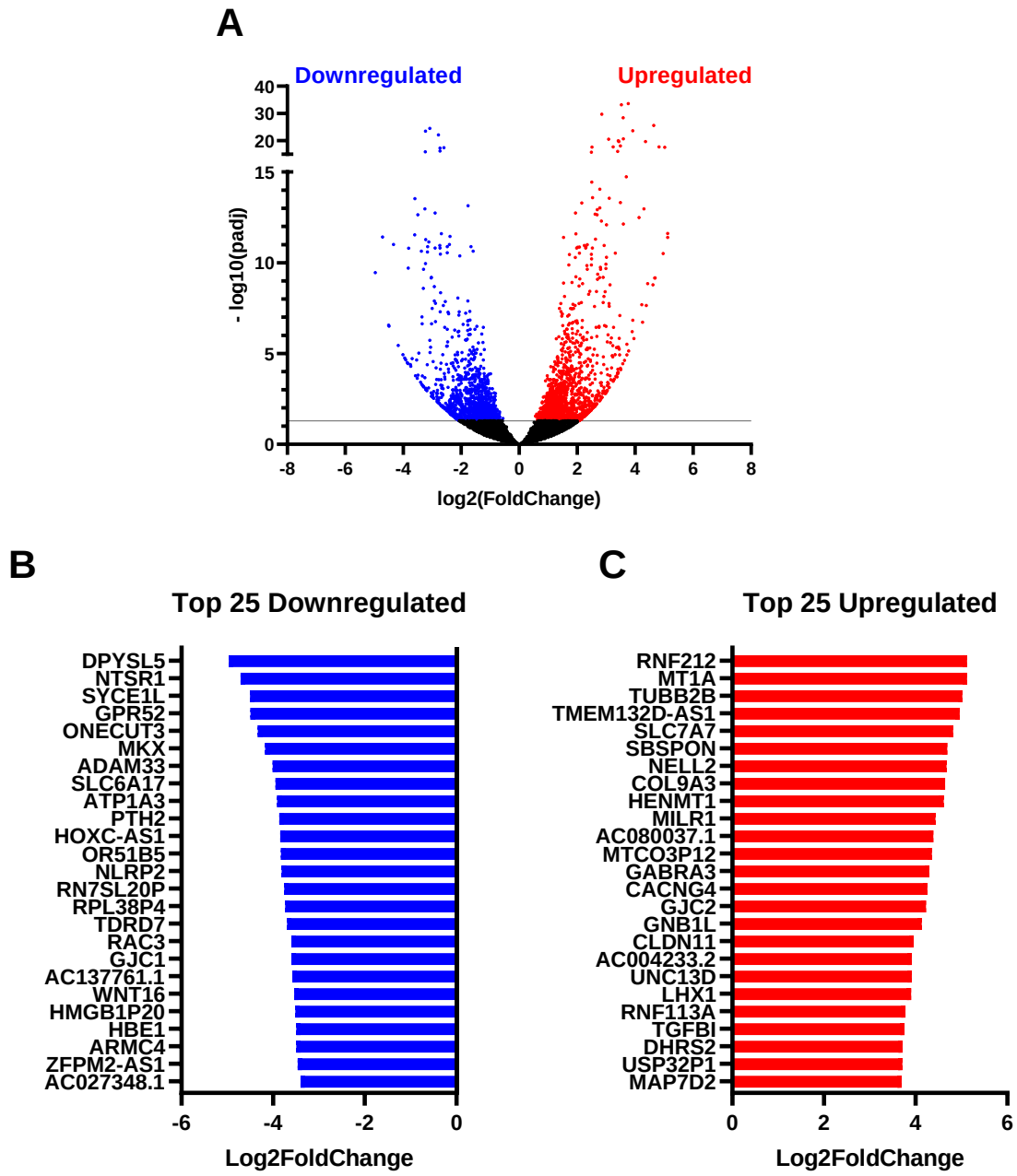

Fig. 2.18: **The basal transcriptome is significantly altered in radioresistant SW837 cells.** Transcriptomic profiling was performed on HCT116 and SW837 cells. Differential expression analysis was performed using BlueBee™ Software, using the DESeq2 R extension script. **A)** Volcano plot demonstrating 2,461 genes significantly altered in SW837 cells, when compared to HCT116 cells, the y-axis corresponds to the -log10(*p*-adj), and the x-axis demonstrates the Log_2 (Fold Change). Dots in blue and red represent the significantly downregulated/upregulated genes (2,461) in SW837 cells, respectively, when compared to HCT116. Dots in black represent the genes which did not reach statistical significance (*p*-adj > 0.05). **B)** The top 25 downregulated genes (by fold change) in SW837 cells, when compared to HCT116 cells. **C)** The top 25 upregulated genes (by fold change) in SW837 cells, when compared to HCT116 cells. Data is presented for 3 (HCT116) or 4 (SW837) independent experiments. Statistical analysis was performed using the Wald test, with corrections for multiple comparisons performed by the Benjamini-Hochberg correction (FDR).

Table 2.5: **Top 30 most significantly altered genes in SW837 cells, when compared to HCT116 cells.**

Gene Name	Up/Down-regulated in SW837	Log_2 Fold Change	*p*-adj
TGFBI	Up	3.759235	2.56E-34
BCAP31	Up	3.524357	6.61E-34
IRAK1	Up	2.848671	2.10E-30
PLA2G16	Up	3.586746	4.28E-29
COL9A3	Up	4.641057	2.57E-26
NECTIN3	Down	-3.08656	3.07E-25
UNC13D	Up	3.914314	2.20E-24
ARHGAP29	Down	-3.23454	3.28E-24
AKAP12	Down	-2.78658	7.57E-23
PASD1	Up	3.594919	2.20E-21
G6PD	Up	3.085395	2.77E-21
KLK6	Up	3.413412	1.10E-20
FAM3A	Up	3.435913	2.29E-20
MTCO3P12	Up	4.355639	2.29E-20
LAGE3	Up	3.490986	8.71E-19
SMPD4	Up	3.239638	2.03E-18
SLC7A7	Up	4.820344	2.03E-18
NAA10	Up	2.50991	2.46E-18
TUBB2B	Up	5.018094	2.84E-18
PHLDB2	Down	-2.59459	3.69E-18
ANXA1	Down	-2.73415	5.29E-18
NR2F1	Down	-2.73196	6.82E-17
WFS1	Up	3.395946	8.37E-17
TIAM1	Down	-3.23933	1.26E-16
BMP7	Up	2.487635	1.63E-16
MAP7D2	Up	3.693246	1.84E-15
FGF19	Up	2.502343	3.60E-15
QPRT	Up	2.782324	8.93E-15
FURIN	Up	2.527345	2.59E-14

Log_2 Fold Change indicates the differential expression of each gene in SW837 cells, when compared to HCT116, with negative values indicating genes downregulated in SW837 cells, and positive values indicating genes upregulated in SW837 cells, when compared to HCT116 cells. The *p*-adj values indicate the statistical significance of the differential expression of each gene between SW837 and HCT116 cells. Statistical analysis performed using the Wald test, with corrections for multiple comparisons performed by the Benjamini-Hochberg correction (FDR).

2.4.16. *Identification of biological functions altered between HCT116 and SW837 cells*

Having demonstrated significant alterations in the basal transcriptome of radioresistant SW837 cells, biostatistical clustering analysis was performed on the differentially expressed genes to identify biological functions differing between the two cell lines. IPA software was utilised to identify altered molecular pathways, based on transcriptomic data.

The most significantly altered biological functions between HCT116 and SW837 cells, based on biostatistical analysis of gene expression data, are demonstrated in **Table 2.6**. The *p*-values represent the statistical probability that selecting genes associated with each function is due to chance alone. As each biological function is comprised of multiple functional pathways, significance is represented as *p*-value range.

The most significantly differing biological function pathway was demonstrated to be 'cell death and survival' (*p* = 3.07E-22 – 5.87E-05) (**Table 2.6**)**.** Other biological functions demonstrated to be altered between HCT116 and SW837 cells, included 'cellular development', 'cellular growth and proliferation', 'cell cycle' and 'DNA replication, recombination and repair' (**Table 2.5**). In addition, altered 'cellular response to therapeutics' was also identified as a biological function altered in SW837 cells, which supports in vitro data demonstrating enhanced radio- and chemo-resistance of SW837 cells (**Sections 2.4.1** and **2.4.3).**

These data demonstrate that the transcriptomic differences between HCT116 and SW837 cells contribute to alterations in biological functional pathways, which may contribute to the radioresistance of SW837 cells.

Table 2.6: **Most significantly altered biological functions between HCT116 and SW837 cells.**

Biological Function	*p*-value range
Cell Death and Survival	3.07E-22-5.87E-05
Cellular Development	2.52E-16-1.4E-04
Cellular Growth and Proliferation	2.52E-16-1.4E-04
Protein Synthesis	1.1E-14-5.19E-05
Cellular Movement	2.21E-14-1.41E-04
Gene Expression	5.44E-12-5.72E-05
Cellular Assembly and Organization	2.2E-11-1.48E-04
Cellular Function and Maintenance	2.2E-11-1.07E-04
Molecular Transport	4.69E-09-6.3E-07
Protein Trafficking	4.69E-09-6.3E-07
Cell-To-Cell Signalling and Interaction	2.06E-08-8.68E-05
Cell Cycle	3.13E-08-1.37E-04
RNA Post-Transcriptional Modification	4.17E-08-1.11E-04
DNA Replication, Recombination, and Repair	6.62E-08-9.97E-05
RNA Damage and Repair	4.55E-07-5.72E-05
Cell Signalling	8.71E-07-1.03E-05
Post-Translational Modification	8.71E-07-1.3E-04
Cellular Response to Therapeutics	2.63E-06-8.71E-06
Cell Morphology	1.95E-05-1.41E-04
Protein Degradation	5.19E-05-5.19E-05
Nucleic Acid Metabolism	8.31E-05-8.31E-05
Small Molecule Biochemistry	8.31E-05-8.31E-05

Biostatistical analysis was performed on significantly altered genes between HCT116 and SW837 cells by IPA analysis to identify projected altered biological functions between the two cell lines. Statistical analysis performed by right-tailed Fisher's exact test using IPA analysis.

2.4.17. *Canonical pathways significantly altered between HCT116 and SW837 cells*

Having demonstrated altered biological functions in SW837 cells, the specific biological pathways involved in these functional processes were subsequently investigated. Transcriptomic data was analysed using IPA software, and Canonical Pathway Analysis was performed. Canonical Pathway Analysis predicts the inhibition/activation of molecular pathways based on the input transcriptomic data and the Ingenuity Knowledge Base.

The most significantly altered canonical pathways between HCT116 and SW837 cells are displayed in **Fig. 2.19**. The *p*-value denotes the significance between the overlap of input experimental data and the Ingenuity Knowledge Base, indicating confidence in pathway involvement. The Z-score refers to software prediction of the activation or inhibition of each affected canonical pathway, with a Z-score ≥ 2, or ≤ -2 indicating significant activation or inhibition of each pathway, respectively.

Fig. 2.19 displays the 10 most significant canonical pathways predicted by IPA analysis to have different activity states between HCT116 and SW837 cells. Oxidative phosphorylation was predicted to be the most significantly activated pathway in SW837 cells, when compared to HCT116 cells (Z-score = 5.145). In addition, the sirtuin signalling pathway was demonstrated to be the most significantly inhibited canonical pathway in SW837 cells, when compared to HCT116 cells (Z-score = -2.496). Mitochondrial dysfunction was also predicted to be significantly altered between HCT116 and SW837 cells, however IPA software was unable to confidently predict activation or inhibition of this pathway due to insufficient evidence in the Knowledge Base (z-score = NaN).

Many of the canonical pathways significantly altered between HCT116 and SW837 cells correspond with processes previously demonstrated to be associated with radioresponse. Some of these pathways, and the specific genes altered in the dataset are demonstrated in **Table 2.7**. Multiple canonical pathways associated with 'Metabolism' were significantly altered in SW837 cells, relative to HCT116, including 'oxidative phosphorylation', 'mitochondrial dysfunction', 'cholesterol biosynthesis' and 'fatty acid biosynthesis'. In addition, 'cell cycle', DNA damage repair', 'oxidative stress' and 'hypoxia' related canonical pathways and genes were demonstrated to be significantly altered between HCT116 and SW837 cells.

These data demonstrate significant differences to canonical pathway activation/inhibition between HCT116 and SW837 cells. Supporting *in vitro* functional data, genes involved in a number of canonical pathways associated with radioresponse, such as metabolism, cell cycle, DNA damage repair and oxidative stress were demonstrated to be altered between the two cell lines, further supporting the contribution of these pathways to the enhanced radioresistance of SW837 cells.

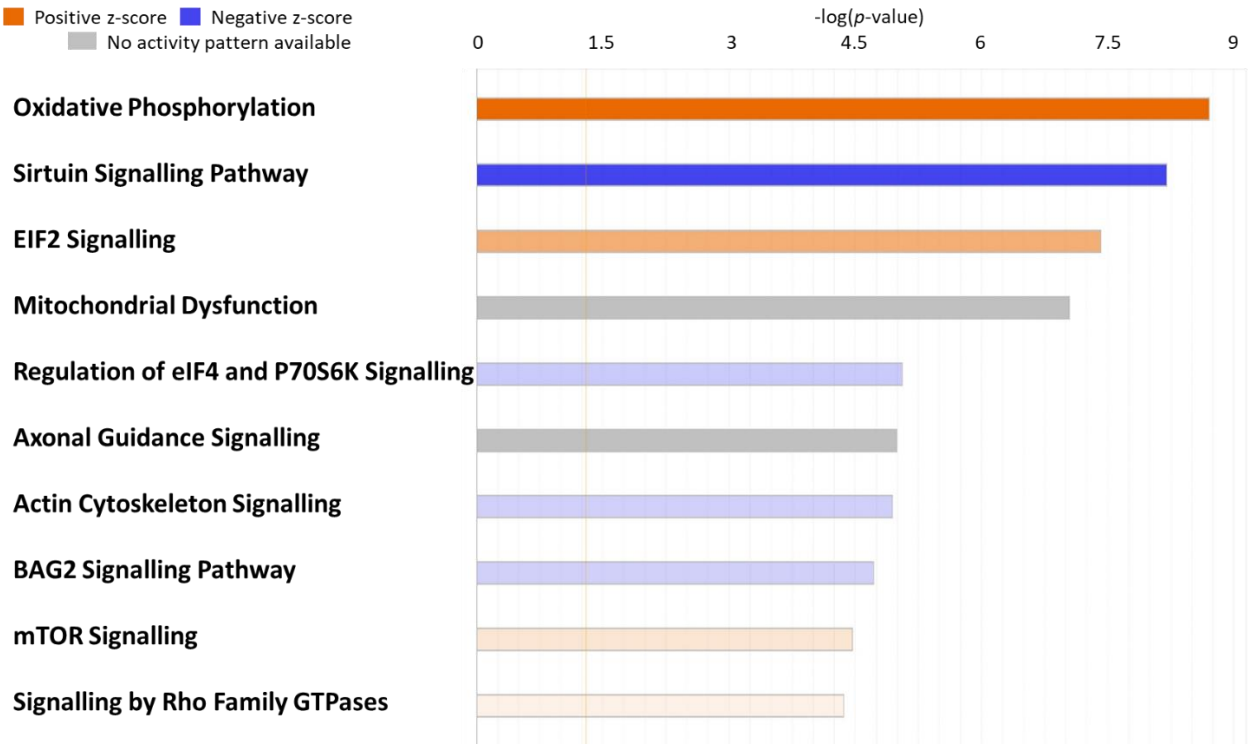

Fig. 2.19: **Top 10 most significantly altered canonical pathways between HCT116 and SW837 cells.** IPA analysis was utilised on transcriptomic data to identify canonical biological pathways altered between HCT116 and SW837 cells. Canonical Pathway Analysis was utilised to predict activation/inhibition of each pathway. An orange bar denotes increasing positive z-score, which indicates predicted activation of pathways. A blue bar denotes decreasing negative z-scores, representing a prediction of inhibition of pathways. Grey bars denote pathways in which the IPA software could not reliably predict activation or inhibition. Data is presented for 3 (HCT116) or 4 (SW837) independent experiments. Statistical analysis was performed using Fisher's Exact testing.

Table 2.7: **Canonical pathways significantly altered in SW837 cells, when compared to HCT116 cells.**

Processes	Ingenuity Canonical Pathways	-log(p-value)	z-score	Genes
Cell Cycle	Cell Cycle: G2/M DNA Damage Checkpoint Regulation	4.14E+00	-0.577	AURKA,CDKN1A,CDKN2A,CKS2,GADD45A,MDM2,MDM4,PLK1,PRKDC,SKP1,TOP2A,TOP2B,WEE1,YWHAB,YWHAH,YWHAQ
	Cell Cycle: G1/S Checkpoint Regulation	4.00E+00	-0.243	CCND3,CDK4,CDK6,CDKN1A,CDKN2A,CDKN2B,E2F1,E2F6,E2F7,GNL3,HDAC3,HDAC7,MDM2,NRG1,PAK1IP1,RB1,RPL11,SKP1,TGFB2
	Cyclins and Cell Cycle Regulation	2.35E+00	0.775	CCND3,CDK4,CDK6,CDKN1A,CDKN2A,CDKN2B,E2F1,E2F6,E2F7,HDAC3,HDAC7,PPM1L,PPP2R1B,PPP2R5B,RB1,SKP1,TGFB2,WEE1
	Cell Cycle Regulation by BTG Family Proteins	1.72E+00	-0.816	BTG1,CDK4,E2F1,E2F6,E2F7,PPM1L,PPP2R1B,PPP2R5B,RB1
	Cell Cycle Control of Chromosomal Replication	1.70E+00	0	CDC45,CDK14,CDK16,CDK4,CDK6,MCM8,MCM9,POLA1,POLA2,RPA3,TOP2A,TOP2B
	Role of CHK Proteins in Cell Cycle Checkpoint Control	9.91E-01	-1	CDKN1A,E2F1,E2F6,E2F7,PLK1,PPM1L,PPP2R1B,PPP2R5B,RAD1,RFC5
DNA Damage Repair	Role of BRCA1 in DNA Damage Response	2.53E+00	-1.265	BABAM2,BARD1,BRCC3,BRIP1,CDKN1A,E2F1,E2F6,E2F7,FANCG,GADD45A,HLTF,PBRM1,PLK1,RB1,RBBP8,RFC5,SMARCC1,UIMC1
	NER	1.46E+00	1.387	CETN2,ERCC3,H3 3A/H33B,H4C3,NEDD8,POLA1,POLA2,POLE3,POLE4,POLR2B,POLR2C,POLR2G,POLR2H,RFC5,RPA3,TOP2A,TOP2B,XPC
	BER	9.39E-01	2.121	CDKN2A,E2F1,FEN1,HMGB1,MBD4,MPG,RFC5,UNG
	DNA Double-Strand Break Repair by NHEJ	6.93E-01	NaN	PRKDC,WRN,XRCC6
Oxidative Stress	Production of Nitric Oxide and Reactive Oxygen Species in Macrophages	1.95E+00	0.365	APOC1,APOL1,APOM,CDC42,CLU,FOS,JAK1,JUN,MAP3K1,MAP3K2,MAPK13,NFKB2,NFKBIA,PIK3C2A,PIK3C3,PIK3R3,PPM1L,PPP1CB,PPP1CC,PPP1R11,PPP1R14C,PPP2R1B,PPP2R5B,PRKCI,RAC1,RAC3,RHOC,RHOT2,RHOU,RHOV,RND3,TNFRSF1B
	Glutathione Redox Reactions I	1.34E+00	-0.447	GPX2,GPX8,GSR,GSTP1,MGST2,PTGES
	Glutathione-mediated Detoxification	7.42E-01	2	GSTA4,GSTM3,GSTP1,MGST2,PTGES
	NRF2-mediated Oxidative Stress Response	6.95E-01	0	ACTG2,AKR7A2,BACH1,CBR1,DNAJC10,DNAJC13,DNAJC19,EPHX1,FOS,FTL,GPX2,GSR,GSTA4,GSTM3,GSTP1,HSP90B1,JUN,JUND,MAP3K1,MGST2,NFE2L2,NQO1,PIK3C2A,PIK3C3,PIK3R3,PPIB,PRKCI,SCARB1

Hypoxia	HIF1α Signalling	6.76E-01	-0.408	ADM,CDKN1A,EIF4EBP1,HSPA8,IGF2,JUN,MDM2,MKNK1,MMP14,NAA10,NCOA1,PDGFC,PIK3C2A,PIK3C3,PIK3R3,PPP3CA,PPP3R1,PRKCI,RAC1,RAC3,RAN,SAT1,SAT2,SLC2A8,STAT3,TGFB2,VEGFA
Metabolism	Oxidative Phosphorylation	8.71E+00	5.145	ATP5F1B,ATP5F1C,ATP5F1E,ATP5MC2,ATP5MC3,ATP5MF,ATP5MG,ATP5PF,ATP5PO,ATPAF1,COX5A,COX6A1,COX6B1,COX7B,COX8A,CYB5B,CYC1,MT-ND5, NDUFA1,NDUFA10,NDUFA12,NDUFA13,NDUFA2,NDUFA8,NDUFB1,NDUFB2,NDUFB5,NDUFB6,NDUFB8,NDUFS2,NDUFS5,NDUFV3,UQCRB,UQCRC2,UQCRQ
	Sirtuin Signalling Pathway	8.20E+00	-2.496	ACLY,ARNTL,ATG12,ATP5F1B,ATP5F1C,ATP5F1E,ATP5PF,CPS1,CYC1,DUSP6,E2F1,G6PD,GADD45A,H1-2,H1-4,H3-3A/H3-3B,IDH2,JUN,KAT2A,MAP1LC3A,MT-ND5,MT-ND6,NDUFA1,NDUFA10,NDUFA12,NDUFA13,NDUFA2,NDUFA8,NDUFB1,NDUFB2,NDUFB5,NDUFB6,NDUFB8,NDUFS2,NDUFS5,NDUFV3,NEDD4,NFE2L2,NFKB2,NQO1,PCK1,PGK1,PPIF,PRKAA2,PRKDC,RBBP8,SCNN1A,SIRT3,SMARCA5,STAT3,TIMM10,TIMM17B,TIMM8B,TOMM34,TOMM7,TSPO,TUBA1A,TUBA1B,TUBA1C,TUBA4A,UCP2,UQCRC2,VDAC3,WRN,XPC,XRCC6
	Mitochondrial Dysfunction	7.04E+00	NaN	APH1A,ATP5F1B,ATP5F1C,ATP5F1E,ATP5MC2,ATP5MC3,ATP5MF,ATP5MG,ATP5PF,ATP5PO,ATPAF1,COX5A,COX6A1,COX6B1,COX7B,COX8A,CYB5B,CYC1,FURIN,GSR,MT-ND5,MT-ND6,NDUFA1,NDUFA10,NDUFA12,NDUFA13,NDUFA2,NDUFA8,NDUFB1,NDUFB2,NDUFB5,NDUFB6,NDUFB8,NDUFS2,NDUFS5,NDUFV3,RHOT2,TXNRD2,UCP2,UQCRB,UQCRC2,UQCRQ,VDAC3
	Superpathway of Cholesterol Biosynthesis	3.21E+00	2.53	ACAT2,DHCR24,DHCR7,EBP,FDFT1,MVD,NSDHL,PMVK,SC5D,SQLE
	GP6 Signalling Pathway	9.96E-01	-1.147	COL12A1,COL18A1,COL1A1,COL26A1,COL27A1,COL4A3,COL5A1,COL6A2,COL6A3,COL7A1,COL9A3,LAMA5,LAMB3,PIK3C2A,PIK3C3,PIK3R3,PRKCI,RAC1,SYK
	Gluconeogenesis I	9.03E-01	2.236	ENO1,MDH1,MDH2,ME3,PGK1
	Fatty Acid β-oxidation	5.75E-01	NaN	ALDH1A3,ALDH2,ALDH3B1
	Pentose Phosphate Pathway	5.06E-01	NaN	G6PD,TALDO1
	Pyrimidine Deoxyribonucleotides De Novo Biosynthesis I	4.04E+00	0.632	AK7,APOBEC3G,DTYMK,DUT,NME3,NME4,NME7,PCK1,RRM2B,TYMS

IPA Canonical Pathway Analysis was utilised to predict pathway activation based on input transcriptomic data and the Ingenuity Knowledge Base. The *p*-value denotes the significance between the overlap of input experimental data and the knowledge base. Z-scores indicate significance of the activation/inhibition status of each predicted pathway. Statistical analysis was performed using Fisher's Exact testing. Nan = not a number, software could not analyse.

2.4.18. *Oxidative Phosphorylation genes are significantly upregulated in SW837 cells*

As oxidative phosphorylation was predicted to be the most significantly activated pathway in SW837 cells, the specific gene alterations occurring in this pathway were assessed.

In total, 33 genes (31.1%) of the 106 genes associated with oxidative phosphorylation in the Ingenuity Knowledge Base were demonstrated to be significantly upregulated in SW837 cells, when compared to HCT116 cells (**Fig. 2.20**). Two oxidative phosphorylation genes (1.96%) (NDUFA13 and MT-ND5) were significantly downregulated in SW837 cells, when compared to HCT116 cells (**Fig. 2.21**).

IPA Molecule Activity Predictor (MAP) analysis was applied to these specific gene alterations in the oxidative phosphorylation pathway to predict and display the activation of oxidative phosphorylation in SW837 cells, when compared to HCT116 (**Fig. 2.21**). Significant upregulation and activation of Complexes III, IV and V were observed in SW837 cells, when compared to HCT116 cells (**Fig. 2.21**). No significant alterations in Complex II gene activation were demonstrated. Alterations to Complex I activation were predicted, however as genes of complex I were both upregulated and downregulated in SW837 cells, activation of Complex I cannot be objectively predicted (**Fig. 2.21**).

Together, these data support the upregulation of oxidative phosphorylation in radioresistant SW837 cells, when compared to radiosensitive HCT116 cells, and support *in vitro* functional analysis data (**Sections 2.4.9 and 2.4.10**) demonstrating an enhanced reliance on elevated oxidative phosphorylation in radioresistant SW837 cells.

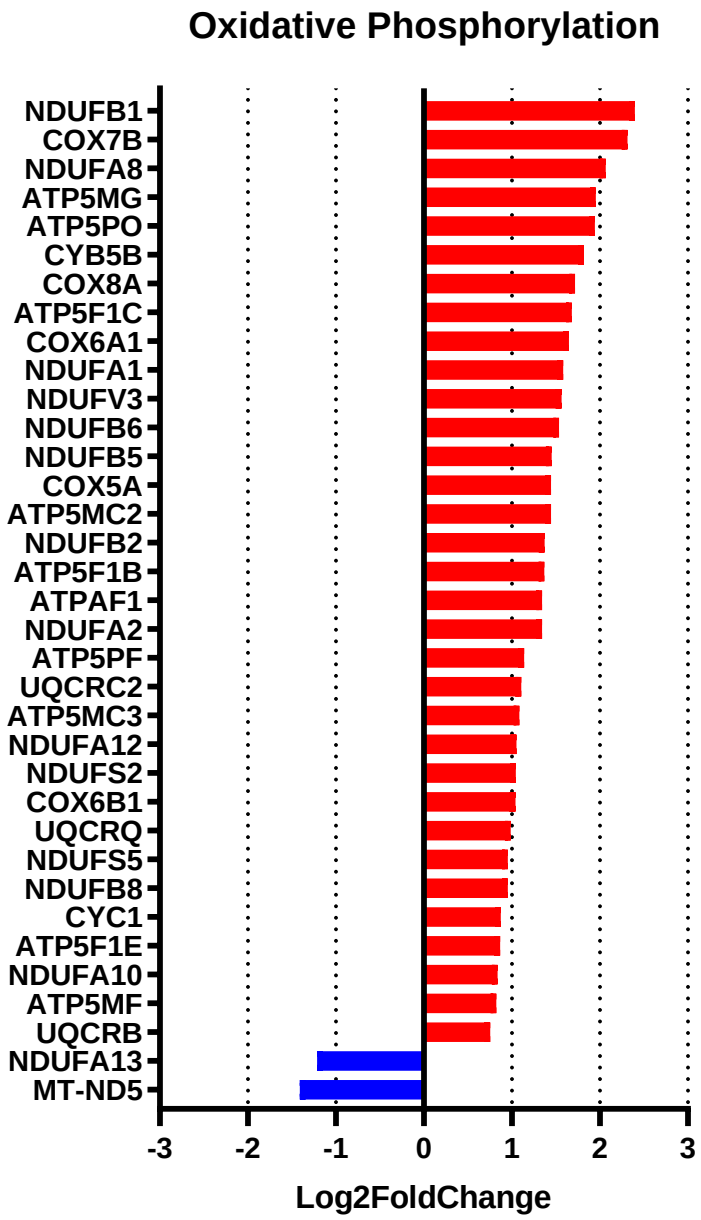

Fig. 2.20: **Oxidative Phosphorylation genes are upregulated in SW837 radioresistant cells, when compared to HCT116 cells.** Transcriptomic profiling was conducted on HCT116 and SW837 cells, and differential expression analysis was performed using BlueBee™ software and DESeq2 R script extensions. Genes in red are significantly upregulated in SW837 cells, when compared to HCT116 cells, while genes in blue are significantly downregulated in SW837 cells, when compared to HCT116 cells. Data is presented as Log_2 Fold Change for 3 (HCT116) or 4 (SW837) independent experiments. Statistical analysis was performed using the Wald test, with corrections for multiple comparisons performed by the Benjamini-Hochberg correction (FDR). Significance was classified as *p*-adj < 0.05.

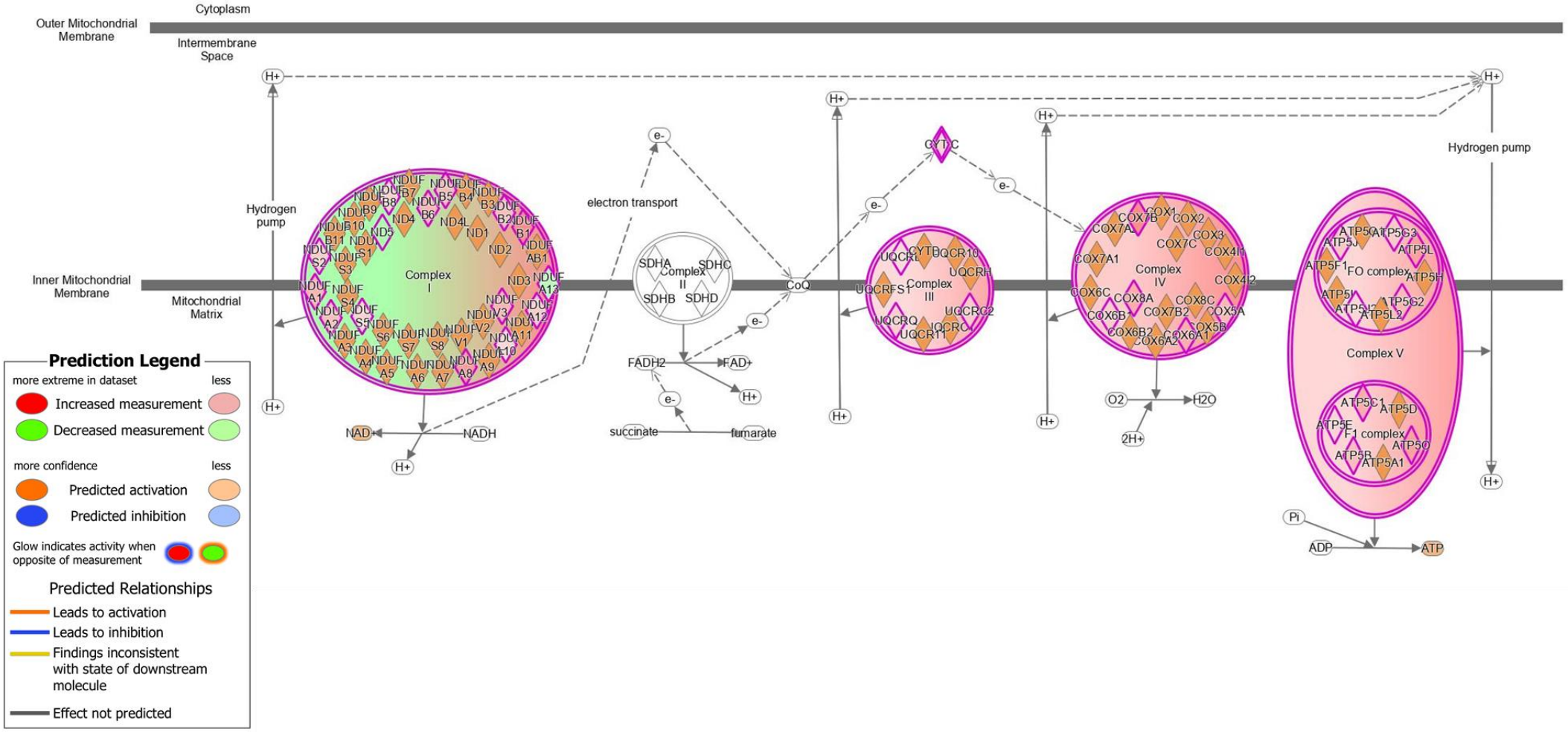

Fig. 2.21: **Oxidative phosphorylation is significantly altered at the transcriptome level in SW837 cells, when compared to HCT116 cells.** IPA MAP software analysis was performed on significantly altered genes in SW837 cells. Oxidative phosphorylation was demonstrated to be significantly upregulated in SW837 cells, when compared to HCT116 cells. An increasing red colour indicates an increasing measurement in the uploaded dataset, while an increasing green colour indicates a decreasing measurement in the uploaded dataset. Orange colour denotes predicted activation of enzymes, and blue colour indicated predicted inhibition of enzymes, based on IPA Knowledge base, and uploaded dataset.

2.5. Summary of main findings of Chapter 2

- HCT116 colon cancer cells are significantly more radiosensitive, when compared to all rectal cancer cell lines profiled (SW837, HRA-19 and SW1463).
- HCT116 cells display a higher proliferative capacity, a more radiosensitive basal cell cycle distribution, and induce G2/M arrest earlier following irradiation with clinically-relevant doses of X-ray radiation, when compared to radioresistant SW837 cells.
- SW837 radioresistant rectal cancer cells display increased resistance to 5-FU, enhanced repair of IR-induced DNA damage, and a reduced reliance on glycolysis when compared to radiosensitive HCT116 colon cancer cells.
- The basal transcriptome is significantly altered in radioresistant SW837 cells, when compared to radiosensitive HCT116 cells.
- IPA analysis revealed significant alterations in pathways commonly associated with radioresponse, in SW837 cells including cell cycle, DNA damage repair, oxidative stress and metabolism.
- Transcriptomic profiling demonstrated that genes involved in oxidative phosphorylation were significantly upregulated in SW837 cells, when compared to HCT116 cells.

2.6. Discussion

This chapter aimed to identify an *in vitro* model of radioresistant and radiosensitive rectal cancer, and to characterise this model to identify underlying mechanisms of radioresistance in rectal cancer.

The majority of studies investigating rectal cancer *in vitro,* use cell lines originally derived from primary colon cancers, not rectal tumours. Although rectal cancer cell lines are available, rarely are they utilised and reported on in publications investigating radioresistance. Colon and rectal cancers are not only anatomically distinct diseases, but there are different underlying molecular mechanisms contributing to both conditions (32-34). In addition, colon cancer and rectal cancer have different standards of care, with radiation being a mainstay of rectal cancer treatment, but rarely being utilised in the management of colon cancer. To counteract these studies, we characterised a panel of rectal adenocarcinoma cell lines (SW837, SW1463 and HRA-19) and a commonly utilised and well characterised colon adenocarcinoma model (HCT116) in terms of radioresistance, with the aim of identifying a

radioresistant and radiosensitive rectal cancer cell line that could be utilised as an *in vitro* model of inherent radioresistance. Rectal adenocarcinoma cell lines, SW837, HRA-19 and SW1463 were demonstrated to be significantly more resistant to X-ray radiation, when compared to radiosensitive HCT116 colon cancer cells. Rectal cancer cell lines were all demonstrated to be similarly resistant to X-ray irradiation. Thus, HCT116 colon cancer cells were chosen as a model of inherently radiosensitive CRC and SW837 rectal cancer cells were chosen as a model of inherently radioresistant rectal cancer for further investigation.

A limitation to investigating mechanisms of radioresistance using cell lines of different origin is that the inherent genetic variability between cell lines may make it difficult to determine the contribution of any identified factors in determining cellular radiosensitivity. Isogenic cell lines aim to mitigate the contribution of this inherent genetic variability while investigating pathways contributing to radioresistance. Various approaches have been previously utilised to generate isogenic models of radioresistance (339, 340). In this study, three clinically-relevant fractionated X-ray radiation treatment regimens were utilised in an attempt to generate an *in vitro* isogenic model of radioresistant CRC using HCT116 and SW837 cell lines. Unfortunately, none of the three regimens examined resulted in the emergence of a radioresistant subline. In the literature, isogenic models of radioresistant HCT116 were previously generated via exposure to fractionated doses of radiation therapy (342). In this study, conducted by Shang et al., HCT116 were exposed to fractionated doses of 4 Gy radiation, until a total of 40 Gy was delivered, culminating in the generation of HCT116-R, an isogenic model of radioresistance (342). However, in this study, the dose of 4 Gy radiation, does not reflect either long-course radiation (delivered in 1.8 Gy fractions) or short-course radiation (delivered in 5 Gy fractions) routinely delivered to patients, reducing the clinical relevance.

While isogenic models of radioresistance do have many advantages over using cell lines of different origin, there are also limitations to the use of isogenic models. Isogenic models are models of acquired radioresistance, which does not reflect the clinical challenge of inherent radioresistance in patient tumours. In addition, while for many studies, the elimination of genetic variability by using matching parental and isogenic cell lines may be beneficial, the genetic variation between cell lines isolated from different patients, may more accurately reflect the genetic variability observed between patients. This variation may aid in the identification of accurate biomarkers, which emerge despite inter-patient genetic

variability. Furthermore, biomarkers of inherent radioresistance would also be of clinical benefit, as they would be used prior to initiation of treatment in patients, enabling enhanced patient stratification.

HCT116 and SW837 cells were utilised as a model of inherently radiosensitive and radioresistant CRC throughout the remainder of this study. Having demonstrated that SW837 rectal cancer cells are more radioresistant, when compared to HCT116 cells, the chemosensitivity of this model was assessed by clonogenic assay. 5-FU is a mainstay of colon and rectal cancer treatment, and so the chemosensitivity to 5-FU treatment was investigated. In addition to being more radioresistant, SW837 rectal cancer cells were demonstrated to be more resistant to 5-FU-induced cytotoxicity at 30 h and 48 h, when compared to HCT116 sensitive cells. This supports the SW837 cells as a highly treatment-resistant model of rectal cancer, supporting previous findings (355, 356).

To identify potential mechanisms underlying the radioresistance of SW837 cells, the inherent model of radioresistance (HCT116 and SW837 cells) was characterised in terms of multiple parameters implicated in radioresistance.

HCT116 radiosensitive cells were demonstrated to display elevated proliferative rates, when compared to radioresistant SW837 cells. Cells with a high proliferative rate, are often the most sensitive to cancer therapeutics. For example, elevated Ki67, which reflects cellular proliferation, is demonstrated to be significantly associated with enhanced sensitivity to radiation therapy in many cancers including small-cell lung cancer (357) and oral squamous cell carcinoma (358). These data suggest that an elevated proliferative rate may contribute to the radiosensitivity of HCT116 cells.

Basal cell cycle phase distribution was also demonstrated to be significantly altered between radioresistant SW837 cells and radiosensitive HCT116 cells. SW837 cells displayed an elevated proportion of cells in the G0/G1 and S phases, when compared to HCT116 cells. Importantly, the S phase of the cell cycle is the most radioresistant phase (52). Furthermore, SW837 cells display a lower proportion of cells in the G2/M phase basally, when compared to radiosensitive HCT116 cells. The G2/M phase is the most radiosensitive phase of the cell cycle (52). Importantly, these data suggest that the basal cell cycle phase distribution may play an important role underlying the radioresistance of SW837 cells.

Cell cycle progression in response to radiation exposure was also demonstrated to differ between radioresistant SW837 and radiosensitive HCT116 cells. At 10 h post irradiation,

HCT116 cell cycle distribution was altered in response to exposure to both 1.8 Gy and 5 Gy clinically-relevant radiation doses. Following irradiation, a reduction in both G0/G1 and S phase cells and an increase in the proportion of G2/M phase cells was observed in HCT116 cells. This reflects activation of cell cycle checkpoints and a G2/M arrest, which is utilised by cells to attempt to repair irradiation-induced DNA damage. This early induction of G2/M arrest may reflect the radiosensitivity of this cell line. In comparison, at 10 h post irradiation, no cell cycle distribution alterations were observed in radioresistant SW837 cells, perhaps reflecting the resistance of these cells to radiation. In SW837 cells, at 24 h post irradiation, the only effect of irradiation exposure was observed, with increased G2/M cells and a trend towards reduced G0/G1 phase cells following treatment with 5 Gy radiation only. This delayed G2/M arrest, only in response to 5 Gy irradiation, and not 1.8 Gy irradiation may reflect the radioresistant phenotype in the SW837 cells. G2/M arrest or blockade is considered to act as an indicator of inherent radiosensitivity (359).

DNA damage, as measured by γH2AX fluorescence by flow cytometry, was demonstrated to be significantly induced at 20 min post exposure to both 1.8 Gy and 5 Gy irradiation in both HCT116 and SW837 cells. Although direct statistical comparisons cannot be made between MFI of HCT116 and SW837, these data seem to indicate that initial susceptibility to radiation-induced DNA DSBs is similar and does not contribute to the differential radioresponse in these cell line models. However, this DNA damage persisted at 6 h, 10 h and 24 h post irradiation in radiosensitive HCT116 cells. In comparison, DNA damage induced by 1.8 Gy irradiation was completely resolved in SW837 cells by 6 h post irradiation, and by 10 h post irradiation DNA damage from 5 Gy irradiation is completely resolved. These data indicate that SW837 radioresistant rectal cancer cells have enhanced repair of IR-induced DNA damage, when compared to HCT116 cells, and that this DNA damage repair may contribute to the inherent radioresistance of this model. These data may also suggest impaired DNA damage repair in HCT116 cells, which is supported by the early and sustained high levels of G2/M arrest observed in the cell cycle investigations (360). Enhanced DNA damage repair capacity is one of the most common features of radioresistant cells, as DSBs are the most critical form of direct radiation induced damage (361).

Exposure to radiation did not induce any apoptosis or necrosis in radioresistant SW837 cells. However, a small increase in the percentage of late apoptotic cells in the HCT116 radiosensitive cells was observed at 24 h following exposure to 5 Gy irradiation, although this

was a increase of only 3%, and therefore may not be clinically relevant. Furthermore, a trend toward increased percentage of cells which were early apoptotic and late apoptotic was demonstrated at 48 h post exposure to 5 Gy irradiation in HCT116 cells. The role of apoptosis in radioresistance is controversial (59), and further assessment of apoptosis by caspase assays or western blot would be necessary to make a conclusion on the potential role of apoptosis in radioresistance in this model.

Seahorse metabolic profiling demonstrated significant differences in the basal metabolic pathway reliance between SW837 and HCT116 cells. SW837 cells were demonstrated to display lower levels of glycolysis, when compared to HCT116. Furthermore, an elevated OCR:ECAR ratio was demonstrated in SW837 cells, which indicates that these cells rely less on glycolysis and therefore more on oxidative phosphorylation, when compared to radiosensitive HCT116 cells. In addition, a mitochondrial metabolic parameter, spare respiratory capacity was demonstrated to be significantly elevated in the SW837 cells, when compared to HCT116 cells. Spare respiratory capacity reflects the ability of a cell to responds to energy demand or stress, such as radiation, and may support the radioresistant phenotype of these cells. In addition, no differences were observed in mitochondrial function between these two cell lines, indicating that these metabolic differences are not simply attributable to increased mitochondrial function or mass. These data support previous research in our department, which demonstrated enhanced reliance on oxidative phosphorylation in radioresistant models of oesophageal adenocarcinoma (212, 213). Furthermore, other mechanisms of radioresistance demonstrated to be altered in SW837 cells, such as cell cycle and DNA damage repair, are dependent on energy metabolism. Therefore, energy metabolism may be a fundamental determinant of radioresistance.

Transcriptomic profiling of both HCT116 and SW837 cells revealed significant differences between the transcriptome of the two cell line models. IPA pathway analysis demonstrated multiple biological functions differing between HCT116 and SW837 cells, including cell death, cellular proliferation and cell cycle. Canonical pathway analysis revealed further information on specific pathways differing between HCT116 and SW837 cells. Alteration in cell cycle related genes were demonstrated, including differential expression of checkpoint related genes, cyclins and cell cycle regulation. These data support the *in vitro* data from functional experiments that demonstrated altered basal cell cycle distribution and progression in HCT116 and SW837 cells. Furthermore, DNA damage repair pathway related

genes were demonstrated to be significantly altered between HCT116 and SW837 cells, with enhanced BER and NER pathway activation in SW837 cells, when compared to HCT116 cells, supporting the data demonstrating enhanced repair of IR-induced DNA damage in SW837 cells.

Importantly, many metabolism-related canonical pathways were demonstrated to be altered at the transcriptome level between HCT116 and SW837 cells. Oxidative phosphorylation was the most significantly upregulated canonical pathway in SW837 cells. In total 33 oxidative phosphorylation genes were demonstrated to be significantly upregulated in radioresistant SW837 cells, when compared to HCT116 cells. These data support the functional experimental findings in which the OCR:ECAR ratio of SW837 cells was demonstrated to be significantly higher than HCT116 cells, indicating an increased reliance on oxidative phosphorylation. These data also support previous findings in OAC, which demonstrate enhanced oxidative phosphorylation being associated with a radioresistant phenotype (212, 213).

In addition, as the results of a number of the functional analyses were supported by transcriptomic profiling, including altered cell cycle and metabolism as potential contributing factors to the differing radioresponse between HCT116 and SW837 cells, these data highlight the importance of combined transcriptomic and functional analysis. Furthermore, the congruence between these functional and transcriptomic findings aids in the validation of experimental findings. In addition, these data demonstrate that transcriptomic analysis may assist in the identification of novel gene biomarkers predictive of radioresponse in rectal cancer.

This chapter identified an *in vitro* model of inherently radioresistant and chemoresistant rectal cancer. Characterisation of this model, demonstrated alterations in basal cell cycle distribution, cell cycle response to radiation, radiation-induced DNA damage repair, apoptosis and energy metabolism. These findings were supported by transcriptomic profiling. Together, these data suggest a potential role for these mechanisms in the radioresistance of rectal cancer. Importantly, microenvironmental conditions in a tumour can be variable and play a crucial role in therapeutic response (362). The next chapter investigates the effect of hypoxia on this model of radioresistance, to assess the impact of the tumour microenvironment on the radioresponse.

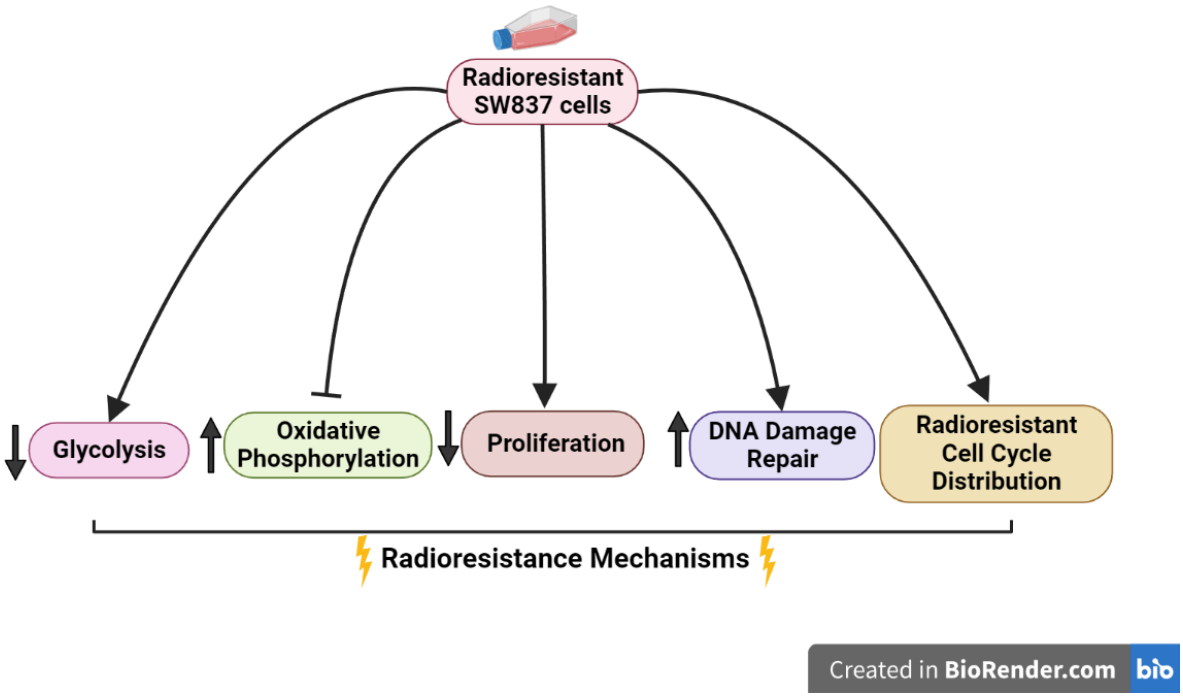

Fig. 2.22: **Summary of main findings of chapter 2.** SW837 rectal cancer cells were demonstrated to be significantly more radioresistant, when compared to HCT116 colon cancer cells. Characterisation of this radioresistant model, when compared to radiosensitive HCT116 cells revealed several potential mechanisms of radioresistance in SW837 cells. SW837 cells were demonstrated to display elevated reliance on oxidative phosphorylation, by real-time metabolic profiling, and supported by transcriptomic analysis. In addition, radioresistant SW837 cells displayed slower basal proliferative rates, and enhanced DNA damage repair following radiation treatment, when compared to radiosensitive HC116 cells. SW837 cells displayed a more radioresistant basal cell cycle distribution. Figure created with BioRender.com.

Chapter 3: Characterisation of an *in vitro* model of radiosensitive and radioresistant colorectal cancer under hypoxia (0.5% O_2)

3.1. Introduction

Hypoxia is a common feature of many solid malignancies, and is often associated with larger, more aggressive tumours. Importantly, hypoxia has been highlighted as a major mechanism for the development of resistance to many cancer therapies, particularly radiation therapy (231).

Hypoxia-inducible factor alpha (HIF-1α), the major mediator in hypoxia, displays a progressive increase in expression along disease progression in many cancers, including CRC (137-144), gastric and oesophageal cancers (145). In addition, elevated HIF-1α expression is associated with poor clinical outcomes in cancer, such as CRC (143, 146), oesophageal (147, 148) and gastric cancers (145). Overexpression of HIF-1α is also associated with poorer survival in oesophageal squamous cell carcinoma patients receiving adjuvant chemotherapy (148). In a study conducted by Shioya *et al.*, HIF-1α expression was predictive of response to hyperthermo-chemoradiotherapy (HCRT) in a cohort of 50 rectal cancer patients with advanced disease (149). Importantly, RFS was reported as 82.8% in the HIF-1α negative group, compared to 47.8% in those with positive HIF-1α expression, suggesting strong prognostic potential in rectal cancer (149).

One of the major mechanisms believed to contribute to the association between hypoxia and radioresistance, is the requirement of oxygen to fix indirect DNA damage induced by radiation exposure, and free radical generation, which contributes to an estimated 70% of radiation-induced damage. Hypoxic conditions have a limited availability of oxygen for such damage fixation. Consequently, a hypoxic tumour microenvironment permits the repair of IR-induced damage, resulting in resistance to radiation treatment (151). Furthermore, hypoxic exposure is also implicated in cell cycle control, with hypoxia demonstrated to induce cell cycle arrest in G1 and G2 phases, to facilitate repair of DNA damage, and induce resistance to cancer therapy (363).

Hypoxia has been demonstrated to have a multi-faceted effect on apoptosis in cancer cells. Non-adaptive cancer cells have been demonstrated to undergo apoptosis when under hypoxic conditions (364). However, oxygen deprivation in colon cancer cells has been demonstrated to significantly reduce mRNA and protein levels of pro-apoptotic proteins (136). Whether cancer cells can adapt to a hypoxic microenvironment can have a major impact on the therapeutic response. For example, HIF-1α expression has been demonstrated to enhance chemotherapy-induced apoptosis in colon cancer cells (150). Furthermore, inhibition of HIF-

1-mediated apoptosis has also been implicated in resistance to 5-FU and cisplatin treatment in gastric cancer cells (365).

Reduced oxygen availability and upregulation of HIF-1α are intrinsically linked to the regulation of metabolic pathways (223-225). In regions of low oxygen availability, cells adapt to conserve oxygen, by downregulating oxidative respiration and oxygen-linked ATP production. This is primarily mediated by the inhibition of complex IV of the electron transport chain, via the activation of the HIF-1 transcription factor (226). In addition to the inhibition of mitochondrial oxidative respiration, cancer cells are forced to upregulate glycolysis for energy production via the activation of HIF-1α (226). HIF-1α has been demonstrated to upregulate the transcription of most glycolytic genes, including GLUT-1, the major glucose transporter and other glycolytic enzymes (157, 223, 227). In addition, HIF-1α induces the upregulation of genes involved in the pentose phosphate pathway, increasing the generation of anabolic intermediates required for cell growth and antioxidant capacity (223). Furthermore, lactate and pyruvate generated as a result of increased glycolytic flux promote the accumulation of HIF-1α, regardless of oxygen availability status, to create a feed-forward mechanism between glycolytic and HIF-1 signalling (225, 228, 229). In this way, cancer cells hijack the inherent metabolic response of cells to hypoxia in order to proliferate and survive anti-cancer therapy. As resistance to therapy is a major clinical issue in the management of rectal cancer, and having demonstrated metabolic alterations between the *in vitro* model of radiosensitive and radioresistant CRC in normoxic conditions in Chapter 2, the impact on hypoxia on metabolism in this model was assessed in this chapter.

3.2. Overall Objective and Specific Aims of Chapter 3

In this chapter, the *in vitro* model of inherent radioresistant/radiosensitive CRC was characterised under hypoxic conditions, to better reflect the tumour microenvironment. The model was characterised in terms of:

- Radioresistance
- Chemoresistance
- Apoptosis basally and following X-ray radiation
- Cell cycle basally and following X-ray radiation
- DNA damage induction and repair following X-ray radiation
- Energy metabolism
- Mitochondrial function
- ATP production

3.3. Materials and Methods

3.3.1. *Reagents and materials*

Laboratory chemicals and reagents were stored according to the manufacturer's instructions. All cell culture reagents were purchased from Gibco, unless otherwise stated. All plastic materials were purchased from Sarstedt unless otherwise stated.

3.3.2. *Cell culture*

Cell culture was carried out as per **section 2.3.2**.

3.3.2.1. *Human colorectal adenocarcinoma cell lines*

The SW837 rectal adenocarcinoma and the HCT116 colon adenocarcinoma cell lines were utilised in this study. The SW837 rectal cancer cell line originated from a stage IV rectal adenocarcinoma from a 53-year-old Caucasian male. Culture conditions are outlined in **section 2.3.2.1**.

3.3.2.2. *Cell line subculturing*

Cell line subculturing was performed as previously described in **section 2.3.2**.

3.3.3. *Hypoxia treatment*

Experiments conducted under hypoxic conditions utilised the H35 Whitley hypoxystation (Don Whitley Scientific), at 37°C, 5% CO_2/0.5% O_2. All plasticware and medium required was deoxygenated by placing in the chamber 24 h prior to use in experiments, to prevent oxygen contamination.

3.3.4. *X-ray radiation*

All irradiations were performed using an X-Strahl cabinet X-ray irradiator (RS225) (X-Strahl) at a dose rate of 1.74 Gy/min, as previously described (**Section 2.3.3.**) Cells to be irradiated under hypoxic conditions were exposed to X-ray radiation in air-locked containers (Don Whitley Scientific).

3.3.4.1. *Clonogenic assessment of radiosensitivity under hypoxia (0.5% O_2)*

As described in **section 2.3.4,** cells in the exponential growth phase were harvested, seeded into 6-well plates at optimised cell densities and allowed to adhere to the plate at 37°C in 5% CO_2/95% atmospheric air. Following 6 h incubation, plates were transferred into a Whitley H35 hypoxystation (Don Whitley Scientific) at 37°C in 0.5% O_2/5% CO_2. Normoxic plates remained incubated at 37°C in 5% CO_2/95% atmospheric air (~ 21% O_2). Following 24 h incubation under normoxic or hypoxic conditions, plates remained under either normoxia or hypoxia and medium was removed from cells to waste, and the RPMI replaced. Importantly,

cells under hypoxia were treated with deoxygenated RPMI, which had been placed in the hypoxystation 24 h prior to treatment, in a vented flask. The following day, cells were exposed to clinically-relevant doses of 1.8 Gy, 5 Gy X-ray radiation, or mock-irradiated, as described (**Section 3.3.4).** Hypoxic cells were irradiated under hypoxic conditions using air-locked containers. Following 24 h incubation post-irradiation, cells were removed from hypoxic conditions, the media removed, and replenished with 1.5 mL/well normoxic RPMI. Cells were incubated at 37°C in 5% CO_2/95% atmospheric air for 7-14 days. Colonies were fixed and counted as described in **sections 2.3.4.2 and 2.3.4.3.**

3.3.4.2. *Clonogenic assessment of 5-Fluorouracil sensitivity under hypoxia (0.5% O_2)*

Cells were harvested by trypsinisation and seeded into 6-well plates at optimised densities (**section 2.3.4**) and allowed to adhere at 37°C in 5% CO_2/95% atmospheric air. At 6 h post seeding, cells to be cultured under hypoxic conditions were transferred to a Whitley H35 hypoxystation at 37°C in 0.5% O_2/5% CO_2. Normoxic plates remained incubated at 37°C in 5% CO_2/95% atmospheric air (~ 21% O_2). After 24 h under hypoxia, medium was removed to waste and cells were treated with 1.5 mL of 15 µM 5-FU, or DMSO vehicle control for 30 h, under hypoxic or normoxic conditions, as appropriate. The 5-FU was then removed and replaced with 1.5 mL / well RPMI. All cells were then incubated at 37°C in 5% CO_2/95% atmospheric air, for 7-14 days. Colonies were fixed and counted as described in **sections 2.3.4.2 and 2.3.4.3**.

3.3.5. *Annexin-V/Propidium Iodide (PI) analysis of apoptosis by flow cytometry under hypoxia (0.5% O_2)*

Cells in the exponential growth phase were harvested, counted and seeded in 12-well plates at 1 mL per well as previously described (**Sections 2.3.2.2 and 2.3.2.5**) (HCT116 at 150,000 and SW837 at 200,000 cells per well). Cells were allowed to adhere for 6 h at 37°C at 5% CO_2/95% atmospheric air. Cells to be cultured under hypoxic conditions were then transferred to a Whitley hypoxychamber at 37°C at 5% CO_2/0.5% O_2, while normoxic cells remained at 37°C at 5% CO_2/95% atmospheric air. At 24 h post hypoxic exposure, media was removed and replaced with 1 mL normoxic/ hypoxic RPMI. Twenty-four hours later, cells were mock-irradiated or exposed to 1.8 Gy X-ray radiation, while remaining under normoxia or hypoxia conditions (**section 3.3.4**). At this timepoint, and at 24 and 48 h post irradiation, cells and supernatants were transferred to 5 mL flow tubes, by trypsinisation (**section 2.3.2.2**) and stained with Annexin-V-FITC or PI as described in **section 2.3.10**. Stained samples were acquired using a

FACS Canto II flow cytometer (BD Biosciences), acquiring 40,000 events per tube. Data was analysed by FlowJo™ version 10.6.2 software.

3.3.6. *Assessment of cell cycle and DNA damage under hypoxia (0.5% O_2).*

Cells in the exponential growth phase, were harvested by trypsinisation, counted and seeded into 12-well plates (HCT116: 150,000 cell/well, SW837 200,000 cell/well) as previously described **Sections 2.3.2.2 and 2.3.2.5**. Cells were allowed to adhere overnight at 37°C in 5% CO_2/95% atmospheric air. Cells for hypoxic culture were transferred to a Whitley H-35 hypoxychamber at 37°C in 5% CO_2/0.5% O_2, while normoxic cells remained at 37°C in 5% CO_2/95% atmospheric air. At 24 h post hypoxic exposure, medium was removed and replaced with 1 mL complete RPMI per well. Twenty-four hours later, cells were mock-irradiated or exposed to clinically-relevant 1.8 Gy X-ray radiation, under normoxic or hypoxic conditions, as appropriate (**section 3.3.4**). At 20 min, 6 h, 10 h, or 24 h post-irradiation, cells were collected into 5 mL flow tubes, and stained with γH2AX-Alexa 488 or PI, as previously described (**section 2.3.11**). Samples were acquired, with a minimum of 10,000 events collected, excluding doublets, using the FACSCanto II flow cytometer (BD Biosciences). γH2AX-AlexaFluor-488 was measured on the FITC channel, while PI was measured on the PerCP-Cy5 channel. Data were analysed using FlowJo™ Version 10.6.2.

3.3.7. *Live-cell metabolic assessment under hypoxia (0.5% O_2)*

HCT116 and SW837 cells were seeded at 15,000 or 30,000 cells/well respectively in 24-well cell culture XFe microplates (Seahorse Technologies, Agilent) in a volume of 100 µL. Cells were allowed to adhere for 6 h at 37°C at 5% CO_2/95% atmospheric air. An additional 150 µL RPMI was added to each well, and cells cultured under hypoxic conditions were transferred to a H35 Whitley hypoxystation at 37°C in 5% CO_2/0.5% O_2, while cell cells for normoxic culture remained at 37°C in 5% CO_2/95% atmospheric air over night. Following 24 h, medium was removed and replaced with 250 µL RPMI, under normoxic or hypoxic conditions, as appropriate. Following 24 h, media was removed and cells were washed with Seahorse basal DMEM, supplemented with 10 mM glucose, 10 mM sodium pyruvate and L-glutamine, and incubated at 37°C in a non-CO_2 incubator for 1 h. OCR and ECAR were assessed using a Seahorse Biosciences XFe24 analyser, under either normoxic or hypoxic (0.5% O_2) conditions, located in the i2 Whitley hypoxystation. Three basal OCR and ECAR measurements were taken in three repeats of mix (3 min), wait (2 min) and measure (3 min). These readings were repeated following the injection of a series of mitochondrial inhibitors, oligomycin-a, FCCP and

antimycin A, as previously described in **section 2.3.6.** Data was then normalised to the crystal violet assay, as described in **section 2.3.9**.

3.3.8. *Assessment of mitochondrial function under hypoxia (0.5% O_2)*

HCT116 and SW837 cells were seeded at 15,000 or 30,000 cells per well, in 100 µL RPMI. Cells were allowed to adhere at 37°C in 5% CO_2/95% atmospheric air. After 6 hours, cells for hypoxic culture were transferred to the Whitley H35 hypoxystation at 37°C in 5% CO_2/0.5% O_2, while cells to be cultured under normoxia remained at 37°C in 5% CO_2/95% atmospheric air. Following 48 h, mitochondrial mass, ROS production and mitochondrial membrane production were assessed using fluorescent probes, 2,7 dichlorofluorescein (DCF), Rhodamine-123 and MitoTracker Green^{FM}, while under normoxic or hypoxic conditions. Medium was removed, and cells were incubated with a fluorescent probe in PBS (Mg^{2+}) for 30 min in the dark at 37°C. The probe was removed and replaced with 100 µL PBS, and the fluorescence measured using a FLx800 microplate reader (Mason Technology). Data was normalised to crystal violet readings as described in **section 2.3.9**.

3.3.9. *ATPlite under hypoxia (0.5% O_2)*

ATP levels were assessed using the ATPlite luminescence ATP detection assay system (Perkin Elmer). Cells were seeded in triplicate in a white-walled 96-well plate, and also into a standard 96-well plate for normalisation and placed at 37°C in 5% CO_2/95% atmospheric air. At 6 h post seeding, cells to be cultured under hypoxic conditions were transferred to the Whitley H35 hypoxystation at 37°C in 5% CO_2/0.5% O_2, while cells to be cultured under normoxia remained at 37°C in 5% CO_2/95% atmospheric air. After 24 h, medium was removed to waste and replaced with 100 µL RPMI. Following 24 h, 50 µL of Mammalian Cell Lysis Solution (Perkin Elmer) was added to each well of the white-walled 96-well plate, and incubated on an orbital shaker, for 5 min at 700 rpm at RT°. A volume of 50 µL Substrate Solution (Perkin Elmer) was added to each well of the white-walled plate, and incubated for 5 min at 700 rpm, at RT°. The plate was subsequently dark-adapted for 10 min at RT°. The luminescence was measured for 1 s on a GloMax Explorer luminescent plate reader (Promega). Luminescence was normalised using the crystal violet assay (**Section 2.3.9**) performed on the corresponding standard 96-well plate.

3.3.10. *Statistical analysis*

All statistical analysis and graphing were performed using Graphpad Prism v9 software. Data is presented as mean ± SEM throughout. All statistical comparisons were carried out using

ANOVA testing, post-hoc Tukey's multiple comparisons testing, or *t*-testing, depending on the experimental set up, as described in figure legends. Results were considered significant where probability (*p)* ≤ 0.05.

3.4. Results

3.4.1. *Exposure to hypoxia (0.5% O_2) enhances the radioresistance of SW837 and HCT116 colorectal cancer cells*

To characterise the radiosensitivity of the inherent model of radioresistant and radiosensitive CRC under hypoxic conditions, the inherent radiosensitivity of the HCT116 and SW837 cells irradiated at 0 Gy, 1.8 Gy, and 5 Gy X-ray radiation under hypoxic conditions (0.5% O_2) was assessed using the gold-standard clonogenic assay.

Following irradiation with 5 Gy X-ray radiation, radiosensitive HCT116 cells were demonstrated to be significantly more resistant to radiation under hypoxic conditions (0.5% O_2), when compared to normoxic conditions (p = 0.0032) (mean SF ± SEM; HCT116 normoxia 5 Gy 3.5 ± 0.52, HCT116 hypoxia 12.36 ± 1.92). Similar surviving fractions were demonstrated following irradiation with 1.8 Gy under hypoxic and normoxic conditions (**Fig. 3.1A**).

No significant alterations in the radiosensitivity of radioresistant SW837 cells were demonstrated following exposure to either 1.8 Gy or 5 Gy radiation under hypoxic conditions (**Fig. 3.1B**), when compared to normoxic conditions**.**

These data demonstrate that hypoxia enhanced the radioresistance of radiosensitive HCT116 colon cancer cells at 5 Gy.

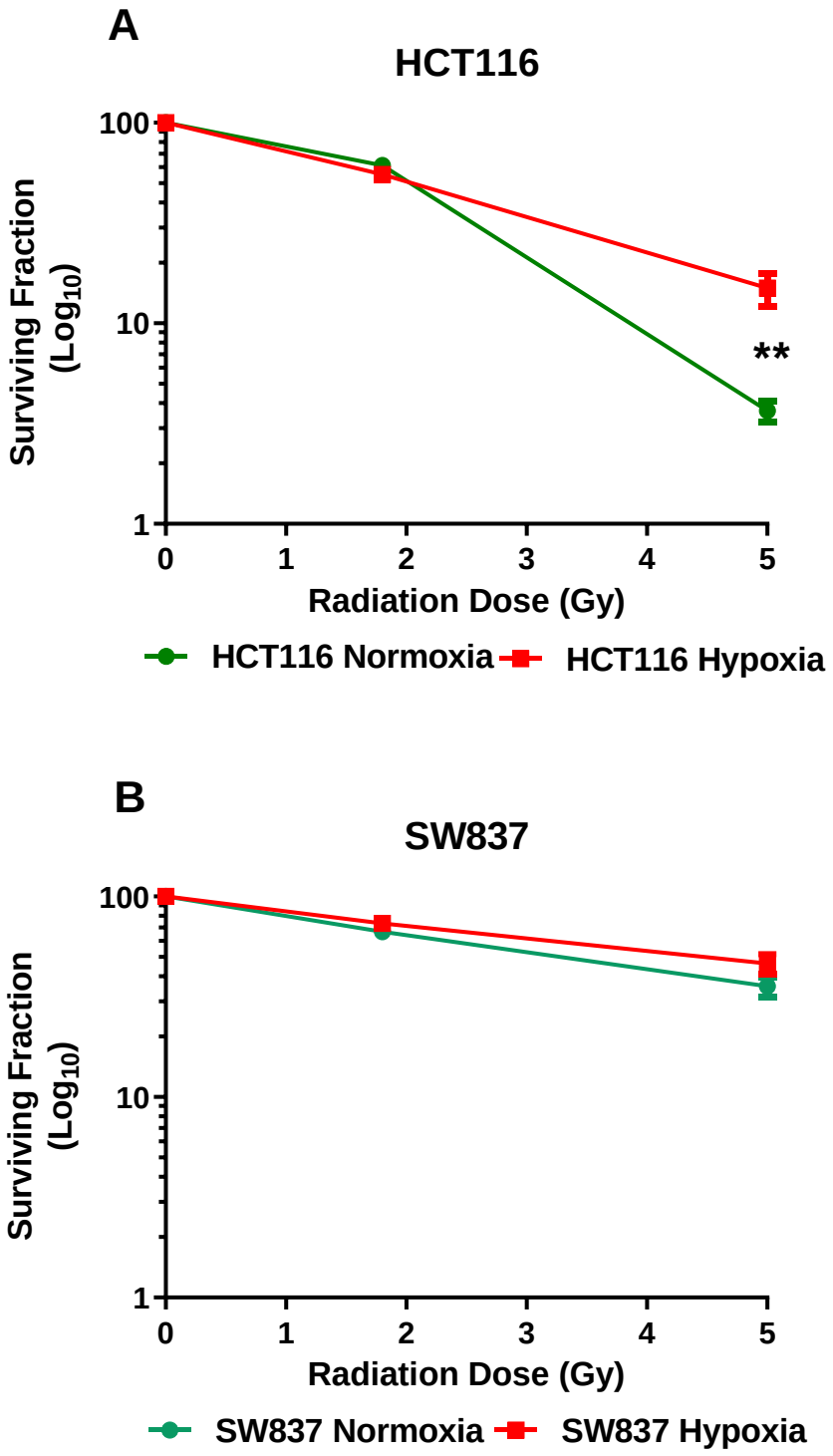

Fig. 3.1: **HCT116 radiosensitive colon cancer cells are more resistant to radiation at 5 Gy under hypoxia (0.5% O_2).** Radiosensitivity was assessed by clonogenic assay under hypoxia and normoxia (21% O_2) following 1.8 Gy and 5 Gy X-ray radiation. Data is expressed as mean ± SEM for 5 (HCT116) or 7 (SW837) independent experiments. Statistical analysis was performed by two-way ANOVA, and post-hoc multiple comparison testing. $^{**}p < 0.01$.

3.4.2. *SW837 cells are more resistant to X-ray radiation in hypoxia conditions when compared to HCT116 cells*

A hypoxic environment is known to contribute to a radioresistance. To determine whether hypoxia altered the inherent radiosensitivity of radiosensitive HCT116 and radioresistant SW837 CRC cells, the gold-standard clonogenic assay was utilised.

Following exposure to a clinically-relevant dose of 1.8 Gy radiation, SW837 rectal cancer cells were significantly more resistant to X-ray radiation, when compared to HCT116 colon cancer cells (p = 0.0284) (Mean SF 1.8 Gy ± SEM; HCT116 55.33 ± 4.8, SW837 73.34 ± 4.84) (**Fig. 3.2**). Furthermore, following 5 Gy irradiation, SW837 cells remain more resistant to irradiation, when compared to HCT116 (p = 0.0009) (Mean SF 5 Gy ± SEM; HCT116 15.07 ± 2.86, SW837 46.34 ± 5.25).

Importantly, these data demonstrate that HCT116 and SW837 cells are a model of radiosensitive and radioresistant CRC under hypoxic conditions.

3.4.3. *HCT116 and SW837 display similar chemosensitivity to 5-FU treatment under hypoxia (0.5% O_2)*

It was previously demonstrated (**Chapter 2, Section 2.4.2**) that radioresistant SW837 rectal cancer cells are also significantly more resistant to 5-FU chemotherapy, when compared to radiosensitive HCT116 cells. To investigate if SW837 cells are more chemoresistant under hypoxia, a clonogenic assay was performed.

As demonstrated in **Section 2.4.2**, HCT116 cells are significantly more sensitive to 5-FU treatment (15 μM for 30 h), when compared to SW837 under normoxic conditions (p = 0.016) (**Fig. 3.3**)**.** However, this effect was lost under hypoxia, with similar surviving fractions demonstrated in SW837 and HCT116 cells (p = 0.398) following 30 h treatment with 5-FU (15 μM) (**Fig. 3.3**)**.** Hypoxia did not significantly alter surviving fraction in either HCT116 (HCT116 Normoxia 88.73 ± 0.7 vs HCT116 Hypoxia 88.55 ± 6.9) or SW387 cells (SF ± SEM SW837 Normoxia 99.83 ± 2.7 vs SW837 Hypoxia 95.22 ± 4.08), relative to their normoxic controls (**Fig. 3.3**). A trend towards a decreased surviving fraction in hypoxic SW837 cells, when compared to normoxia was demonstrated.

These data demonstrate that, under hypoxia, SW837 cells are not more resistant to 5-FU treatment at this timepoint, or this dose, when compared to radiosensitive HCT116 cells.

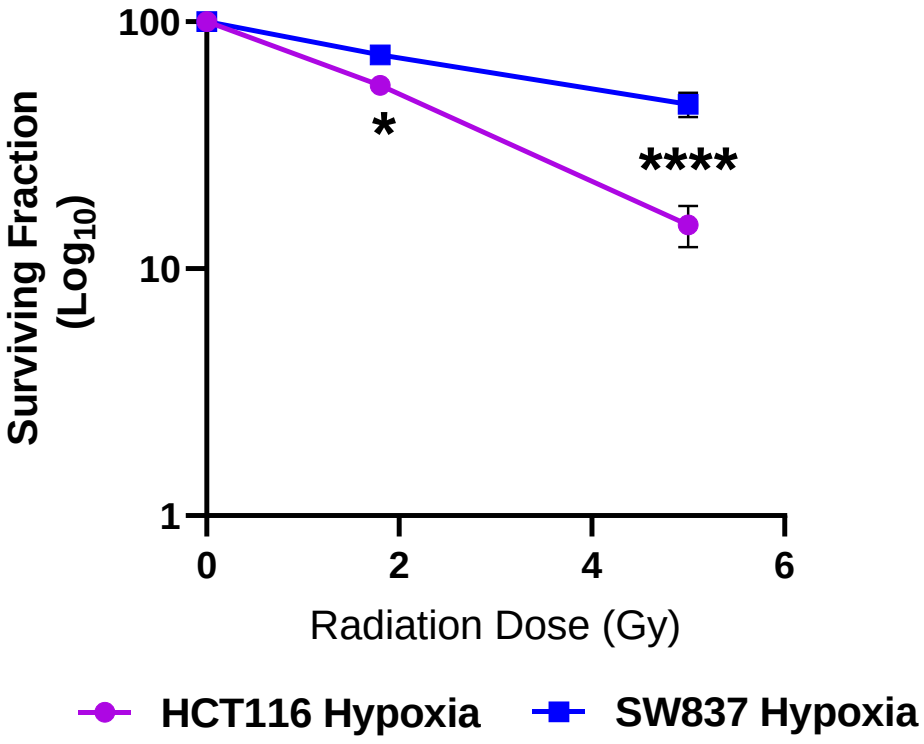

Fig. 3.2: **SW837 rectal cancer cells are significantly more radioresistant, when compared to HCT116 colon cancer cells under hypoxia (0.5% O_2).** Radiosensitivity was assessed by clonogenic assay under hypoxia following 1.8 Gy and 5 Gy X-ray radiation. Data is presented as mean ± SEM for 5 (HCT116) or 7 (SW837) independent experiments. Statistical analysis was performed by two-way ANOVA, and post-hoc multiple comparison testing. *$p < 0.05$, ****$p < 0.0001$.

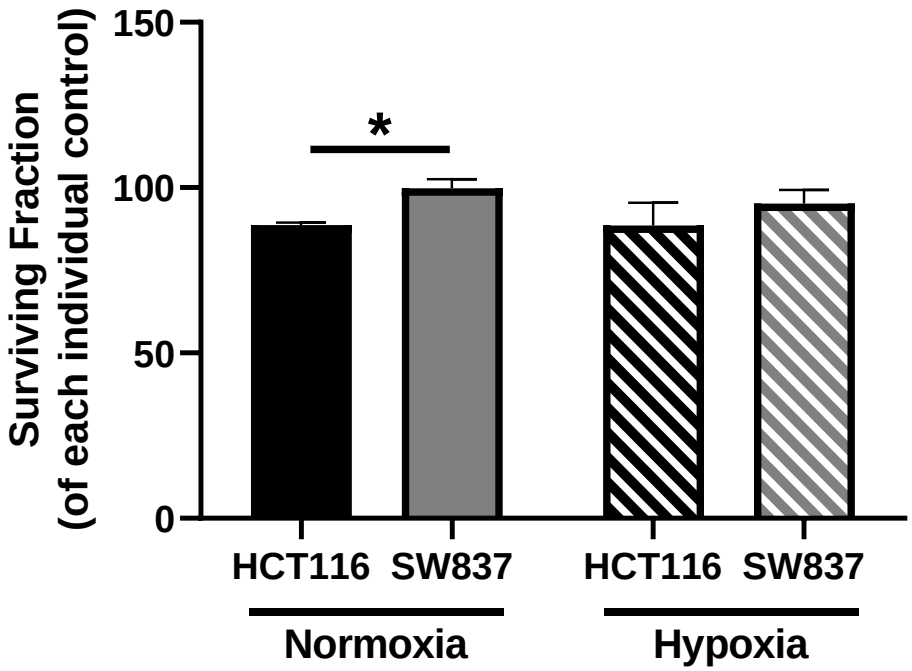

Fig. 3.3: **SW837 and HCT116 cells display similar surviving fraction following 5-FU chemotherapy treatment under hypoxia (0.5% O_2).** Chemosensitivity was assessed by the gold-standard clonogenic assay. Cells were treated for 30 h with 5-FU (15 µM) or DMSO vehicle control under normoxic or hypoxic conditions. Data is presented as mean ± SEM for 3 (HCT116) or 4 (SW837) independent experiments. Statistical analysis was performed using paired/un-paired *t*-testing. *$p < 0.05$.

3.4.4. *Hypoxia (0.5% O_2) induces basal cell death in HCT116 cells*

To investigate the effect of hypoxia on cell death in HCT116 and SW837 cells, apoptosis was assessed by PI and AV-FITC staining and flow cytometry under normoxia and hypoxia.

At 24 h following hypoxic exposure, no differences were demonstrated to the percentage of SW837 live cells, necrotic cells, early apoptotic cells or late apoptotic cells, when compared to cells in normoxia (**Fig. 3.4A-D**). At 24 h post hypoxic exposure, in HCT116 cells, a slight but significant reduction to the proportion of necrotic cells was demonstrated in hypoxia, when compared to normoxia (p = 0.0322) (mean AV- PI+ % cells ± SEM; HCT116 normoxia 2.67 ± 0.49, HCT116 hypoxia 1.25 ± 0.27) (**Fig. 3.4C**).

Furthermore, following 72 h in hypoxia, a significant reduction to the proportion of live cells was demonstrated in HCT116 cells, when comparing unirradiated controls in normoxia, to those in hypoxia (p = 0.048) (mean AV-PI- % cells ± SEM; HCT116 0 Gy normoxia 91.85 ± 1.1, HCT116 0 Gy hypoxia 49.10 ± 13) (**Fig. 3.6A**). Also at this timepoint, hypoxia induced a significant increase to the proportion of HCT116 cells in late apoptosis (p = 0.0499) (mean % AV+PI+ ± SEM; HCT116 0 Gy normoxia 3.5 ± 0.56, HCT116 0 Gy hypoxia 21.18 ± 5.095) (**Fig. 3.6D**).

These data demonstrate that hypoxia significantly induces cell death in HCT116 cells, but not SW837 cells.

3.4.5. *Radiation induces apoptosis in HCT116 and SW837 cells under hypoxia (0.5% O_2)*

To investigate the effect of hypoxia on radiation-induced apoptosis in HCT116 and SW837 cells, apoptosis was assessed by PI and AV-FITC staining and flow cytometry. Cells were irradiated/mock-irradiated after 24 h in hypoxic or normoxic conditions, and apoptosis was assessed at 24 h and 48 h post radiation, with cells remaining in normoxia and hypoxia throughout.

At 24 h post radiation, no difference in the proportion of live cells was demonstrated following radiation exposure in either HCT116 or SW837 cells, when compared to unirradiated controls (**Fig. 3.5A**). A significant increase in the proportion of HCT116 cells undergoing early apoptosis was demonstrated following exposure to 1.8 Gy radiation under normoxia, when compared to unirradiated control (p = 0.035) (mean AV + PI - ± SEM; HCT116 0 Gy Normoxia 5.4 ± 1.88) (**Fig. 3.5B**). However, at 24 h post radiation, no differences in the proportion of HCT116 or SW837 cells in early apoptosis (**Fig. 3.5B**), necrosis (**Fig. 3.5C**) or late apoptosis (**Fig.**

3.5D) were demonstrated following radiation exposure, when compared to unirradiated controls under hypoxia.

Following a total 72 h in hypoxia, there was a significant decrease in the proportion of live HCT116 cells, compared to normoxia controls in unirradiated (p = 0.048) and irradiated cells (p = 0.0075) (mean AV-PI- % cells ± SEM; HCT116 0 Gy normoxia 91.85 ± 1.1, HCT116 0 Gy hypoxia 49.10 ± 13, HCT116 1.8 Gy normoxia 91.4 ± 0.66, HCT116 1.8 Gy Hypoxia 44.3 ± 7.47) (**Fig. 3.6A**). No differences were demonstrated in the proportion of live cells following irradiation under normoxia or hypoxia at 48 h post-radiation in HCT116 cells (**Fig. 3.6**). No differences were observed to the live cells in SW837 cells at this timepoint, following either hypoxia or radiation exposure (**Fig. 3.6**). Exposure to 1.8 Gy radiation significantly increased the percentage of cells in early apoptosis in HCT116 under normoxia at 48 h post radiation (p = 0.011) (mean AV+PI- % cells ± SEM; HCT116 0 Gy normoxia 3.25 ± 0.7, HCT116 1.8 Gy normoxia 4.33 ± 0.56) (**Fig. 3.6B**). While there was a trend towards increased proportion of HCT116 cells in early apoptosis in hypoxia, when compared to normoxia, this did not reach statistical significance. There was a trend towards radiation induced early apoptosis in SW837 cells at 48 h post radiation, although this did not reach statistical significance (p = 0.058).

There was a significant increase in the proportion of necrotic HCT116 cells following 1.8 Gy irradiation in hypoxia, when compared to irradiated cells under normoxic conditions (p 0.0212) (mean % necrotic cells ± SEM HCT116 1.8 Gy normoxia 1.3 ± 0.36, HCT116 1.8 Gy hypoxia 22.85 ± 4.5) (**Fig. 3.6C**). No difference to necrotic cells was observed in SW837 cells.

After a total 72 h in hypoxia, there was a significant increase in late apoptosis in HCT116, when compared to normoxia in unirradiated (p = 0.0499) and irradiated cells (p 0.0153) (mean % AV+PI+ ± SEM; HCT116 0 Gy normoxia 3.5 ± 0.56, HCT116 0 Gy hypoxia 21.18 ± 5.095; HCT116 1.8 Gy normoxia 2.968 ± 0.08, HCT116 1.8 Gy hypoxia 23.3 ± 4.087) (**Fig. 3.6D**). Exposure to 1.8 Gy radiation had no significant impact on the number of late apoptotic HCT116 cells under normoxia or hypoxia. There were no differences demonstrated in SW837 cells at this timepoint under hypoxia or following radiation exposure.

These data demonstrate that radiosensitive HCT116 cells are more sensitive to hypoxia-induced apoptosis basally and following radiation, when compared to SW837 cells.

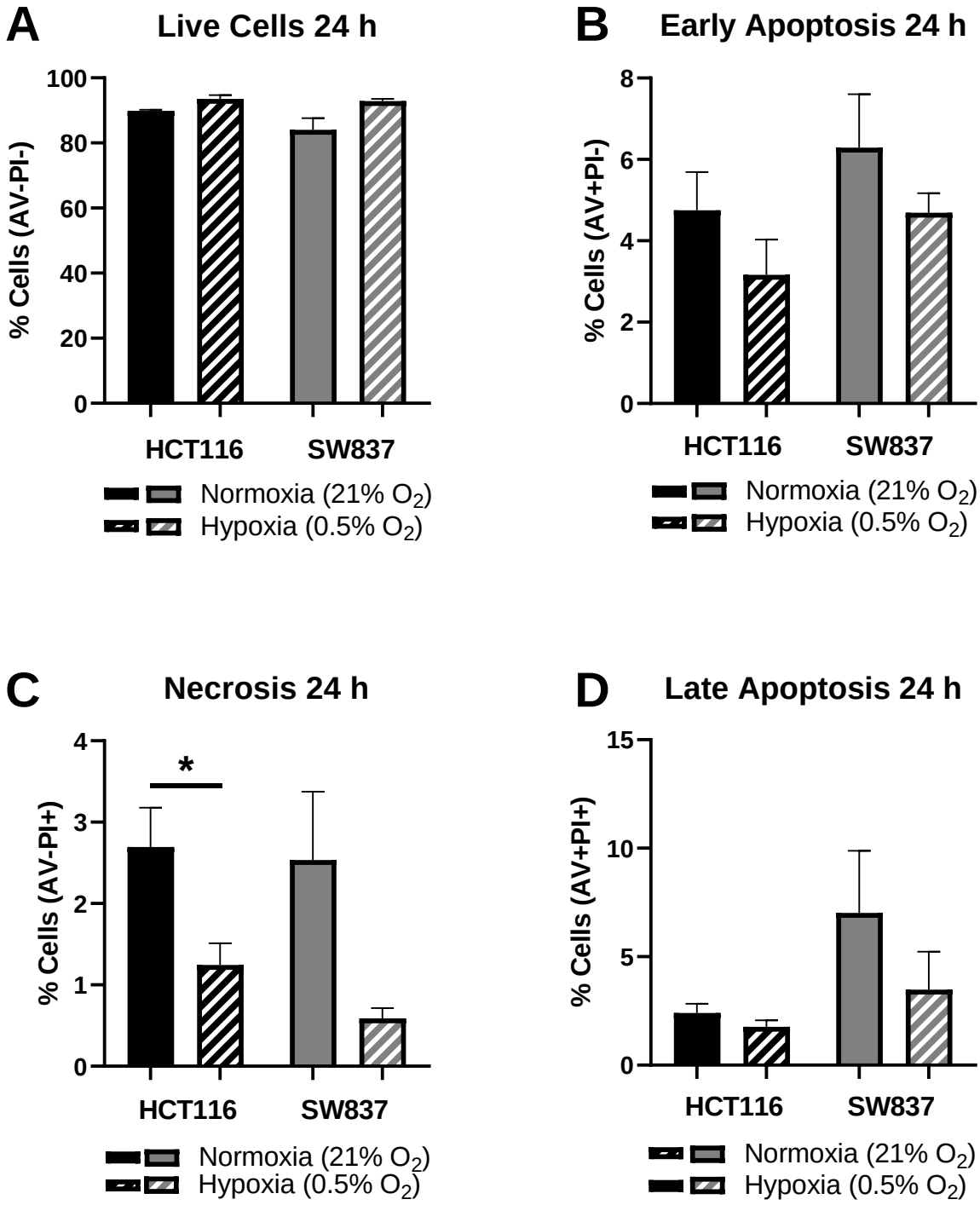

Fig. 3.4: **Hypoxic exposure (24 h) induces cell death in HCT116 cells.** Apoptosis was assessed by PI and Annexin V -FITC staining and flow cytometry in HCT116 and SW837 cells. **A)** Proportion of live cells (AV-PI-) **B)** Proportion of early apoptotic cells (AV+PI-) **C)** Proportion of late apoptotic cells (AV+PI+) **D)** Proportion of necrotic cells (AV-PI+) in HCT116 and SW837 cells after 24 h in normoxia or hypoxia. Data is presented as mean ± SEM for 4 independent experiments. Statistical analysis was performed using a series of paired/unpaired t-tests. *p < 0.05.

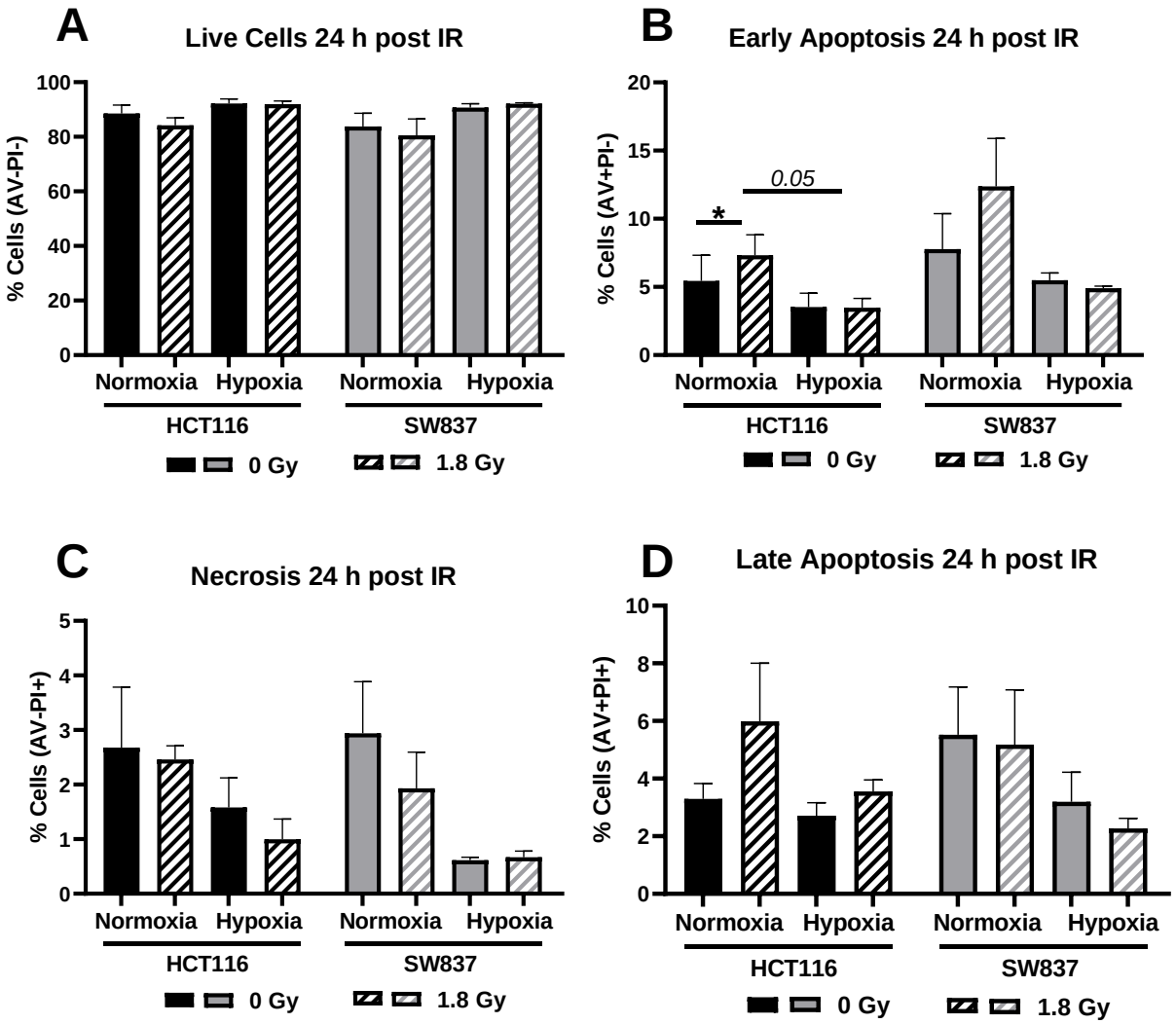

Fig. 3.5: **Apoptosis in HCT116 and SW837 cells following hypoxic exposure (48h total), and irradiation (24 h post).** Cell death following radiation treatment was assessed in HCT116 and SW837 cells by PI and Annexin V-FITC staining and flow cytometry, under normoxic (21% O_2) and hypoxic (0.5% O_2) conditions. **A)** Proportion of live cells (AV-PI-) in HCT116 and SW837 cells at 24 h following 1.8 Gy radiation in normoxia (N) and hypoxia (H). **B)** Proportion of early apoptotic cells (AV+PI-) in HCT116 and SW837 cells at 24 h following 1.8 Gy radiation in normoxia and hypoxia. **C)** Proportion of late apoptotic cells (AV+PI+) in HCT116 and SW837 cells at 24 h following 1.8 Gy radiation in normoxia and hypoxia **D)** Proportion of necrotic cells (AV-PI+) in HCT116 and SW837 cells at 24 h following 1.8 Gy radiation in normoxia and hypoxia. Data is presented as mean ± SEM for 4 independent experiments. Statistical analysis was performed using paired/unpaired *t*-testing. **p* < 0.05.

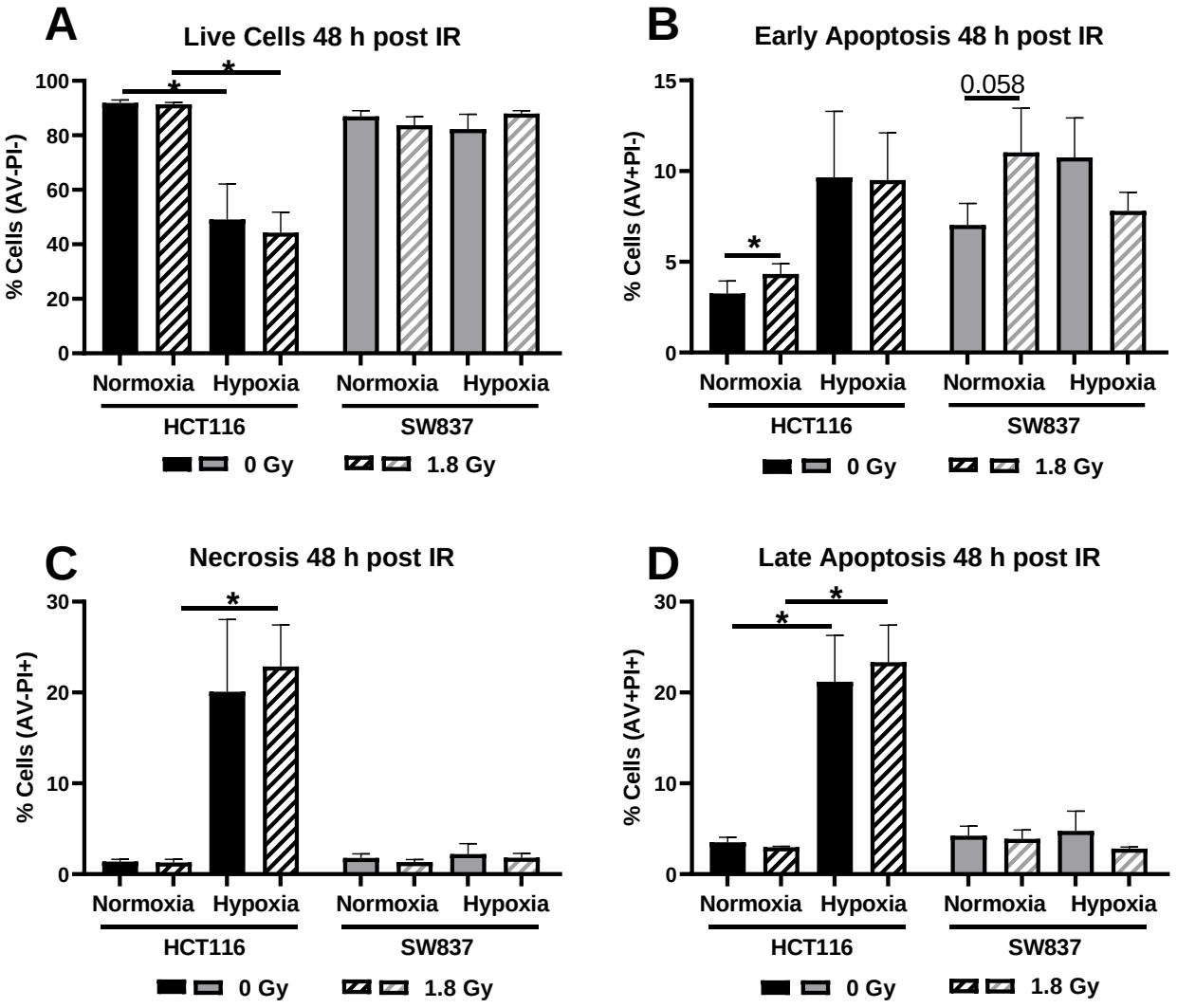

Fig. 3.6: **Apoptosis in HCT116 and SW837 cells following hypoxic exposure (72 h total), and irradiation (48 h post).** Cell death following radiation treatment was assessed in HCT116 and SW837 cells by PI and Annexin V-FITC staining and flow cytometry, under normoxic (21% O_2) and hypoxic (0.5% O_2) conditions. **A)** Proportion of live cells (AV-PI-) in HCT116 and SW837 cells 48 h following 1.8 Gy radiation in normoxia or hypoxia. **B)** Proportion of early apoptotic cells (AV+PI-) in HCT116 and SW837 cells 48 h following 1.8 Gy radiation in normoxia or hypoxia. **C)** Proportion of late apoptotic cells (AV+PI+) in HCT116 and SW837 cells 48 h following 1.8 Gy radiation in normoxia or hypoxia **D)** Proportion of necrotic cells (AV-PI+) in HCT116 and SW837 cells 48 h following 1.8 Gy radiation in normoxia or hypoxia. Data is presented as mean ± SEM for 4 independent experiments. Statistical analysis was performed using a series of paired/unpaired t-testing. *$p < 0.05$.

3.4.6. *Hypoxia (0.5% O_2) significantly alters basal cell cycle distribution in HCT116 and SW837 cells*

Having demonstrated that there are differences in the basal cell cycle distribution between HCT116 and SW837 cells under normoxia (**Chapter 2, Section 2.4.5**), the impact of a hypoxic microenvironment (0.5% O_2) on basal cell cycle distribution was assessed in both cell lines by PI staining and flow cytometry.

Following 24 h exposure to hypoxia, the proportion of HCT116 cells in the G0/G1 phase was significantly reduced (p = 0.0028) (Mean % G0/G1 ± SEM; HCT116 normoxia 43.43 ± 1.93 vs HCT116 Hypoxia 28.8 ± 2.42), when compared to normoxic cells (**Fig. 3.7A**). In contrast, the proportion of SW837 cells in the G0/G1 phase was significantly increased under hypoxic exposure (p = 0.0047) (SW837 normoxia 61.86 ± 1.89 vs SW837 Hypoxia 71.1 ± 1.77), when compared to normoxic cells (**Fig. 3.7A**). When comparing the HCT116 cell line to SW837 cells, under normoxic conditions there was a significantly higher proportion of cells in the G0/G1 phase in SW837 cells, when compared to HCT116 cells under normoxia (p =0.0003). Under hypoxia, SW837 cells displayed a significantly elevated proportion of cells in the G0/G1 phase, when compared to HCT116 cells under hypoxia (p < 0.0001) (**Fig. 3.7A**).

Hypoxic exposure induced a significant increase in the proportion of cells in the S phase, when compared to normoxic cells in HCT116 (p = 0.02) (mean % S phase ± SEM; HCT116 normoxia 191.88 ± 2.68 vs HCT116 hypoxia 33.18 ± 4.34) and in SW837 cells (p = 0.033) (SW837 normoxia 15.99 ± 2.06 vs SW837 hypoxia 9.07 ± 1.09) (**Fig. 3.7B**). In addition, under hypoxia, a significant decrease in S phase cells was demonstrated in SW837 cells, when compared to HCT116 cells (p = 0.0005) (**Fig. 3.7B**).

No significant differences to the proportion of cells in the G2/M phase was demonstrated in HCT116 or SW837 cells under hypoxia, when compared to normoxia (**Fig. 3.7C**). There were significantly less cells in the G2/M phase in SW837 cells, when compared to HCT116 under normoxia (p = 0.005) (Mean % G2/M phase ± SEM; HCT116 Normoxia 28 ± 2.47 vs SW837 normoxia 18.18 ± 0.96) (**Fig. 3.7C**). This was also demonstrated under hypoxic conditions, with a significantly lower proportion of cells in the G2/M phase in SW837 cells, when compared to HCT116 (p = 0.011) (HCT116 hypoxia 25.6 ± 2.69 vs SW837 hypoxia 16.72 ± 0.95) (**Fig. 3.7C**).

These data demonstrate that hypoxic exposure alters basal cell cycle distribution in HCT116 and SW837 cells.

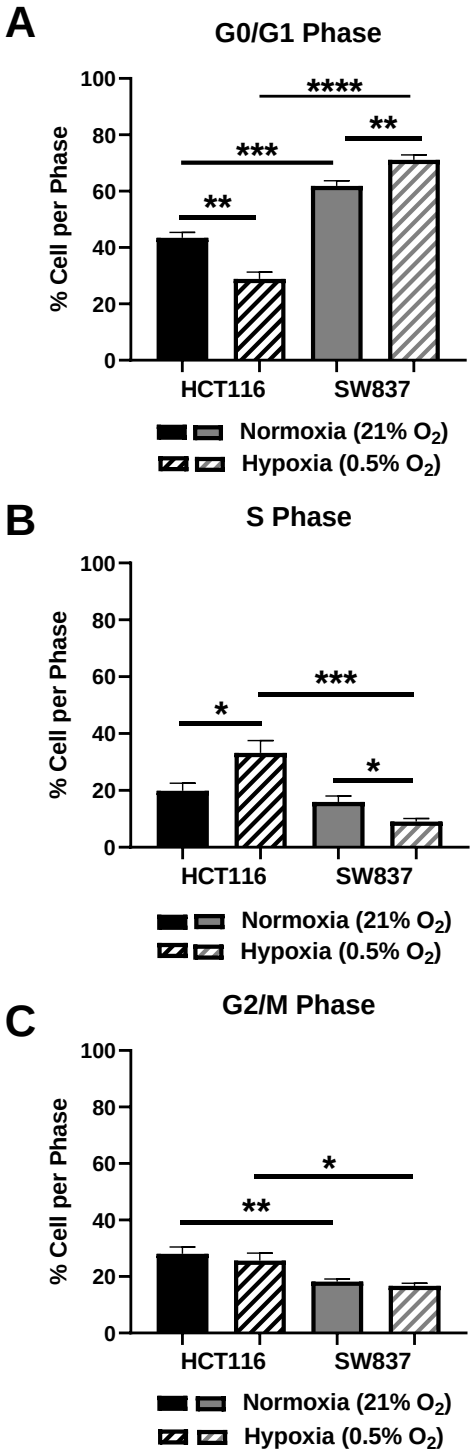

Fig. 3.7: **Hypoxia alters basal cell cycle distribution in HCT116 and SW837 cells.** Cell cycle distribution was assessed after 24 h culture under hypoxia (0.5% O_2) or normoxia (21% O_2). **A)** Proportion of HCT116 and SW837 cells in G0/G1 phase under normoxia and hypoxia. **B)** Proportion of HCT116 and SW837 cells in S phase under normoxia and hypoxia. **C)** Proportion of HCT116 and SW837 cells in G2/M phase under normoxia and hypoxia. Data is presented as mean ± SEM for 4 independent experiments. Statistical analysis was performed by paired or unpaired *t*-testing, as appropriate. *$p < 0.05$, **$p < 0.01$, ***$p < 0.001$, ****$p < 0.0001$.

3.4.7. *Hypoxia affects cell cycle progression following radiation in HCT116 and SW837 cells*

Having demonstrated that hypoxic exposure significantly alters basal cell cycle distribution in HCT116 and SW837 cells (**Section 3.4.5**), the progression of cells through the cell cycle following radiation was subsequently assessed under hypoxic conditions.

In HCT116 cells, no significant differences were demonstrated to the proportion of cells in the G0/G1 phase at 20 min, following 1.8 Gy radiation, under normoxic or hypoxic conditions (**Fig. 3.8A**). However, when comparing irradiated cells, a significant decrease in the proportion of G0/G1 phase HCT116 cells was demonstrated under hypoxia, when compared to normoxia control (p = 0.028) (**Fig. 3.8A**).

At 6 h following radiation exposure, a significant decrease in the proportion of G0/G1 phase cells was demonstrated in irradiated HCT116 cells, under normoxia, when compared to unirradiated control (p = 0.0012) (Mean ± SEM; HCT116 normoxia 0 Gy 53.1 ± 2.26 vs HCT116 normoxia 1.8 Gy 41.34 ± 2.81), but not under hypoxia (**Fig. 3.8A**). In addition, at 6 h post radiation, there was a significant decrease in the proportion of cells in G0/G1 phase under hypoxic exposure, when compared to normoxia in unirradiated and irradiated cells (p = 0.0035, p = 0.018 respectively) (**Fig. 3.8A**). At 10 h post radiation exposure, a significant decrease in the proportion of G0/G1 HCT116 cells was demonstrated following 1.8 Gy radiation, under normoxic (p = 0.0007) (Mean % G0/G1 ± SEM; HCT116 normoxia 0 Gy 57.14 ± 4.19 vs HCT116 normoxia 1.8 Gy 42.76 ± 3.85) but not hypoxic conditions (**Fig. 3.8A**). At 24 h post radiation, a significant decrease in the proportion of G0/G1 phase cells was demonstrated in irradiated cells, when compared to unirradiated controls, under normoxia (p = 0.021) (HCT116 normoxia 0 Gy 59.56 ± 2.6 vs HCT116 normoxia 1.8 Gy 49.82 ± 2.8), with no significant differences observed under hypoxia. At 24 h post radiation, hypoxic exposure significantly decreased the proportion of G0/G1 phase cells in both unirradiated and irradiated cells (p = 0.0003, p = 0.0004 respectively) (**Fig. 3.8A**).

In HCT116 cells, no significant differences were demonstrated to the proportion of S phase cells at 20 min, 6 h or 10 h post radiation under normoxic or hypoxic conditions (**Fig. 3.8B**). At 24 h, a decrease to the proportion of S phase cells was demonstrated following radiation, under normoxia (p = 0.047) (Mean % S phase ± SEM; HCT116 normoxia 0 Gy 10.23 ± 2.4 vs HCT116 normoxia 1.8 Gy 6.36 ± 1.88) (**Fig. 3.8B**). In addition, the proportion of cells in the S phase was significantly elevated in irradiated cells, under hypoxic conditions, when compared to normoxia (p = 0.016) (**Fig. 3.8B**).

No significant differences to the proportion of cells in the G2/M phase in HCT116 were demonstrated at 20 min or 6 h post radiation, following radiation, or under hypoxic conditions (**Fig. 3.8C**). At 10 h post radiation, radiation induced a significant increase in the proportion of HCT116 cells in G2/M phase, under normoxia (p= 0.006) (Mean % G2/M ± SEM; HCT116 0 Gy normoxia 20.84 ± 2.88 vs HCT116 1.8 Gy normoxia 39.22 ± 5.48), however, no significant differences were demonstrated under hypoxia (**Fig. 3.8C**). At 24 h post radiation, a significant increase in the percentage of cells in the G2/M phase was demonstrated under normoxic conditions in irradiated cells, when compared to unirradiated control (p = 0.0018) (HCT116 0 Gy normoxia 21.9 ± 2.42 vs HCT116 1.8 Gy normoxia 32.88 ± 1.9) (**Fig. 3.8C**).

In SW837 cells, at 20 min post radiation, exposure to hypoxia induced a significant increase in the proportion of cells in the G0/G1 phase, when compared to normoxic cells in both unirradiated (p = 0.0047) (Mean % G0/G1 ± SEM; SW837 0 Gy Normoxia 61.86 ± 1.89 vs SW837 0 Gy hypoxia 71.1 ± 1.77) and irradiated cells (p = 0.0096) (SW837 1.8 Gy normoxia 61.98 ± 2.5 vs SW837 1.8 Gy hypoxia 69.46 ± 2.48) (**Fig. 3.9A**). At 6 h post radiation, exposure to radiation induced significant decrease in the proportion of cells in the G0/G1 phase under normoxia (p = 0.035) (SW837 0 Gy normoxia 61.32 ± 2.18 vs SW837 1.8 Gy normoxia 53.92 ± 2.64) and under hypoxia (p = 0.002) (SW837 0 Gy hypoxia 75.06 ± 2.03 vs SW837 1.8 Gy hypoxia 71.2 ± 2.49) (**Fig. 3.9A**). Exposure to hypoxia induced a significant increase in the proportion of G0/G1 phase cells in both unirradiated and irradiated cells (p = 0.0017, p = 0.0002 respectively) (**Fig. 3.9A**). At 10 h post radiation, a significant decrease in the proportion of G0/G1 phase cells was demonstrated in irradiated cells, when compared to unirradiated controls under normoxia (p = 0.001) (SW837 0 Gy normoxia 62.74 ± 1.89 vs SW837 1.8 Gy normoxia 51.04 ± 2.61) and under hypoxic conditions (p = 0.034) (SW837 0 Gy hypoxia 78.22 ± 1.04 vs SW837 1.8 Gy hypoxia 74.26 ± 1.5) (**Fig. 3.9A**). Furthermore, at 10 h post radiation, hypoxic exposure induced a significant increase in the proportion of cells in the G0/G1 phase in both unirradiated and irradiated cells (p = 0.0001, p = 0.0001 respectively). At 24 h post radiation, radiation induced a significant decrease in the proportion of G0/G1 phase cells, under hypoxic conditions only (p = 0.036) (SW837 0 Gy hypoxia 76.9 ± 2.76 vs SW837 1.8 Gy hypoxia 73.32 ± 1.86) (**Fig. 3.9A**). In addition, hypoxic exposure induced a significant increase in the proportion of G0/G1 cells in unirradiated cells (p = 0.028).

In SW837 cells, exposure to hypoxia induced a decrease in the proportion of S phase cells in unirradiated (p = 0.033) (Mean % S phase ± SEM; SW837 0 Gy normoxia 15.99 ± 2.06

vs SW837 0 Gy hypoxia 9.07 ± 1.09) and irradiated cells (p = 0.0002) (SW837 1.8 Gy normoxia 18.1 ± 2.09 vs SW837 1.8 Gy hypoxia 10.73 ± 1.81) (**Fig. 3.9B**). Similar findings were demonstrated at 6 h post radiation, with a significant decrease to the proportion of S phase cells in unirradiated (p = 0.005) (SW837 0 Gy normoxia 15.24 ± 1.09 vs SW837 0 Gy hypoxia 7.49 ± 1.28) and irradiated cells (p = 0.0051) (SW837 1.8 Gy normoxia 19.24 ± 2.9 vs SW837 1.8 Gy hypoxia 9.13 ± 1.62) (**Fig. 3.9B**). At 10 h post radiation, a significant decrease in the proportion of S phase cells was demonstrated with hypoxic exposure in both unirradiated and irradiated cells (p = 0.001, p = 0.033 respectively)) (SW837 0 Gy normoxia 16.1 ± 1.7 vs SW837 0 Gy hypoxia 7.4 ± 0.93) (SW837 1.8 Gy normoxia 16.95 ± 2.78 vs SW837 1.8 Gy hypoxia 8.43 ± 0.9). Furthermore, at 24 h post radiation, hypoxia induced a reduction in the proportion of S phase cells in both unirradiated cells (p= 0.028) (SW837 0 Gy normoxia 14.5 ± 1.6 vs SW837 0 Gy hypoxia 7.42 ± 0.98) and irradiated cells (p = 0.016) (SW837 1.8 Gy normoxia 12.98 ± 1.36 vs SW837 1.8 Gy hypoxia 8.13 ± 1.05) (**Fig. 3.9B**).

While no significant differences were demonstrated in the proportion of G2/M phase cells in SW837 at 20 min post radiation, a significant decrease in the proportion of cells in G2/M phase at 6 h post radiation was demonstrated, in hypoxic cells, when compared to normoxia in irradiated cells (p = 0.0009) (SW837 1.8 Gy normoxia 24.24 ± 0.69 vs SW837 1.8 Gy hypoxia 17.54 ± 1.11) (**Fig. 3.9C**). In addition, at this timepoint, hypoxic exposure alone induced a significant decrease in the proportion of cells in the G2/M phase in unirradiated cells, when compared to normoxia (p = 0.0147) (Mean % G2/M phase ± SEM; SW837 0 Gy normoxia 20.88 ± 1.23 vs SW837 0 Gy hypoxia 15.56 ± 0.98) (**Fig. 3.9C**). Exposure to radiation induced G2/M arrest at 10 h post radiation, under normoxia (p = 0.0018) (SW837 0 Gy normoxia 17.8 ± 1.04 vs SW837 1.8 Gy normoxia 28.6 ± 1.89) and hypoxia (p = 0.044) (SW837 0 Gy hypoxia 12.63 ± 0.92 vs SW837 1.8 Gy hypoxia 17.34 ± 1.47) (**Fig. 3.9C**). Furthermore, exposure to hypoxia was demonstrated to significantly decrease the proportion of cells in the G2/M phase, when compared to normoxic conditions in unirradiated cells (p = 0.008, p = 0.022 respectively) (**Fig. 3.9C**). At 24 h post radiation, while no significant differences to the proportion of G2/M phase cells was demonstrated following radiation under normoxia, a significant increase in G2/M phase cells was demonstrated under hypoxia in irradiated cells, when compared to unirradiated controls (p = 0.0009) (SW837 0 Gy hypoxia 12.37 ± 1.8 vs SW837 1.8 Gy hypoxia 15 ± 1.6) (**Fig. 3.9C**).

These data demonstrate that hypoxic exposure alters cell cycle progression following radiation exposure in HCT116 and SW837 cells.

3.4.8. *Radiation-induced DNA damage is efficiently repaired under hypoxic conditions in HCT116 and SW837 cells*

Having demonstrated enhanced DNA damage repair in radioresistant SW837 cells, when compared to HCT116 cells under normoxic conditions (**Chapter 2, Section 2.4.8**), DNA damage induction and repair following radiation with a clinically-relevant dose was assessed under hypoxic conditions, by detection of γH2AX by flow cytometry.

In radiosensitive HCT116 cells, a significant induction of γH2AX DNA damage was demonstrated at 20 min post radiation in hypoxic cells (p = 0.0224) (Mean relative MFI ± SEM; HCT116 1.8 Gy 1.1 ± 0.027) (**Fig. 3.10A**). However, at 6 h, 10 h and 24 h post treatment, no significant differences were demonstrated to DNA damage levels, indicating resolution of radiation-induced damage by this timepoint under hypoxic conditions in HCT116 cells.

In hypoxic SW837 cells, a similar induction of DNA damage following radiation was demonstrated at 20 min post radiation, when compared to unirradiated control (p = 0.04) (SW837 1.8 Gy 1.39 ± 0.1) (**Fig. 3.10B**). γH2AX levels had returned to baseline by 6 h post radiation exposure, with no significant differences in DNA damage levels at 6 h, 10 h or 24 h post radiation, suggesting repair of radiation-induced DSB.

These data demonstrate that under hypoxic conditions, radiation-induced DSB are quickly repaired in both HCT116 and SW837 cells.

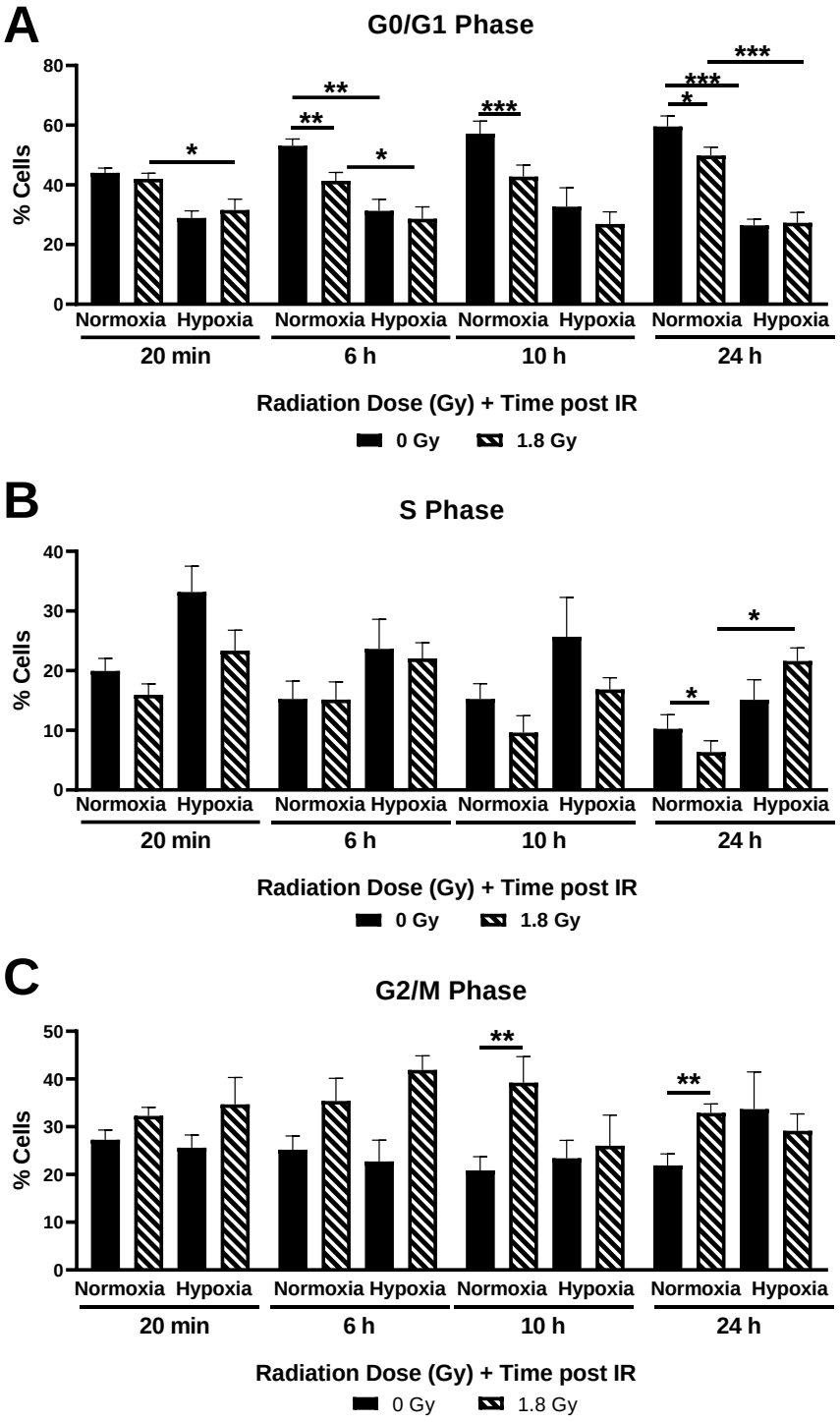

Fig. 3.8: **Hypoxia (0.5% O_2) affects cell cycle progression following radiation treatment in HCT116 cells.** HCT116 cells were placed in normoxia or hypoxia for 24 h prior to being mock-irradiated or exposed to 1.8 Gy X-ray radiation. Cell cycle distribution was assessed at 20 min, 6 h, 10 h, and 24 h post radiation, by PI staining and flow cytometry. **A)** Proportion of HCT116 cells in G0/G1 phase following radiation, under normoxia or hypoxia. **B)** Proportion of HCT116 cells in S phase following radiation, under normoxia or hypoxia. **C)** Proportion of HCT116 cells in G2/M phase following radiation, under normoxia or hypoxia. Data is presented as mean ± SEM for 4 independent experiments. Statistical analysis was performed by paired ANOVA and post-hoc multiple comparisons testing. *$p < 0.05$, **$p < 0.01$, ***$p < 0.001$.

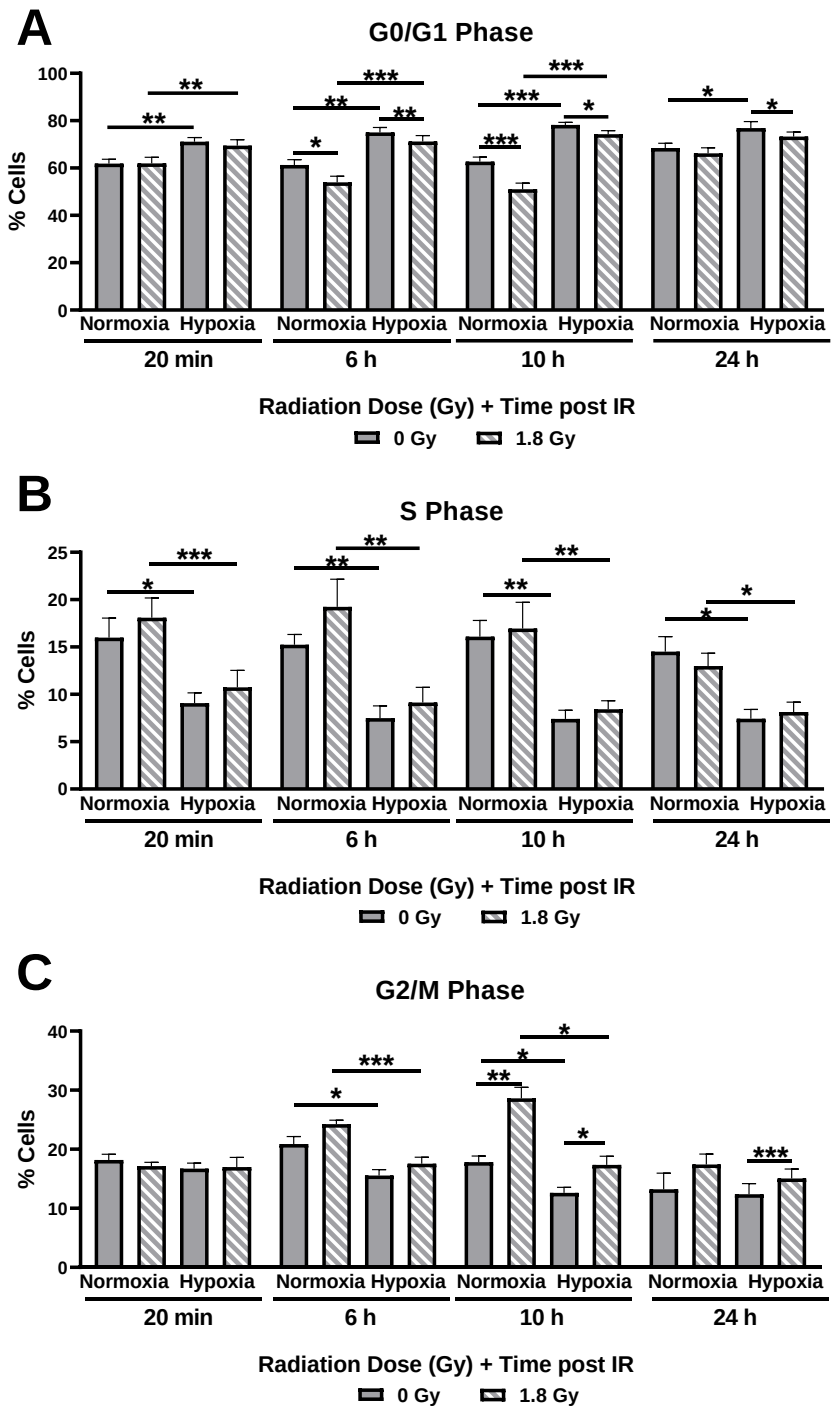

Fig. 3.9: **Hypoxia (0.5% O_2) affects cell cycle progression following radiation treatment in SW837 cells.** SW837 cells were placed in normoxia or hypoxia for 24 h prior to being mock-irradiated or exposed to 1.8 Gy X-ray radiation. Cell cycle distribution was assessed at 20 min, 6 h, 10 h, and 24 h post radiation, by PI staining and flow cytometry. **A)** Proportion of SW837 cells in G0/G1 phase following radiation, under normoxia or hypoxia. **B)** Proportion of SW837 cells in S phase following radiation, under normoxia or hypoxia. **C)** Proportion of SW837 cells in G2/M phase following radiation, under normoxia or hypoxia. Data is presented as mean ± SEM for 4 independent experiments. Statistical analysis was performed by paired ANOVA and post-hoc multiple comparisons testing. *$p < 0.05$, **$p < 0.01$, ***$p < 0.001$.

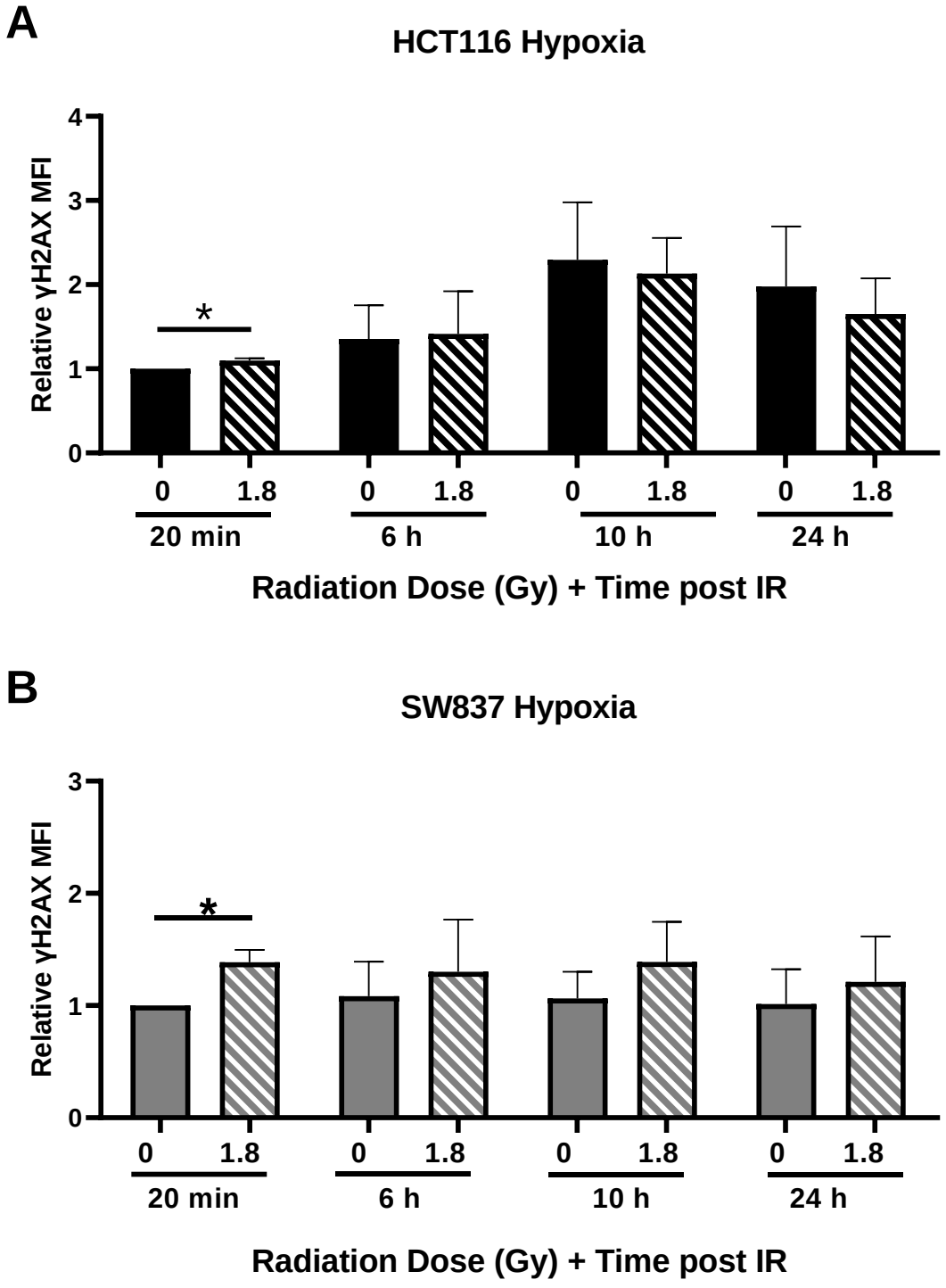

Fig. 3.10: **Radiation-induced DNA damage is efficiently repaired in HCT116 and SW837 cells under hypoxic conditions (0.5% O_2).** HCT116 and SW837 cells were exposed to hypoxia for 24 h prior to irradiation, and DNA damage levels assessed at 20 min, 6 h, 10 h, and 24 h post radiation exposure by flow cytometry. **A)** DNA damage levels in HCT116 following radiation, under hypoxic conditions. **B)** DNA damage levels in SW837 cells following radiation, under hypoxic conditions. Data is presented as relative mean MFI ± SEM for 4 independent experiments. Statistical analysis was performed by paired *t*-testing. **p* < 0.05.

3.4.9. *Hypoxia (0.5% O_2) alters basal energy metabolism in radiosensitive HCT116 and radioresistant SW837 cells*

Hypoxia is demonstrated to affect energy metabolism. As metabolism was demonstrated to be altered in HCT116 and SW837 cells in normoxic conditions (**Chapter 2 Section 2.4.9**), basal metabolism of SW837 and HCT116 cells under hypoxic conditions (0.5% O_2), was assessed using the Seahorse™ XFe24 analyser (Agilent). This assay allows for the assessment of oxidative phosphorylation, by surrogate marker oxygen consumption rate (OCR) and glycolysis levels, by surrogate marker extracellular acidification rate (ECAR) in live cells in real-time.

Basally, hypoxic conditions induced a significant reduction in OCR in SW837 cells, when compared to normoxic conditions (p = 0.038) (mean normalised OCR ± SEM; SW837 normoxia 428.5 ± 74.65, SW837 hypoxia 214 ± 43.28) (**Fig. 3.11A**). A trend towards reduced OCR in HCT116 cells following hypoxia was demonstrated, although this did not reach statistical significance (p = 0.13) (mean normalised OCR ± SEM; HCT116 normoxia 645.8 ± 237.1, HCT116 hypoxia 136.4 ± 22.46) (**Fig. 3.11A**).

Hypoxia resulted in a trend towards reduced ECAR in HCT116 and SW837 CRC cells, although there was no statistically significant difference (p = 0.4 and p = 0.1) (mean normalised ECAR ± SEM; HCT116 normoxia 97.79 ± 27.4, HCT116 hypoxia 73.4 ± 4.71, SW837 normoxia 62.91 ± 6.23, SW837 hypoxia 86.92 ± 11.09) (**Fig. 3.11B**).

To further characterise alterations in metabolic reliance of HCT116 and SW837 CRC cells under hypoxia, the OCR:ECAR was calculated by dividing the basal OCR values by the basal ECAR values. Culture in hypoxic conditions was demonstrated to significantly shift the metabolic reliance of both HCT116 and SW837 cells, significantly reducing the reliance on oxidative phosphorylation (p = 0.0033 and p = 0.009) (mean normalised OCR: ECAR ratio; HCT116 normoxia 5.76 ± 0.85:1, HCT116 hypoxia 1.92 ± 0.16: 1, SW837 normoxia 6.78 ± 0.64:1, SW837 hypoxia 2.77 ± 0.86:1) (**Fig. 3.11C**).

These data demonstrate that a hypoxic microenvironment causes a metabolic shift, specifically a reduction in reliance on oxidative phosphorylation in both HCT116 and SW837 cells.

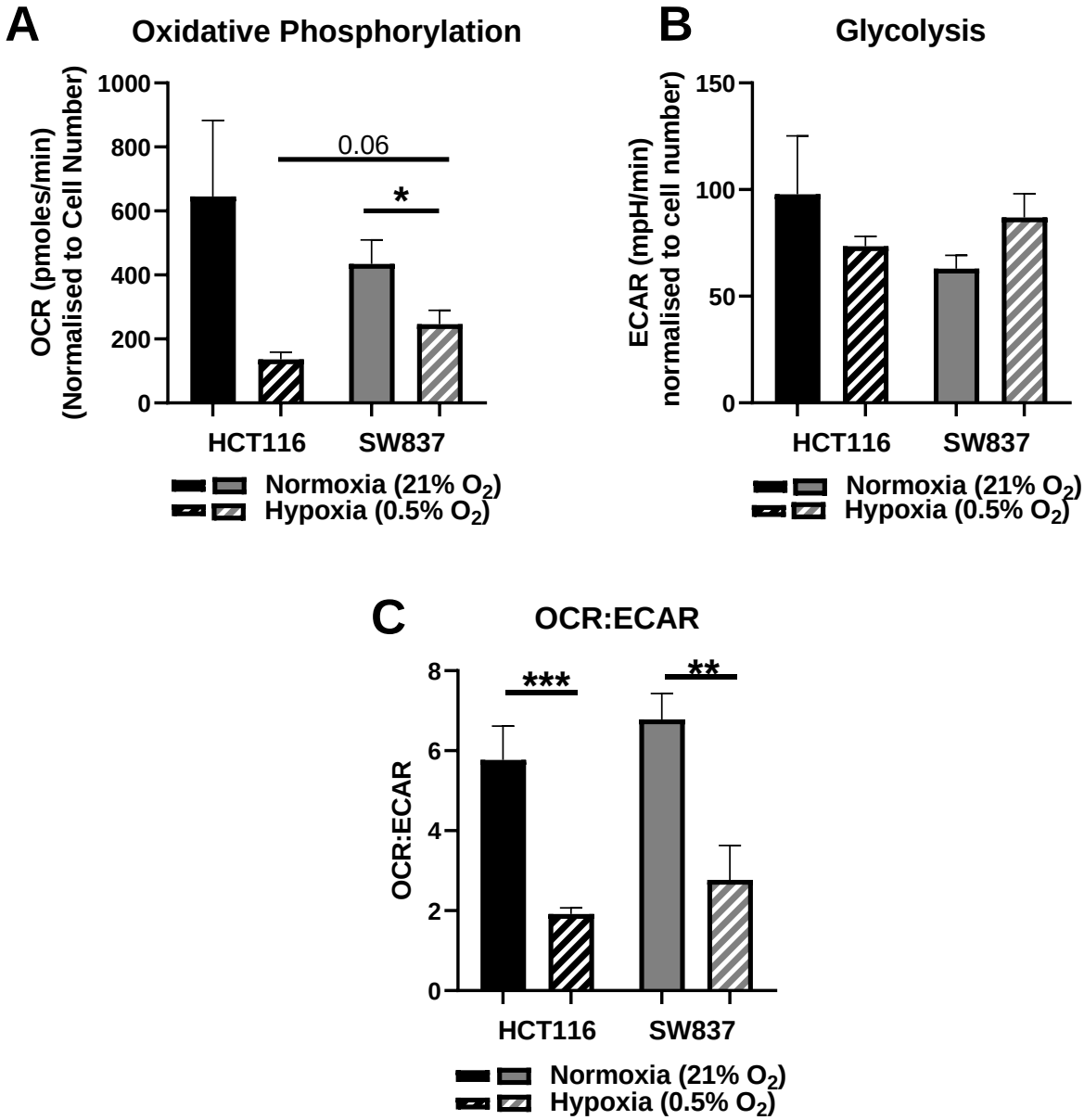

Fig. 3.11: **Hypoxia (0.5% O_2) alters basal metabolic reliance of HCT116 and SW837 colorectal cancer cells.** The OCR and ECAR rates of HCT116 colon and SW837 rectal cancer cell lines under hypoxia (0.5% O_2) and normoxia (21% O_2) were assessed by Seahorse XFe24 analyser. **A)** Basal OCR (oxidative phosphorylation) of HCT116 and SW837 cell lines under normoxia and hypoxia. **B)** Basal ECAR (glycolysis) of HCT116 and SW837 cells. **C)** OCR: ECAR of HCT116 and SW837 cells. Data is presented as mean ± SEM for 4 independent experiments. Statistical analysis was performed by paired *t*-testing between the normoxic and hypoxic conditions, or unpaired *t*-testing between different cell lines. *$p < 0.05$, **$p < 0.01$, ***$p < 0.001$.

3.4.10. *Hypoxia alters mitochondrial metabolic parameters in HCT116 and SW837 cells*

To further assess the metabolic reliance of HCT116 and SW837 cells under hypoxia, the effects of a series of mitochondrial inhibitor drugs on OCR was assessed by Seahorse MitoStress™ assay.

Non-mitochondrial oxygen consumption was demonstrated to be significantly increased under hypoxic conditions, when compared to normoxic conditions in HCT116 (p = 0.0467) and SW837 cells (p = 0.0176) (mean non-mitochondrial oxygen consumption ± SEM: HCT116 normoxia 49.25, HCT116 hypoxia 89.02 ± 4.926, SW837 normoxia 54.98 ± 17.7, SW837 hypoxia 149.3 ± 23.07) (**Fig. 3.12A**).

There was a significant reduction in basal respiration in SW837 cells (p = 0.0181) and a trend towards reduced basal respiration in HCT116 cells (p = 0.0507) under hypoxia, when compared to normoxia (mean basal respiration ± SEM; HCT116 normoxia 596.5 ± 224.3, HCT116 hypoxia 47.34 ± 21.46, SW837 normoxia 379.7 ± 64.03, SW837 hypoxia 96.72 ± 60.09) (**Fig. 3.12B**). Maximal respiration was also significantly reduced under hypoxic conditions, when compared to normoxia in HCT116 and SW837 cells (p = 0.0362, p = 0.0076 respectively) (mean maximal respiration ± SEM; HCT116 normoxic 645.6 ± 224.7, HCT116 hypoxia 39.06 ± 20.72, SW837 normoxia 530.6 ± 79.7, SW837 hypoxia 95.46 ± 76.18) (**Fig. 3.12C**).

No significant differences were demonstrated in proton leak under hypoxia, when compared to normoxia in HCT116 or SW837 cells (**Fig. 3.12D**). Oxygen-linked ATP turnover was significantly reduced under hypoxia in HCT116 and SW837 cells (p = 0.0367, p = 0.0168) (mean oxygen-linked ATP turnover ± SEM; HCT116 normoxia 502.8 ± 192, HCT116 hypoxia -12.73 ± 16.16, SW837 normoxia 317.2 ± 58.05, SW837 hypoxia 38 ± 62.28) (**Fig. 3.12E**). A trend towards reduced spare respiratory capacity was demonstrated in HCT116 cells under hypoxia, although this did not reach significance (p = 0.079). Spare respiratory capacity was significantly lower in SW837 cells under hypoxia, when compared to normoxia (p = 0.0011) (mean spare respiratory capacity ± SEM; SW837 normoxia 151 ± 19.66, SW837 hypoxia -1.27 ± 16.87) (**Fig. 3.12F**).

These data demonstrate that hypoxic exposure has a significant impact on mitochondrial metabolism in HCT116 and SW837 cells.

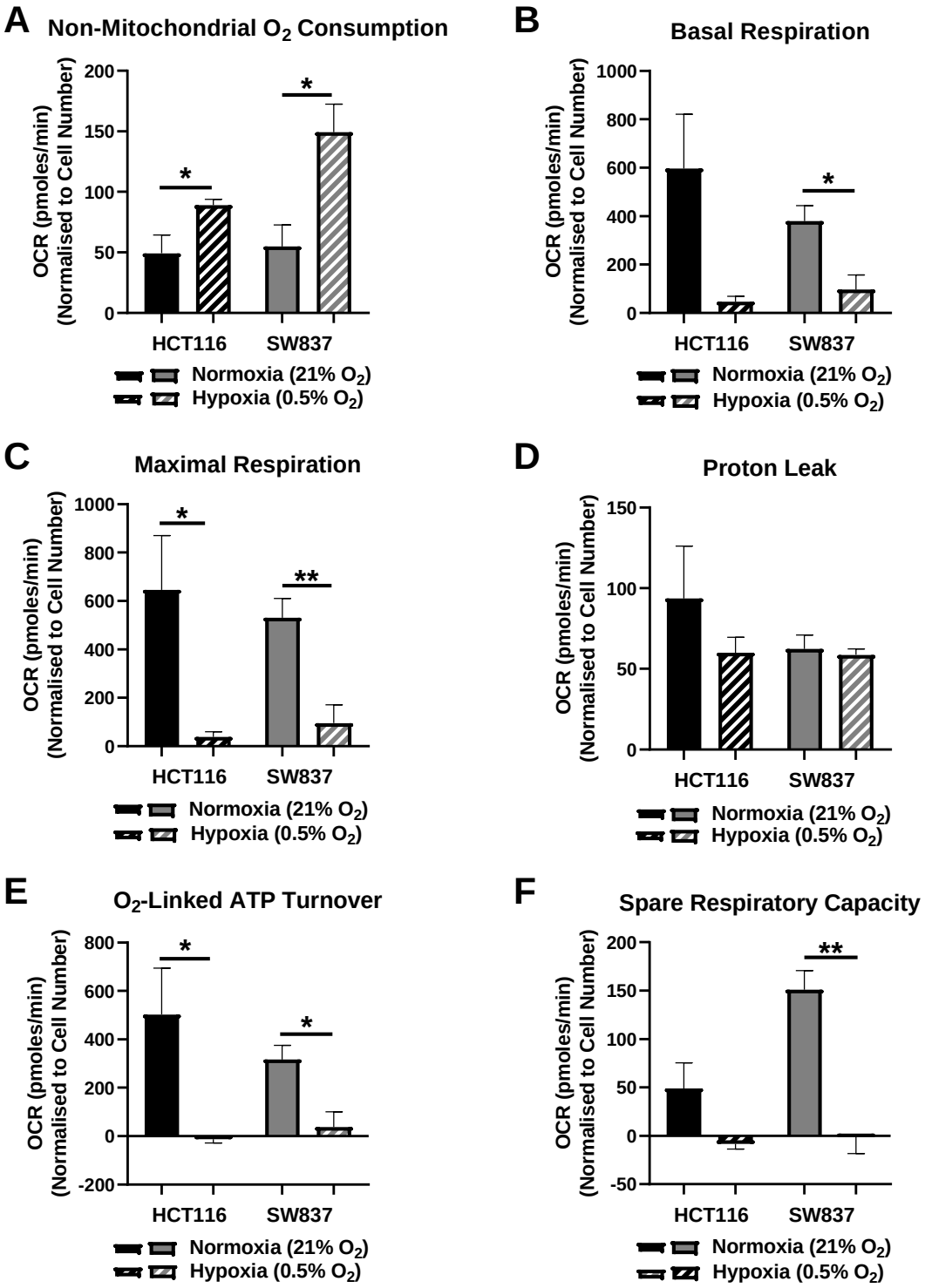

Fig. 3.12: **Profiling of mitochondrial metabolic parameters in HCT116 and SW837 colorectal cancer cells under hypoxia.** Mitochondrial metabolic parameters were assessed in HCT116 and SW837 cells under hypoxia (0.5% O_2) and normoxia (21% O_2) using Seahorse™ XFe24 analyser and a series of mitochondrial inhibitors. **A)** Non-mitochondrial oxygen consumption. **B)** Basal respiration. **C)** Maximal respiration. **D)** Proton leak. **E)** Oxygen-linked ATP production. **F)** Spare-respiratory capacity. Data is presented as mean ± standard error of the mean (SEM) for 4 independent experiments. Statistical analysis was performed using one-way ANOVA and post-hoc Tukey's multiple comparisons testing. *$p < 0.05$ **$p < 0.01$.

3.4.11. *Mitochondrial function is altered under hypoxia (0.5% O_2) in HCT116 and SW837 cells*

Having profiled the impact of hypoxia exposure on metabolism in HCT116 and SW837 cells, basal mitochondrial function was assessed using three surrogate markers of mitochondrial function (mitochondrial mass, ROS production and mitochondrial membrane potential).

Culture under hypoxic conditions resulted in a significant increase in mitochondrial mass in radioresistant SW837 rectal cancer cells, when compared to normoxic conditions (p = 0.0203) (Mean normalised MitoTracker™ fluorescence ± SEM: SW837 normoxia 5.1 ± 0.4, SW837 hypoxia 8.13 ± 0.86) (**Fig. 3.13A**). There were no significant differences in mitochondrial mass under hypoxic conditions in radiosensitive HCT116 cells, when compared to normoxia (HCT116 normoxia 6.6 ± 1.2, HCT116 hypoxia 4.86 ± 0.27).

Hypoxia resulted in a significant decrease in ROS accumulation in radiosensitive HCT116 cells, when compared to HCT116 cells cultured under normoxic conditions (p = 0.0135) (mean normalised DCF-DA fluorescence ± SEM: HCT116 normoxia 6.63 ± 0.67, HCT116 hypoxia 3.09 ± 0.51) (**Fig. 3.13B**). No significant differences in ROS production were demonstrated in radioresistant SW837 cells under hypoxia, compared to normoxic conditions (SW837 normoxia 4.87 ± 0.49, SW837 hypoxia 6.19 ± 0.57).

Mitochondrial membrane potential was demonstrated to be significantly increased under hypoxic conditions, when compared to normoxic conditions, in both SW837 and HCT116 CRC cells (p = 0.032, p = 0.0032) (mean Rhodamine-123 normalised fluorescence ± SEM; SW837 normoxia 52.2 ± 8.52, SW837 hypoxia 99.81 ± 17.45, HCT116 normoxia 27.53 ± 4.05, HCT116 hypoxia 52.56 ± 3.4) (**Fig. 3.13C**).

Together, this demonstrates significant alterations to mitochondrial function under hypoxic conditions (0.5% O_2), in SW837 and HCT116 CRC cells.

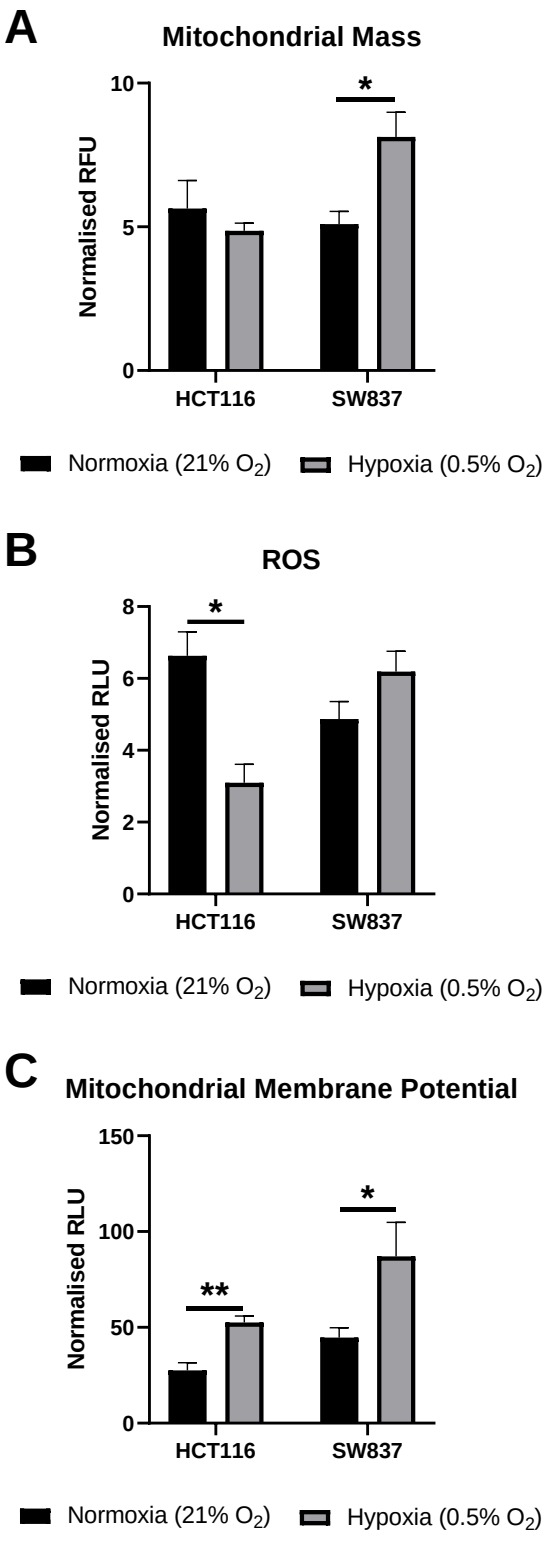

Fig. 3.13: **Mitochondrial function is significantly altered under hypoxic conditions (0.5% O_2) in SW837 and HCT116 colorectal cancer cell lines.** Mitochondrial function was assessed using a series of fluorescent probes in SW837 and HCT116 cells. **A)** Mitochondrial mass was assessed using MitoTracker Green FM. **B)** ROS production was assessed using 2,7 DCF-DA. **C)** Mitochondrial membrane potential was assessed using Rhodamine-123. Data is presented as mean ± SEM of 4 independent experiments. Statistical analysis was performed using paired *t*-testing. *$p < 0.05$, **$p < 0.01$.

3.4.12. *Characterisation of ATP production under hypoxia (0.5% O_2)*

Having demonstrated that hypoxic exposure significantly affects oxygen-linked ATP turnover by seahorse assay (**Section 3.4.9**), ATP levels were assessed by ATPlite™ luminescence ATP detection assay.

No significant differences in quantitative ATP levels were demonstrated between normoxic and hypoxic conditions in HCT116 or SW837 cells (**Fig. 3.14**)**,** suggesting that downregulation of oxidative phosphorylation dependent ATP production under hypoxia, is supplemented by glycolysis-derived ATP production.

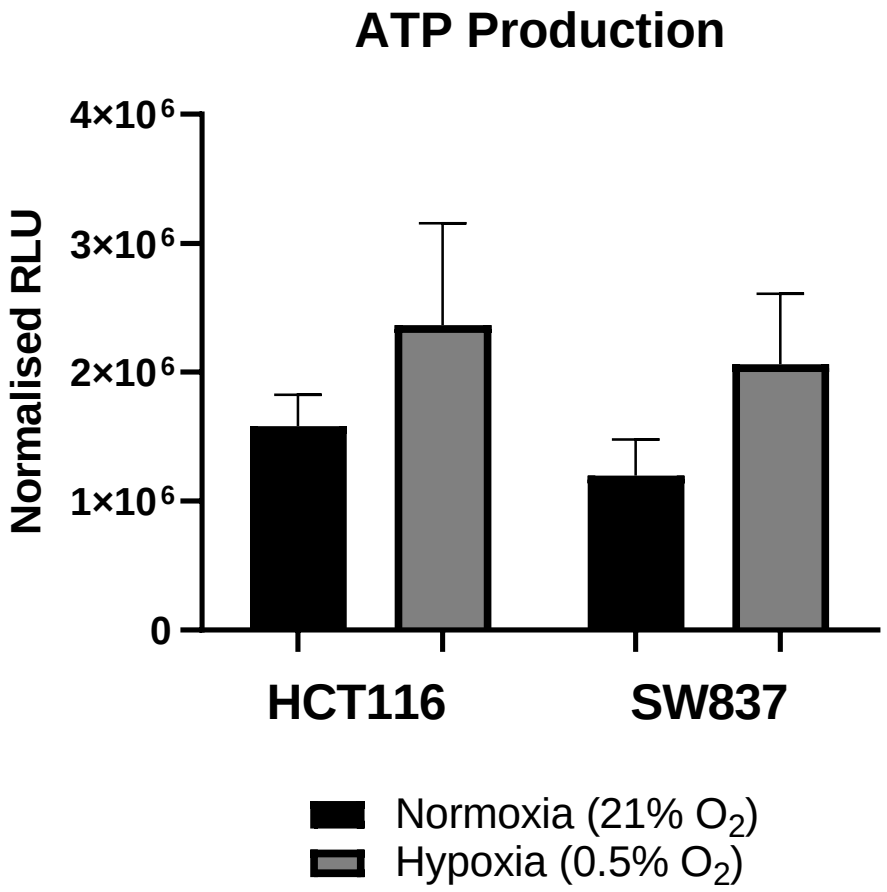

Fig. 3.14: **Characterisation of ATP production in HCT116 and SW837 colorectal cancer cell lines, under hypoxia (0.5% O_2)**. ATP production was assessed by ATPlite luminescent assay under hypoxia (0.5% O_2) and normoxia (21% O_2). No significant alterations in ATP were demonstrated in HCT116 and SW837 cells under hypoxia, when compared to normoxia. Data is presented as mean ± SEM of 5 independent experiments. Statistical analysis was performed by paired *t*-testing.

3.5. Summary of results of Chapter 3

- SW837 rectal cancer cells are significantly more radioresistant under hypoxic conditions (0.5% O_2), when compared to HCT116 colon cancer cells.
- SW837 and HCT116 cells display similar sensitivity to 5-FU treatment under hypoxia.
- HCT116 display enhanced radiation-induced apoptosis under hypoxic conditions.
- Hypoxia alters cell cycle distribution and progression in HCT116 and SW837 cells.
- Radiation-induced DNA damage is efficiently repaired under hypoxic conditions in HCT116 and SW837 cells.
- Hypoxia induces a metabolic shift in HCT116 and SW837 cells, specifically reducing reliance on oxidative metabolism, and enhancing reliance on glycolysis.
- Exposure to hypoxia alters mitochondrial function in HCT116 and SW837 cells.

3.6. Discussion

This chapter aimed to characterise the *in vitro* inherent model of radioresistant and radiosensitive CRC, SW837 and HCT116 cells, identified in Chapter 2, under hypoxic conditions.

Hypoxia is a common feature of solid tumours, as a consequence of rapid proliferation, insufficient blood supply and ultimate reduced oxygen availability. The hypoxic tumour microenvironment is a major contributor to the development of therapeutic resistance in cancer (363, 364). Due to the importance of hypoxia in the therapeutic response, the inherent *in vitro* model of radioresistant and radiosensitive CRC was assessed under hypoxic conditions.

Hypoxia is known to contribute to enhanced therapeutic resistance in many cancer types (225, 344, 364). This enhanced radioresistance was demonstrated in HCT116 cells cultured and irradiated under hypoxia, which displayed enhanced survival following 5 Gy radiation, when compared to HCT116 cells cultured under normoxic conditions. Importantly, under hypoxia, SW837 cells remained significantly more radioresistant, when compared to HCT116 cells. These data support this model as a robust *in vitro* model of inherent radioresistance/radiosensitivity, irrespective of oxygen availability.

In chapter 2, it was demonstrated that radioresistant SW837 cells were also significantly more resistant to 5-FU chemotherapy, when compared to radiosensitive HCT116 cells. Under hypoxia, no difference in chemoresistance was observed between HCT116 or

SW837 cells, after 30 h treatment with 5-FU (15 μM). However, a trend towards reduced surviving fraction in SW837 cells following 5-FU treatment under hypoxia, when compared to that under normoxia was demonstrated. This indicates that SW837 cells may become slightly more sensitive to 5-FU under hypoxia.

The impact of hypoxia on cell death was assessed by flow cytometry, at 24 h, 48 h and 72 h following hypoxic exposure. While SW837 radioresistant cells displayed no significant differences to cell death following hypoxia, HCT116 radiosensitive cells were demonstrated to be sensitive to hypoxia. By 72 h total hypoxic exposure, there was a significant decrease in the proportion of live HCT116 cells, when compared to normoxia. These cells had undergone cell death, with significant increases in the proportion of late apoptotic and necrotic cells under hypoxia in HCT116. In addition, HCT116 cells displayed enhanced apoptosis following exposure to 1.8 Gy irradiation at 48 h post radiation under normoxia, supporting previous findings in Chapter 2, however these effects were not observed under hypoxia. These data suggest that apoptosis may not contribute to the radiosensitivity of HCT116 cells under hypoxia.

In addition, HCT116 cells appear to be more susceptible to hypoxia-induced stress, when compared to SW837 cells and ultimately undergo cell death. It has been demonstrated that cancer cells, which are classed as 'non-adaptive' undergo apoptosis via HIF1-α and p53-dependent pathways following hypoxia (136). Research suggests that this hypoxia induced apoptosis is due in part to altered metabolism under hypoxic conditions, including reduced ATP availability from inhibited oxidative phosphorylation (366, 367). It was previously demonstrated in Chapter 2, that radioresistant SW837 rectal cancer cells display enhanced spare respiratory capacity, when compared to HCT116 cells. Spare respiratory capacity reflects the mitochondrial capacity of cells, which is exploited to meet high energy demands in response to cellular stresses, including hypoxia (368, 369), and perhaps this is contributing to the differential effects of hypoxia exposure between HCT116 and SW837 cells.

Hypoxia and metabolism are intrinsically linked (228, 370). Under hypoxia, the reduced oxygen availability results in a reduction in oxidative metabolism, and an enhanced glycolytic rate, which is oxygen-independent, and HIF1-α inducible (226). Following hypoxic exposure, a significant reduction to OCR was demonstrated in radioresistant SW837 cells. In addition, a shift in the OCR:ECAR was demonstrated in both HCT116 and SW837 cells, supporting a switch from oxidative phosphorylation to glycolysis in these cell lines. Importantly, non-

mitochondrial oxygen consumption was significantly reduced following hypoxic exposure in both HCT116 and SW837 cell lines, which reflects the shift from using the little remaining oxygen for use in oxidative phosphorylation. Spare respiratory capacity was significantly reduced in SW837 rectal cancer cells, demonstrating that these cells use this adaptive capacity once exposed to hypoxic stress. These findings have been supported in the literature, with research demonstrating that hypoxic exposure (<0.1% for 24 h) induces a decrease in spare respiratory capacity, alongside a metabolic shift from mitochondrial metabolism and pyruvate to lactate (371).

In addition, significant reductions to oxygen-linked ATP turnover were demonstrated in HCT116 and SW837 cells under hypoxia and reflect this shift from oxidative phosphorylation to glycolysis under hypoxic conditions, which produces a far reduced yield of ATP. These findings of reduced O_2-linked ATP turnover, and spare respiratory capacity under hypoxia, were supported in a recent study by Jiang *et al.* in an *in vitro* model of gastric adenocarcinoma (372).

In addition, hypoxic exposure was demonstrated to induce significant mitochondrial dysfunction. In SW837 cells, mitochondrial mass was significantly upregulated following hypoxic exposure. This may be a compensatory mechanism, in a bid to counteract the reduced oxidative phosphorylation levels as a result of low oxygen availability. In support, it is demonstrated in models of hepatocellular carcinoma, that hypoxia exposure induced enhanced mitochondrial biogenesis (373). In addition, enlarged mitochondria induced by hypoxia has been proposed as a potential mechanism by which cancer cells are primed to resist cell death and increase radioresistance (374-376). Furthermore, ROS production was demonstrated to be significantly decreased in HCT116 cells following exposure to hypoxia. Importantly, the impact of hypoxia on ROS production in cancer cells, and it's implication in therapeutic response is controversial (377). Due to the importance of ROS in radioresistance, perhaps this reduction in ROS production in HCT116 cells may be contributing to the enhanced radioresistance observed in these cells under hypoxia.

Hypoxic exposure was demonstrated to affect cell cycle distribution in HCT116 and SW837 cells. An enhanced proportion of G0/G1 phase cells and a reduction in S phase and G2/M phase cells was demonstrated in hypoxic SW837 cells, when compared to normoxic cells. These alterations to cell cycle distribution were also demonstrated under hypoxia in an *in vitro* breast cancer model, which also was more resistant to hypoxia (378). In contrast, a

reduction in G0/G1, and increase in S phase cells upon hypoxic exposure was demonstrated in HCT116 cells. Increased S phase cells upon hypoxia exposure has also previously been demonstrated in HCT116 cells, and as this is a radioresistant phase, it may contribute to the elevated radioresistance demonstrated in hypoxic HCT116 cells (376, 379).

Interestingly, the G2/M arrest, which is a common response to radiation to facilitate DNA damage repair, was induced under both normoxic and hypoxic conditions in HCT116 and SW837 cells following radiation exposure, however to a lesser extent under hypoxia. When assessing DNA damage induction and repair, it was demonstrated that DNA damage induced by radiation was efficiently repaired by 6 h post radiation in both HCT116 and SW837 cells, under hypoxic conditions. Many studies have demonstrated that hypoxic exposure enhances both HRR and NHEJ DNA damage repair mechanisms, the major DNA damage repair pathways utilised by cells to repair radiation induced DSBs (376, 380). In addition, hypoxia is demonstrated to prime cancer cells for DSB repair initiation, and also to be associated with enhanced resolution of γH2AX foci (376, 380-382). However, this impact of hypoxia on DNA damage repair mechanisms is controversial, with some research also suggesting that hypoxia may downregulate DNA repair, warranting further investigation (383). Overall, these data suggest that a hypoxic microenvironment supports radiation-induced DNA damage repair, potentially contributing to enhanced therapy resistance demonstrated under such conditions.

This chapter demonstrates that the *in vitro* model of inherent radioresistant CRC is robust under hypoxic conditions. Characterisation of this model under hypoxia also demonstrated alterations to apoptosis, cell cycle, metabolism and mitochondrial function, demonstrating that the tumour microenvironment has major implications on this model. Having characterised this model under normoxic and hypoxic conditions, and demonstrated its relevance as a model of radioresistance, the next chapter aims to investigate the potential of utilising anti-metabolic drugs to enhance therapeutic response in this model.

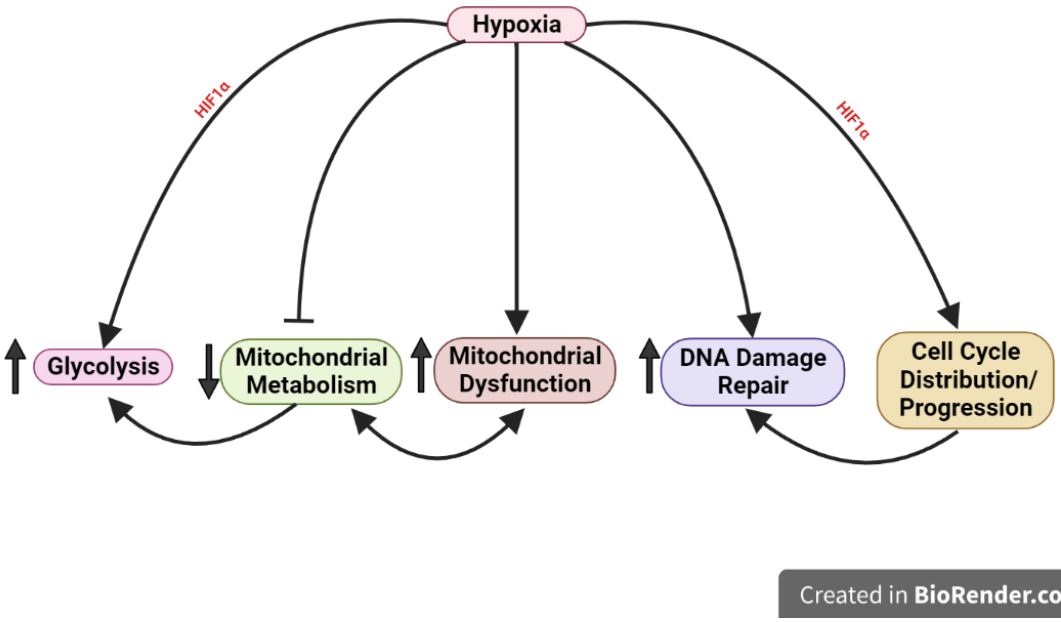

***Fig. 3.15*: Summary of main findings of chapter 3**. Hypoxia was demonstrated to alter the metabolic reliance of HCT116 and SW837 CRC cells, specifically by reducing the reliance on oxidative phosphorylation towards enhanced glycolysis. This may be due to the lack of oxygen availability to fuel oxidative phosphorylation, and HIF-1α mediated enhanced glycolysis. Hypoxia was also demonstrated to induce mitochondrial dysfunction, including increased mitochondrial mass, decreased ROS production and altered mitochondrial membrane potential in CRC cells. Radiation-induced DNA damage was efficiently repaired in CRC cells under hypoxia. Exposure to hypoxia significantly altered cell cycle distribution and progression in CRC cells, which may contribute to enhanced DNA damage repair. Figure created using BioRender.com.

Chapter 4: Targeting energy metabolism to enhance therapeutic response in an *in vitro* model of inherently radiosensitive and radioresistant colorectal cancer

4.1. Introduction

The standard of care for locally-advanced rectal cancer treatment is neoCRT followed by surgery (6). Unfortunately, the response rates to neoCRT remain low, with only approximately 20-30% of patients achieving a pCR, which is associated with improved outcomes (44-47). Importantly, as treatment is given in the neoadjuvant setting, this can result in a delay to surgery, which may have major clinical implications (44). There is currently a global unmet need to identify biomarkers predicting response to therapy, and to develop novel therapeutic strategies to enhance treatment response in those rectal cancer patients who are resistant to the current standard of care.

The development of novel drugs to enhance response to radiation therapy, radiosensitisers, is a vast and growing field, with many different pathways proposed as potential targets to enhance response (384). Very few drugs are approved clinically for their use as radiosensitisers. The standard of care for locally advanced rectal cancer involves neoadjuvant radiation therapy given concomitantly with the chemotherapeutic 5-FU (6). 5-FU is an anti-metabolite chemotherapeutic drug, which enters cells by hijacking uracil transporters. Intracellularly, 5-FU once converted to its active form disrupts RNA synthesis to induce its cytotoxic effects (61). In addition to its cytotoxic activity, 5-FU also exerts radiosensitising effects (62). However, the low pCR rates achieved by rectal cancer patients following neoadjuvant treatment with radiation therapy and 5-FU, highlights the need for the development of novel radiosensitisers to boost treatment outcomes in the neoadjuvant setting. In recent years, tumour metabolism has emerged as having a potential role in the development of therapeutic resistance (177, 208, 348). In particular, oxidative phosphorylation, a mitochondrial energy metabolism pathway, has been previously demonstrated by our department, to be associated with a radioresistant phenotype *in vitro* and *ex vivo* in oesophageal adenocarcinoma (212, 213).

Pyrazinib (P3) is a novel small molecule drug, which is under investigation in our department. P3 has been demonstrated to display anti-angiogenic and anti-metabolic effects in an *in vitro* zebrafish model, and also has been demonstrated to be an anti-metabolic drug with radiosensitising ability in an isogenic model of radioresistant oesophageal adenocarcinoma (212). Buckley *et al*. previously demonstrated that P3 is a potent inhibitor of oxidative phosphorylation, while also inhibiting glycolysis *in vitro.* As oesophageal adenocarcinoma and rectal cancer are two gastrointestinal cancers with similar treatment

regimens and similar poor therapeutic response rates, this suggests that P3 may act as a novel anti-metabolic radiosensitiser in rectal cancer.

Enhanced oxidative phosphorylation is demonstrated to be associated with poor therapeutic response (212, 213). In Chapter 2, it was demonstrated that the radioresistant SW837 rectal cancer cells display reduced reliance on glycolysis, and significant upregulation of oxidative phosphorylation genes, when compared to radiosensitive HCT116 cells. One drug which is a known inhibitor of oxidative phosphorylation and is approved for use in the clinic is metformin (279, 385). Metformin, a Complex I inhibitor, is primarily used in the management of type II diabetes (386). In recent years observational studies emerged in which diabetics with rectal or oesophageal cancer, treated with metformin during their treatment for cancer, were demonstrated to display enhanced responses to their cancer therapies (300-302). Findings such as these led to further studies investigating the potential action of metformin as a radiosensitising drug. Previous research has demonstrated efficacy of metformin as a radiosensitiser in models of CRC (231, 305). However, the potential of metformin as a novel anti-metabolic radiosensitiser in rectal cancer is largely unknown.

In this chapter, the novel small molecule compound P3, and the clinically-approved drug metformin were assessed for their impact on metabolism and radiosensitivity in the *in vitro* model of radioresistant and radiosensitive CRC.

4.2. Overall Objective and Specific Aims of Chapter 4

In this chapter, the novel small-molecule compound P3 and the clinically-approved drug metformin were assessed for their impact on metabolism and radiosensitivity in a model of inherent radiosensitive/radioresistant CRC (HCT116 and SW837 cells). The effect of P3 and metformin was assessed on the following parameters:

- Basal energy metabolism
- Mitochondrial function
- ATP production
- Proliferation
- Clonogenic replicative integrity
- Radiosensitivity

4.3. Materials and Methods

4.3.1. *Reagents and Materials*

All laboratory chemicals and reagents were stored according to manufacturer's instructions. All cell culture reagents were purchased from Gibco, unless otherwise stated. All plastic materials were purchased from Sarstedt, unless otherwise stated.

4.3.2. *Drugs*

Pyrazinib (P3) (E)-2-(2-Pyrazin-2-yl-vinyl)-phenol), a novel small-molecule compound, derived from the parent compound Quininib (2-[(e)-2-(quinoline-2yl)vinyl]phenol) was synthesised by Celtic Catalysts (Ireland) and Onyx Scientific (UK). P3 was dissolved in 100% DMSO to make 10 mM stock solutions, and stored at -20°C. Metformin (metformin hydrochloride) was purchased from Sigma-Aldrich, and prepared in distilled water to stock concentrations of 200 mM, and stored at -20°C.

5-FU was purchased from Sigma-Aldrich, and prepared in 100% DMSO, for storage at -20°C.

4.3.3. *Cell Culture*

Cell culture was carried out as per **section 2.3.2**.

4.3.3.1. *Human Colorectal Adenocarcinoma Cell Lines*

SW837 and HCT116 cells were obtained from the ECACC. The SW837 rectal cancer cells were originally obtained from a stage IV rectal adenocarcinoma from a 53-year-old Caucasian male. The HCT116 colon cancer line originated from a colon adenocarcinoma from an adult male. Culture conditions are outlined in **section 2.3.2.1.**

4.3.4. *Irradiation*

All irradiations were performed using an X-Strahl cabinet X-ray irradiator (RS225) (X-Strahl) at a dose rate of 1.74 Gy/min, as previously described (**Section 2.3.3**.) Cells to be irradiated under hypoxic conditions were exposed to X-ray radiation in air-locked containers.

4.3.5. *Hypoxia treatment*

Experiments conducted under hypoxic conditions utilised the H35 Whitley hypoxystation (Don Whitley Scientific), at 37°C, 5% CO_2/0.5% O_2. Seahorse experiments under hypoxia were conducted in the i2 hypoxychamber (Don Whitley Scientific). All plasticware and media utilised were deoxygenated in the hypoxia chamber for at least 24 h prior to use.

4.3.6. *Live-cell metabolic assessment of P3 or metformin-treated cells under normoxia or hypoxia (0.5% O_2)*

Cells were seeded at optimised seeding densities (10,000 cells per well for HCT116, 30,000 cells per well for SW837) in a 24-well cell culture XFe24 microplate (Agilent Technologies) at a volume of 100 µL and allowed to adhere at 37°C, 5% CO_2/95% atmospheric air. At 6 h post seeding, an additional 150 µL complete media was added to each well. Cells cultured under hypoxic conditions were transferred to a H35 Whitley hypoxystation at 37°C in 5% CO_2/0.5% O_2 (**Section 4.3.5**), while cells for normoxic culture remained at 37°C in 5% CO_2/95% atmospheric air.

At 24 h post seeding, medium was removed to waste, and cells were treated with either P3-vehicle control (0.2% DMSO), a series of concentrations of P3 (1 µM, 5 µM, 10 µM, 12.5 µM, 15 µM, 20 µM), H_2O control (5%) or metformin (1 mM, 2.5 mM, 10 mM) under normoxic or hypoxic conditions, as appropriate. At 24 h post treatment, cells were washed with unbuffered Seahorse XF Base DMEM (Agilent*/* (supplemented with 10 mM glucose (Sigma), 10 mM sodium pyruvate (Sigma) and L-glutamine) and normoxic plates placed in a non-CO_2 incubator for 1 h at 37°C, while hypoxic plates remained in the H35 hypoxystation. OCR and ECAR were measured using the Seahorse XFe24 Extracellular Flux Analyser, under either normoxia or hypoxia (0.5% O_2) in the i2 hypoxystation (Don Whitley). Three baseline measurements of OCR and ECAR were taken over 24 min, consisting of 2 repetitions of mix (3 min)/ wait (2 min)/ measurement (3 min), to establish basal respiration. These steps were repeated following the injection of a series of mitochondrial inhibitors (oligomycin (Sigma), FCCP (Sigma) and antimycin-A(Sigma), as described in **section 2.3.6**. All OCR/ECAR readings were normalised using the crystal violet assay (**Section 2.3.9**).

4.3.7. *Assessment of mitochondrial function of P3 or metformin-treated cells under normoxia or hypoxia (0.5% O_2)*

Three surrogate markers of mitochondrial function, reactive oxygen species (ROS), mitochondrial membrane potential and mitochondrial mass were assessed using a series of fluorescent probes (2,7 DCF), Rhodamine-123 and MitoTracker Green^{FM}) were used, as previously described (212).

HCT116 cells (10,000 cells per well) and SW837 cells (30,000 cells per well) were seeded in triplicate in a 96-well plate and placed at 37°C in 5% CO_2/95% atmospheric air. At 6 h post seeding, cells for hypoxic culture were transferred to the Whitley H35 hypoxystation at

37°C in 5% CO_2/0.5% O_2, while cells to be cultured under normoxia remained at 37°C in 5% CO_2/95% atmospheric air. At 24 h post seeding, the medium was removed and cells were treated with P3-vehicle control (0.2% DMSO), a series of concentrations of P3 (1 µM, 5 µM, 10 µM, 12.5 µM, 15 µM or 20 µM), metformin vehicle (H_2O) control or metformin (1 mM, 2.5 mM, 10 mM), under normoxia or hypoxia. At 24 h post treatment, the media was removed and cells were incubated with a fluorescent probe (in PBS Mg) for 30 min, in the dark at 37°C, while remaining under normoxia or hypoxia, as appropriate. The probe was removed, fresh PBS was added and the fluorescence was immediately read using a FLx800 Fluorescence microplate reader (Mason Technology). Fluorescence values were subsequently normalised to cell number using the crystal violet assay (**Section 2.3.9**).

4.3.8. *ATPlite assay on cells treated with P3 or metformin*

ATP levels were measured using the ATPLite Luminescence ATP Detection Assay System (Perkin Elmer).

Cells were seeded (SW837: 30,000 cells/well) in triplicate into a white-walled 96-well plate (Perkin Elmer). Cells were also seeded into a standard 96-well plate, for subsequent normalisation. At 24 h post seeding, medium was removed to waste and cells were treated with 100 µL DMSO control (0.2%), various concentration of P3 (1 µM, 5 µM, 10 µM, 12.5 µM, 15 µM or 20 µM), H_2O control or metformin (1 mM, 2.5 mM or 10mM) in both the white-walled and normalisation plate. At 24 h post treatment, 50 µL of Mammalian Cell Lysis Solution (Perkin Elmer) was added to each well of the white-walled 96-well plate, and incubated on an orbital shaker, for 5 min at 700 rpm at RT°. This step lyses the cells, releasing and stabilising the ATP. A volume of 50 µL Substrate Solution (Perkin Elmer) was added to each well of the white-walled plate, and incubated for 5 min at 700 rpm, at RT°. The plate was subsequently dark-adapted for 10 min at RT°. The luminescence was measured for 1 s on a FLx800 Fluorescence Microplate Reader (Mason Technology Ireland). Luminescence was normalised using the crystal violet assay (**Section 2.9**) performed on the corresponding standard 96-well plate.

4.3.9. *Clonogenic optimisation of 5-FU as a radiosensitiser*

In order to determine the optimal schedule of 5-FU treatment as a positive control for radiosensitisation, a clonogenic assay was performed.

HCT116 and SW837 cells were harvested in the exponential growth phase and seeded in a single-cell suspension into 6-well plates at previously-optimised seeding densities (**Section**

2.3.4). Cells were allowed to adhere to the plates overnight in 5% CO_2/95% atmospheric air, at 37°C. Either 24 h or 42 h after seeding, cells were treated with a range of doses of 5-FU (5 µM, 10 µM, 15 µM or 20 µM) or DMSO vehicle control (0.001%), and incubated in 5% CO_2/95% atmospheric air, at 37°C. Exactly 48 h post seeding (24 h or 6 h post drug treatment), cells were irradiated with clinically relevant doses of 1.8 Gy or 5 Gy X-ray radiation (**Section 4.3.4**), or mock-irradiated. At 24 h post radiation, drug treatments were removed, and replaced with 1.5 mL RPMI. Cells were incubated in 5% CO_2/95% atmospheric air, at 37°C for 7-14 days, until colonies formed, but had not merged. Colonies were then fixed/stained and counted as previously described (**Sections 2.3.4.2 and 2.3.4.3**).

4.3.10. *Clonogenic assessment of effect of P3/metformin as radiosensitisers under hypoxic (0.5% O_2) or normoxic conditions*

To investigate the ability of various drugs to radiosensitise CRC cell lines, clonogenic assays were performed on treated cells, under normoxic (21% O_2) or hypoxic conditions (0.5% O_2).

Cells in the exponential growth phase were harvested, seeded into 6-well plates at optimised cell densities (**Section 2.3.4**), and allowed to adhere to the plate at 5% CO_2/95% atmospheric air, at 37°C. Following 6 h incubation, plates to be cultured under hypoxia were transferred into a Whitley H35 hypoxystation (Don Whitley Scientific) in 0.5% O_2/5% CO_2 at 37°C. Normoxic plates remained incubated at 5% CO_2/95% atmospheric air (~21% O_2) at 37°C. Following 24 h incubation under normoxic or hypoxic conditions, plates remained under either normoxia or hypoxia and medium was removed to waste. Cells were treated with P3 (1 µM, 5 µM, 10 µM, 12.5 µM, 15 µM, 20 µM, 50 µM, 100 µM or 200 µM), DMSO control (0.2%, 0.5% or 2%), metformin (1 mM, 2.5 mM or 10mM) or H_2O control (5%) for 24 h prior to radiation. The following day, as a positive control, appropriate wells were treated with an optimised dose of 15 µM 5-FU, or its DMSO (0.001%) control, 6 h pre-irradiation. At 24 h post P3/metformin treatment, cells were exposed to clinically-relevant doses of 1.8 Gy, 5 Gy X-ray radiation, or mock-irradiated, as described (**Section 2.3.3**). Hypoxic cells were irradiated under hypoxic conditions (**Section 4.3.5)**. Following 24 h incubation post-radiation, cells were removed from hypoxic conditions, and the drug treatment removed, and replenished with normoxic RPMI (1.5 mL/well) in both normoxic and hypoxic plates. Cells were incubated in 5% CO_2/95% atmospheric, at 37°C for 7-14 days. Colonies were fixed and counted as described (**Sections 2.3.4.2 and 2.3.4.3)**.

4.3.11. *Statistical analysis*

All statistical analysis and graphing were performed using Graphpad Prism v9 software. Data is presented as mean ± SEM throughout. All statistical comparisons were carried out using ANOVA testing, post-hoc Tukey's multiple comparisons testing, or *t*-testing, depending on the experimental set up, as described in fig. legends. Results were considered significant where probability (*p)* ≤ 0.05.

4.4. Results

4.4.1. *P3 treatment inhibits metabolism in a dose-dependent manner in radioresistant SW837 cells*

The effect of 24 h treatment with the novel compound P3 (1 µM, 5 µM, 10 µM, 12.5 µM, 15 µM, 20 µM) or 0.2% DMSO vehicle control on oxidative phosphorylation (OCR) and glycolysis (ECAR) in SW837 cells or was assessed using the Seahorse^{TM} XFe24 analyser.

Treatment with P3 (15 µM and 20 µM doses (p = 0.004, p = 0.004 respectively) (Mean % OCR of control (mean ± SEM); 15 µM 73.02 ± 2.24, 20 µM 68.2 ± 2.65) for 24 h was demonstrated to significantly reduce OCR, when compared to the DMSO control) (**Fig. 4.1A**).

ECAR was also demonstrated to be significantly reduced in SW837 cells at 10 µM (p = 0.019), 12.5 µM (p = 0.0361), and 20 µM (p = 0.0029) doses (mean % ECAR of control; 10 µM 88.32 ± 3.027, 12.5 µM 85.82 ± 1.79, 15 µM 72.78 ± 7.28, 20 µM 60.81 ± 2.92) (**Fig. 4.1B**).

These data demonstrate that P3 has anti-metabolic activity in a dose-dependent manner in radioresistant rectal cancer cells.

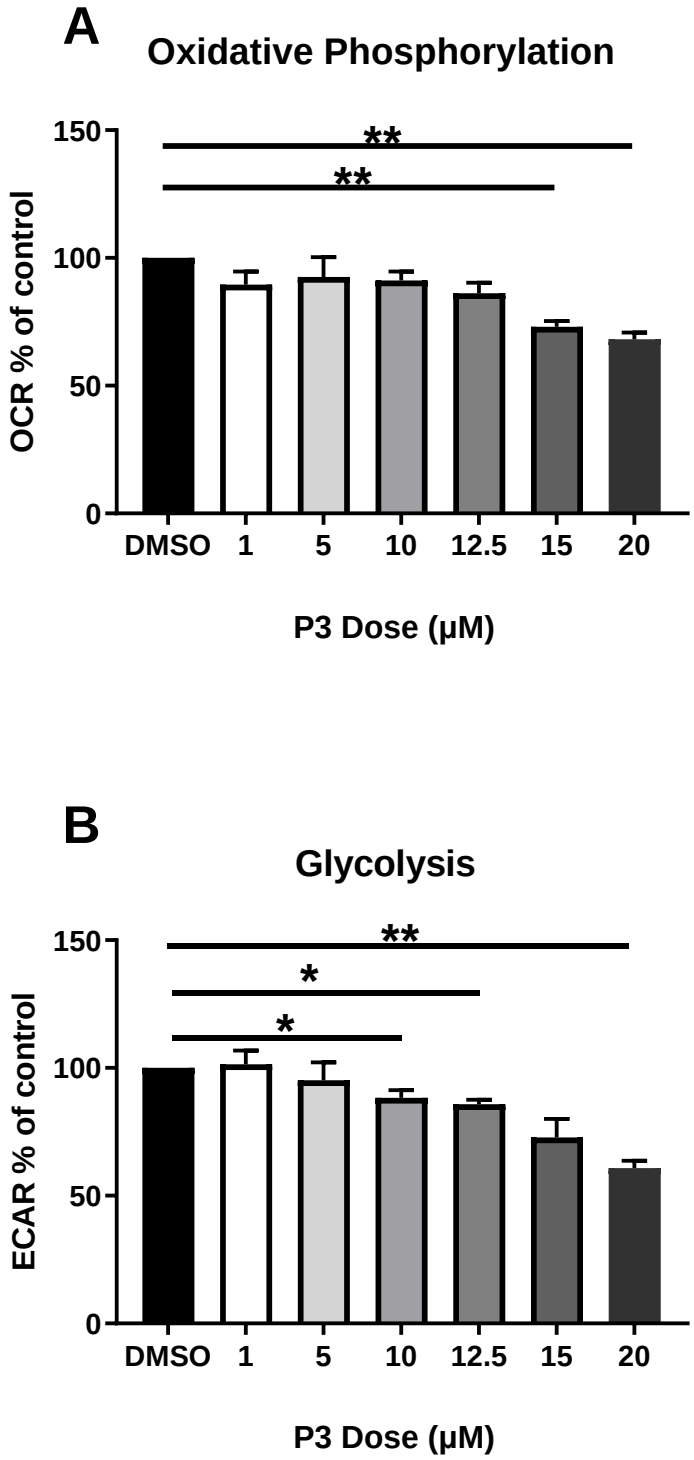

Fig. 4.1: **P3 treatment reduces both oxidative phosphorylation and glycolysis rates in radioresistant SW837 rectal cancer cells, in a dose-dependent manner.** OCR and ECAR values were assessed using the Seahorse XFe24 analyser. **A)** OCR % of DMSO control of SW837 cells treated with a range of P3 doses. **B)** ECAR % of DMSO control of SW837 cells treated with a range of P3 doses. Data is presented as mean ± SEM from at least 3 independent experiments (12.5 μM *n*=3) (1 μM, 5 μM, 15 μM, 20 μM *n*=4)(10 μM *n*=10). Statistical analysis was performed by paired ANOVA. **p* < 0.05, ***p* < 0.01.

4.4.2. *P3 treatment inhibits mitochondrial metabolic parameters in radioresistant SW837 cells*

To further interrogate the anti-metabolic effects of P3, SW837 cells treated with a range of doses of P3 (1 µM, 5 µM, 10 µM, 12.5 µM, 15 µM, 20 µM) or 0.2% DMSO vehicle control, for 24 h, were exposed to a series of mitochondrial inhibitors and the effect on OCR was assessed using the Seahorse XFe24 analyser.

No effect on non-mitochondrial oxygen consumption was demonstrated following P3 treatment in SW837 cells, when compared to vehicle control (**Fig. 4.2A**). Basal respiration, reflecting the oxygen consumption used by cells to meet basal energy demands, was demonstrated to be significantly reduced following 24 h treatment with P3 at doses of 12.5 µM (p = 0.038), 15 µM (p = 0.0046) and 20 µM (p = 0.0041) (**Fig. 4.2B**) (Basal respiration (% control) ± SEM; 12.5 µM 75.53 ± 3.16, 15 µM 69.81 ± 2.64, 20 µM 65.18 ± 2.93). Maximal respiration was demonstrated to be significantly reduced following treatment with P3 at doses of 12.5 µM (p = 0.0128), 15 µM (p = 0.0007) and 20 µM (p = 0.001) (**Fig. 4.2C**) (mean max. respiration (% control) ± SEM; 12.5 µM 70.54 ± 2.195, 15 µM 66.65 ± 1.53, 20 µM 59.2 ± 2.15). Spare respiratory capacity was also demonstrated to be significantly reduced following 24 h treatment with P3 at doses of 15 µM (p = 0.006) and 20 µM (p = 0.0024) (**Fig. 4.2D**) (Mean spare respiratory capacity (% control) ± SEM; 15 µM 61 ± 3.733, 20 µM 49.08 ± 3.573).

Oxygen-linked ATP turnover was demonstrated to be significantly reduced in SW837 cells following 24 h treatment with P3 at doses of 12.5 µM (p = 0.0121), 15 µM (p = 0.0206) and 20 µM (p = 0.0037) (**Fig. 4.2E**) (mean ATP turnover (% control) ± SEM; 12.5 µM 76.28 ± 1.718, 15 µM 68.6 ± 4.61, 20 µM 65.58 ± 2.783). Proton leak, reflecting the oxygen consumption used by these cells, which is not linked to ATP synthesis, was also demonstrated to be significantly reduced following P3 treatment at a concentration of 20 µM (p = 0.008) (**Fig. 4.2F**) (Mean proton leak (% control) ± SEM); 20 µM 63.20 ± 3.878). Coupling efficiency, which reflects the basal oxygen consumption for ATP synthesis, compared to that used by proton leak was not altered following 24 h P3 treatment, at any concentration (**Fig. 4.2G**).

These data demonstrate that P3 significantly reduces basal and maximal respiration, spare respiratory capacity and ATP turnover in SW837 radioresistant cells.

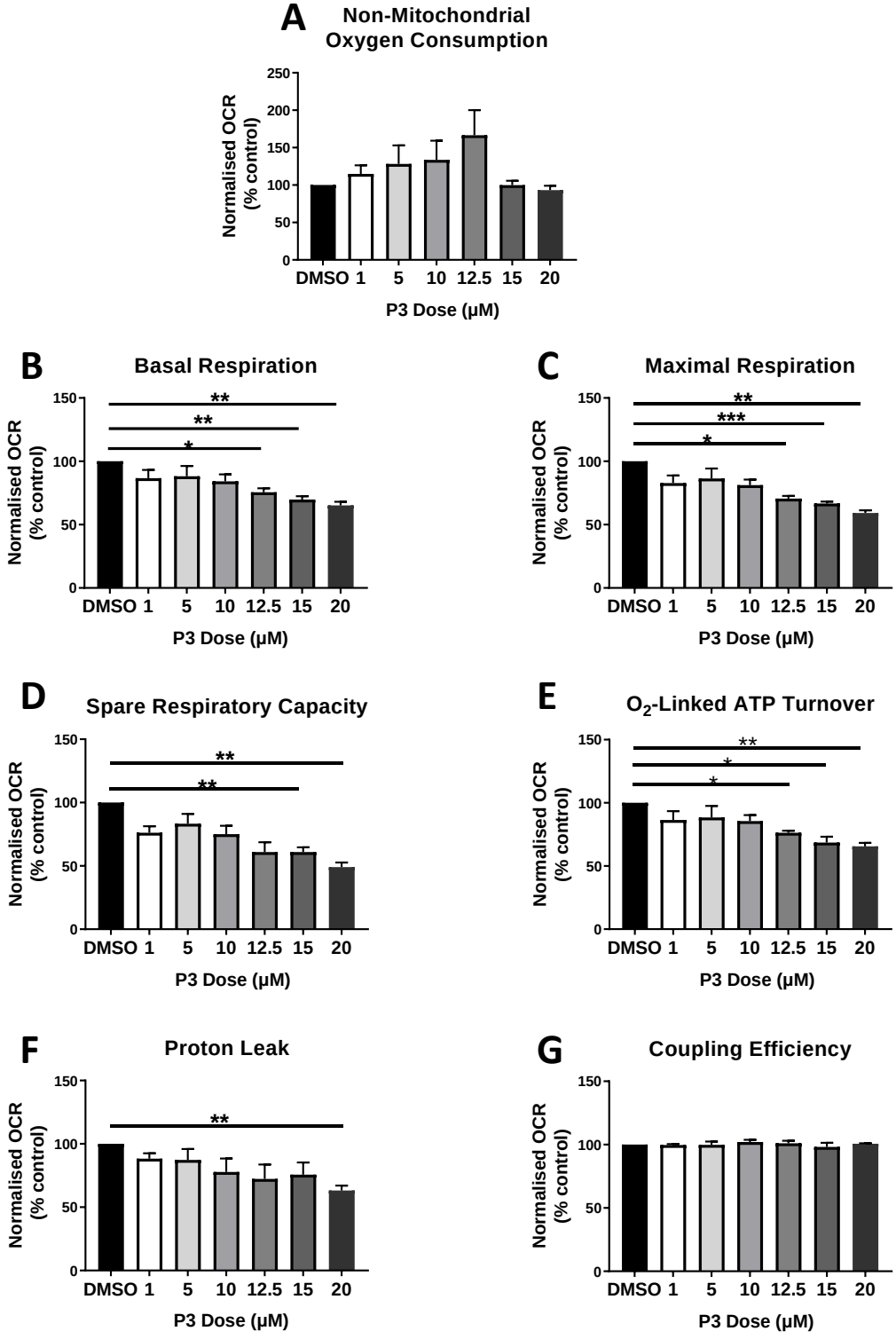

Fig. 4.2: **P3 inhibits mitochondrial metabolic parameters in a dose-dependent manner in SW837 rectal cancer cells.** Mitochondrial metabolic parameters were assessed following P3 treatment (24 h) using the Seahorse XFe24 analyser and a series of mitochondrial inhibitors in SW837 cells. **A)** Non-mitochondrial respiration. **B)** Basal respiration. **C)** Maximal respiration. **D)** Spare respiratory. **E)** O_2-linked ATP turnover. **F)** Proton leak. **G)** Coupling Efficiency. Data is presented as mean ± SEM for 4 independent experiments. Statistical analysis was performed by paired mixed-effects analysis. *$p < 0.05$, **$p < 0.01$, ***$p < 0.001$.

4.4.3. *P3 treatment inhibits glycolytic metabolic parameters in radioresistant SW837 cells*

To further interrogate the impact of P3 treatment on metabolism in SW837 cells, glycolytic parameters were assessed following injection of oligomycin A (354).

Total glycolytic capacity, which reflects the ECAR reading following inhibition of mitochondrial metabolism by oligomycin A injection, was demonstrated to be significantly reduced in SW837 cells following 24 h treatment with 20 μM P3, when compared to vehicle control (0.2% DMSO) (p = 0.0439) (total glycolytic capacity as % control (mean ± SEM) 20 μM 74.55 ± 4.915) (**Fig. 4.3A**). Treatment with 12.5 μM P3 displayed a trend towards reduced total glycolytic capacity, although this did not reach statistical significance (p = 0.058).

Glycolytic reserve capacity, which reflects the potential glycolytic capacity reserved for use under stress conditions, was also demonstrated to be significantly lower in P3 treated SW837 cells, when compared to DMSO control, at 15 μM and 20 μM doses (p = 0.0437, p = 0.0223 respectively) (glycolytic reserve capacity as % control (mean ± SEM): 15 μM 86.86 ± 2.54, 20 μM 80.41 ± 2.96) (**Fig. 4.3B**).

These data demonstrate that the novel drug P3 induces significant inhibition to glycolytic metabolism in radioresistant SW837 rectal cancer cells.

4.4.4. *P3 treatment significantly inhibits ATP production in radioresistant SW837 cells*

Having demonstrated that P3 treatment significantly inhibits oxygen-linked ATP turnover in SW837 cells (**Fig. 4.2**), ATP production was quantitatively assessed by ATPlite™ luminescence ATP detection assay.

Treatment with 20 μM P3 for 24 h was demonstrated to significantly inhibit ATP production in SW837 cells, when compared to vehicle control (0.2% DMSO) (p = 0.01) (mean relative luminescence ± SEM; 20 μM P3 0.84 ± 0.043) (**Fig. 4.4**).

These data demonstrate that P3 treatment significantly reduces ATP production in SW837 cells.

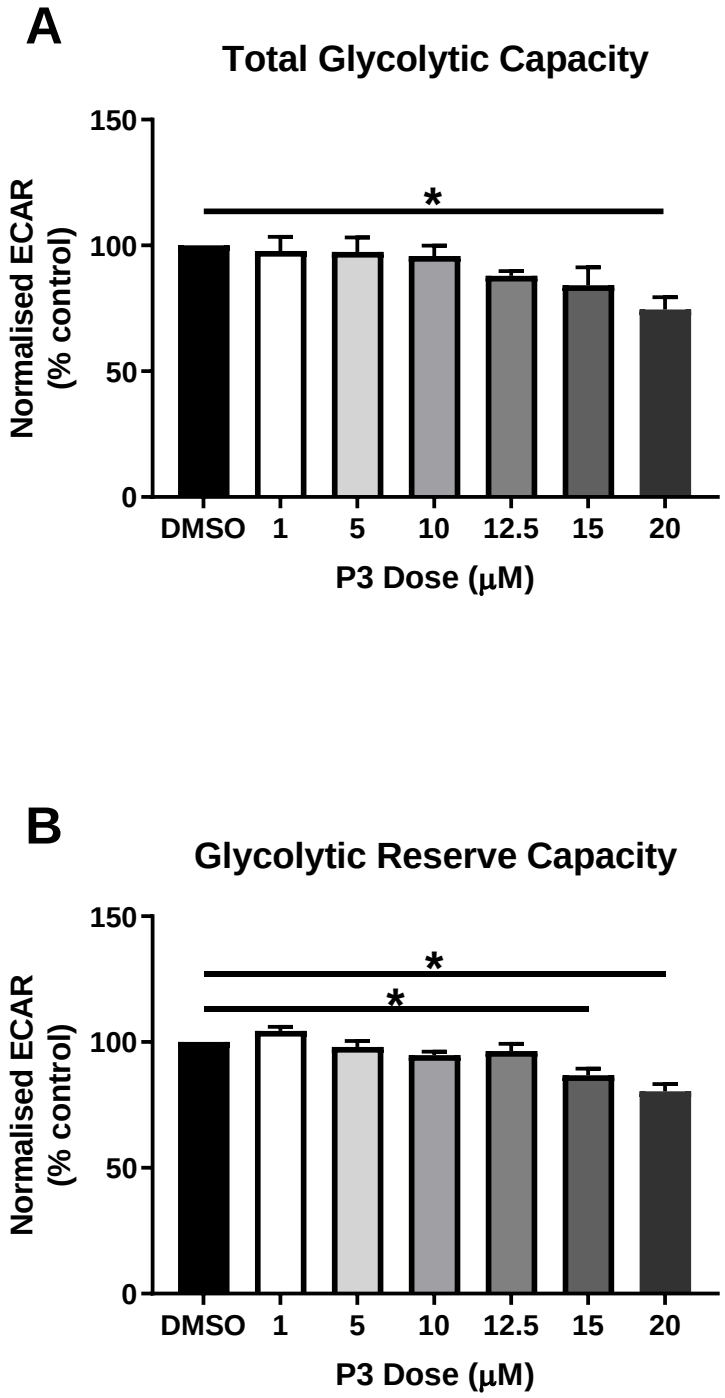

***Fig. 4.3*: P3 treatment inhibits glycolytic parameters in a dose-dependent manner in radioresistant SW837 cells.** Glycolytic parameters were assessed following P3 treatment (24 h), or DMSO control (0.2%) using the Seahorse XFe24 analyser and injection of Oligomycin A in SW837 cells. **A)** Total glycolytic capacity **B)** Glycolytic reserve capacity. Data is presented as mean ± SEM for 4 independent experiments. Statistical analysis was performed by paired mixed-effects analysis. *$p < 0.05$

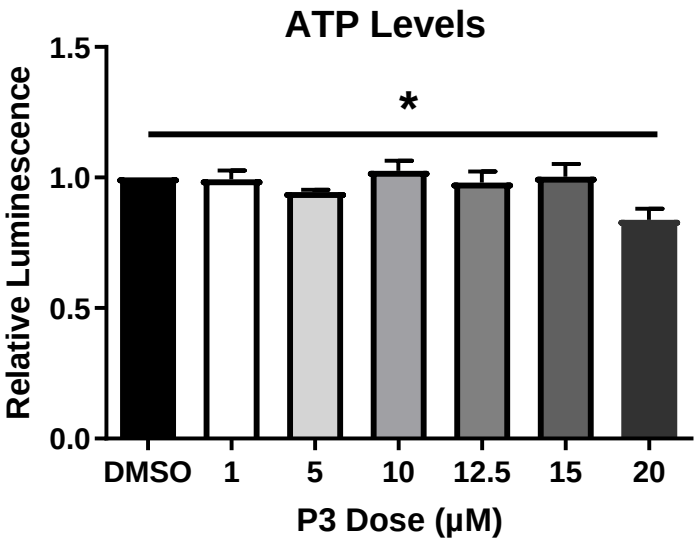

Fig. 4.4: **P3 treatment significantly reduces ATP production in SW837 cells.** ATP production was assessed by ATPlite luminescent assay after 24 h drug exposure. Data is presented as mean ± SEM from 3 independent experiments. Statistical analysis was performed by paired mixed effects analysis. *$p < 0.05$.

4.4.5. *P3 treatment significantly induces mitochondrial dysfunction in radioresistant SW837 cells*

Having demonstrated that P3 treatment alters mitochondrial metabolism in SW837 cells (**Section 4.4.1 and 4.4.2**), the effect of P3 treatment on mitochondrial function (mitochondrial mass, ROS production and mitochondrial membrane potential) in SW837 cells was assessed. SW837 cells were treated with a range of doses of P3 (1 µM, 5 µM, 10 µM, 12.5 µM, 15 µM, 20 µM) or 0.2% DMSO vehicle control, for 24 h and mitochondrial function was assessed by fluorescent probes.

Mitochondrial mass was demonstrated to be significantly increased following treatment with 5 µM and 20 µM P3, when compared to DMSO control ($p = 0.039$, $p = 0.006$) (Mean fluorescence relative to control ± SEM; 5 µM 136 ± 10.29, 20 µM 141.2 ± 5.86) (**Fig. 4.5A**). Treatment with P3 significantly induced ROS production at 5 µM, 10 µM and 15 µM, when compared to DMSO control ($p = 0.046$, $p = 0.039$, $p = 0.027$ respectively) (Mean fluorescence relative to control; 5 µM 162.9 ± 19.1, 10 µM 187.3 ± 24.9, 15 µM 224.6 ± 30.67) (**Fig. 4.5B**). A trend towards increased ROS production in SW837 cells treated with 12.5 µM P3 was demonstrated, but this did not reach statistical significance ($p = 0.058$). Mitochondrial membrane potential was demonstrated to be significantly increased in SW837 cells treated with 12.5 µM and 20 µM P3, when compared to DMSO control ($p = 0.0006$, $p = 0.033$) (Mean fluorescence relative to control; 12.5 µM 117.5 ± 1.13, 20 µM 123.6 ± 6.3) (**Fig. 4.5C**).

These data demonstrate that P3 treatment significantly alters mitochondrial function in SW837 cells.

4.4.6. *Optimisation of 5-FU treatment in HCT116 and SW837 cells*

The current standard of care for rectal cancer involves neoadjuvant radiation therapy and 5-FU treatment. 5-FU has demonstrated radiosensitising effects (65). In order to identify a radiosensitising dose of 5-FU *in vitro* to act as an accurate positive control for radiosensitisation, a clonogenic assay was performed in HCT116 and SW837 cells treated with a range of doses of 5-FU prior to radiation treatment. Cells were treated with 5-FU (5 µM, 10 µM, 15 µM or 20 µM) for 24 h or 6 h before treatment with 1.8 Gy or 5 Gy radiation, 5-FU treatment was removed at 24 h post irradiation and radiosensitivity was assessed by clonogenic assay.

HCT116 were significantly sensitised to 1.8 Gy radiation following treatment with 15 µM and 20 µM 5-FU for 6 h prior to irradiation ($p = 0.003$, $p = 0.0007$ respectively), when

compared to DMSO control (Mean surviving fraction ± SEM; 15 μM 28.15 ± 2.74, 20 μM 19.97 ± 4.46 vs. DMSO 61.04 ± 5.8) (**Fig. 4.6A**). In addition, HCT116 cells were also significantly sensitised to 1.8 Gy radiation following treatment with 10 μM, 15 μM and 20 μM of 5-FU for 24 h prior to irradiation, (p 0.035, p = 0.021, p = 0.0104 respectively), when compared to DMSO control (Mean surviving fraction ± SEM; 10 μM 39.45 ± 8.65, 15 μM 36.63 ± 5.77, 20 μM 32.75 ± 8.14 vs. DMSO 64.34 ± 8.16) (**Fig. 4.6B**).

5-FU treatment 6 h prior to irradiation also significantly radiosensitised HCT116 cells to 5 Gy X-ray radiation at all 5-FU doses tested (p < 0.0001 for all) (Mean surviving fraction ± SEM; 5 μM 2.3.2 ± 0.19, 10 μM 0.76 ± 0.11, 15 μM 0.34 ± 0.19, 20 μM 0.42 ± 0.38 vs. DMSO 5.69 ± 0.43) (**Fig. 4.6C)**. In addition, HCT116 cells were also significantly sensitised to 5 Gy radiation following treatment with 5 μM (p = 0.0001) and 10 μM, 15 μM and 20 μM (p < 0.0001 for all) of 5-FU for 24 h prior to irradiation, when compared to DMSO control (mean surviving fraction ± SEM; 5 μM 1.61 ± 0.12, 10 μM 0.89 ± 0.15, 15 μM 0.72 ± 0.25, 20 μM 0.59 ± 0.29 vs DMSO 4.87 ± 0.58) (**Fig. 4.6D**).

In radioresistant SW837 rectal cancer cells, 5-FU treatment did not radiosensitise cells at 1.8 Gy following 5-FU treatment for either 6 h or 24 h prior to irradiation (**Fig. 4.7A, 4.7B**). However, SW837 cells were significantly more sensitive to 5 Gy radiation following treatment with 15 μM 5-FU for 6 h prior to irradiation, when compared to vehicle control (p = 0.0375) (Mean relative surviving fraction ± SEM; 15 μM 6 hr pre-radiation 31.58 ± 0.82 vs DMSO 36.81 ± 0.930) (**Fig. 4.7C**). No differences to radiosensitivity were demonstrated in SW837 cells following treatment with 5-FU for 24 h prior to 5 Gy radiation (**Fig. 4.7D**).

These data demonstrate that 5-FU sensitises HCT116 and SW837 CRC cells to X-ray radiation *in vitro*. Pre-treatment of cells with 15 μM of 5-FU for 6 h prior to irradiation was utilised as a positive control for radiosensitisation for all subsequent experiments.

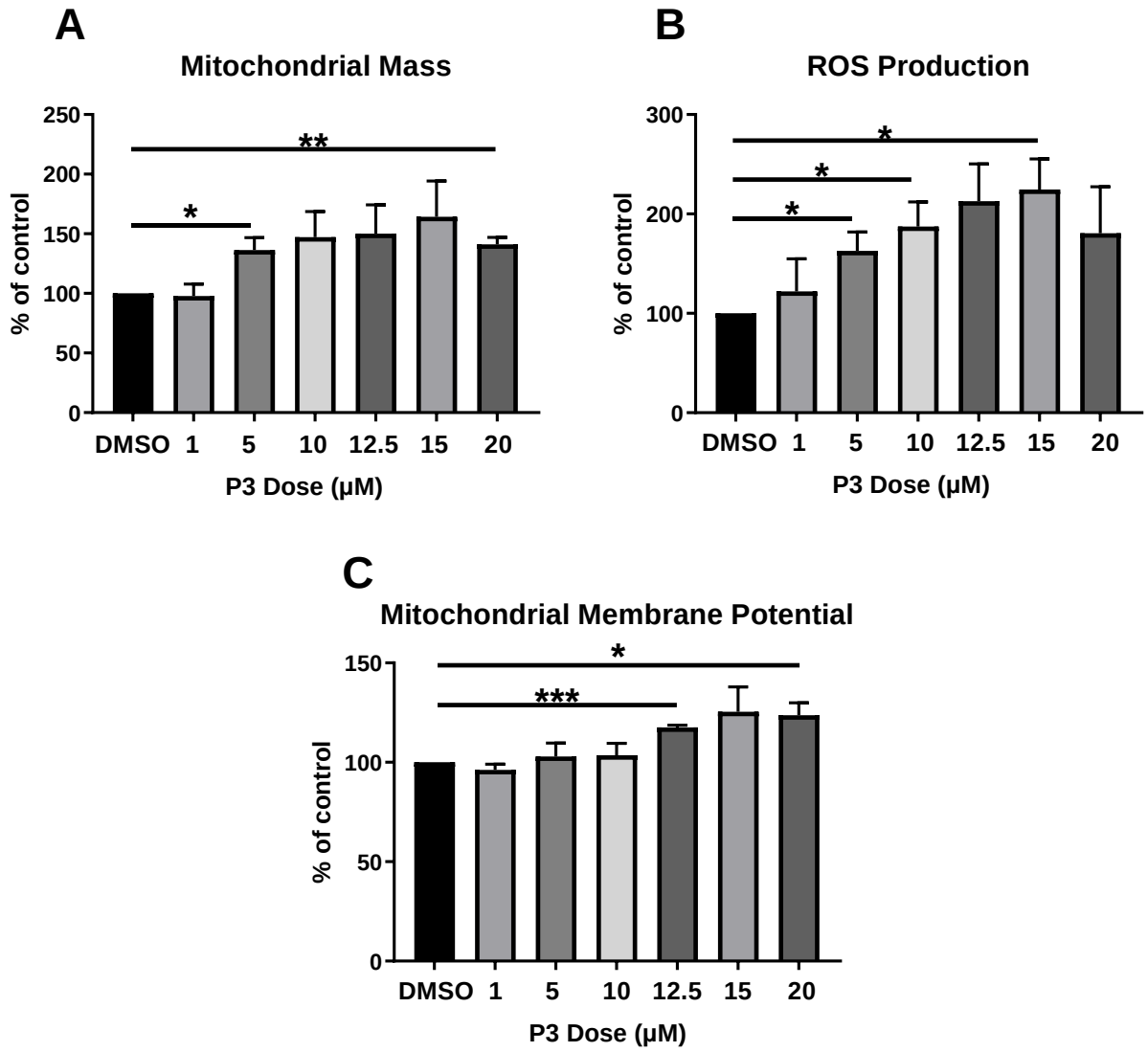

Fig. 4.5: **P3 treatment induces mitochondrial dysfunction in SW837 cells.** Mitochondrial function was assessed using a series of fluorescent probes in SW837 cells, following 24 h treatment with a range of doses of P3 (1 µM, 5 µM, 10 µM, 12.5 µM, 15 µM, 20 µM) or DMSO control. **A)** Mitochondrial mass was assessed using MitoTracker Green FM. **B)** ROS production was assessed using 2,7 DCF-DA. **C)** Mitochondrial membrane potential was assessed using Rhodamine-123. Data is presented as mean ± SEM of 4 independent experiments. Statistical analysis was performed by paired ANOVA. *$p < 0.05$, ** $p < 0.01$, ***$p < 0.001$.

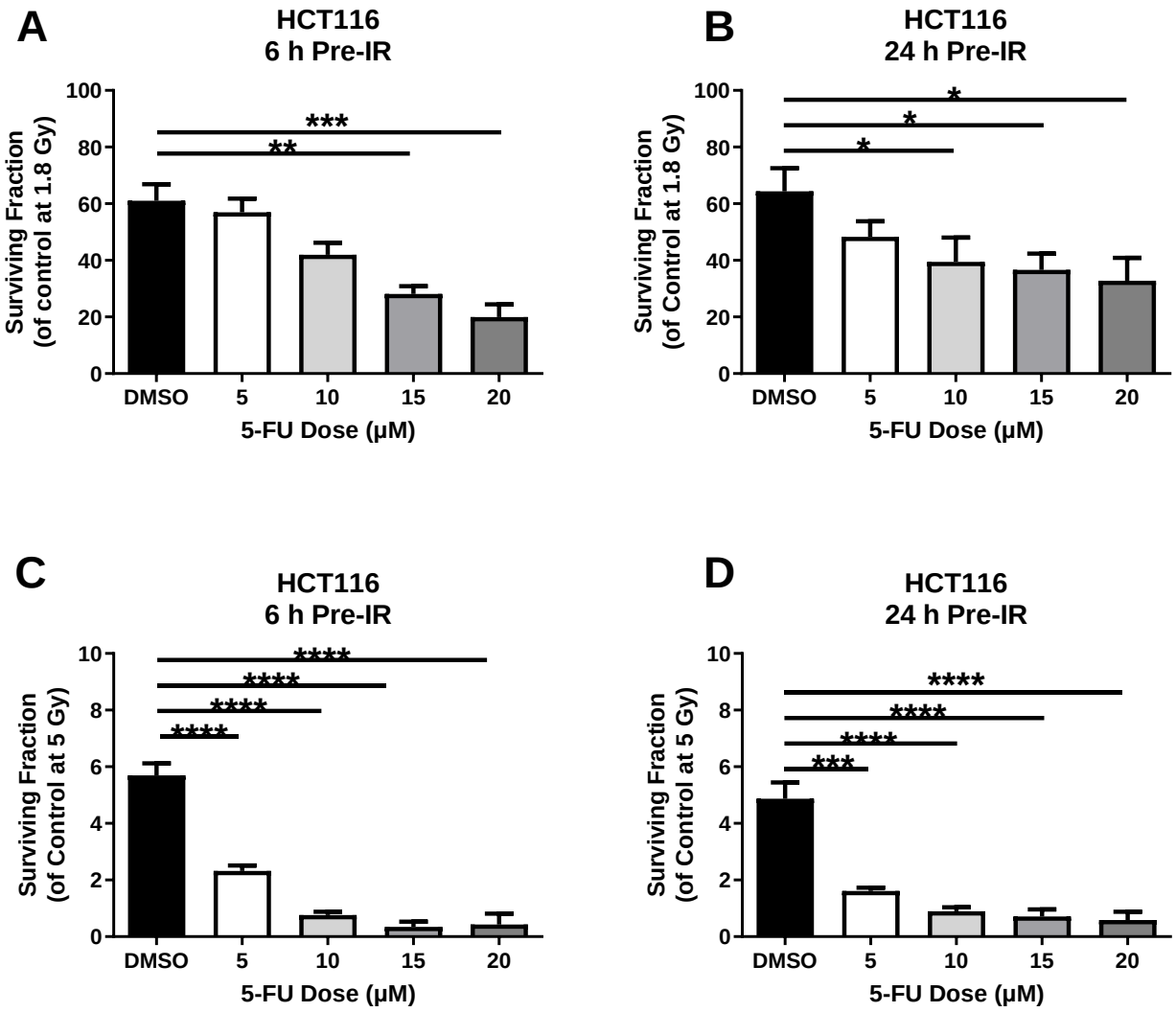

Fig. 4.6: **5-FU significantly sensitises radiosensitive HCT116 cells to X-ray radiation.** Radiosensitivity was assessed by the gold-standard clonogenic assay in HCT116 cells treated with a range of doses of 5-FU (5 μM, 10 μM, 15 μM and 20 μM) or DMSO vehicle control, either 6 h or 24 h prior to irradiation with 1.8 Gy or 5 Gy. **A)** 5-FU treatment 6 h prior to 1.8 Gy. **B)** 5-FU treatment 24 h prior to 1.8 Gy. **C)** 5-FU treatment 6 h prior to 5 Gy radiation. **D)** 5-FU treatment 24 h prior to 5 Gy radiation. Data is presented as mean ± SEM for 3 independent experiments. Statistical analysis was performed by paired ANOVA, and Tukey's multiple comparisons testing. *$p < 0.05$, **$p < 0.01$, ***$p < 0.001$, ****$p < 0.0001$.

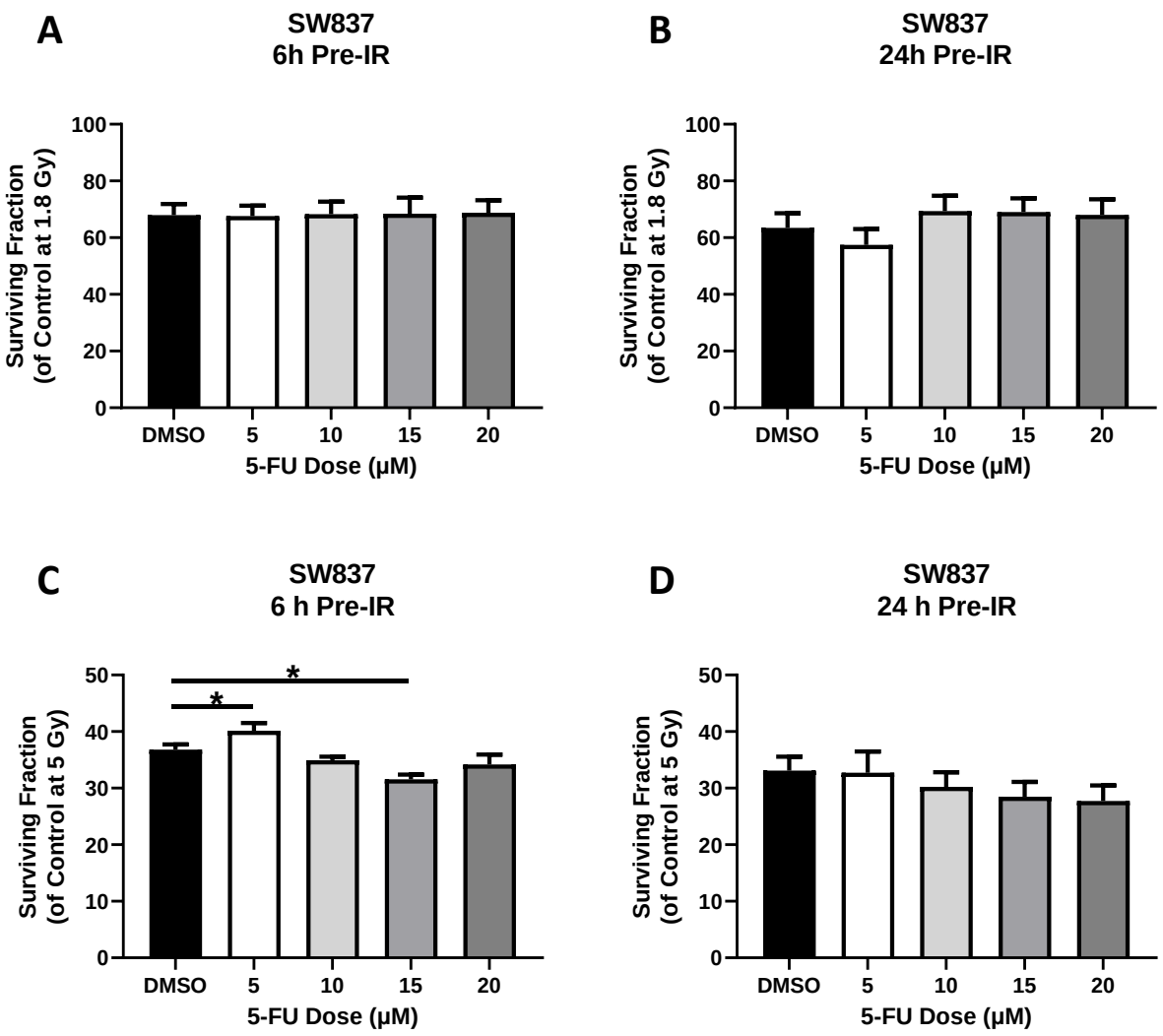

Fig. 4.7: **5-FU significantly sensitises radioresistant SW837 cells to X-ray radiation.** Radiosensitivity was assessed by the gold-standard clonogenic assay in SW837 cells treated with a range of doses of 5-FU (5 μM, 10 μM, 15 μM and 20 μM) or DMSO vehicle control, either 6 h or 24 h prior to radiation exposure. **A)** 5-FU treatment 6 h prior to 1.8 Gy. **B)** 5-FU treatment 24 h prior to 1.8 Gy. **C)** 5-FU treatment 6 h prior to 5 Gy radiation. **D)** 5-FU treatment 24 h prior to 5 Gy radiation. Data is presented as mean ± SEM for 4 independent experiments. Statistical analysis was performed by paired ANOVA, and Tukey's multiple comparisons testing. *$p < 0.05$.

4.4.7. *P3 treatment does not radiosensitise HCT116 or SW837 cells*

To investigate the potential utility of P3 as a radiosensitiser in rectal cancer cells, radioresistant SW837 cells were treated with P3 (1μM, 5μM, 10μM, 12.5μM, 15μM, 20 μM) or vehicle control (0.2% DMSO) for 24 h before irradiation with 0 Gy, 1.8 Gy, 2 Gy, 4 Gy or 6 Gy X-ray radiation and radiosensitivity was assessed by clonogenic assay.

No significant alterations were demonstrated in the surviving fraction of SW837 cells following 24 h pre-treatment with any dose of P3 or 5-FU at 1.8 Gy, 2 Gy, 4 Gy or 6 Gy X-ray radiation (**Fig. 4.8A-D**).

Having demonstrated that 24 h exposure with P3 doses lower than 20 μM did not radiosensitise SW837 cells, the impact of increasing P3 concentration on the radiosensitivity of both radiosensitive HCT116 and radioresistant SW837 cells at clinically-relevant doses of 1.8 Gy and 5 Gy radiation was assessed. Furthermore, as a hypoxic microenvironment is prevalent in tumours, and known to contribute to radioresistance, the potential of novel compound P3 as a radiosensitising drug under both normoxic and hypoxic conditions was investigated.

In radiosensitive HCT116 cells, no enhanced radiosensitisation was observed at 1.8 Gy radiation under normoxia by P3, however 5-FU significantly radiosensitised HCT116 cells under these conditions ($p = 0.033$) (relative mean surviving fraction ± SEM, 15 μM 5-FU 0.78 ± 0.076) (**Fig.4.9A**). Under hypoxia, P3 did not radiosensitise HCT116 cells at 1.8 Gy radiation, although a trend towards reduced surviving fraction was observed following treatment with 200 μM P3, when compared to its control, this did not reach statistical significance ($p = 0.08$) (**Fig. 4.9B**).

Following exposure to 5 Gy radiation, 10 μM P3 reduced surviving fraction of HCT116 cells, when compared to control ($p = 0.0171$) (mean relative surviving fraction ± SEM; 10 μM 0.76 ± 0.03) (**Fig. 4.9C**). In addition, following 5 Gy radiation exposure under normoxia, there was an increase in surviving fraction in HCT116 treated with 100 μM P3, when compared to vehicle control ($p = 0.032$) (Mean relative surviving fraction 100 μM 2 ± 0.31) (**Fig. 4.9C**). Under hypoxia, no significant differences to radiosensitivity at 5 Gy were observed following treatment with P3 in HCT116. 5-FU treatment did significantly radiosensitise HCT116 cells at 5 Gy under hypoxic conditions ($p = 0.0023$) (relative mean surviving fraction ± SEM; 5-FU 0.27 ± 0.1) (**Fig. 4.9D**).

In radioresistant SW837 rectal cancer cells, no effect on radiosensitivity was demonstrated following treatment with P3 at either 1.8 Gy or 5 Gy radiation in normoxia or hypoxia (**Fig.4.10A-D**). 5-FU significantly radiosensitised SW837 cells to 5 Gy radiation under normoxia only (p = 0.0009) (Mean surviving fraction ± SEM; 15 μM 5-FU 0.55 ± 0.07) (**Fig. 4.10C**).

These data demonstrate that P3 does not sensitise radioresistant SW837 rectal cancer cells to clinically-relevant doses of X-ray radiation under normoxia or hypoxia.

4.4.8. *High dose (200 μM) P3 is cytotoxic in HCT116 cells but not SW837 cells*

Having demonstrated that P3 significantly inhibits metabolic parameters at low concentrations (≤20 μM) in SW837 cells, the cytotoxicity of low doses of P3 (1 μM, 5 μM, 10 μM, 12.5, 15 μM and 20 μM) in SW837 cells was assessed by crystal violet and clonogenic assay.

Low dose P3 (1 μM, 5 μM, 10 μM, 12.5, 15 μM and 20 μM) treatment for 24 h did not impact cell number, as assessed by crystal violet (**Fig. 4.11A**). In addition, clonogenic survival was similar between P3-treated cells, and vehicle control in SW837 cells (**Fig. 4.11B**).

The effect of increasing dose of P3 on cytotoxicity was assessed in HCT116 and SW837 cells under normoxia and hypoxia (0.5% O_2) by the gold-standard clonogenic assay. Cells were treated with a range of doses of P3 (10 μM, 20 μM, 50 μM, 100 μM and 200 μM) or vehicle controls for 48 h, under normoxic and hypoxic conditions

In HCT116 cells, P3 was demonstrated to be significantly cytotoxic at 200 μM, when compared to control under both normoxia (p = 0.011) and hypoxia (p = 0.0082) (mean relative surviving fraction (as %) ± SEM; 200 μM P3 normoxia 74.72 ± 5.68, 200 μM P3 hypoxia 58.54 ± 8.5) (**Fig. 4.12A-B**). No cytotoxicity was demonstrated following P3 treatment in SW837 cells under normoxia or hypoxia (**Fig. 4.13A-B**).

These data demonstrate that P3 is cytotoxic at 200 μM in HCT116 cells only.

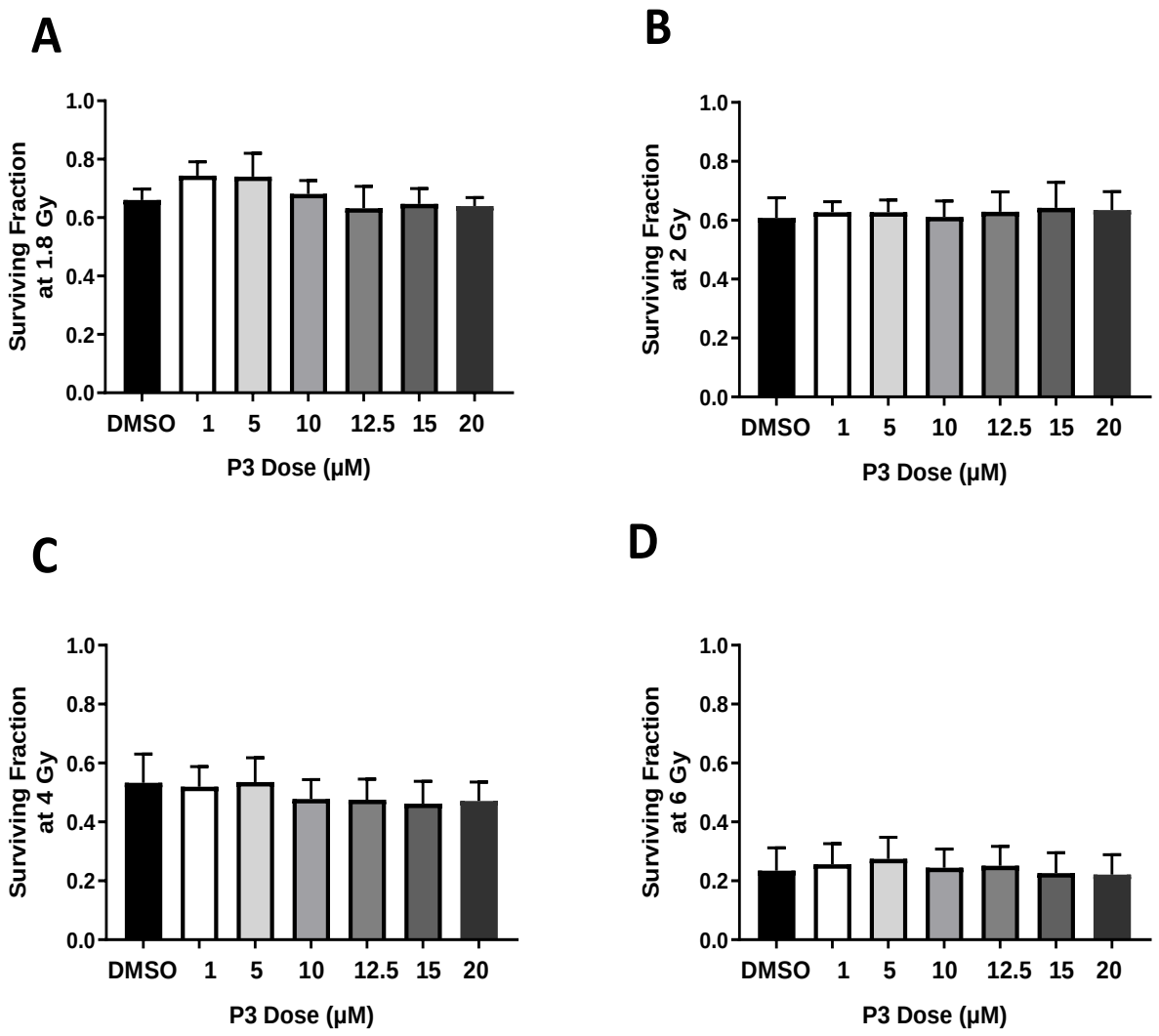

Fig. 4.8: **P3 treatment (1-20 μM) does not sensitize SW837 cells to 1.8 Gy, 2 Gy, 4 Gy or 6 Gy X-ray radiation.** Radiosensitivity was assessed by clonogenic assay. Controls were mock-irradiated. **A)** Surviving Fractions of SW837 cells at 1.8 Gy following 24 h treatment with DMSO (0.2%), or a series of concentrations of P3**. B**) Surviving fraction of SW837 cells at 2 Gy following 24 h treatment with DMSO, or a series of concentrations of P3. **C)** Surviving fraction of SW837 cells at 4 Gy following 24 h treatment with DMSO, or a series of concentrations of P3. **D)** Surviving fraction of SW837 cells at 6 Gy following 24 h treatment with DMSO, or a series of concentrations of P3. Data is presented as mean ± SEM for 4 independent experiments. Statistical analysis was performed using a one-way repeated-measures ANOVA, and post-hoc Tukey's multiple comparisons testing.

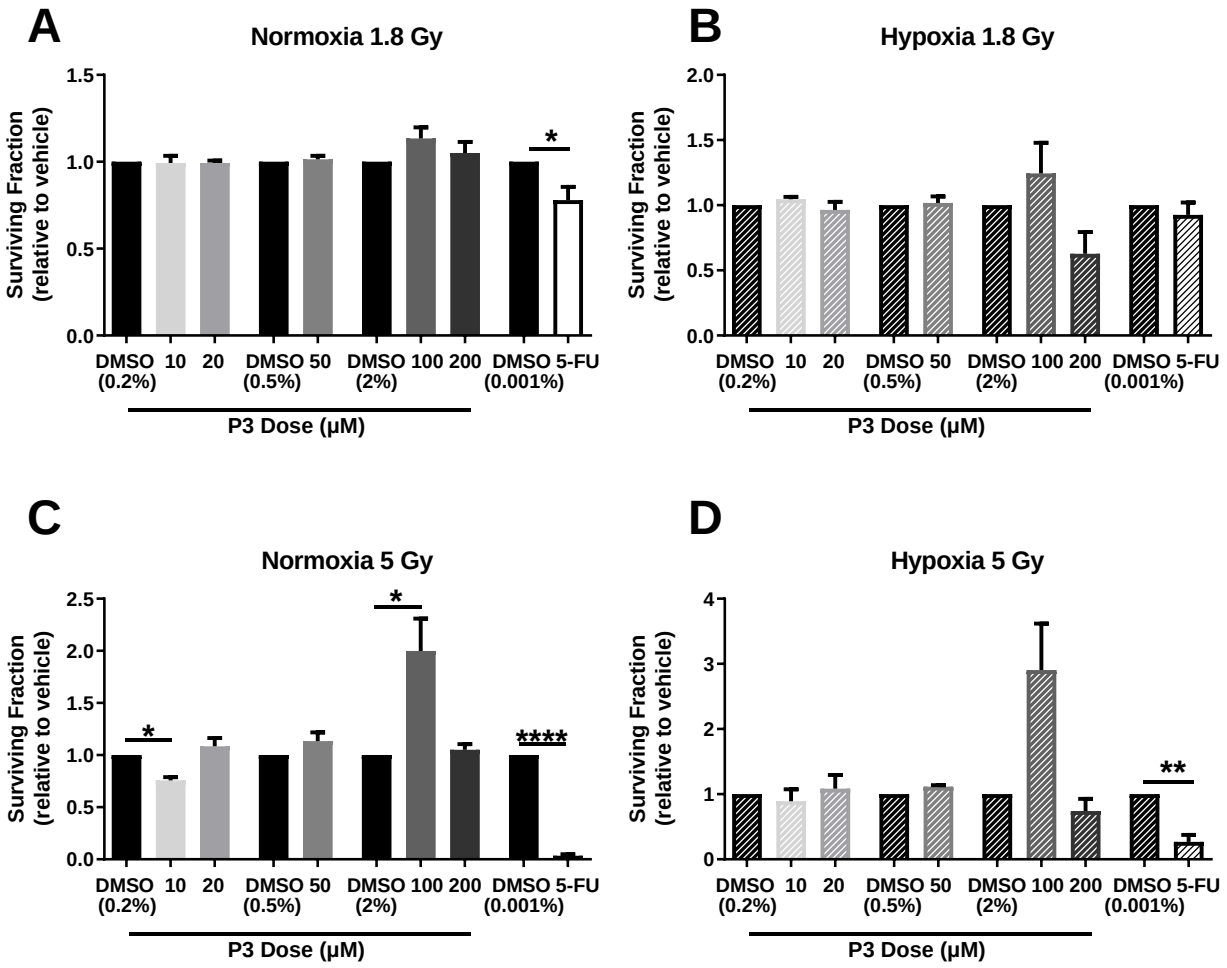

Fig. 4.9: **P3 treatment (10-200 μM) does not sensitise radiosensitive HCT116 cells to X-ray radiation.** Radiosensitivity was assessed by clonogenic assay, under normoxic and hypoxic (0.5% O_2) conditions. **A)** Surviving fractions of HCT116 cells at 1.8 Gy following 24 h pre-treatment with DMSO, or a series of concentrations of P3 under normoxia. **B)** Surviving fractions of HCT116 cells at 1.8 Gy following 24 h pre-treatment with DMSO, or a series of concentrations of P3 under hypoxia. **C**) Surviving fractions of HCT116 cells at 5 Gy following 24 h pre-treatment with DMSO, or a series of concentrations of P3 under normoxia. **D)** Surviving fractions of HCT116 cells at 5 Gy following 24 h pre-treatment with DMSO, or a series of concentrations of P3 under hypoxia. Data is presented as mean ± SEM from *n*= 5 (100, 200 μM P3 and 5-FU) or *n*=3 (10 μM, 20 μM and 50 μM P3). Statistical analysis was performed using paired ANOVA and multiple comparisons testing. *$p < 0.05$, **$p < 0.01$, ****$p < 0.0001$.

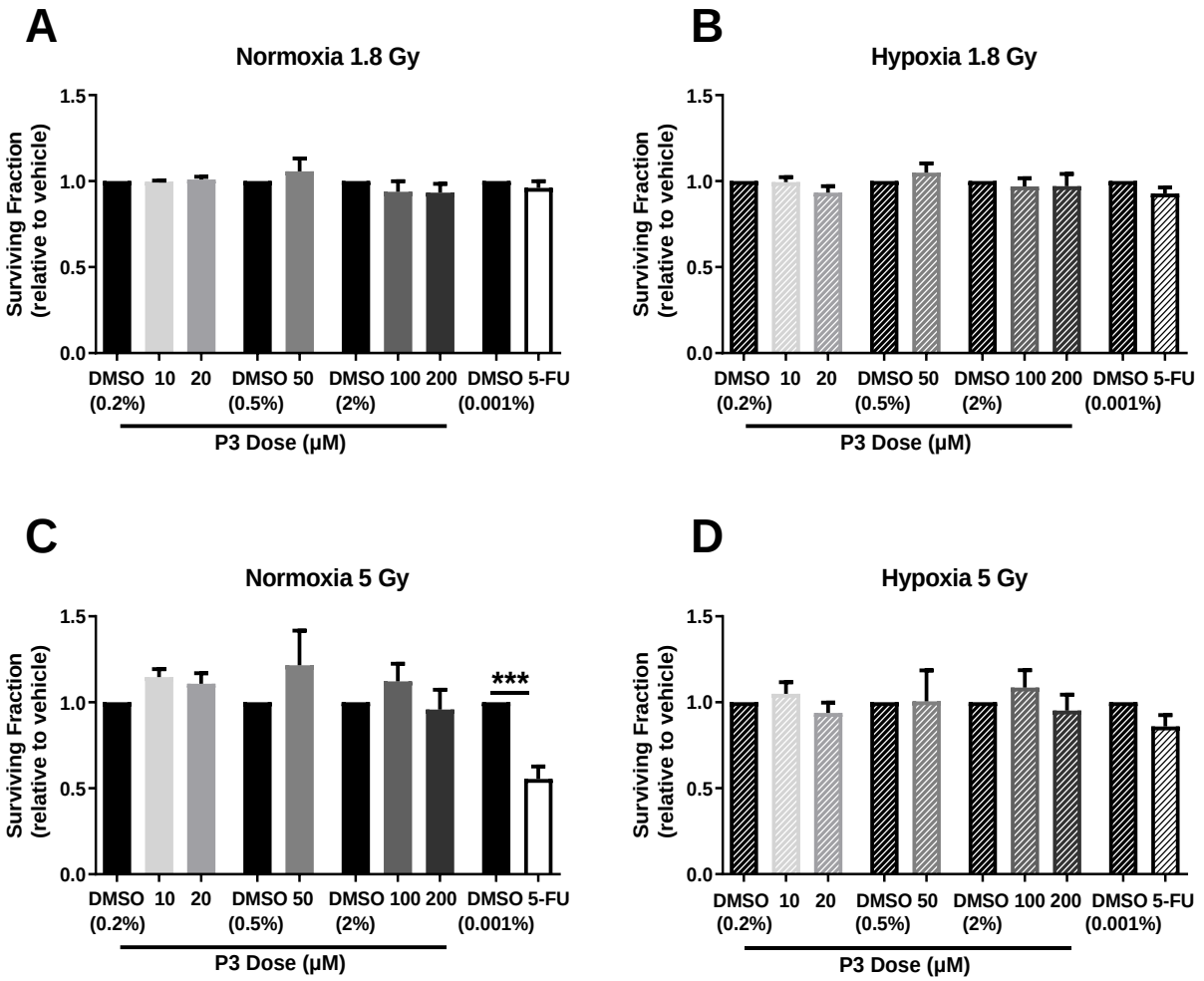

Fig. 4.10: **P3 treatment (10-200 µM) does not sensitise radioresistant SW837 cells to X-ray radiation.** Radiosensitivity was assessed by clonogenic assay, under normoxic and hypoxic (0.5% O_2) conditions. **A)** Surviving fractions of SW837 cells at 1.8 Gy following 24 h pre-treatment with DMSO, or a series of concentrations of P3 under normoxia. **B)** Surviving fractions of SW837 cells at 1.8 Gy following 24 h pre-treatment with DMSO, or a series of concentrations of P3 under hypoxia. **C**) Surviving fractions of SW837 cells at 5 Gy following 24 h pre-treatment with DMSO, or a series of concentrations of P3 under normoxia. **D)** Surviving fractions of SW837 cells at 5 Gy following 24 h pre-treatment with DMSO, or a series of concentrations of P3 under hypoxia. Data is presented as mean ± SEM from *n*= 7 (100, 200 µM P3 and 5-FU) or *n*=3 (10 µM, 20 µM and 50 µM P3). Statistical analysis was performed using paired ANOVA and multiple comparisons testing. ***$p < 0.001$.

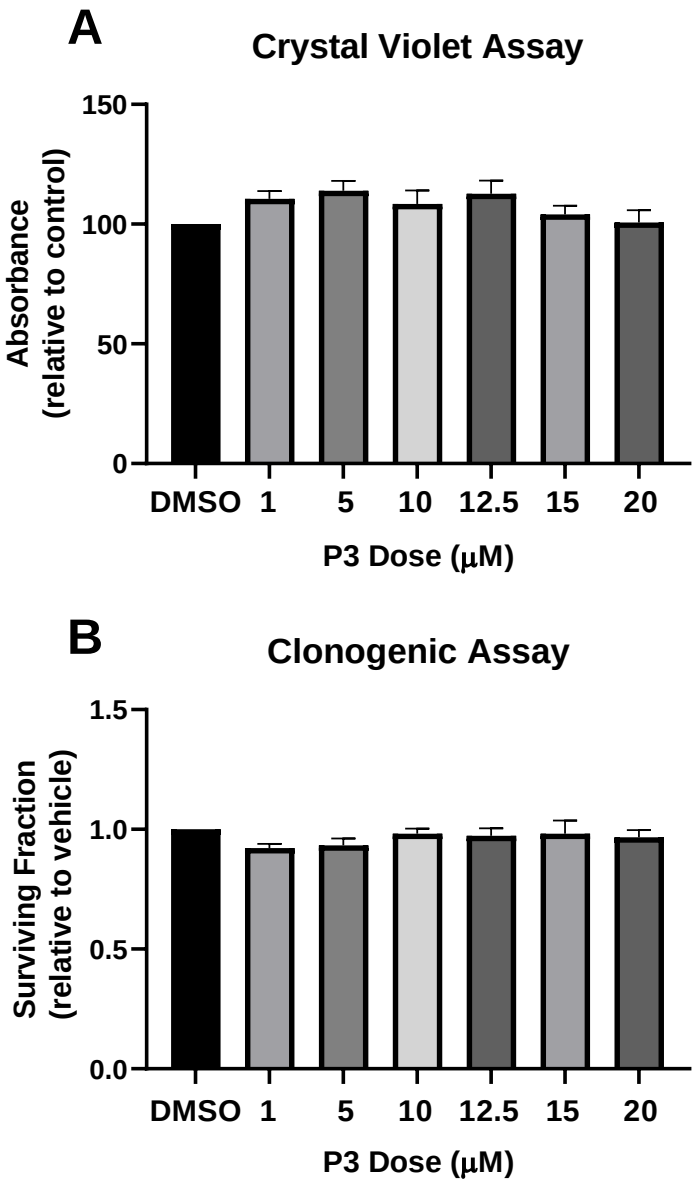

Fig. 4.11: **P3 treatment (1-20 μM) does not alter cell number or clonogenicity of SW837 cells.** The effect of P3 on cell number and surviving fraction was assessed using the **A)** crystal violet assay and **B)** clonogenic assay respectively, following treatment with P3 (1 μM, 5 μM, 10 μM, 12.5 μM, 15 μM, 20 μM) or 0.2% DMSO as a vehicle control. Data is presented as mean ± SEM from 4 independent experiments. Statistical analysis was performed using repeated-measures ANOVA and post-hoc Tukey's multiple comparisons testing.

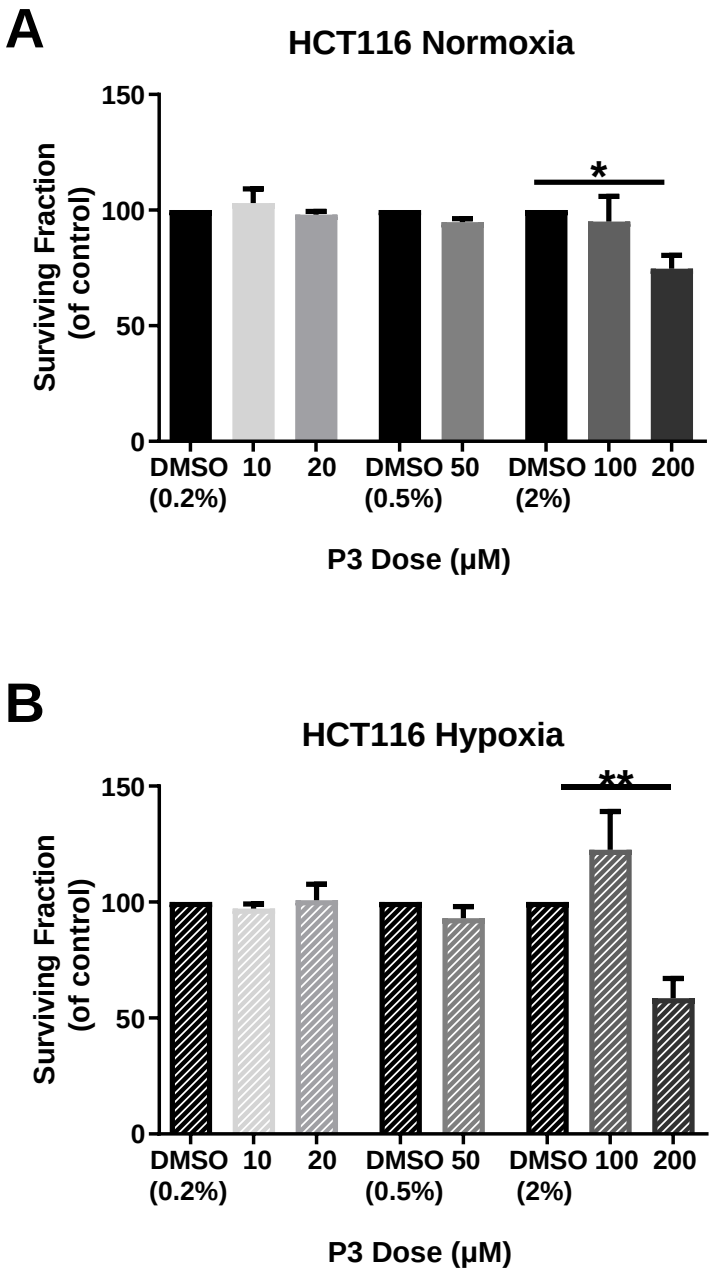

Fig. 4.12: **P3 (200 µM) is cytotoxic in radiosensitive HCT116 cells.** Cytotoxicity of P3 was assessed by clonogenic assay, following treatment with a range of doses of P3 (10 µM, 20 µM, 50 µM, 100 µM and 200 µM) and matching DMSO controls for 48 h, under normoxic or hypoxic conditions. **A)** Effect of P3 treatment on cytotoxicity in HCT116 cells under normoxia. **B)** Effect of P3 treatment on cytotoxicity in HCT116 cells under hypoxia. Data is presented as mean ± SEM from *n*=5 (100, 200 µM P3) or *n*=3 (10 µM, 20 µM and 50 µM P3) experiments. Statistical analysis was performed using paired ANOVA and multiple comparisons testing. **p* < 0.05, **p* < 0.01.

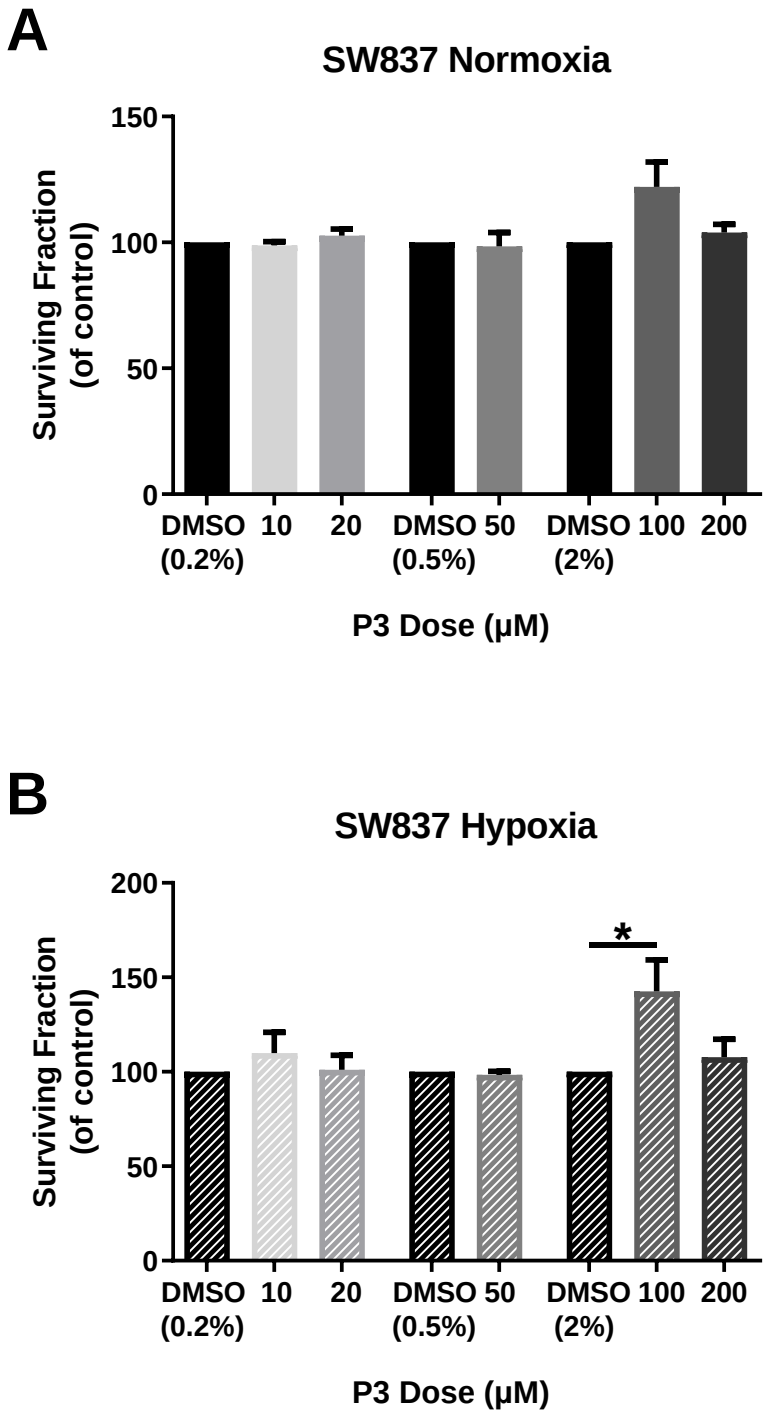

Fig. 4.13: **P3 treatment (doses ≥ 10 µM) is not cytotoxic in radioresistant SW837 cells.** Cytotoxicity of P3 was assessed by clonogenic assay, following treatment with a range of doses of P3 (10 µM, 20 µM, 50 µM, 100 µM and 200 µM) and matching DMSO controls for 48 h, under normoxic or hypoxic conditions. **A)** Effect of P3 treatment on cytotoxicity in SW837 cells under normoxia. **B)** Effect of P3 treatment on cytotoxicity in SW837 cells under hypoxia. Data is presented as mean ± SEM for from *n*=7 (100, 200 µM P3) or *n*=3 (10 µM, 20 µM and 50 µM P3) experiments. Statistical analysis was performed using paired ANOVA and multiple comparisons testing. **p* < 0.05.

4.4.9. *Metformin inhibits OCR and increases ECAR in HCT116 and SW837 cells under normoxia and hypoxia*

Having demonstrated that the novel anti-metabolic compound P3 does not radiosensitise HCT116 or SW837 cells to radiation, an established drug, metformin, was investigated for its impact on energy metabolism in this cell line model. To determine if metformin alters cellular metabolism in HCT116 and SW837, cells were treated with 2.5 mM or 10 mM metformin, or H_2O vehicle control for 24 h under either normoxic or hypoxic (0.5% O_2) conditions, and metabolic rates assessed by Seahorse assay.

Metformin treatment significantly reduced OCR, a measure of oxidative phosphorylation, in HCT116 cells under normoxia at 2.5 mM and 10 mM, when compared to vehicle control ($p < 0.0001$, $p < 0.0001$, respectively) (Mean relative OCR (%) ± SEM; HCT116 2.5 mM 6.71 ± 1.02, HCT116 10 mM 5.33 ± 2.58) (**Fig. 4.14A**)**.** Furthermore, 10 mM metformin significantly inhibited OCR in HCT116 under hypoxic conditions ($p = 0.023$) (60.12 ± 9.47) (**Fig. 4.14A**). In radioresistant SW837 rectal cancer cells, metformin significantly inhibited OCR under normoxic conditions at 2.5 mM ($p < 0.0001$) and 10 mM ($p < 0.0001$), relative to vehicle control (Mean relative OCR (%) ± SEM; SW827 2.5 mM 8.16 ± 2.31, SW837 10 mM 6.14 ± 0.95) (**Fig. 4.14B**)**.** In addition, 2.5 mM metformin treatment significantly inhibited OCR under hypoxia ($p = 0.0307$) (55.05 ± 11.6) (**Fig. 4.14B**)**.** While a trend towards inhibited OCR by 10 mM metformin treatment under hypoxia was demonstrated, this did not reach statistical significance ($p = 0.12$) (68.73 ± 14.5).

In HCT116 cells, while there were trends towards elevated ECAR rates, a measure of glycolysis, following treatment with both 2.5 mM and 10 mM metformin, these did not reach statistical significance ($p = 0.023$, $p = 0.20$) (Mean relative ECAR (as %) ± SEM; HCT116 2.5 mM metformin 145.6 ± 20.39, HCT116 10 mM metformin 161.6 ± 25.1) (**Fig. 4.15A**). However, under hypoxia, 10 mM metformin treatment significantly increased ECAR in HCT116 cells ($p = 0.004$) (112.7 ± 2.196). Metformin treatment significantly upregulated ECAR in SW837 cells under normoxia at 2.5 mM and 10 mM, when compared to vehicle control ($p = 0.0136$, $p = 0.035$ respectively) (Mean relative ECAR (as %) ± SEM; SW837 2.5 mM metformin 254.3 ± 29.53, 10 mM metformin 239.8 ± 38.25) (**Fig. 4.15B**). No differences to ECAR were observed in SW837 cells following metformin treatment under hypoxia.

These data demonstrate that metformin inhibits oxidative phosphorylation in HCT116 and SW837 CRC cells and induces a concurrent upregulation of glycolysis.

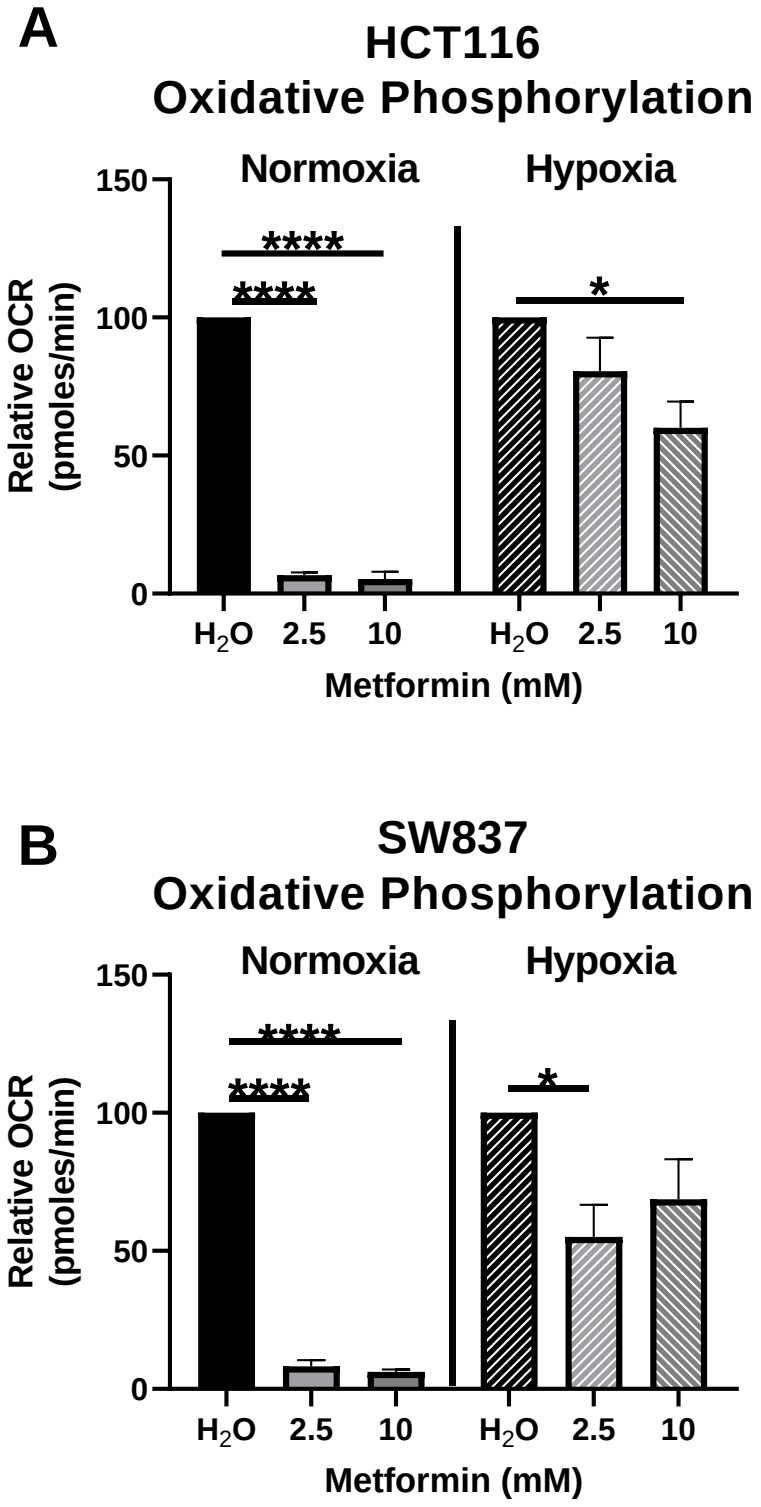

Fig. 4.14: **Metformin treatment significantly inhibits OCR in HCT116 and SW837 cells under normoxia (21% O_2) and hypoxia (0.5% O_2).** Cells were treated for 24 h with metformin (2.5 mM or 10 mM) or vehicle control (H_2O) and basal metabolism was assessed using a Seahorse XFe24 analyser. **A)** OCR in HCT116 cells under normoxic and hypoxic conditions. **B)** OCR in SW837 cells under normoxic and hypoxic conditions. Data is presented as mean ± SEM from 4 independent experiments. Statistical analysis was performed by paired ANOVA. *p < 0.05, ****p < 0.0001.

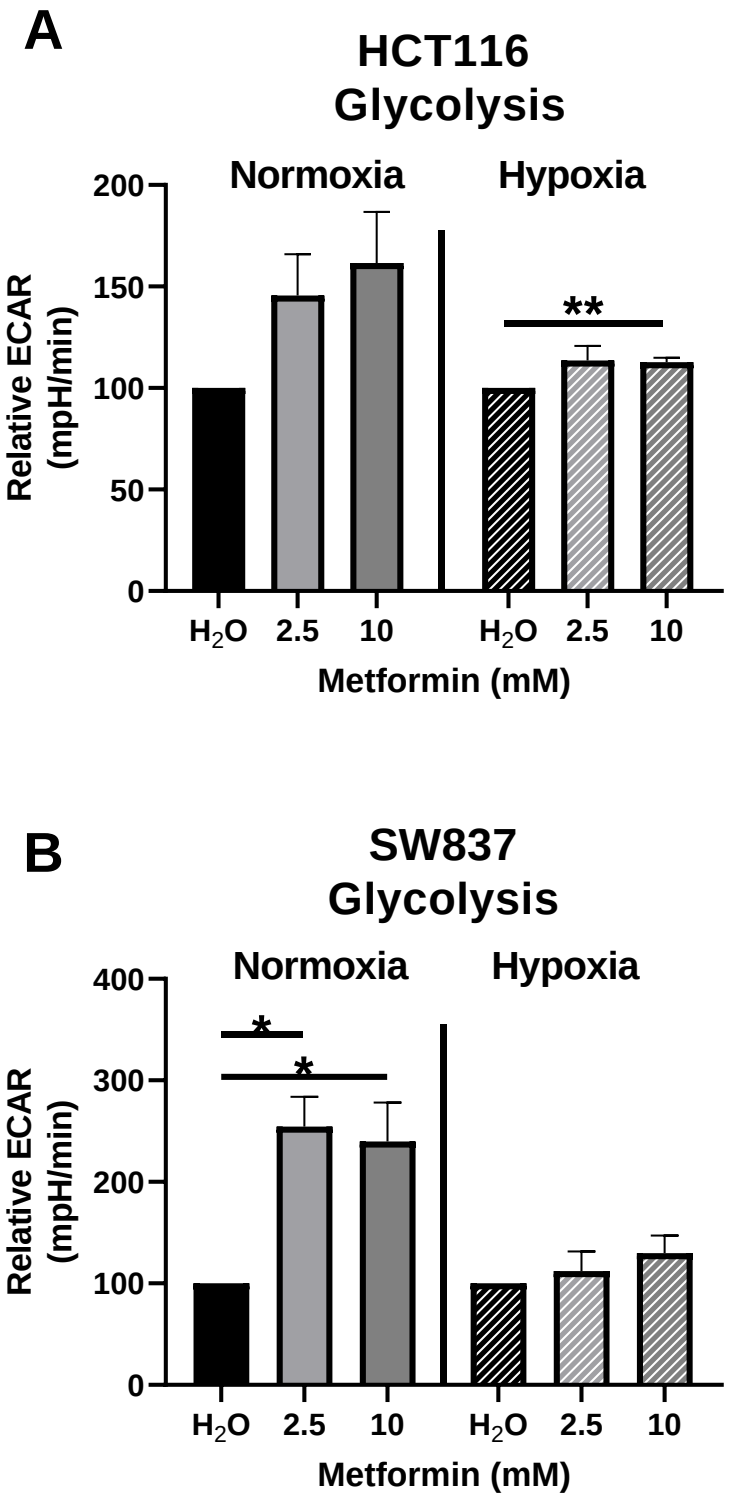

Fig. 4.15: **Metformin treatment significantly increases ECAR in HCT116 and SW837 cells.** Cells were treated for 24 h with metformin (2.5 mM or 10 mM) or vehicle control (H_2O) and basal metabolism was assessed using a Seahorse XFe24 analyser. **A)** ECAR in HCT116 cells under normoxic and hypoxic conditions. **B)** ECAR in SW837 cells under normoxic or hypoxic conditions. Data is presented as mean ± SEM from 4 independent experiments. Statistical analysis was performed by paired ANOVA. *$p < 0.05$, **$p < 0.01$.

4.4.10. *Metformin induces mitochondrial dysfunction under normoxic, but not hypoxic conditions in HCT116 and SW837 cells*

As metformin was demonstrated to significantly impair mitochondrial metabolism in SW837 and HCT116 cells, the effect of metformin treatment under normoxic and hypoxic conditions on mitochondrial function was assessed using three surrogate markers of mitochondrial function; mitochondrial mass, reactive oxygen species (ROS) and mitochondrial membrane potential.

Under normoxia, a trend towards increased mitochondrial mass was demonstrated in HCT116 cells in hypoxia following 24 h treatment with metformin (10 mM), when compared to vehicle control, although this did not reach statistical significance (p = 0.09) (**Fig. 4.16A**). Metformin treatment (10 mM for 24 h) significantly increased ROS production and mitochondrial membrane potential in HCT116 under normoxia (p = 0.0194, p = 0.0067 respectively) (Mean DCF-DA fluorescence ± SEM; H_2O 6.63 ± 0.67, 10 mM metformin 7.61 ± 0.73) (Mean Rhodamine-123 fluorescence ± SEM; H_2O 27.53 ± 4.05, 10 mM metformin 50.1 ± 6.42) (**Fig. 4.16B, 4.16C**). Under hypoxia (0.5% O_2), no significant differences in mitochondrial function were demonstrated in HCT116 cells following metformin treatment (**Fig. 4.16A-C**).

In SW837 cells, mitochondrial mass was significantly increased following 24 h treatment with 10 mM metformin, when compared to H_2O vehicle control in normoxia (p = 0.0406) (Mean MitoTracker fluorescence ± SEM; H_2O 5.099 ± 0.44, 10 mM metformin 10.55 ± 1.936) (**Fig. 4.17A**). ROS production was significantly increased under normoxia following treatment with 10 mM metformin for 24 h, when compared to vehicle control (H_2O) (p = 0.0295) (Mean DCF-DA fluorescence ± SEM; H_2O 4.87 ± 0.49, 10 mM metformin 4.87 ± 1.24) (**Fig. 4.17B**). Furthermore, mitochondrial membrane potential was significantly increased following 24 h treatment with 2.5 mM and 10 mM metformin, when compared to H_2O control under normoxia (p = 0.0295, p = 0.0229 respectively) (mean rhodamine-123 fluorescence ± SEM; H_2O 52.2 ± 8.52, 2.5 mM metformin 164.8 ± 35.85, 10 mM metformin 143.5 ± 25.98) (**Fig. 4.17C**). Under hypoxia (0.5% O_2), no alterations in mitochondrial function were demonstrated following metformin treatment in SW837 cells (**Fig. 4.17A-C**).

These data demonstrate that metformin induces significant mitochondrial dysfunction in both HCT116 and SW837 cells under normoxia, but not hypoxia.

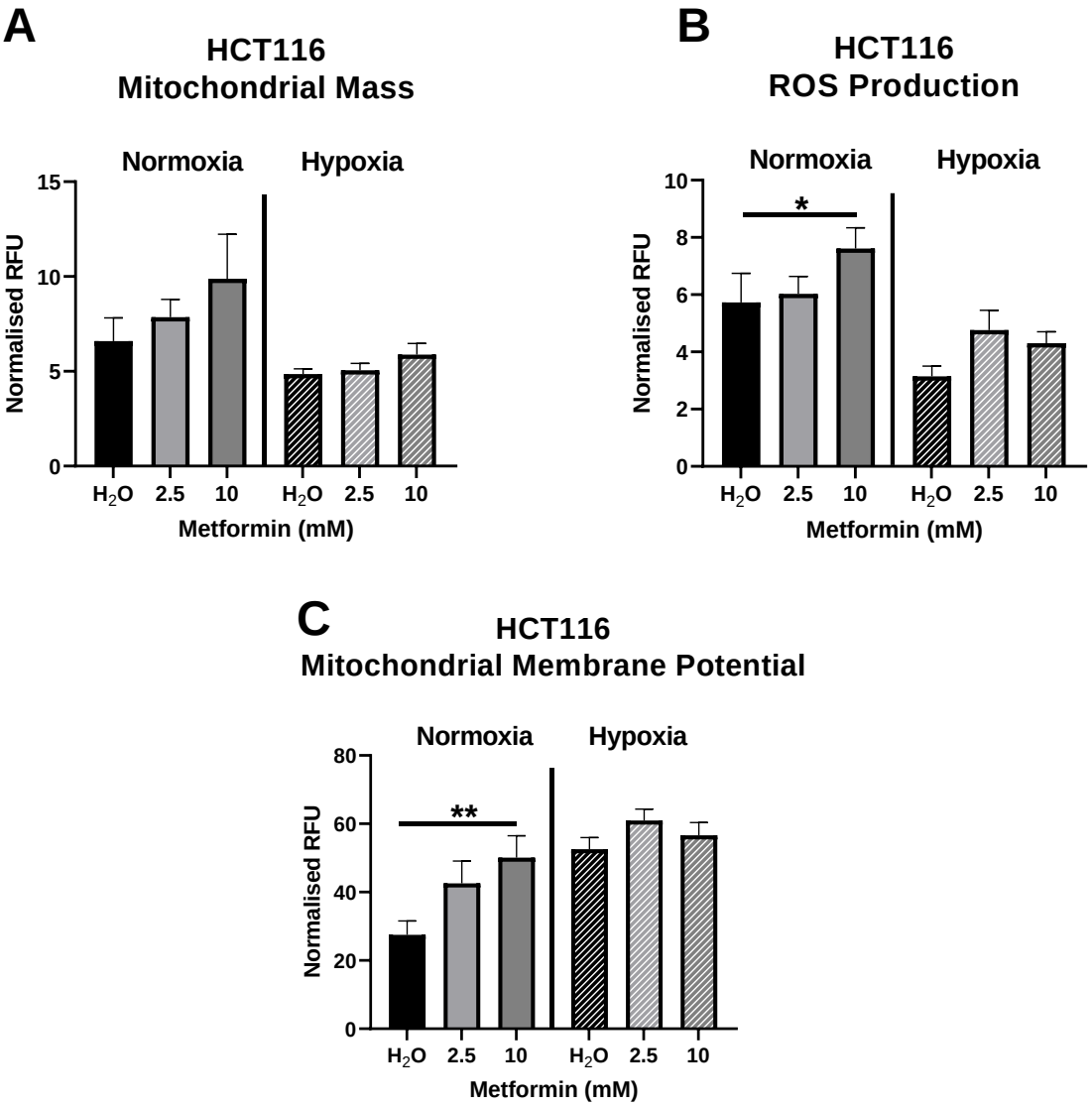

Fig. 4.16: **Metformin treatment induces mitochondrial dysfunction in HCT116 cells.** Mitochondrial function was assessed in HCT116 cells following 24 h treatment with metformin under normoxia and hypoxia using a series of fluorescent probes. **A)** Mitochondrial mass was assessed using MitoTracker Green FM. **B)** ROS production was assessed using 2,7 DCF-DA. **C)** Mitochondrial membrane potential was assessed using Rhodamine-123. Data is presented as mean ± SEM from 5 independent experiments. Statistical analysis was performed by paired ANOVA. *$p < 0.05$, **$p < 0.01$.

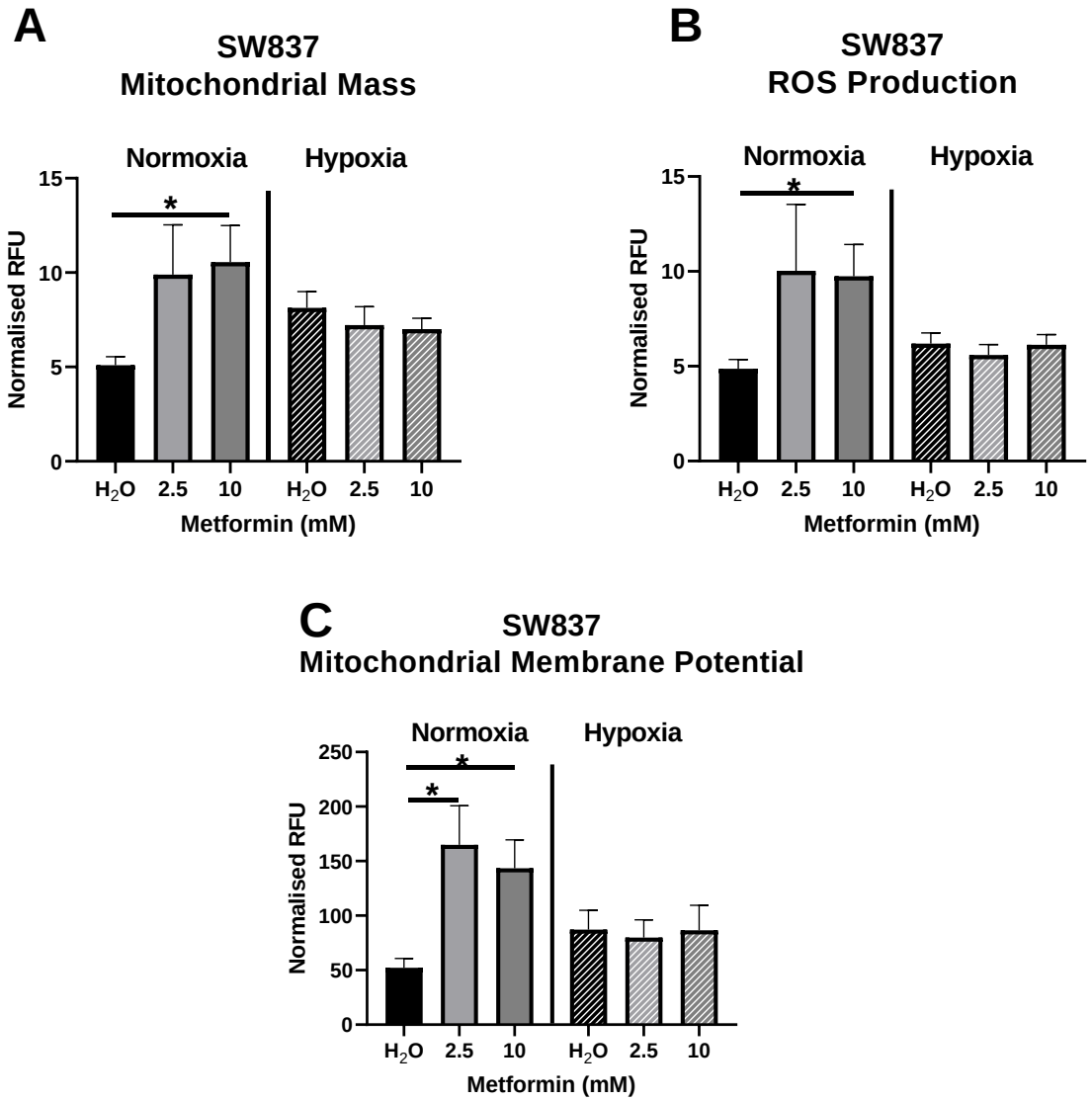

Fig. 4.17: **Metformin treatment induces mitochondrial dysfunction in SW837 cells.** Mitochondrial function was assessed in SW837 cells following 24 h treatment with metformin under normoxia and hypoxia using a series of fluorescent probes. **A)** Mitochondrial mass was assessed using MitoTracker Green FM. **B)** ROS production was assessed using 2,7 DCF-DA. **C)** Mitochondrial membrane potential was assessed using Rhodamine-123. Data is presented as mean ± SEM from 5 independent experiments. Statistical analysis was performed by paired ANOVA. *$p < 0.05$.

4.4.11. *Metformin induces cytotoxicity in HCT116 and SW837 cells*

Having demonstrated that metformin significantly alters metabolic parameters, the cytotoxicity of metformin in HCT116 and SW837 cells was assessed using the gold-standard clonogenic assay, under normoxic and hypoxic conditions.

Treatment with metformin (48 h) was demonstrated to induce significant cytotoxicity in HCT116 colon cancer cells under normoxia at 10 mM concentration, relative to vehicle control ($p = 0.0001$) (Mean relative surviving fraction ± SEM; HCT116 10 mM metformin 40.67 % ± 4.06) (**Fig. 4.18A**)**.** Under hypoxia, metformin induced cytotoxicity at 1 mM ($p = 0.008$), 2.5 mM ($p = 0.0003$) and 10 mM ($p < 0.0001$), when compared to vehicle control (Mean relative surviving fraction ± SEM; 1 mM 38.11 ±10.07, 2.5 mM 27.03 ± 6.39, 10 mM 9.47 ± 1.74) (**Fig. 4.18B**)**.**

No significant cytotoxicity was demonstrated in SW837 cells treated with metformin under normoxia (**Fig. 4.19A**)**,** However under hypoxia, metformin treatment significantly induced cytotoxicity at 10 mM ($p = 0.038$), when compared to vehicle control (mean relative surviving fraction ± SEM; 10 mM 69.82 ± 8.49) (**Fig. 4.19B**)**.**

These data demonstrate that radiosensitive HCT116 cells are sensitive to metformin-induced cytotoxicity under normoxia and hypoxia, but metformin is only cytotoxic in SW837 cells under hypoxic conditions.

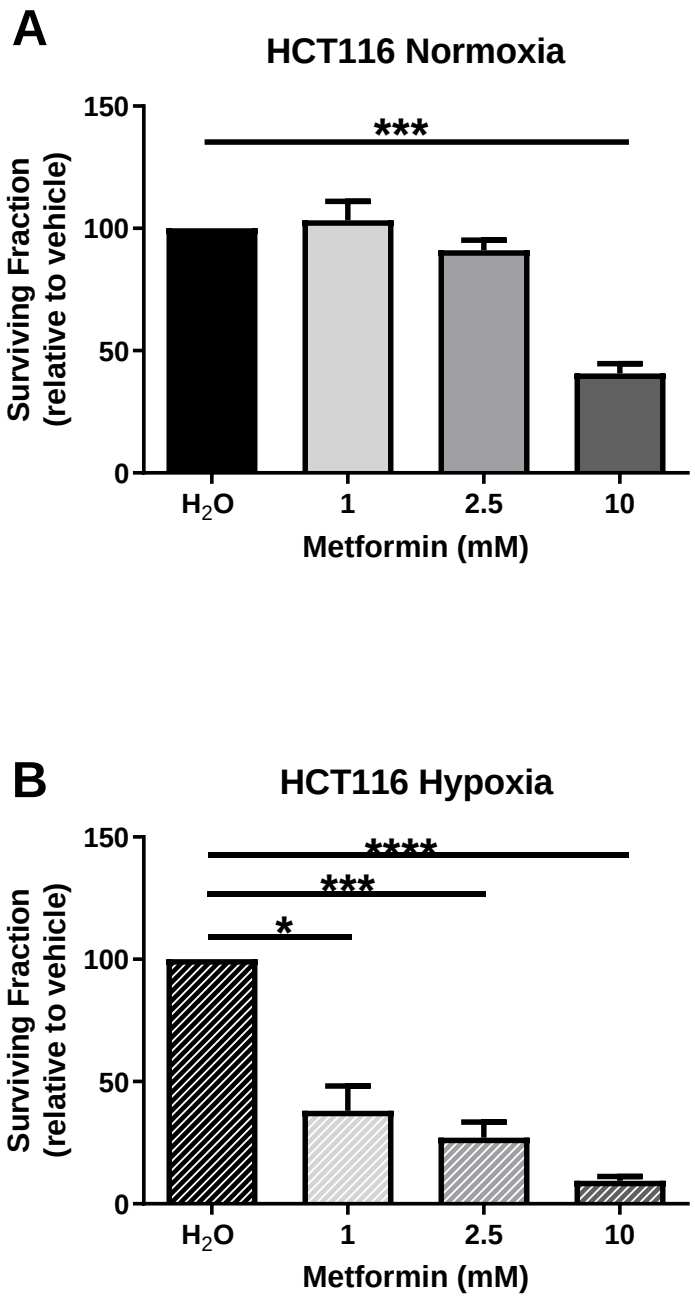

Fig. 4.18: **Metformin treatment induces significant cytotoxicity in HCT116 cells under normoxic and hypoxic conditions.** The effect of metformin (1 mM, 2.5 mM, 10 mM, for 48 h) or vehicle control (H_2O) on cytotoxicity was assessed using the gold-standard clonogenic assay in HCT116 cells, under normoxia and hypoxia. **A)** The effect of metformin treatment on cytotoxicity in HCT116 cells under normoxia. **B)** The effect of metformin treatment on cytotoxicity in HCT116 cells under hypoxia. Data is presented as mean ± SEM for 4 independent experiments. Statistical analysis was performed using paired ANOVA, with post-hoc Tukey's multiple comparisons testing. *$p < 0.05$, ***$p < 0.001$, ****$p < 0.0001$.

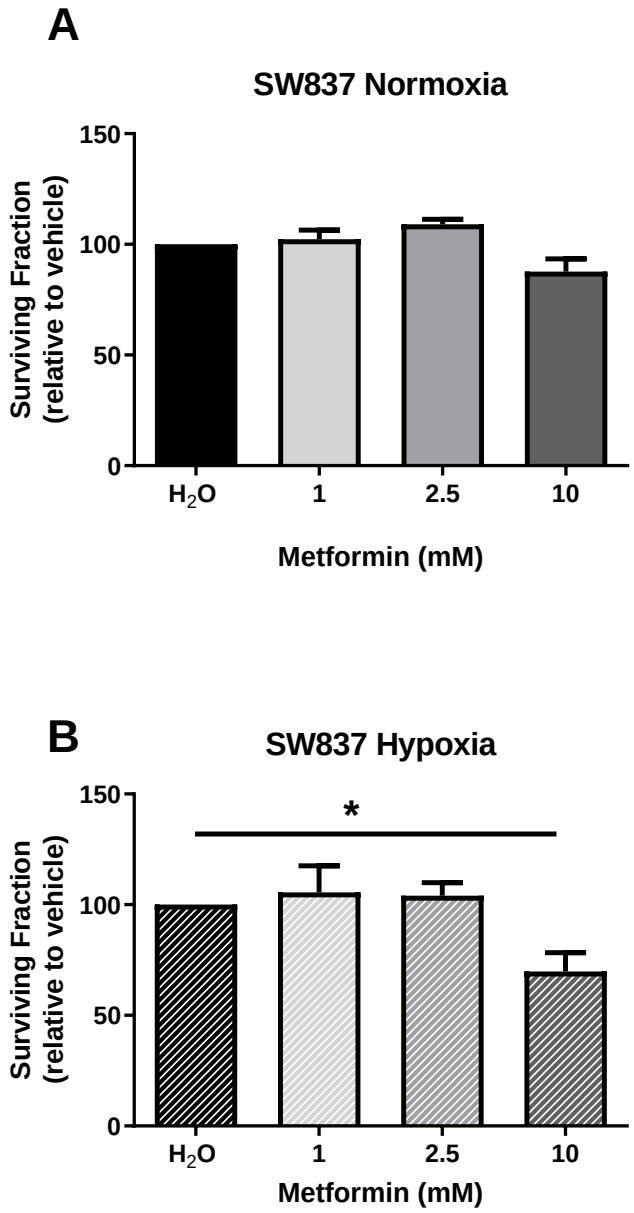

Fig. 4.19: **Metformin treatment induces significant cytotoxicity in SW837 cells under hypoxic conditions.** The effect of metformin (1 mM, 2.5 mM, 10 mM, for 48 h) or vehicle control (H_2O) on cytotoxicity was assessed using the gold-standard clonogenic assay in SW837 cells, under normoxia and hypoxia. **A)** The effect of metformin treatment on cytotoxicity in SW837 cells under normoxia. **B)** The effect of metformin treatment on cytotoxicity in SW837 cells under hypoxia. Data is presented as mean ± SEM for 4 independent experiments. Statistical analysis was performed using paired ANOVA, with post-hoc Tukey's multiple comparisons testing. *$p < 0.05$.

4.4.12. *Metformin significantly radiosensitises HCT116 and SW837 cells*

The potential radiosensitising effects of metformin (1 µM, 2.5 µM, 10 µM) at clinically relevant doses of 1.8 Gy and 5 Gy radiation under normoxia and hypoxia was assessed in HCT116 and SW837 cells by clonogenic assay.

Under normoxia, metformin treatment (2.5 mM and 10 mM) significantly sensitised HCT116 cells to 1.8 Gy radiation, when compared to vehicle control (p = 0.0072, p = 0.0014 respectively) (relative mean surviving fraction ± SEM; 2.5 mM metformin 0.67 ± 0.033, 10 mM metformin 0.523 ± 0.075) (**Fig. 4.20A**)**.** In addition, the optimised radiosensitising dose of 5-FU (15 µM 5-FU 6 h pre-radiation, **Section 4.4.6**) significantly radiosensitised HCT116 cells to 1.8 Gy under normoxia (p = 0.033) (relative mean surviving fraction ± SEM, 15 µM 5-FU 0.78 ± 0.076) (**Fig. 4.20A**). While a trend towards decreased surviving fraction in HCT116 cells treated with 10 mM Metformin, when compared to 5-FU treated cells, was demonstrated, this did not reach statistical significance (p = 0.08).

Furthermore, under hypoxia (0.5% O_2), metformin significantly radiosensitised HCT116 to 1.8 Gy radiation at 2.5 mM and 10 mM dose (p = 0.0016, p = 0.0013 respectively) (relative mean surviving fraction ± SEM; 2.5 mM metformin 0.259 ± 0.079, 10 mM metformin 0.33 ± 0.067) (**Fig. 4.20B**). 5-FU, the clinical standard of care chemotherapeutic did not radiosensitise HCT116 cells to 1.8 Gy under hypoxia (**Fig. 4.20B**). Importantly, the radiosensitising effects of metformin were superior to that seen with 5-FU under hypoxia, with the surviving fraction of HCT116 cells following 1.8 Gy radiation being significantly lower in cells treated with either 2.5 mM or 10 mM Metformin, when compared to 5-FU-treated cells (p = 0.016, p = 0.001 respectively) (**Fig. 4.20B**).

Under normoxia, metformin significantly radiosensitised HCT116 cells to 5 Gy radiation, relative to vehicle control, following 24 h treatment with 1 mM, 2.5 mM and 10 mM (p = 0.039, p = 0.19, p = 0.008 respectively) (relative mean surviving fraction ± SEM; 1 mM 0.69 ± 0.068, 2.5 mM 0.51 ± 0.1, 10 mM 0.41 ± 0.09) (**Fig. 4.20C**). Treatment with the optimised radiosensitising dose of 5-FU also significantly radiosensitised HCT116 cells to 5 Gy radiation under normoxia (p < 0.0001) (relative mean surviving fraction ± SEM; 15 µM 5-FU 0.035 ± 0.013). In addition, metformin treatment with 1 mM, 2.5 mM and 10 mM resulted in a significantly lower surviving fraction following 5 Gy radiation, when compared to that of 5-FU (p = 0.003, p = 0.009, p = 0.019 respectively) (**Fig. 4.20C**).

Under hypoxia, metformin radiosensitised HCT116 cells to 5 Gy radiation at 2.5 mM and 10 mM doses (p = 0.0013, p = 0.0004 respectively) (relative mean surviving fraction ± SEM; 2.5 mM Metformin 0.212 ± 0.057, 10 mM Metformin 0.331 ± 0.067) (**Fig. 4.20D**). In addition, 5-FU significantly radiosensitised HCT116 cells to 5 Gy radiation (p = 0.0023) (relative mean surviving fraction ± SEM; 5-FU 0.27 ± 0.1).

Furthermore, radioresistant SW837 cells were significantly radiosensitised to 1.8 Gy X-ray radiation by 24 h metformin treatment at 2.5 mM and 10 mM (p = 0.0075, p = 0.0338 respectively) (Mean relative surviving fraction ± SEM; 2.5 mM 0.86 ± 0.027 10 mM 0.88 ± 0.037) (**Fig. 4.21A**), when compared to vehicle control**.** Importantly, the clinical gold-standard radiosensitising drug, 5-FU, did not induce radiosensitisation in SW837 cells exposed to 1.8 Gy radiation under normoxia. The radiosensitising effects of metformin were superior to that of the clinical standard 5-FU, with the surviving fraction of cells treated with 10 mM metformin being significantly lower than that of 5-FU treated cells, following 1.8 Gy radiation (p = 0.039) (Mean relative surviving fraction ± SEM; 10 mM metformin 0.88 ± 0.037 vs 15 µM 5-FU 0.98 ± 0.045). Under hypoxic conditions, no impact of metformin, or 5-FU was demonstrated on radiosensitivity to 1.8 Gy in SW837 cells (**Fig. 4.21B**).

Metformin did not radiosensitise SW837 cells to 5 Gy radiation under normoxic or hypoxic conditions **(Fig. 4.21C-D**). 5-FU did radiosensitise SW837 cells to 5 Gy radiation under normoxia (p = 0.0009), when compared to vehicle (DMSO), and was superior to Metformin (2.5 mM and 10 mM) at this radiation dose (p = 0.014, p = 0.007 respectively). However, 5-FU treatment did not radiosensitise SW837 cells to radiation under hypoxia (**Fig. 4.21B, 4.21D**) (Mean relative surviving fraction ± SEM; SW837 5-FU 5 Gy 0.55 ± 0.073).

These data demonstrate that metformin, a clinically approved anti-diabetic drug and metabolic modulator significantly radiosensitises HCT116 cells under normoxia and hypoxia. Furthermore, metformin significantly radiosensitises radioresistant SW837 rectal cancer cells at the clinically-relevant dose of 1.8 Gy under normoxia. Importantly, the radiosensitising effects of metformin on both cells lines at 1.8 Gy were superior to the radiosensitising effects demonstrated by the current standard of care chemotherapeutic 5-FU.

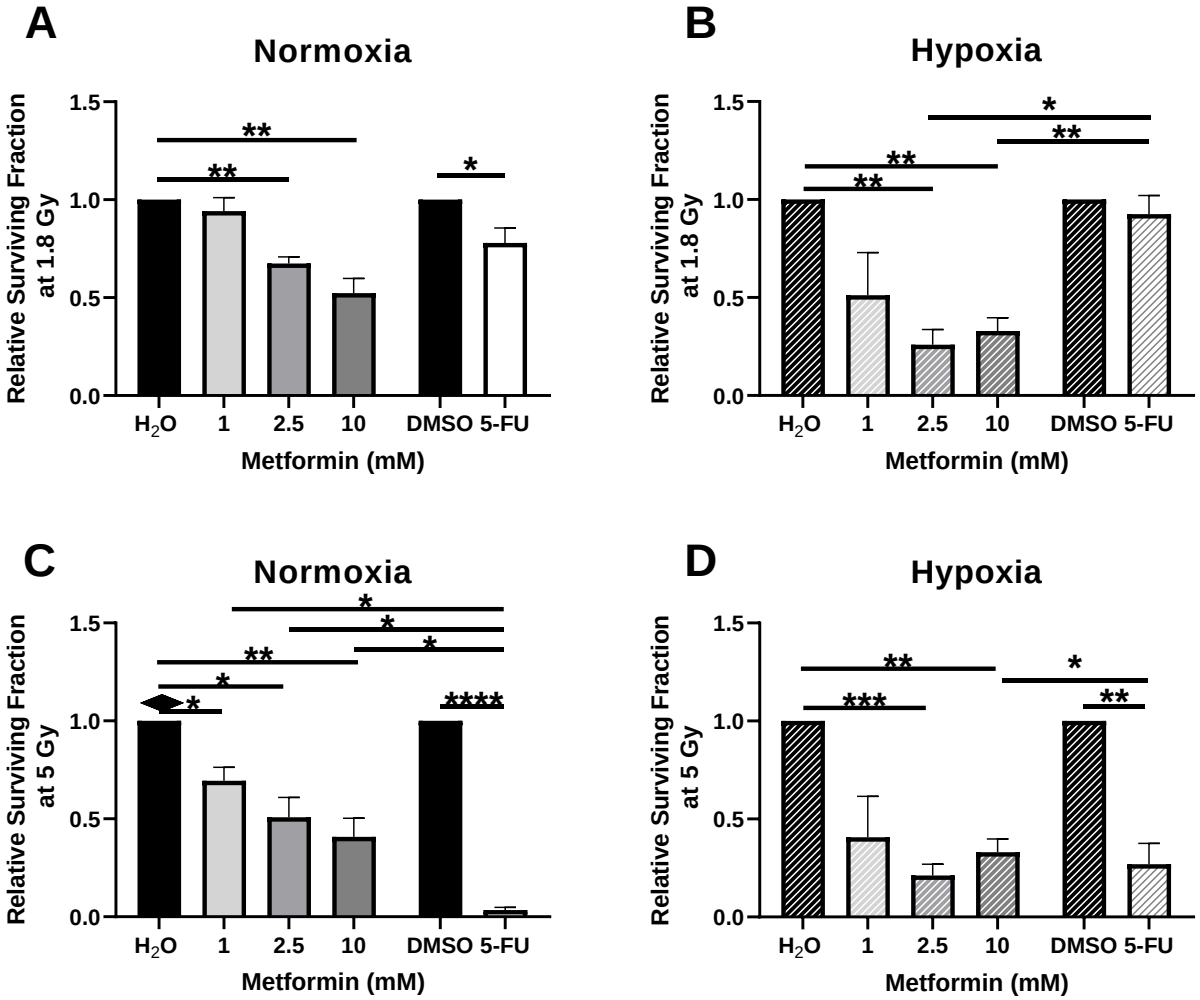

Fig. 4.20: **Metformin treatment significantly sensitises radiosensitive HCT116 cells to X-ray radiation under normoxia and hypoxia.** Radiosensitivity was assessed by clonogenic assay on HCT116 cells treated with metformin (1 mM, 2.5 mM, 10 mM) or H_2O vehicle control for 24 h prior to radiation exposure, or 5-FU (15 µM 6 h prior to radiation) or DMSO control (0.001%) under normoxic and hypoxic conditions. **A)** Surviving fractions of HCT116 cells at 1.8 Gy following pre-treatment with metformin, 5-FU or vehicle controls under normoxia. **B)** Surviving fractions of HCT116 cells at 1.8 Gy following pre-treatment with metformin, 5-FU or vehicle controls under hypoxia. **C)** Surviving fractions of HCT116 at 5 Gy following pre-treatment with metformin, 5-FU or vehicle controls under normoxia. **D)** Surviving fractions of HCT116 cells at 5 Gy following pre-treatment with metformin, 5-FU or vehicle controls under hypoxia. Data is presented as mean ± SEM for 5 independent experiments. Statistical analysis was performed using paired ANOVA, with post-hoc Tukey's multiple comparisons testing or *t*-testing. *$p < 0.05$, **$p < 0.01$, ***$p < 0.001$, ****$p < 0.0001$.

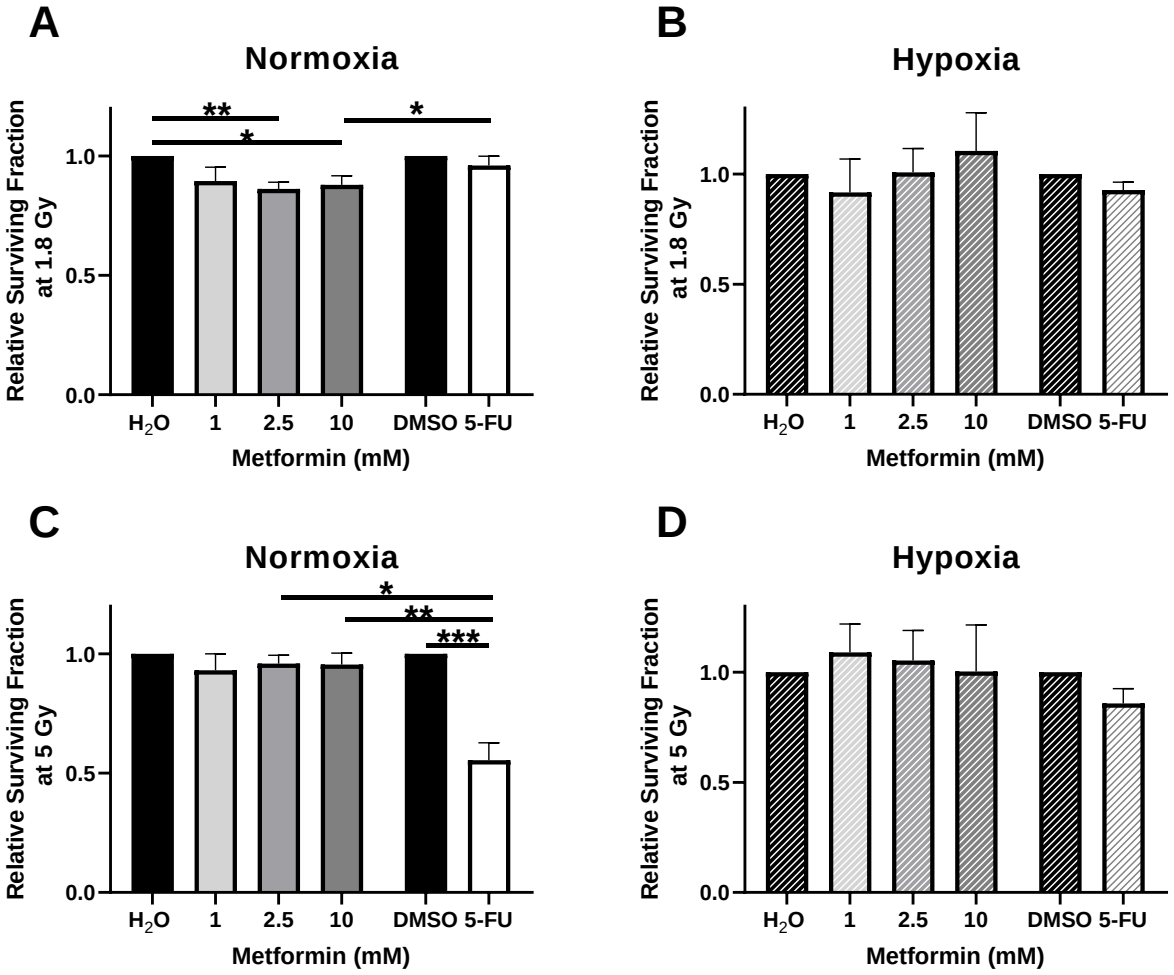

Fig. 4.21: **Metformin treatment significantly sensitises radioresistant SW837 cells to 1.8 Gy X-ray radiation under normoxia.** Radiosensitivity was assessed by clonogenic assay on SW837 cells treated with metformin (1 mM, 2.5 mM, 10 mM) or H_2O vehicle control for 24 h prior to radiation exposure, or 5-FU (15 µM 6 h prior to radiation) or DMSO control (0.001%) under normoxic and hypoxic conditions. **A)** Surviving fractions of SW837 cells at 1.8 Gy following pre-treatment with metformin, 5-FU or vehicle controls under normoxia. **B)** Surviving fractions of SW837 cells at 1.8 Gy following pre-treatment with metformin, 5-FU or vehicle controls under hypoxia. **C)** Surviving fractions of SW837 cells at 5 Gy following pre-treatment with metformin, 5-FU or vehicle controls under normoxia. **D)** Surviving fractions of SW837 cells at 5 Gy following pre-treatment with metformin, 5-FU or vehicle controls under hypoxia. Data is presented as mean ± SEM for 5 independent experiments. Statistical analysis was performed using paired ANOVA, with post-hoc Tukey's multiple comparisons testing or *t*-testing. **p* < 0.05, ***p* < 0.01, ****p* < 0.001.

4.5. Summary of Results of Chapter 4:

- The novel small molecule drug P3 significantly inhibits both OCR and ECAR in radioresistant SW837 cells in a dose-dependent manner and alters parameters of both mitochondrial and glycolytic metabolism.
- P3 treatment significantly alters mitochondrial function in radioresistant SW837 cells.
- P3 treatment does not radiosensitise either radioresistant SW837 cells or radiosensitive HCT116 cells, under hypoxic or normoxic conditions.
- P3 is cytotoxic at 200 μM in HCT116 cells under normoxia and hypoxia.
- Metformin treatment significantly inhibits OCR in both SW837 and HCT116 cells under normoxic and hypoxic conditions and increases ECAR.
- Metformin treatment significantly induces mitochondrial dysfunction (increasing ROS production, mitochondrial mass and mitochondrial membrane potential) under normoxia only.
- Metformin is cytotoxic to HCT116 cells under both normoxia and hypoxia, and to SW837 cells under hypoxia only.
- Metformin treatment significantly sensitises both HCT116 and SW837 cells to 1.8 Gy X-ray radiation under normoxia, and HCT116 cells under hypoxia, and this radiosensitising effect is superior to the clinically-utilised chemotherapeutic 5-FU.

4.6. Discussion

Resistance to therapy is a major clinical problem in the management of rectal cancer. Unfortunately, despite being the standard of care, only an estimated 20-30% of rectal cancer patients achieve a pCR following neoCRT, which is a predictor of improved outcomes (44). There is an urgent need to develop novel therapeutic strategies to enhance therapy response in those rectal cancer patients who are resistant to the current standard of care.

Recent evidence has highlighted a potential role for altered tumour metabolism in radioresistance (208, 212, 213, 240, 250, 266, 387-390). Previous research by our group has demonstrated that oxidative phosphorylation is associated with a radioresistant phenotype in upper gastrointestinal cancer, oesophageal adenocarcinoma, both *in vitro* and *in vivo* (213). In Chapter 2, it was demonstrated that radioresistant SW837 cells display a lower reliance on glycolysis, and upregulation of oxidative phosphorylation related genes, when compared to radiosensitive HCT116 cells, further supporting the importance of oxidative metabolism in radioresistance.

The development of drugs which target energy metabolism may be an effective strategy to enhance therapeutic response (391). P3, a novel quininib analogue, has been previously demonstrated in our laboratory to have anti-angiogenic and anti-metabolic effects in a zebrafish model and *ex vivo* treatment-naïve OAC biopsies and anti-metabolic and radiosensitising effects in an isogenic model of radioresistant oesophageal adenocarcinoma (212, 392). To investigate the potential anti-metabolic effect of P3 in rectal cancer, SW837 cells were treated for 24 h with a series of concentrations of P3, and the impact on metabolism assessed by Seahorse technology. Importantly, the SW837 rectal cancer line is not only radioresistant, but also has reduced reliance on glycolysis. In previous studies, P3 exerts its most potent anti-metabolic effects on oxidative phosphorylation, the pathway frequently associated with radioresistance. P3 was demonstrated to significantly inhibit OCR in SW837 cells at 15 µM and 20 µM doses, while in previous research in OAC, a dose of 10 µM for 24 h was sufficient to inhibit OCR. Importantly, in the SW837 cells, P3 also significantly inhibited ECAR, indicating a dual anti-metabolic role of P3 in cancer cells.

In addition, P3 was demonstrated to significantly reduce basal and maximal respiration rates following 24 h treatment with P3 at doses of 12.5 µM, 15 µM and 20 µM. Similarly, spare respiratory capacity was demonstrated to be significantly inhibited at doses of 15 µM and 20 µM. These findings indicate that SW837 cells lose their ability to respond to energy demand,

following 24 h treatment with P3. Furthermore, O_2-linked ATP turnover was demonstrated to be significantly inhibited following 24 h treatment with P3 at doses of 12.5 µM, 15 µM and 20 µM, supporting previous findings in radioresistant oesophageal adenocarcinoma cells (212). In addition, quantitative ATP levels were significantly reduced following treatment with 20 µM P3 in SW837 cells. This lower ATP production is most likely a result of inhibition of both oxidative and glycolytic metabolism. Importantly, ATP production is known to be associated with radiation resistance, in part due to its role in DNA damage repair (393). P3 treatment was also demonstrated to have significant effects on mitochondrial function, including increasing ROS production, mitochondrial mass and mitochondrial membrane potential in radioresistant SW837 cells. Mitochondrial function is also demonstrated to be associated with radioresponse of various cancers (391).

Low-dose P3 (≤ 20 µM) did not affect the proliferation or reproductive integrity of CRC cells, suggesting that the reduction in metabolic rates is not simply due to a reduction in cell number or proliferation rates, indicating that P3 may be having direct anti-metabolic effects. However, 200 µM P3 was demonstrated to induce cytotoxicity in HCT116 cells, and this is the first report of P3-induced cytotoxicity *in vitro* to date. Despite the previously demonstrated radiosensitising effects of P3 in OAC cells (212), P3 did not significantly sensitise HCT116 or SW837 cells to 1.8 Gy or 5 Gy X-ray radiation at any of the doses investigated under normoxic or hypoxic conditions.

One potential explanation for the lack of P3-mediated radiosensitisation in this model of inherent radioresistant and radiosensitive CRC is that the precise target of P3 in cells is as of yet unknown. Current studies are attempting to elucidate the precise target, and subsequent mechanism of action, of P3 as an anti-metabolic radiosensitiser in OAC, however. It is possible that this target is not expressed by or is in lower availability in the CRC cells utilised in this study (212, 392). Furthermore, these data indicate that whilst P3 is anti-metabolic, it does not radiosensitise CRC cells, suggesting that dual-inhibition of oxidative phosphorylation and glycolysis does not alter radioresponse.

In this chapter, the radiosensitising effect of the clinically utilised chemotherapeutic 5-FU was assessed in CRC cells. 5-FU has been utilised in the clinic as a radiosensitising drug for decades, and is utilised in neoadjuvant treatment in combination with radiation therapy, as the standard of care for treatment of locally-advanced rectal cancer (337, 394). In this chapter, 5-FU was demonstrated to enhance radiosensitivity in both HCT116 and SW837 cells *in vitro*.

This permitted the use of 5-FU as a positive control for radiosensitisation in assessments of metformin as a radiosensitiser. Importantly, the utilisation of 5-FU in this study, also permitted comparison between the efficacy of metformin as a novel radiosensitiser and the current clinical gold-standard.

Metformin is a clinically-approved drug used in the management of T2DM, which has an elusive precise mechanism of action. One known mechanism of metformin is as an inhibitor of complex I of the ETC (279, 386). In recent years, metformin has been assessed for its potential use as a radiosensitiser in various cancers (215-218). In observational studies, patients with diabetes treated with metformin during their cancer treatment, either neoCRT, or peri-operative chemotherapy, have demonstrated higher rates of pCR, when compared to those not on metformin in rectal (300) and oesophageal cancers (301, 302). Furthermore, metformin treatment is demonstrated to enhance radiosensitivity *in vitro* and in xenograft models of CRC (231, 305) and pancreatic cancer (395).

In this chapter, metformin was assessed for its impact on energy metabolism in HCT116 and SW837 cells. Metformin treatment resulted in significant inhibition of OCR in both cell lines, supporting its role as an ETC inhibitor. In addition, metformin was demonstrated to enhance ECAR in these cell lines, potentially as a compensatory mechanism for the severely reduced oxidative metabolism rates.

In addition, metformin treatment was demonstrated to have significant impact on mitochondrial function in HCT116 and SW837 cells, increasing mitochondrial mass, mitochondrial membrane potential and ROS production. Previous research has demonstrated that metformin treatment in cancer cells increases mitochondrial mass readings, by inducing mitochondrial swelling and mitochondrial biogenesis using *in vitro* models of lung and prostate cancer (396). Furthermore, these findings of increased mitochondrial mass following metformin treatment were supported in an *in vivo* model of prostate cancer (396). In addition, increased mitochondrial mass was demonstrated in *in vitro* and *ex vivo* models of endometrial cancer, following treatment with metformin (397). High mitochondrial membrane potential (MMP) is directly associated with high oxidative stress (398), and so these results again support the role of metformin as an anti-metabolic drug, targeting mitochondria. In this chapter, metformin treatment was demonstrated to significantly increase ROS production in HCT116 and SW837 cells. Previous research has demonstrated significant induction of ROS production using *in vitro* models of pancreatic cancer (399), lung and breast cancer (400). In

addition, a study by Mogavero *et al.* demonstrated significant induction of ROS production in HCT116 cells, supporting the findings in this chapter (401).

Importantly, metformin was demonstrated to significantly radiosensitise HCT116 colon cancer cells to radiation therapy, under both normoxic and hypoxic conditions. In addition, this metformin-induced radiosensitisation was superior to that of the clinical-standard radiosensitiser drug 5-FU, at doses of 1.8 Gy radiation. While metformin significantly reduced the clonogenic surviving fraction of HCT116 cells following 5 Gy radiation, it is important to note that HCT116 cells are already significantly radiosensitive at 5 Gy and therefore, it is difficult to extrapolate the radiosensitising effects of 5-FU at this dose of radiation.

Importantly, it was demonstrated that metformin also induced radiosensitisation in SW837 cells under normoxic conditions. This radiosensitising effect was superior to that demonstrated for the current standard of care, 5-FU, highlighting the potential for metformin as a novel radiosensitiser in treatment resistant rectal cancer cells. These findings support previous evidence in the literature of the radiosensitising effects of metformin in various cancer types, including pancreatic cancer (402), fibroscarcoma and breast cancer (403). Radiosensitisation induced by metformin treatment in radiosensitive HCT116 cells is supported by multiple studies in the literature (232, 305, 404). However, while the effect of metformin treatment on cytotoxicity in SW837 cells has been previously assessed (405), to our knowledge, this is the first study to investigate and demonstrate metformin-induced radiosensitisation in this highly radioresistant cell line.

The impact of metformin on metabolism and as a radiosensitiser was investigated under both normoxic and hypoxic conditions. One reason this is important is that hypoxia is a common feature of solid malignancies and is also associated with enhanced therapeutic resistance (231). In addition, as previously demonstrated (**Chapter 3, Section 3.4.1**), hypoxia significantly enhanced the radioresistance of both HCT116 and SW837 cells. Furthermore, hypoxia is intrinsically linked to metabolism and the regulation of metabolic pathways (223-225). In addition, evidence suggests that one mechanism by which anti-metabolic drugs may act as therapeutic radiosensitisers is a result of the enhanced oxygen availability that results from oxidative phosphorylation inhibition, permitting enhanced fixation of radiation induced damage (217, 231). For example, the mitochondrial complex I inhibitor, Papavarine, reduces OCR and hypoxia and induces radiosensitisation in a model of non-small cell lung cancer (406)

In this chapter, it was demonstrated that metformin treatment significantly radiosensitises HCT116 cells to a clinically-relevant dose of 1.8 Gy radiation under normoxia and hypoxia, and that this radiosensitisation is superior to that of clinically-utilised radiosensitising drug 5-FU. Importantly, previous research by Zannella *et al*. supports these findings, demonstrating that metformin treatment improved tumour oxygenation, and radiotherapy responses in a xenograft model of HCT116 colon cancer (231). While metformin, and the clinically-utilised radiosensitising drug 5-FU failed to sensitize SW837 cells to radiation under hypoxia, this is possibly be due to the inherently highly radioresistant cells becoming significantly more radioresistant due to hypoxic exposure alone.

Together these data indicate that while dual metabolic inhibition by P3 does not induce radiosensitisation in this CRC model, inhibition of oxidative phosphorylation, and induction of glycolysis in this model by metformin is associated with enhanced radioresponse in HCT116 and SW837 cells. While metabolic inhibition alone may not underpin radiosensitivity, metabolism and metabolic flexibility is a requirement for many established mechanisms of radioresistance, including cell cycle, cell death and DNA damage repair. The next chapter aims to investigate these potential underlying mechanisms by which metformin sensitises CRC cells to radiation.

Chapter 5: Investigation of the mechanisms underlying metformin-induced radiosensitivity in colorectal cancer *in vitro*

5.1. Introduction

In chapter 4, it was demonstrated that metformin altered CRC cell metabolism *in vitro*, and importantly, was demonstrated to sensitise both radiosensitive and radioresistant CRC cells. This radiosensitising effect of metformin has been previously identified in various cancer types, (231, 300-302, 305), however, the exact mechanism(s) underlying metformin-induced radiosensitivity are incompletely understood. In particular, the potential role of metformin treatment in the radiation response of rectal cancer are poorly understood.

Numerous molecular mechanisms have been proposed to contribute to the anti-neoplastic and therapeutic sensitising effects of metformin in cancer. One such mechanism is activation of LKB1 and AMPK, which results in mTOR inhibition, and alterations to cellular metabolism (278). The main subcellular target of metformin is the mitochondrion, with metformin demonstrated to inhibit Complex I of the ETC, inhibiting oxidative metabolism, and subsequently altering the AMP/ATP ratio in cells (231, 279). In addition to these anti-metabolic effects, the anti-neoplastic effects of metformin may also be mediated by alterations in cell cycle, inhibition of protein synthesis, immune activation, angiogenesis inhibition and induction of cell death (278).

Research to identify and develop radiosensitising drugs has highlighted a number of potential molecular pathways and targets of interest, which are exploited by cancer cells to overcome radiation induced cell death (384). One such mechanism is cell cycle. In cancer cells, G2/M arrest following radiation exposure is a common feature, to permit repair of radiation-induced DNA damage. This G2/M checkpoint has been proposed as a potential target to enhance radiosensitivity in cancer cells (96, 97, 407). Metformin has been demonstrated to inhibit this G2/M blockade, with subsequent elevation in cells in the G0/G1 phase in various cancer types, although the impact of metformin treatment on cell cycle in rectal cancer is currently unknown (308-310).

Other major pathways targeted in the development of radiosensitising drugs are DNA damage repair pathways. DSBs are the most critical form of DNA damage induced by exposure to radiation therapy, and if not repaired, result in cell death (57). DNA damage repair pathways play an important role in the regulation of cell cycle, apoptosis and cellular signalling. Upregulation of DNA damage repair pathways is a common feature of radioresistant cancer cells, to facilitate the repair of IR-induced DNA lesions, such as DSBs (361). As a result, drugs targeting key DNA damage repair pathway mediators, including ATM/ATR and CHK1/CHK2

have been developed as radiosensitisers. Metformin treatment has been demonstrated to impair DNA damage repair in various cancer types (306, 307). In CRC, metformin was demonstrated to impair DNA damage repair proteins, particularly those associated with homologous recombination (Rad-51 and ERCC1) *in vitro* and *ex vivo* in colon cancer (305), however, the impact of metformin on DNA damage repair in rectal cancer is largely unknown.

While the role of programmed cell death in the radioresponse is controversial (112), growing evidence has highlighted its potential importance (59). In Chapter 4, it was demonstrated that metformin induces significant cytotoxicity as assessed by crystal violet assay and clonogenic assay. Research has demonstrated that metformin does induce apoptosis in various cancer types, although the contribution of this apoptosis to enhanced radiosensitivity is currently unknown (311-313, 405, 408).

In Chapter 4, it was demonstrated that metformin significantly induces ROS production in HCT116 and SW837 cells. Oxidative stress and antioxidant capacity are known determinants of cellular radioresponse (133, 134). Metformin has been demonstrated to enhance oxidative stress in various cancers (296, 311-313), however, whether this contributes to the radiosensitising effect of metformin treatment is currently unknown.

Having demonstrated in Chapter 4 that metformin treatment significantly radiosensitises HCT116 and SW837 cells to radiation therapy, this chapter investigated the potential underlying mechanism(s) of this metformin-induced radiosensitivity.

5.2. Overall Objective and Specific Aims of Chapter 5

In this chapter, the potential mechanisms of metformin-induced radiosensitisation were investigated.

The specific aims of this chapter were:

- Investigate metformin-induced effects on basal cell cycle distribution in HCT116 and SW837 cells under normoxic and hypoxic conditions.
- Investigate the impact of metformin treatment on cell cycle progression following exposure to radiation in HCT116 and SW837 cells, under normoxia and hypoxia.
- Determine the effect of metformin treatment on cell death, basally and in combination with radiation treatment in HCT116 and SW837 cells under normoxic and hypoxic conditions.
- Investigate the effect of metformin on DNA damage induction and repair, in combination with radiation treatment in HCT116 and SW837 cells under normoxia and hypoxia.
- Investigate the impact of metformin treatment on GSH/GSSG antioxidant production in HCT116 and SW837 cells.
- Determine the impact of metformin treatment on the transcriptome of HCT116 and SW837 cells.
- Validate metabolic effects of metformin treatment in *ex vivo* rectal cancer biopsies.
- Investigate the impact of metformin treatment on the protein secretome of rectal cancer.
- Assess the effect of metformin treatment on metabolism and the protein secretome of normal (non-cancer) rectal tissue

5.3. Materials and Methods

5.3.1. *Reagents and materials*

All laboratory chemicals and reagents were stored according to manufacturer's instructions. All cell culture reagents were purchased from Gibco, unless otherwise stated. All plastic materials were purchased from Sarstedt, unless otherwise stated.

5.3.2. *Drugs*

Metformin (metformin hydrochloride) was purchased from Sigma-Aldrich, and prepared in distilled water to stock concentrations of 200 mM, and stored at -20°C.

5.3.3. *Cell culture*

Cell culture was carried out as per section 2.3.2.

5.3.3.1. *Human colorectal adenocarcinoma cell lines*

SW837 and HCT116 cells were obtained from the ECACC. The SW837 rectal cancer cells were originally obtained from a stage IV rectal adenocarcinoma from a 53-year-old Caucasian male. The HCT116 colon cancer line originated from a colon adenocarcinoma from an adult male.

5.3.4. *Irradiation*

All irradiations were performed using an X-Strahl cabinet X-ray irradiator (RS225) (X-Strahl) at a dose rate of 1.74 Gy/min, as previously described (**Section 2.3.3**). Cells to be irradiated under hypoxic conditions were exposed to X-ray radiation in air-locked containers.

5.3.5. *Hypoxia treatment*

Cells were cultured under hypoxic conditions (0.5% O_2 /5% CO_2) at 37°C in the Don Whitley H-35 hypoxychamber. All treatment medium and plastic ware were deoxygenated in the chamber for at least 24 h prior to use.

5.3.6. *Assessment of metformin treatment on cell cycle and DNA damage under normoxia and hypoxia (0.5% O_2).*

Cells in the exponential growth phase, were harvested by trypsinisation, counted and seeded into 12-well plates as previously described (**Sections 2.3.2.2 and 2.3.2.5)** (HCT116: 150,000 cell/well, SW837 200,000 cell/well). Cells were allowed to adhere overnight in 5% CO_2/95% atmospheric air, at 37°C. Cells for hypoxic culture were transferred to a Whitley hypoxychamber at 37°C in 5% CO_2/0.5% O_2, while normoxic cells remained at 37°C in 5% CO_2/95% atmospheric air. At 24 h post hypoxic exposure, medium was removed and cells were treated with 1 mL metformin (10 mM) or vehicle control (H_2O) while under normoxic or hypoxic conditions. Twenty-four hours after treatment, cells were mock-irradiated or exposed

to clinically-relevant 1.8 Gy X-ray radiation, under normoxic or hypoxic conditions, as appropriate (**Section 5.3.5**). At 20 min, 6 h, 10 h, or 24 h post-irradiation, cells were collected into 5 mL flow tubes by trypsinisation and stained with γH2AX-Alexa 488 or PI, as previously described (**Section 2.3.11**). Samples were acquired, with a minimum of 10,000 events collected, excluding doublets, using the FACSCanto II flow cytometer (BD Biosciences). γH2AX-AlexaFluor-488 was measured on the FITC channel, while PI was measured on the PerCP-Cy5 channel. Data were analysed using FlowJo™ Version 10.6.2.

5.3.7. *Annexin-V/Propidium Iodide analysis of apoptosis in metformin treated cells by flow cytometry under normoxia and hypoxia (0.5% O_2)*

Cells in the exponential growth phase were harvested, counted and seeded in 12-well plates at 1 mL per well as previously described (**Sections 2.3.2.2 and 2.3.2.5**) (HCT116 at 150,000 and SW837 at 200,000 cells per well). Cells were allowed to adhere for 6 h at 37°C in 5% CO_2/95% atmospheric air. Cells to be cultured under hypoxic conditions were then transferred to a Whitley hypoxychamber at 37°C in 5% CO_2/0.5% O_2, while normoxic cells remained at 37°C in 5% CO_2/95% atmospheric air. At 24 h post hypoxic exposure, media was removed and replaced with 1 mL metformin (10 mM) or vehicle control (H_2O) while under normoxic or hypoxic conditions. Twenty-four hours later, cells were mock-irradiated or exposed to 1.8 Gy X-ray radiation, while remaining under normoxia or hypoxia conditions (**Section 5.3.5**). At this timepoint, and at 24 and 48 h post irradiation, cells and supernatants were transferred to 5 mL flow tubes by trypsinisation, (**Section 2.3.2.2**) and stained with Annexin-V-FITC or PI as described in **section 2.3.10**. Stained samples were acquired using a FACS Canto II flow cytometer (BD Biosciences), acquiring 40,000 events per tube. Data was analysed by FlowJo™ version 10.6.2 software 10.6.2 software.

5.3.8. *Glutathione GSH/GSSG-Glo™ Assay*

Reduced glutathione (GSH) and oxidised glutathione (GSSG) levels were assessed in Metformin or H_2O vehicle-treated HCT116 and SW837 cells using the GSH/GSSG-Glo™ luminescent assay (Promega) according to the manufacturer's instructions.

HCT116 and SW837 cells were seeded in RPMI in white-walled 96-well plates (Promega) at 15,000 cells per well. Cells were cultured at 37°C in 5% CO_2/95% atmospheric air. At 24 h post seeding, medium was removed to waste, and cells were treated with 100 µL of metformin (10 mM) or H_2O vehicle control in RPMI and incubated at 37°C in 5% CO_2/95% atmospheric air. After 24 h treatment, media was removed to waste and cells were lysed with

either Total or Oxidised Glutathione Reagent, which was prepared in advance, at 50 µL per well. The plate was then agitated by shaking on a plate mixer for 5 min at RT°. Luciferin Generation Reagent was added to each well at 50 µL per well. The plate was shaken briefly using a plate shaker and allowed to incubate for 30 min at RT°. A volume of 100 µL Luciferin Detection Reagent was added to each well, the plate shaken briefly, and incubated at RT° for 15 min. Luminescence was measured at 1 s integration time using the Explorer Luminometer (Promega). An identical plate of cells was set up and treated as with the experimental plate and was used for normalisation of assay results by crystal violet assay (**Section 2.3.9**).

5.3.9. *RNA collection and isolation*

HCT116 and SW837 cells were seeded in 1.5 mL RPMI in 6-well plates (250,000/350,000 cells per well) and incubated at 37°C in 5% CO_2/95% atmospheric air. At 24 h post seeding, medium was removed to waste and cells were treated with metformin (10 mM) or H_2O vehicle control (2%). At 24 h post treatment medium was removed to waste, and cells were washed with 500 µL PBS. The wash was removed to waste and cells were lifted by trypsinisation (500 µL) and incubation at 37°C for 5 min. A volume of 500 µL RPMI was added to each well to neutralise the trypsin, and the cell suspensions were transferred to 1.5 mL Eppendorf tubes. Cells were pelleted by centrifugation at 1300 rpm for 3 min at 4°C. Supernatant was carefully removed, and cell pellets were washed and resuspended in 700 µL cold PBS. Cells were centrifuged at 1300 rpm for 3 min at 4°C. Supernatants were removed, and cell pellets were stored at -80°C until RNA isolation.

To isolate RNA, the MiRNeasy Mini Kit (Qiagen) was used according to the manufacturer's instructions. A volume of 700 µL QIAzol lysis reagent was added to the cell pellet, and thoroughly mixed by pipetting. The suspension was vortexed briefly. The homogenate was incubated at RT° for 5 min, before a volume of 140 µL 1-bromo-3-chloropropane (BCP) was added and the tube was shaken vigorously for 15 s. The homogenate was allowed to rest for 1 min at RT°, before being centrifuged at 12,000 x g for 15 min at 4°C, to allow for phase separation. The upper aqueous phase was transferred to a new 1.5 mL collection tube, and 525 µL of ethanol (Sigma) was added to each tube and mixed by pipetting. A volume of 700 µL of each sample was transferred to a RNeasy Mini spin column in a 2 mL collection tube. The samples were then centrifuged at 10,000 x g for 15 s at RT°. The flow-through was discarded and any remaining sample was added to each spin column and centrifuged as the step previous. A volume of 700 µL RWT buffer was added to each spin

column, and samples were centrifuged at 10,000 x g for 15 s at RT°. Buffer RPE (500 µL) was added to each spin column and centrifuged at 10,000 x g for 15 s at RT°. This step was repeated and the sample was centrifuged for 2 min to dry the membrane. The spin column was transferred to another collection tube and centrifuged for 1 min at full speed. The spin column was transferred to a new 1.5 mL collection tube, and 30 µL RNase-free water was added to each sample. Samples were centrifuged at 8000 x g for 1 min to elute the RNA.

5.3.10. *RNA quantification*

RNA was quantified using a Nanodrop 1000 spectrophotometer (version 3.1, Nanodrop technology). Initially, 1 µL RNase-free water was loaded to each probe to blank the instrument. The water was gently wiped away, and 1 µL of each sample of isolated RNA was loaded to each probe on the instrument and concentration measured in ng/µL. To assess RNA quality, the 260:280 and the 260:230 ratios were also recorded.

5.3.11. *Transcriptomic analysis*

Transcriptomic profiling by RNA-Seq, was conducted using Lexogen QuantSeq 3'mRNA-Seq, and a NovaSeq 6000 sequencing platform, as previously described (**Section 2.3.16**).

Briefly, RNA libraries were prepared for sequencing using the QuantSeq 3' mRNA-Seq Library prep kit (Lexogen), according to the manufacturers instructions. First strand synthesis of RNA samples was conducted, and RNA samples were denatured. The RNA template was degraded prior to initiation of second strand synthesis of cDNA. The dsDNA library was purified using magnetic beads, to remove contaminants from reaction components. The library was amplified by PCR, using an optimised number of 15 PCR cycles, as described (**Section 2.3.16**). An equal molar amount was pooled for sequencing, with 320 pM loaded onto the NovaSeq flow cell for sequencing using the NovaSeq 6000 and an SP v1.5 sequencing kit, with 1 x 100 bp reads. Raw sequencing files were uploaded to the BlueBee platform for analysis (**Section 5.2.12**).

5.3.12. *Transcriptomic data analysis*

Raw files from transcriptomic profiling were assessed using the BlueBee Bioinformatics platform (Lexogen). Raw reads were trimmed and aligned for automated gene counting. Once gene reads and counts were complete, differential expression analysis was performed using the DESeq2 R script extension within BlueBee software, which compares gene expression counts between samples and performs the Wald test, with Benjamini-Hochberg correction. Genes were considered differentially expressed with an adjusted *p* value (*p*adj) < 0.05.

Differential expression data was subsequently assessed by bioinformatics software, Ingenuity Pathway Analysis (IPA) (Qiagen), to cluster differentially expressed genes and assess pathway activation and inhibition within samples.

5.3.13. *IPA analysis*

Significantly differentially expressed genes, and corresponding Log2 Fold Change values were imported to IPA bioinformatics software. Core analysis in IPA was performed, which utilises the Qiagen Knowledge Base, to identify networks and predict specific biological function and pathway involvement in the uploaded experimental transcriptomic dataset.

Downstream Effects Analysis in IPA was utilised to predict alterations to downstream biological functions in uploaded experimental datasets. A networking algorithm utilises information about gene relationships and activation pathways from the literature and the Qiagen Knowledge Base to predict biological function alterations in experimental data. The overlap between genes in the dataset, and those known to be involved in each biological function is used to predict alterations to biological functions. As each biological function is comprised of multiple functional pathways, significance is represented as *p*-value range.

Canonical Pathway Analysis in IPA, utilising the Qiagen Knowledge Base, was utilised to predict involvement and activation or inhibition of specific biological pathways in the experimental dataset. The *p*-value denotes the significance between the overlap of input experimental data and the Ingenuity Knowledge Base, indicating confidence in pathway involvement. The Z-score refers to software prediction of the activation or inhibition of each affected canonical pathway, with a Z-score ≥ 2, or ≤ -2 indicating significant activation or inhibition of each pathway, respectively.

5.3.14. *Patient recruitment and sample collection*

Ethical approval for patient sample collection for this study was granted by the Joint St. James's Hospital/AMNCH ethical review board and the Beacon Hospital Research Ethics Committee. Patients undergoing lower gastrointestinal investigations or endoscopy for rectal cancer diagnosis were recruited between January 2018 and October 2021 from St. James's Hospital, Dublin and Beacon Hospital, Dublin.

Pre-treatment rectal tumour biopsies were obtained from consenting patients at diagnostic endoscopy. Normal (non-cancer) rectal tissue biopsies were obtained during colonoscopy from consenting patients who did not have a cancer diagnosis. Patient data was pseudonymised and coded with a unique biobank identifier. Histological confirmation of

tumour tissue and non-malignant tissue in biopsies was performed by an experienced GI pathologist using haematoxylin and eosin staining.

5.3.15. *Protein isolation from biopsies*

Protein was isolated from patient tissue biopsies using the AllPrep DNA/RNA/Protein Mini Kit, according to manufacturers specifications.

Briefly, tissue biopsies were homogenised in a 2 mL tube, with 600 µL buffer RLT (supplemented with β-mercaptoethanol) and a stainless-steel bead. Biopsies were homogenised using the Qiagen tissue lyser for 2 min at 20 Hz, until fully homogenised. Homogenised tissue lysates were centrifuged at full speed for 3 min, and the supernatant transferred to an AllPrep DNA spin column in a 2 mL collection tube. The samples were centrifuged for 30 s at 8000 x *g*. The spin column was stored at 4°C, until required for DNA purification. A volume of 400 µL ethanol (100%) was added to the flow through and mixed by pipetting. A volume of 700 µL of the sample, and any precipitate, was transferred to an RNeasy spin column in a 2 mL tube and centrifuged for 15 s at 8000 x *g*. RNA was subsequently isolated from the spin column, as per manufacturers instructions, and stored at -80 °C. The flow-through was utilised for protein purification. One volume of buffer APP was added to samples, mixed vigorously and incubated at RT° for 10 min to permit protein precipitation. The samples were centrifuged at full speed for 10 min and the supernatant discarded. A volume of 500 µL ethanol (70%) was added to the protein pellet, the samples centrifuged at full speed for 1 min, and the supernatant decanted. Protein pellets were allowed to air-dry for 10 min at RT°. Protein pellets were dissolved in 70 µL of sodium dodecyl sulfate (5%) (SDS)(Sigma), supplemented with protease inhibitor cocktail tablet (1 tablet per 10 mL) (Roche), and stored at -20°C until protein was quantified using the BCA assay.

5.3.16. *Bicinchoninic acid (BCA) assay*

To quantify the protein content of patient biopsies, the Pierce bicinchoninic acid (BCA) protein assay kit (Thermo Fisher) was utilised.

A standard curve using albumin standards, with the top standard of 2000 µg/mL, was used. A volume of 10 µL of each standard or sample (1 in 2 dilution with PBS) was loaded into a 96-well plate. A volume of 200 µL working reagent (50:1 BCA reagent A: BCA reagent B) was added to each sample and standard well, and mixed. The plate was incubated for 30 min at 37°C. The plate was allowed to cool to RT° and absorbance was read at 562 nm using a

VersaMax microplate reader (Molecular Devices). The standard curve was generated, and the protein content of each sample determined.

5.3.17. *Real-time metabolic profiling of rectal tumour and non-cancer rectal tissue biopsies*

Following informed consent, 2 biopsies per patient (either rectal cancer or non-cancer rectal tissue) were collected at colonoscopy, placed on saline-soaked gauze and transported to the laboratory. Each biopsy was placed into an individual well of an XF24 Islet Capture Microplate (Agilent Technologies) and secured into place by islet capture screens. A volume of 1 mL complete M199 (Gibco) (supplemented with FBS (10%), penicillin-streptomycin (1%), Fungizone™ (1%), gentamycin (0.1%) and insulin (1 μg/mL)) was placed in each well. The plate was placed at 37°C, in 5% CO_2/95% atmospheric air for 30 min to equilibrate.

Three basal measurements of OCR and ECAR were measured over 24 min of three repeats of mix (3 min)/ wait (2 min)/ measurement (3 min) using the Seahorse XFe24 analyser. The biopsies were treated with metformin (10 mM) or H_2O control in complete M199 medium (1 mL volume). Biopsies were cultured for 24 h at 37°C in 5% CO_2/95% atmospheric air, and basal measurements of OCR and ECAR measured over 24 min as described. Biopsies and matching TCM or NCM were collected, snap-frozen in liquid nitrogen, and stored at -80°C until required.

The effect of treatment was assessed as the change in OCR/ECAR measurements following vehicle/metformin treatment, when compared to each corresponding baseline measurement. Metabolic rates were normalised to protein content using the BCA assay (Pierce) (**Sections 5.2.15 and 5.2.16**).

5.3.18. *Multiplex enzyme-linked immunosorbent assay (ELISA) profiling of secretome of rectal cancer and non-cancer rectal tissue*

The protein secretome of rectal cancer and non-cancer rectal tissue biopsies was assessed using TCM and NCM from biopsies treated with metformin (10 mM) or H_2O vehicle control for 24 h, using the Meso Scale Diagnostics (MSD) Discovery multiplex ELISA platform.

To assess angiogenic, vascular injury, pro-inflammatory, cytokine and chemokine secretions from TCM and NCM, a 54-plex ELISA kit separated across 7 plates was used (Meso Scale Diagnostics, USA). The multiplex kit was used to quantify the secretions of CRP, Eotaxin, Eotaxin-3, FGF(basic), Flt-1, GM-CSF, ICAM-1, IFN-γ, IL-10, IL-12/IL-23p40, IL-12p70, IL-13, IL-15, IL-16, IL-17A, IL-17A/F, IL-17B, IL-17C, IL-17D, IL-1RA, IL-1α, IL-1β, IL-2, IL-21, IL-22, IL-23, IL-27, IL-3, IL-31, IL-4, IL-5, IL-6, IL-7, IL-8, IL-8 (HA), IL-9, IP-10, MCP-1, MCP-4, MDC, MIP-1α,

MIP-1β, MIP-3α, PlGF, SAA, TARC, Tie-2, TNF-α, TNF-β, TSLP, VCAM-1, VEGF-A, VEGF-C and VEGF-D from TCM. All assays were run as per manufacturer's recommendation, an overnight supernatant incubation protocol was used for all assays except Angiogenesis Panel 1 and Vascular Injury Panel 2 which were run according to the same day protocol. TCM and NCM were run undiluted on all assays except Vascular Injury Panel 2, where a 1:4 dilution was used. Secretion data for all factors was normalised to cell lysate protein content by using a BCA assay (**Section 5.2.16)**.

5.3.19. *Statistical analysis*

All statistical analysis and graphing were performed using Graphpad Prism v9 software. Data is presented as mean ± standard error of the mean (SEM) throughout. Statistical comparisons were carried out using analysis of variance (ANOVA) testing, post-hoc Tukey's multiple comparisons testing or *t*-testing, depending on the experimental set up, as described in figure legends. For transcriptomic data analysis, BlueBee, DESeq2 R extension and IPA software were utilised for statistical analysis. DESeq2 utilised Wald testing, while IPA utilised Fisher's Exact Test, as stated in figure/table legends. Analysis on patient samples used Mann-Whitney U or Wilcoxon signed rank test, as appropriate. Results were considered significant where probability (p) ≤ 0.05.

5.4. Results

5.4.1. *Metformin treatment alters basal cell cycle distribution in HCT116 and SW837 cells under normoxic conditions*

To investigate the impact of metformin treatment on basal cell cycle, HCT116 and SW837 cells were treated with metformin for 24 h, 30 h, 34 h or 48 h with metformin (10 mM) or H_2O vehicle control and the basal cell cycle distribution assessed by PI staining and flow cytometry.

At 24 h post treatment, no significant alterations were demonstrated in the proportion of G0/G1, S or G2/M phase HCT116 cells treated with metformin (10 mM), when compared to H_2O vehicle control (**Fig. 5.1 A**). Metformin treatment significantly reduced the proportion of G0/G1 phase cells at 30 h post treatment, when compared to H_2O (p = 0.022) (Mean % G0/G1 phase ± SEM; HCT116 H_2O 53.1 ± 2.26 vs HCT116 metformin 46.22 ± 2.99) (**Fig. 5.1B**). At 34 h post treatment, a trend towards reduced proportion of G0/G1 phase cells in metformin treated cells was observed, but this did not reach statistical significance (p = 0.078) (Mean % G0/G1 cells ± SEM; HCT116 H_2O 57.14 ± 4.19 vs HCT116 metformin 40.3 ± 3.94) (**Fig. 5.1C**)**.** At 48 h post treatment, metformin significantly reduced the proportion of G0/G1 phase HCT116 cells, when compared to vehicle control (p = 0.0036) (Mean % G0/G1 ± SEM; HCT116 H_2O 59.56 ± 3.56 vs. HCT116 metformin 42.08 ± 1.97) (**Fig. 5.1D**). Metformin treatment did not significantly alter the proportion of HCT116 cells in the G2/M phase basally at any timepoint (**Fig. 5.1A-D**). However, by 48 h post treatment, metformin treatment resulted in a significant increase to the proportion of HCT116 cells in S phase (**Fig. 5.1C**).

In SW837 cells, at 24 h post treatment, metformin did not affect cell cycle distribution (**Fig. 5.2A**). At30 h post treatment, metformin significantly increased the proportion of SW837 G0/G1 phase cells, when compared to vehicle control *(p* = 0.01) (Mean % G0/G1 cells ± SEM; SW837 H_2O 61.32 ± 2.18 vs SW837 metformin 66 ± 1.96) (**Fig. 5.2B**).This G0/G1 phase arrest persisted at 34 h post metformin treatment, with significantly more SW837 cells in G0/G1 phase in metformin treated cells, when compared to vehicle control (p = 0.035) (Mean % G0/G1 phase ± SEM; SW837 H_2O 62.74 ± 1.89 vs. SW837 metformin 65.6 ± 2.29) (**Fig. 5.2C**). No significant differences to cell cycle distribution were observed at 48 h post treatment in SW837 cells (**Fig. 5.2D**).

These data demonstrate that metformin treatment alters basal cell cycle distribution in HCT116 and SW837 cells under normoxia, at various timepoints. HCT116 cell cycle distribution is most affected by metformin treatment, when compared to SW837 cells.

5.4.2. *Metformin treatment affects basal cell cycle distribution in HCT116 and SW837 cells under hypoxic conditions (0.5% O_2)*

Having demonstrated that metformin treatment alters basal cell cycle distribution in HCT116 and SW837 CRC cells under normoxic conditions, the effect of metformin on cell cycle was subsequently assessed under hypoxic conditions, by PI staining and flow cytometry.

In HCT116 cells, a trend towards increased G0/G1 cells with metformin treatment was observed at 30 h post treatment, although this did not reach statistical significance (p = 0.06) (**Fig. 5.3B**). Similarly, while trends towards increased G0/G1 phase cells with metformin treatment were observed at 34 h post treatment, no statistical differences were observed (**Fig. 5.3C**). By 48 post metformin treatment, the proportion of G0/G1 phase cells were significantly increased in HCT116 cells, when compared to vehicle control (p = 0.0423) (Mean % G0/G1 ± SEM; HCT116 H_2O 26.5 ± 2.67 vs HCT116 metformin 33.45 ± 2.46) (**Fig. 5.3D**).

At 24 h post treatment, a trend towards reduced HCT116 cells in the S phase was observed in metformin treated cells, although this did not reach statistical significance (p = 0.07) (**Fig. 5.3A**). Similar trends were observed at 30 h post treatment in metformin treated cells, although this did not reach statistical significance (p = 0.088) (**Fig. 5.3B**). No significant alterations to the proportion of S phase cells were demonstrated at 34 h or 48 h post treatment (**Fig. 5.3C-D**). Metformin did not affect the proportion of G2/M phase HCT116 cells under hypoxia at any timepoint examined (**Fig. 5.3A-D**).

In SW837 cells, at 30 h post treatment, a trend towards reduced G0/G1 phase cells following metformin treatment was demonstrated, but this did not reach statistical significance (p = 0.09) (**Fig. 5.4B**). Furthermore, at 34 h post treatment, metformin treatment significantly reduced the proportion of G0/G1 phase cells, when compared to vehicle control (p = 0.0009) (Mean G0/G1 cells ± SEM; SW837 H_2O 78.22 ± 1.04 vs SW837 metformin 71.98 ± 1.62,) (**Fig. 5.4C**).

In SW837 cells, under hypoxic conditions, the proportion of S phase cells was significantly increased with metformin treatment, when compared to H_2O at 24 h post treatment (p = 0.04) (Mean % S phase ± SEM; SW837 H_2O 13.92 ± 3.03 vs. SW837 metformin

17.37 ± 2.34) (**Fig. 5.4A**). The proportion of G2/M phase cells in hypoxic SW837 cells was demonstrated to be significantly lower at 24 h post metformin treatment, when compared to H_2O control (p = 0.015) (Mean % G2/M ± SEM; SW837 H_2O 26.5 ± 1.46 vs SW837 metformin 21.57 ± 1.49) (**Fig. 5.4A**).

These data demonstrate that metformin affects the basal cell cycle distribution of HCT116 and SW837 cells under hypoxic conditions.

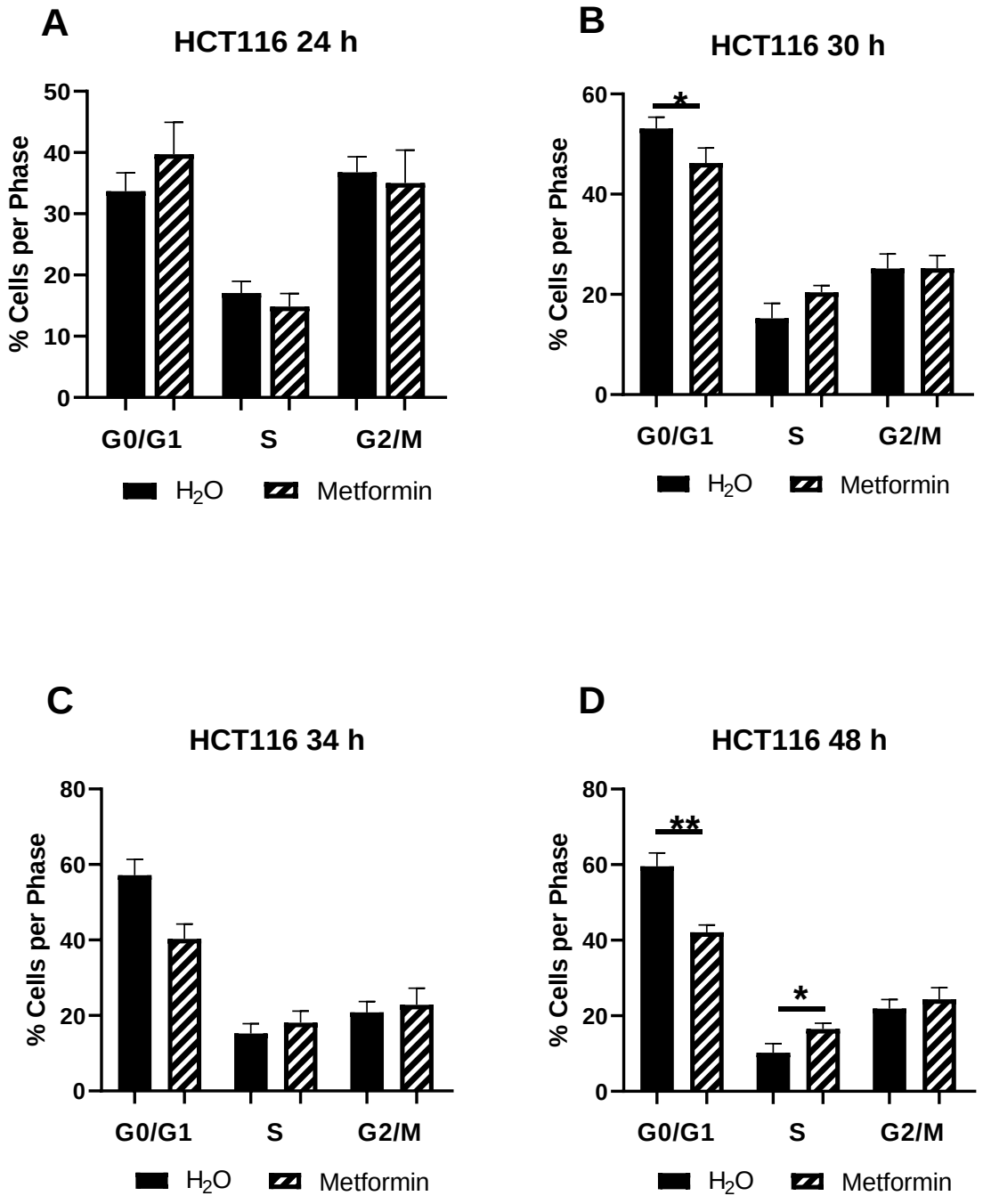

Fig. 5.1: **Metformin treatment significantly alters HCT116 cell cycle distribution under normoxia.** HCT116 cells were treated with metformin (10 mM) or H_2O vehicle control for 24, 30, 34 and 48 h, and cell cycle distribution assessed by PI staining and flow cytometry. **A)** Effect of 24 h metformin treatment on cell cycle distribution. **B)** Effect of 30 h metformin treatment on cell cycle distribution. **C)** Effect of 34 h metformin treatment on cell cycle distribution. **D)** Effect of 48 h metformin treatment on cell cycle distribution. Data is presented as mean ± SEM for 3 (24 h) or 5 independent experiments. Statistical analysis was performed using paired *t*-testing. *$p < 0.05$, **$p < 0.01$.

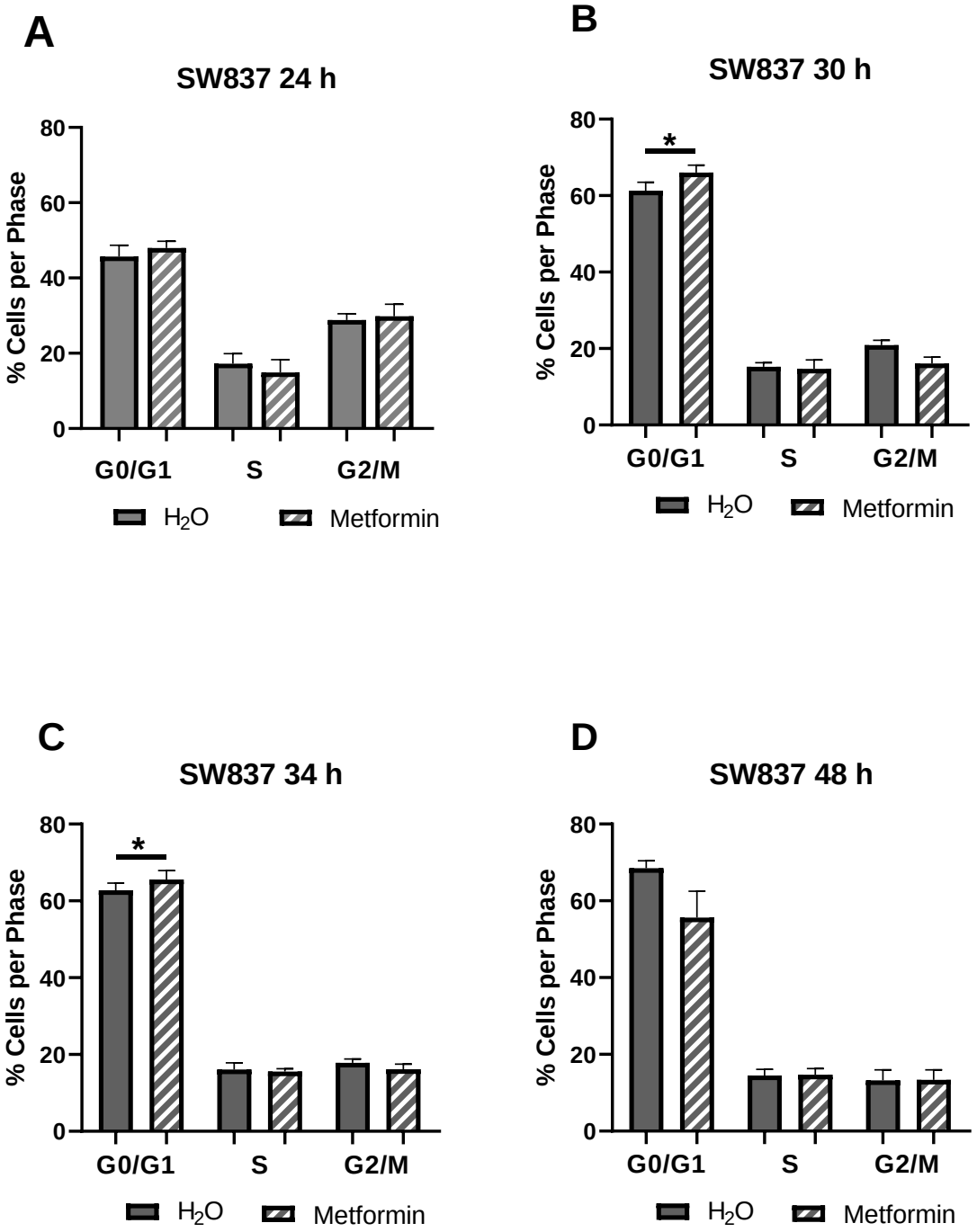

Fig. 5.2: **Metformin treatment significantly alters SW837 cell cycle distribution under normoxia.** SW837 cells were treated with metformin (10 mM) or H_2O vehicle control for 24, 30, 34 and 48 h, and cell cycle distribution assessed by PI staining and flow cytometry. **A)** Effect of 24 h metformin treatment on cell cycle distribution. **B)** Effect of 30 h metformin treatment on cell cycle distribution. **C)** Effect of 34 h Metformin treatment on cell cycle distribution. **D)** Effect of 48 h metformin on cell cycle distribution. Data is presented as mean ± SEM for 3 (24 h) or 5 independent experiments. Statistical analysis was performed using paired *t*-testing. **p* < 0.05.

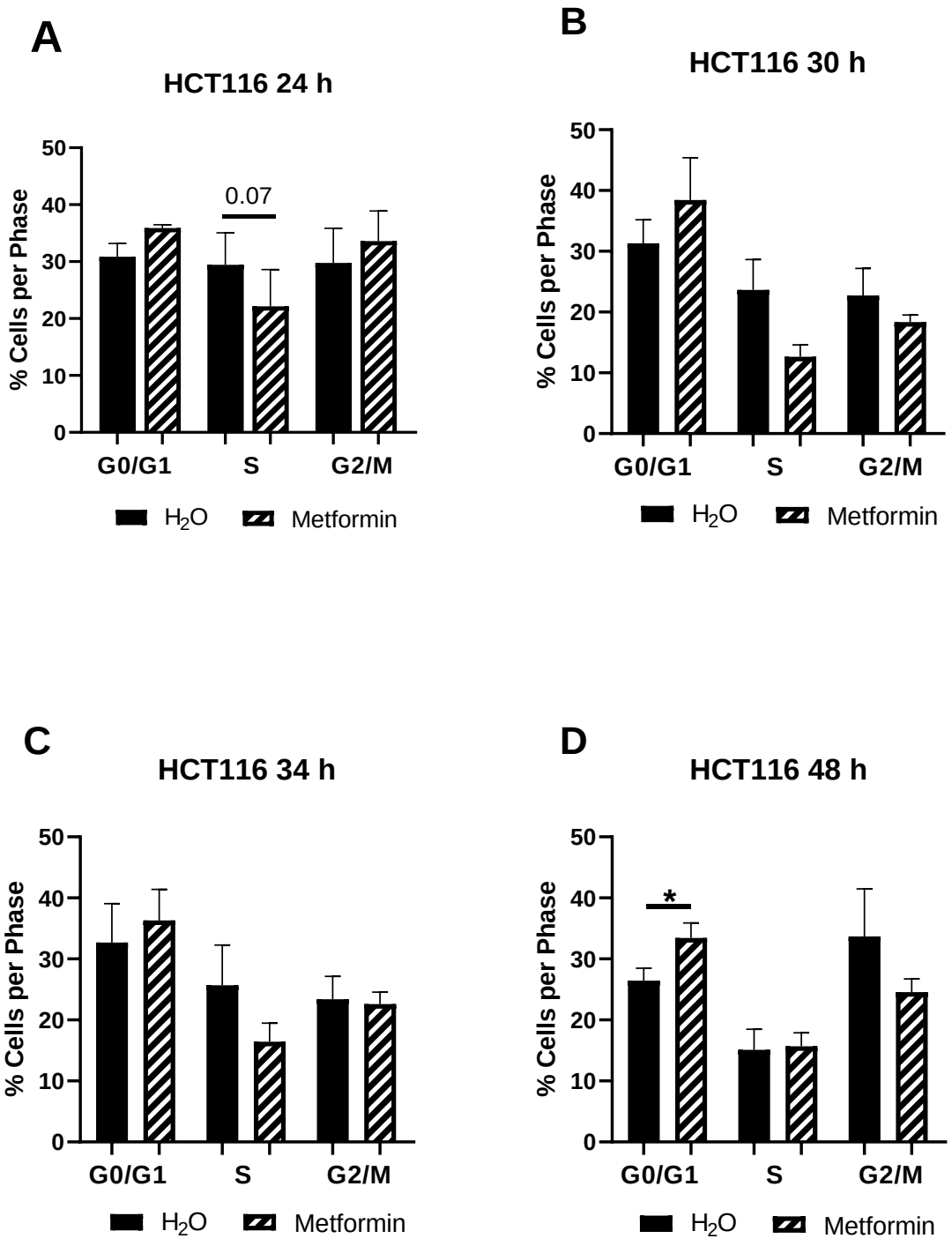

Fig. 5.3: **Metformin treatment significantly alters HCT116 cell cycle distribution under hypoxia.** HCT116 cells were treated with metformin (10 mM) or H_2O vehicle control for 24, 30, 34 and 48 h under hypoxia (0.5% O_2), and cell cycle distribution assessed by PI staining and flow cytometry. **A)** Effect of 24 h metformin treatment on cell cycle distribution. **B)** Effect of 30 h metformin treatment on cell cycle distribution. **C)** Effect of 34 h metformin treatment on cell cycle distribution. **D)** Effect of 48 h metformin treatment on cell cycle distribution. Data is presented as mean ± SEM for 3 (24 h) or 5 independent experiments. Statistical analysis was performed using paired *t*-testing. *$p < 0.05$.

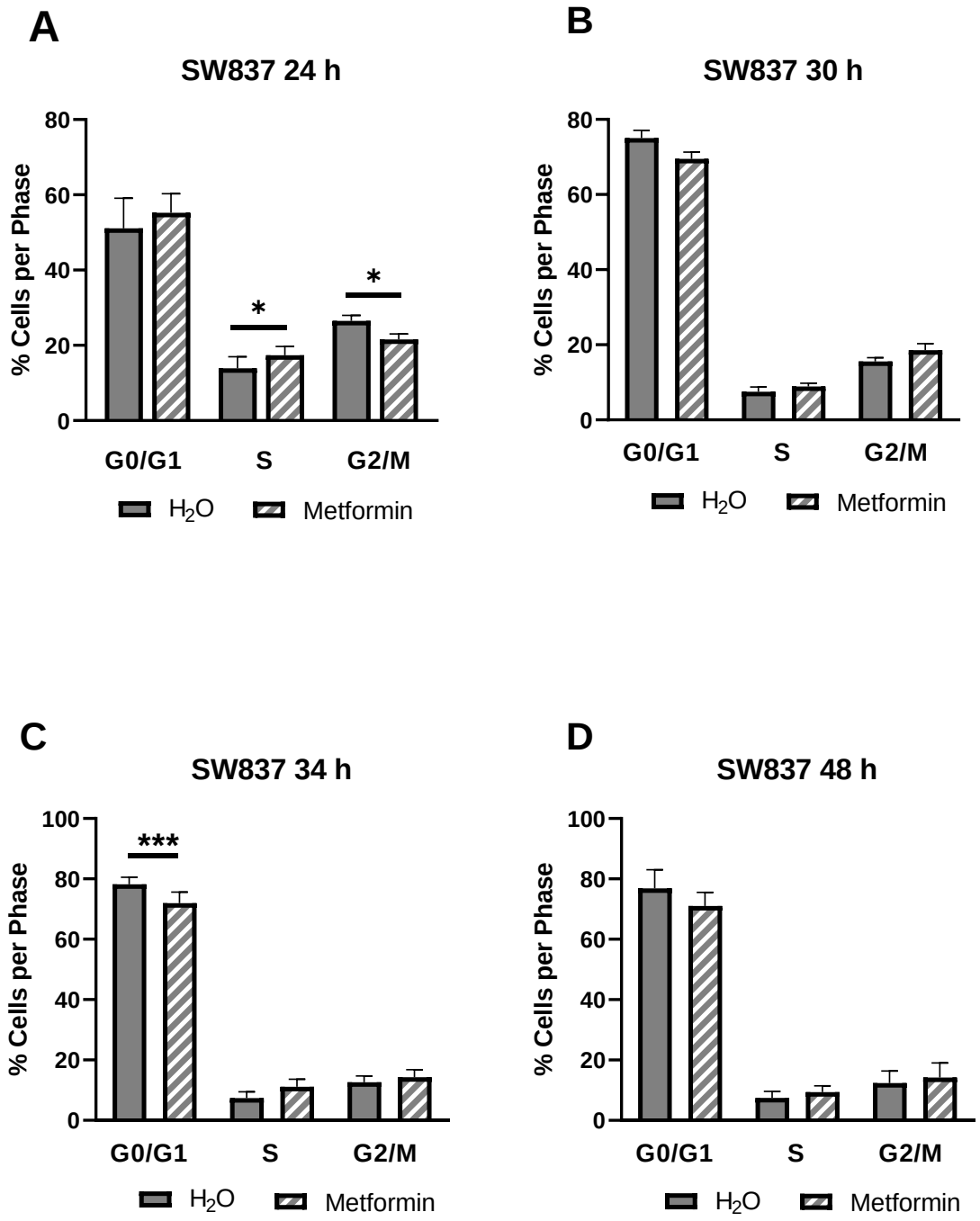

Fig. 5.4: **Metformin treatment significantly alters SW837 cell cycle distribution under hypoxia.** SW837 cells were treated with metformin (10 mM) or H_2O vehicle control for 24, 30, 34 and 48 h under hypoxia (0.5% O_2), and cell cycle distribution assessed by propidium iodide staining and flow cytometry. **A)** Effect of 24 h metformin treatment on cell cycle distribution. **B)** Effect of 30 h metformin treatment on cell cycle distribution. **C)** Effect of 34 h Metformin treatment on cell cycle distribution. **D)** Effect of 48 h metformin treatment on cell cycle distribution. Data is presented as mean ± SEM for 3 (24 h) or 5 independent experiments. Statistical analysis was performed using paired *t*-testing. **p* < 0.05, *p**** < 0.001.

5.4.3. *Combined metformin and X-ray radiation treatment alters cell cycle distribution in HCT116 and SW837 cells under normoxic conditions*

Having demonstrated that metformin affects basal cell cycle distribution in HCT116 and SW837 cells, the effect of combined X-ray radiation and metformin treatment on cell cycle distribution was investigated. HCT116 and SW837 cells were pre-treated with metformin (10 mM) or H_2O vehicle control for 24 h, mock-irradiated or exposed to 1.8 Gy radiation, and the cell cycle distribution assessed at 20 min, 6 h, 10 h and 24 h post irradiation.

In HCT116 cells, by 6 h post radiation, while radiation alone significantly reduced the proportion of G0/G1 phase cells (p = 0.0012), the combination of metformin and 1.8 Gy radiation significantly increased the proportion of G0/G1 cells, when compared to irradiated vehicle control (p = 0.022) (Mean % G0/G1 ± SEM; HCT116 1.8 Gy H_2O 41.34 ± 2.81 vs HCT116 1.8 Gy metformin 48.08 ± 3.36) (**Fig. 5.5A**). However, by 24 h post radiation, combination treatment of metformin and 1.8 Gy radiation was demonstrated to significantly further reduce the proportion of G0/G1 phase cells, when compared to vehicle control (p = 0.037 respectively) (Mean % G0/G1 ± SEM; HCT116 1.8 Gy H_2O 49.82 ± 2.79 vs HCT116 1.8 Gy metformin 43.58 ± 2.75) (**Fig. 5.5A**).

At 20 min post radiation, the addition of 1.8 Gy radiation to metformin treatment significantly reduced the proportion of S phase HCT116 cells, when compared to unirradiated metformin treated cells (p = 014) (Mean % S phase ± SEM; HCT116 0 Gy metformin 22.76 ± 1.9 vs HCT116 1.8 Gy metformin 18.14 ± 1.08) (**Fig. 5.5B**). At 10 h post radiation, the combination of metformin and 1.8 Gy treatment significantly increased the proportion of S phase cells, when compared to irradiated vehicle control (p=0.0022) (Mean % S phase ± SEM; HCT116 1.8 Gy H_2O 6.9 ± 1.13 vs. HCT116 1.8 Gy metformin 19.43 ± 1.48) (**Fig. 5.5B**)**.** At 24 h post radiation, while radiation exposure alone reduced the proportion of S phase cells (p = 0.047), combination metformin and radiation treatment significantly increased the proportion of S phase cells, when compared to irradiated vehicle controls (p= 0.0064) (Mean % S phase cells ± SEM; HCT116 1.8 Gy H_2O 6,36 ± 1.88 vs HCT116 1.8 Gy metformin 16.58 ± 1.7) (**Fig. 5.5B**).

At 20 min post radiation, combination metformin and 1.8 Gy radiation treatment resulted in a trend towards reduced G2/M cells, when compared to irradiated vehicle controls (p = 0.07) (**Fig. 5.5C**). At 6 h post irradiation, metformin treatment significantly reduced the proportion of G2/M phase cells in irradiated HCT116 cells, when compared to irradiated

vehicle control (p = 0.0232) (Mean % G2/M ± SEM; HCT116 1.8 Gy H_2O 35.38 ± 4.75 vs. HCT116 1.8 Gy metformin 25.06 ± 2.16) (**Fig. 5.5C**). Similarly, while exposure to 1.8 Gy radiation induced G2/M accumulation at 10 h and 24 h post irradiation (p = 0.0066 and p = 0.0018, respectively) (Mean % G2/M ± SEM; HCT116 0 Gy H_2O 10 h 20.84 ± 2.88 vs HCT116 1.8 Gy H_2O 10 h 39.22 ± 5.48; HCT116 1.8 Gy H_2O 24 h 39.22 ± 5.48 vs HCT116 1.8 Gy H_2O 24 h 21.9 ± 4.91)**,** combination metformin and 1.8 Gy radiation treatment significantly reduced the proportion of G2/M phase cells at 10 h and 24 h post radiation, when compared to irradiated vehicle controls (p = 0.0018 and p = 0.0126 respectively) (Mean % G2/M ± SEM; HCT116 1.8 Gy H_2O 10 h 39.22 ± 5.48 vs HCT116 1.8 Gy metformin 10 h 21.9 ± 4.91; HCT116 1.8 Gy H_2O 24 h 32.88 ± 1.9 vs. HCT116 1.8 Gy metformin 24 h 24.94 ± 3.24) (**Fig. 5.5C**)**.**

In SW837 rectal cancer cells, at 20 min following radiation, combination metformin and 1.8 Gy radiation treatment significantly increased the proportion of SW837 cells in the G0/G1 phase, when compared to irradiated vehicle control (p = 0.017) (Mean % G0/G1 cells ± SEM; SW837 1.8 Gy H_2O 61.98 ± 2.55 vs. SW837 1.8 Gy metformin 66.78 ± 3.39) (**Fig. 5.6A**).

At 6 h post radiation exposure (30 h post metformin treatment), G0/G1 arrest was demonstrated in metformin treated SW837 cells at in both unirradiated and irradiated cells, when compared to vehicle controls (p = 0.01, p = 0.0097 respectively) (Mean % G0/G1 cells ± SEM; SW837 0 Gy H_2O 61.32 ± 2.18 vs SW837 0 Gy metformin 66 ± 1.96, SW837 1.8 Gy H_2O 53.92 ± 2.64 vs SW837 1.8 Gy metformin 63.14 ± 2.47) (**Fig. 5.6A**). Exposure to radiation induced a slight but significant reduction of SW837 cells in G0/G1 phase in both vehicle and metformin treated cells, when compared to unirradiated cells (p = 0.0097, p = 0.036). At 10 h post radiation, metformin treatment increased the proportion of SW837 cells in the G0/G1 phase, when compared to vehicle controls at both 0 Gy and 1.8 Gy radiation (p = 0.035, p= 0.005 respectively) (Mean % G0/G1 phase ± SEM; SW837 0 Gy H_2O 62.74 ± 1.89 vs. SW837 0 Gy metformin 65.6 ± 2.29, SW837 1.8 Gy H_2O 51.04 ± 2.6 vs. SW837 1.8 Gy metformin 59.68 ± 1.98) (**Fig. 5.6A**). In addition, exposure to 1.8 Gy radiation significantly reduced the proportion of G0/G1 phase cells in both vehicle and metformin treated cells, although to a lesser extent in metformin treated cells (p = 0.0022, p = 0.0052). By 24 h post radiation (total 48 h metformin treatment), while a clear trend towards reduced proportion of G0/G1 cells was demonstrated in metformin treated cells at both 0 Gy and 1.8 Gy, when compared to vehicle controls, this did not reach statistical significance (p = 0.1, p = 0.08 respectively) (Mean

% G0/G1 ± SEM; SW837 0 Gy H_2O 68.48 ± 1.95 vs. SW837 0 Gy metformin 55.64 ± 6.85, SW837 1.8 Gy H_2O 66.18 ± 2.33 vs SW837 1.8 Gy Metformin 51.22 ± 8.65) (**Fig. 5.6A**).

At all timepoints post radiation, no significant differences were demonstrated in the proportion of S phase SW837 cells treated with either metformin or radiation (**Fig. 5.6B**).

At 6 h post radiation exposure (total 30 h post metformin treatment), while metformin treatment in unirradiated cells did not significantly decrease the proportion of G2/M phase cells, when compared to vehicle control (p = 0.075), combination metformin and 1.8 Gy radiation significantly reduced the proportion of G2/M phase cells, when compared to irradiated vehicle control (p = 0.009) (Mean % G2/M cells ± SEM; SW837 1.8 Gy H_2O 24.82 ± 0.8 vs. SW837 1.8 Gy metformin 18.13 ± 1.56) (**Fig. 5.6C**). At 10 h post radiation, while radiation alone induced significant G2/M arrest, when compared to unirradiated cells (p = 0.002), combination metformin and 1.8 Gy radiation exposure significantly reduced the proportion of G2/M phase SW837 cells, when compared to irradiated vehicle control (p = 0.024) (Mean % G2/M cells ± SEM; SW837 1.8 Gy H_2O 28.6 ± 1.89 vs SW837 1.8 Gy metformin 19.1 ± 1.71) (**Fig. 5.6C**).

In summary, these data demonstrate that metformin treatment in combination with radiation induces significant alterations to cell cycle progression, with differing effects on the HCT116 and SW837 cell lines.

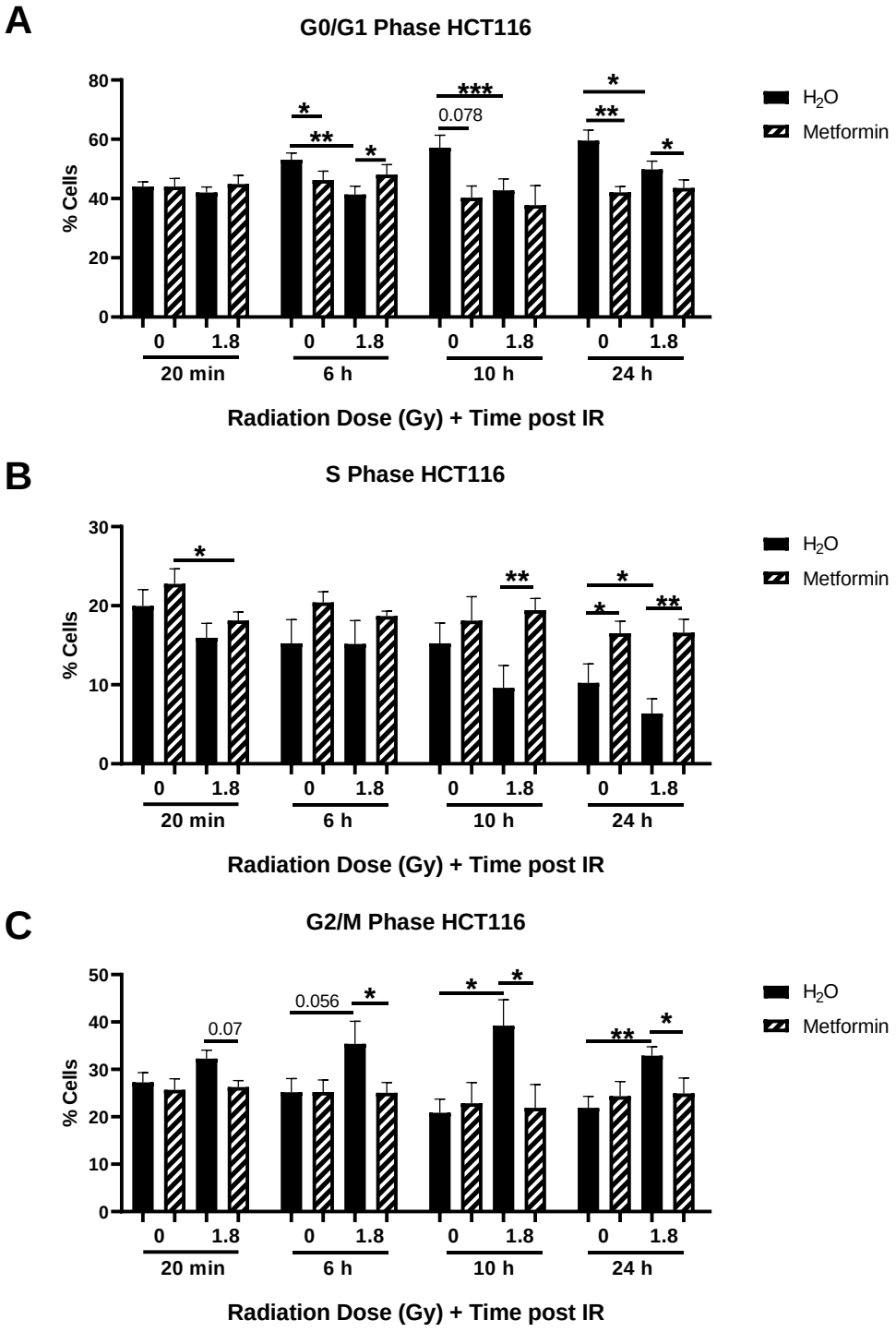

Fig. 5.5: **Combined metformin and X-ray radiation treatment alters cell cycle progression in HCT116 cells under normoxia.** HCT116 cells were treated with 10 mM metformin or H_2O control for 24 h before exposure to 1.8 Gy radiation Controls (0 Gy) were mock irradiated. Cell cycle distribution was assessed at 20 min, 6 h, 10 h and 24 h post irradiation by PI staining and flow cytometry. **A)** Proportion of HCT116 cells in G0/G1 phase following metformin and radiation treatment. **B)** Proportion of HCT116 cells in S phase following metformin and radiation treatment. **C)** Proportion of HCT116 cells in G2/M phase following metformin and radiation treatment. Data is presented as mean ± SEM for 5 independent experiments. Statistical analysis was performed by paired *t*-testing. **p* < 0.05, ***p* < 0.01, ****p* < 0.001.

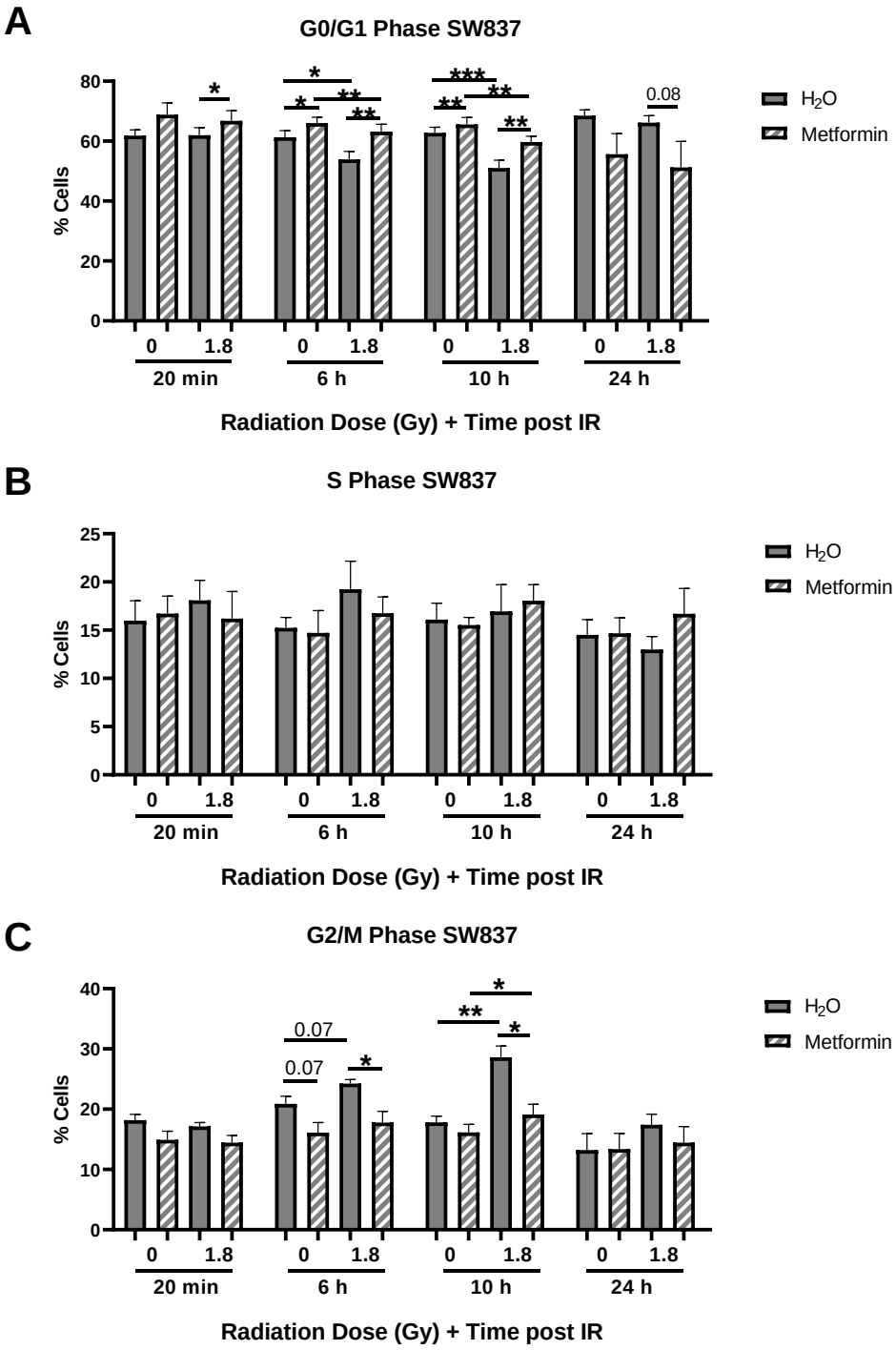

Fig. 5.6: **Combined metformin and X-ray radiation treatment alters cell cycle progression in SW837 under normoxia.** SW837 cells were treated with 10 mM metformin or H_2O control for 24 h before exposure to 1.8 Gy radiation. Controls were mock irradiated. Cell cycle distribution was assessed at 20 min, 6 h, 10 h and 24 h post radiation by propidium iodide staining and flow cytometry. **A)** Proportion of G0/G1 phase in SW837 cells following metformin and radiation treatment. **B)** Proportion of S phase in SW837 cells following metformin and radiation treatment. **C)** Proportion of G2/M phase in SW837 cells following metformin and radiation treatment. Data is presented as mean ± SEM for 5 independent experiments. Statistical analysis was performed by paired *t*-testing. **p* < 0.05, ***p* < 0.01, ****p* < 0.001.

5.4.4. *Combined metformin and X-ray radiation treatment alters cell cycle distribution in HCT116 and SW837 cells under hypoxic conditions*

To further investigate whether the radiosensitising effects of metformin are mediated in part by altered cell cycle following radiation, cell cycle distribution following pre-treatment with metformin or H_2O vehicle control and 1.8 Gy radiation was assessed in hypoxic (0.5% O_2) conditions in SW837 and HCT116 cells at 20 min, 6 h, 10 h and 24 h post radiation exposure.

In HCT116 cells under hypoxia, a trend towards increased G0/G1 cells was demonstrated in irradiated cells in combination with metformin, when compared to irradiated vehicle control, although this did not reach statistical significance (p = 0.07) (**Fig. 5.7A).** By 24 h post radiation, the proportion of G0/G1 phase cells was significantly increased in HCT116 cells following combination metformin and 1.8 Gy radiation treatment, when compared to irradiated vehicle control (p = 0.038) (Mean % G0/G1 ± SEM; HCT116 1.8 Gy H_2O 24.9 ± 3.12 vs. HCT116 1.8 Gy Metformin 35.75 ± 3.1) (**Fig. 5.7A**).

In hypoxic HCT116 cells, no significant differences in the proportion of S phase cells were observed at 20 min, 6 h or 10 h post irradiation (**Fig. 5.7B**). At 24 h post radiation exposure, metformin in combination with 1.8 Gy radiation significantly reduced the proportion of S phase cells, when compared to irradiated vehicle control (p = 0.0324) (Mean % S Phase ± SEM; HCT116 1.8 Gy H_2O 22.55 ± 2.6 vs. HCT116 1.8 Gy metformin 13.54 ± 1.89) (**Fig. 5.7B**).

At 6 h post radiation, combination metformin and 1.8 Gy radiation treatment significantly decreased the proportion of hypoxic HCT116 cells in the G2/M phase, when compared to irradiated vehicle control cells (p = 0.048) (Mean % G2/M ± SEM; HCT116 1.8 Gy H_2O 40.5 ± 3.65 vs. HCT116 1.8 Gy metformin 21.33 ± 5.21) (**Fig. 5.7C**).

In hypoxic SW837 cells, combined metformin and radiation treatment significantly reduced the proportion of cells in the G0/G1 phase by 20 min post radiation (p = 0.02), when compared to irradiated vehicle control (Mean % G0/G1 cells ± SEM; SW837 1.8 Gy H_2O 69.46 ± 2.48 vs SW837 1.8 Gy metformin 64.64 ± 2.12) (**Fig. 5.8A**). Combination metformin and 1.8 Gy radiation treatment significantly decreased the proportion of SW837 cells in the G0/G1 phase, when compared to unirradiated metformin treated cells (p = 0.024) (**Fig. 5.8A**). At 6 h post radiation, the proportion of G0/G1 SW837 cells was significantly reduced in SW837 cells treated with a combination of metformin and 1.8 Gy, when compared to irradiated vehicle control (p = 0.06) (Mean % G0/G1 cells ± SEM; SW837 1.8 Gy H_2O 71.2 ± 2.49 vs SW837 1.8 Gy

metformin 65.98 ± 3.55) (**Fig. 5.8A**). Furthermore, at 10 h post radiation, combination metformin and 1.8 Gy radiation treatment significantly reduced the proportion of G0/G1 phase cells, when compared to irradiated vehicle control (p = 0.037) (Mean G0/G1 cells ± SEM; SW837 1.8 Gy H_2O 74.26 ± 1.5 vs SW837 1.8 Gy metformin 69.02 ± 2.38) (**Fig. 5.8A**).

At 24 h post radiation, a trend towards reduced proportion of G0/G1 phase cells in SW837 cells treated with combination metformin and 1.8 Gy radiation was demonstrated, when compared to irradiated vehicle control, but did not reach statistical significance (p = 0.061) (Mean % G0/G1 ± SEM; SW839 1.8 Gy H_2O 73.32 ± 1.86 vs SW837 1.8 Gy metformin 65.88 ± 2.05) (**Fig. 5.8A**). Combination treatment of metformin and 1.8 Gy radiation further reduced the proportion of G0/G1 SW837 cells under hypoxia, when compared to unirradiated metformin treated cells (p = 0.022) (**Fig. 5.8A**).

Under hypoxia, no differences in the proportion of S phase cells following treatment with metformin or radiation was demonstrated in SW837 cells at 20 min (**Fig. 5.8B**)**.** At 6 h following radiation, a trend towards increased proportion of S phase cells was demonstrated in cells treated with combination metformin and 1.8 Gy radiation, when compared to irradiated vehicle control, although this did not reach statistical significance (p = 0.057) (**Fig. 5.8B**). In addition, a trend towards increased S phase SW837 cells was demonstrated in combined metformin and 1.8 Gy treated cells at 6 h, when compared to unirradiated cells, but this did not reach statistical significance (p = 0.065). At 10 h post radiation, the addition of metformin significantly increased the proportion of S phase SW837 cells following irradiation, when compared to irradiated vehicle control (p= 0.02) (Mean % S phase cells ± SEM; SW837 1.8 Gy H_2O 8.43 ± 0.9 vs SW837 1.8 Gy metformin 12.44 ± 1.26) (**Fig. 5.8B**).

At 24 h post radiation, a significant increase in the proportion of G2/M phase cells was demonstrated in irradiated cells treated in combination with metformin, when compared to irradiated vehicle control (p = 0.047) (Mean % G2/M ± SEM; SW837 1.8 Gy H_2O 15.06 ± 1.61 vs SW837 1.8 Gy metformin 18.2 ± 1.61) (**Fig. 5.8C**). Furthermore, at 24 h post radiation, combination metformin and 1.8 Gy radiation treatment significantly increased the proportion of G2/M phase cells, when compared to unirradiated controls (p = 0.013 respectively) (Mean % G2/M cells ± SEM; SW837 0 Gy metformin 14.23 ± 2.17 vs SW837 1.8 Gy metformin 18.2 ± 1.61) (**Fig. 5.8C**).

In summary, these data demonstrate that combination metformin and radiation treatment affect cell cycle progression following radiation exposure under hypoxic conditions in HCT116 and SW837 cells.

5.4.5. *Metformin induces DNA damage in HCT116 cells under normoxia*

Having demonstrated that metformin affects cell cycle progression, and induces radiosensitisation in HCT116 and SW837 cells, the impact of metformin treatment on DNA damage was assessed. HCT116 and SW837 cells were treated with metformin (10 mM) or H_2O vehicle control for 24/30/34/48 h under normoxic (21% O_2) and hypoxic (0.5% O_2) conditions and DNA damage was assessed by γH2AX-Alexa 488 fluorescence and flow cytometry.

In normoxic HCT116 cells, a trend towards increased DNA damage was observed at 24 h and 30 h post metformin treatment, when compared to vehicle control, however, this did not reach statistical significance (p = 0.08, p = 0.089 respectively) (**Fig. 5.9A**). By 34 h following metformin exposure, there was a significant increase in DNA damage in metformin treated HCT116 cells, when compared to vehicle control (p = 0.046) (Mean relative γH2AX fluorescence ± SEM; HCT116 0 Gy H_2O 1.46 ± 0.72 vs HCT116 0 Gy metformin 2.67 ± 1.14) (**Fig. 5.9A**).

In normoxic SW837 cells, treatment with metformin did not induce DNA damage at 24, 30, 34 or 48 h post treatment (**Fig. 5.9B**). However, a trend towards enhanced DNA damage levels in metformin treated SW837 cells was observed at 48 h post treatment, although this did not reach statistical significance (p = 0.069) (**Fig. 5.9B**).

Under hypoxic conditions, metformin treatment did not induce DNA damage in either HCT116 (**Fig. 5.10A**) or SW837 (**Fig. 5.10B**) cells at any timepoint examined.

These data indicate that metformin treatment significantly induces DNA damage in HCT116 cells under normoxia but does not induce DNA damage under hypoxic conditions in HCT116 or SW837 cells.

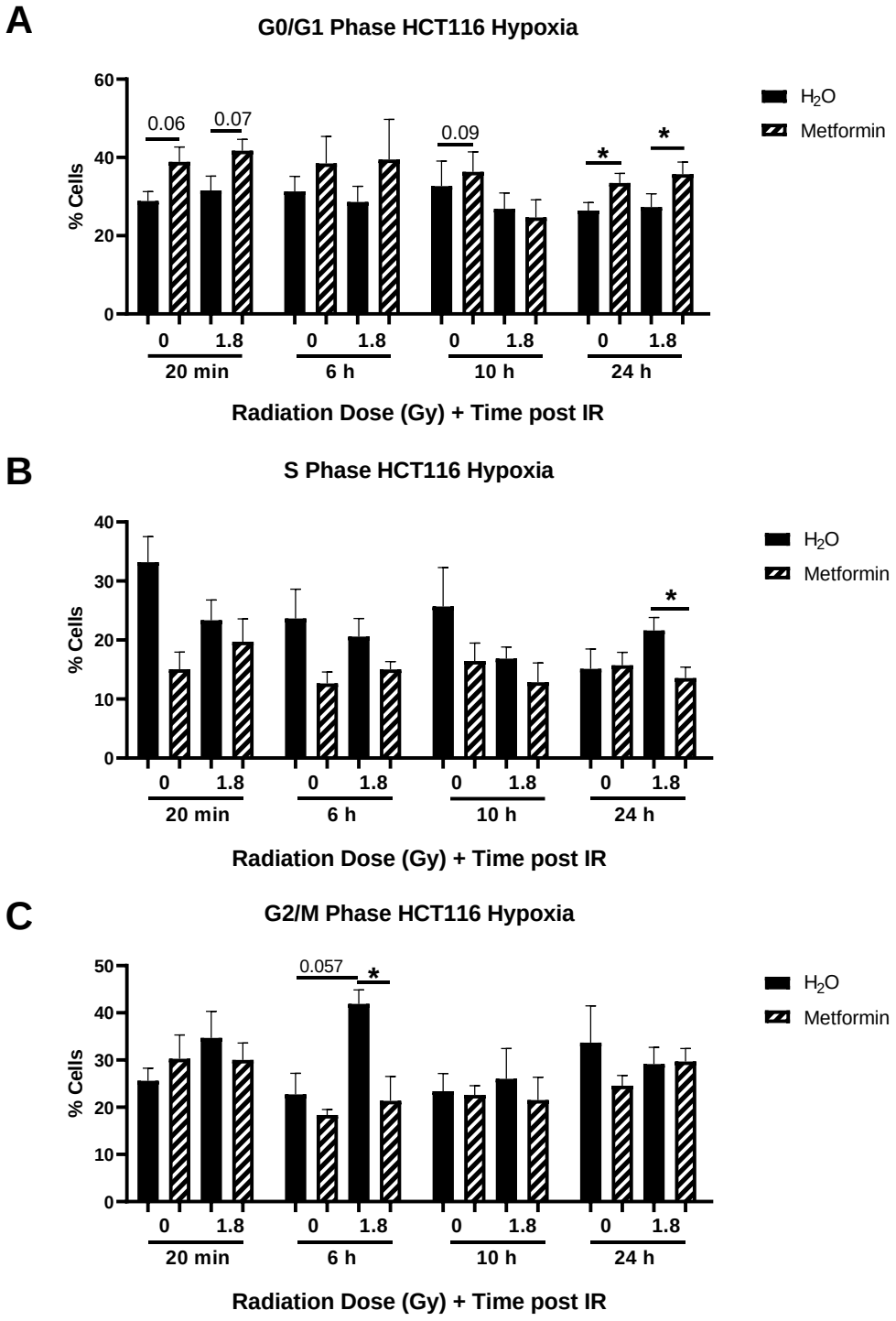

Fig. 5.7: **Combined metformin and X-ray radiation treatment alters cell cycle progression in HCT116 cells under hypoxia.** HCT116 cells were treated with 10 mM metformin or H_2O control for 24 h before exposure to 1.8 Gy radiation, under hypoxia. Controls were mock-irradiated. Cell cycle distribution was assessed at 20 min, 6 h, 10 h and 24 h post radiation by PI staining and flow cytometry. **A)** Proportion of G0/G1 phase in HCT116 cells following metformin and radiation treatment. **B)** Proportion of S phase in HCT116 cells following metformin and radiation treatment. **C)** Proportion of G2/M phase in HCT116 cells following metformin and radiation treatment. Data is presented as mean ± SEM for 4 independent experiments. Statistical analysis was performed by paired *t*-testing. **p*<0.05.

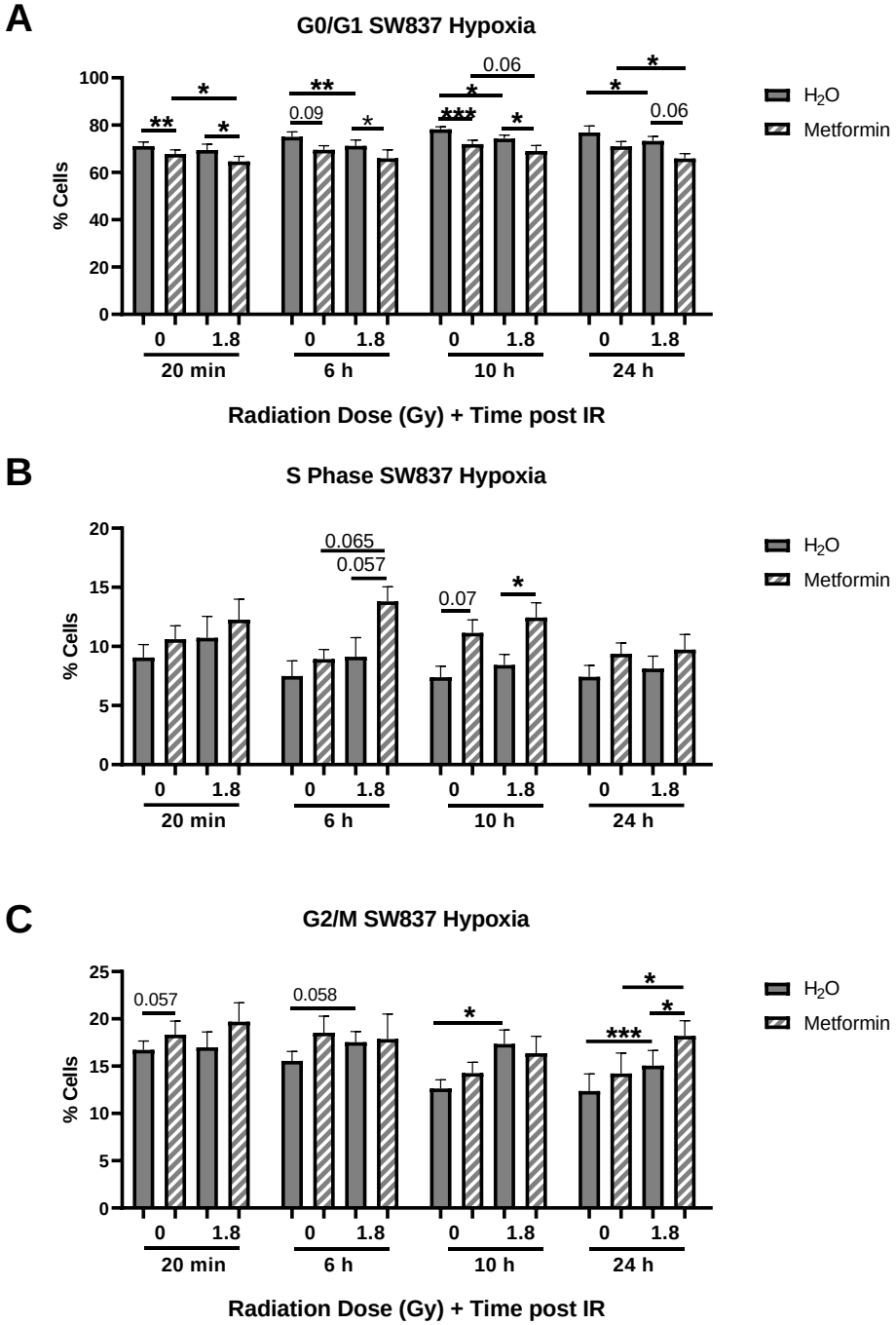

Fig. 5.8: **Combined metformin and X-ray radiation treatment alters cell cycle in SW837 cells under hypoxia.** SW837 cells were treated with 10 mM metformin or H_2O control for 24 h before exposure to 1.8 Gy radiation, under hypoxia. Controls were mock-irradiated. Cell cycle distribution was assessed at 20 min, 6 h, 10 h and 24 h post radiation by propidium iodide staining and flow cytometry. **A)** Proportion of G0/G1 phase in SW837 cells following metformin and radiation treatment. **B)** Proportion of S phase in SW837 cells following metformin and radiation treatment. **C)** Proportion of G2/M phase in SW837 cells following metformin and radiation treatment. Data is presented as mean ± SEM for 4 independent experiments. Statistical analysis was performed by paired *t*-testing. **p*<0.05, ***p*<0.01, ****p*<0.001.

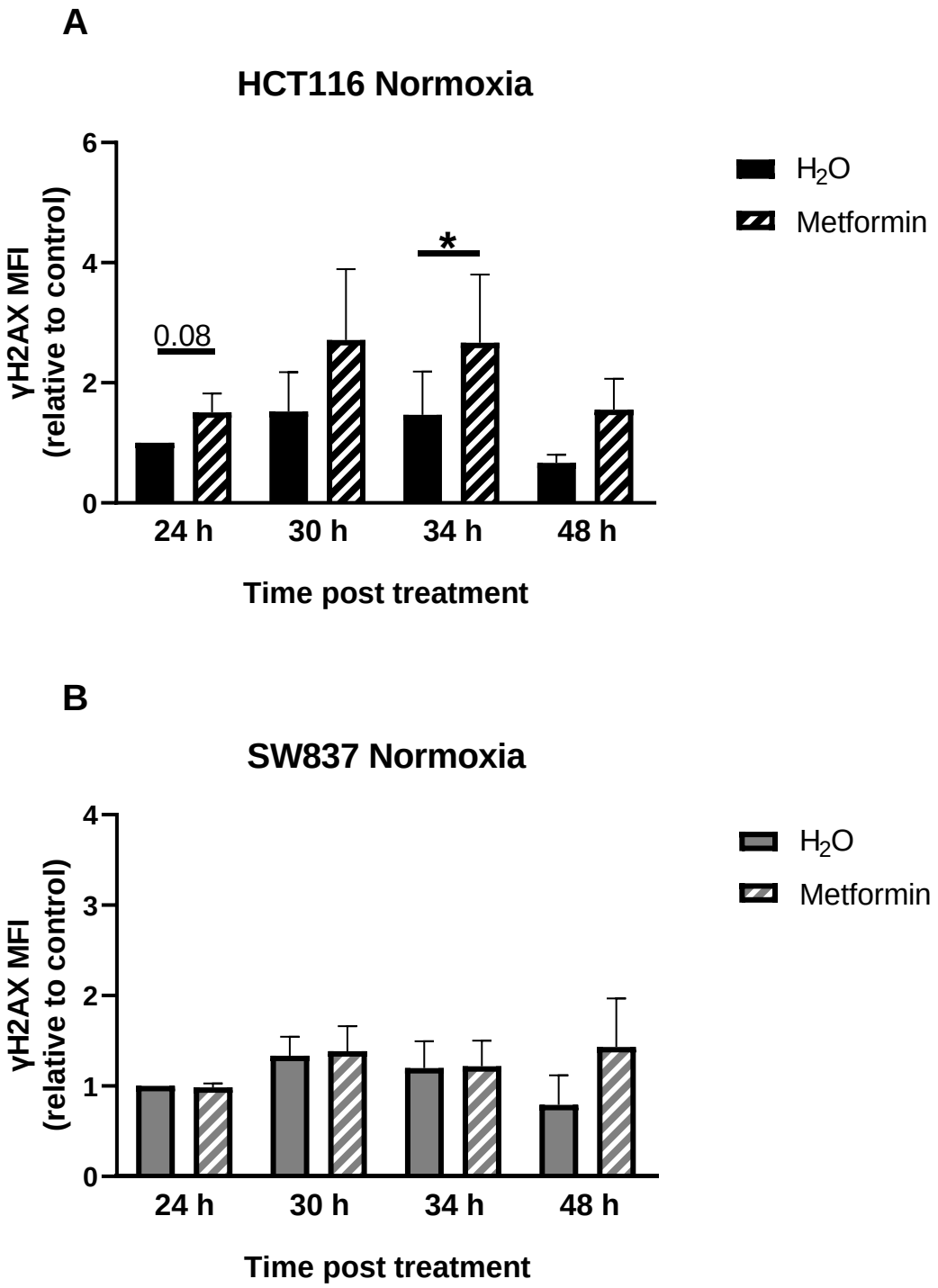

Fig. 5.9: **Metformin treatment induces DNA damage in HCT116 cells under normoxia.** HCT116 and SW837 cells were treated with metformin (10 mM) or H_2O vehicle control for 24/30/34/38 h, and DNA damage assessed by γH2AX fluorescence and flow cytometry. **A)** DNA damage in HCT116 cells following metformin treatment. **B)** DNA damage in SW837 cells following metformin treatment. Data is presented as mean ± SEM from 4 independent experiments. Statistical analysis was performed by paired *t*-testing. **p*<0.05.

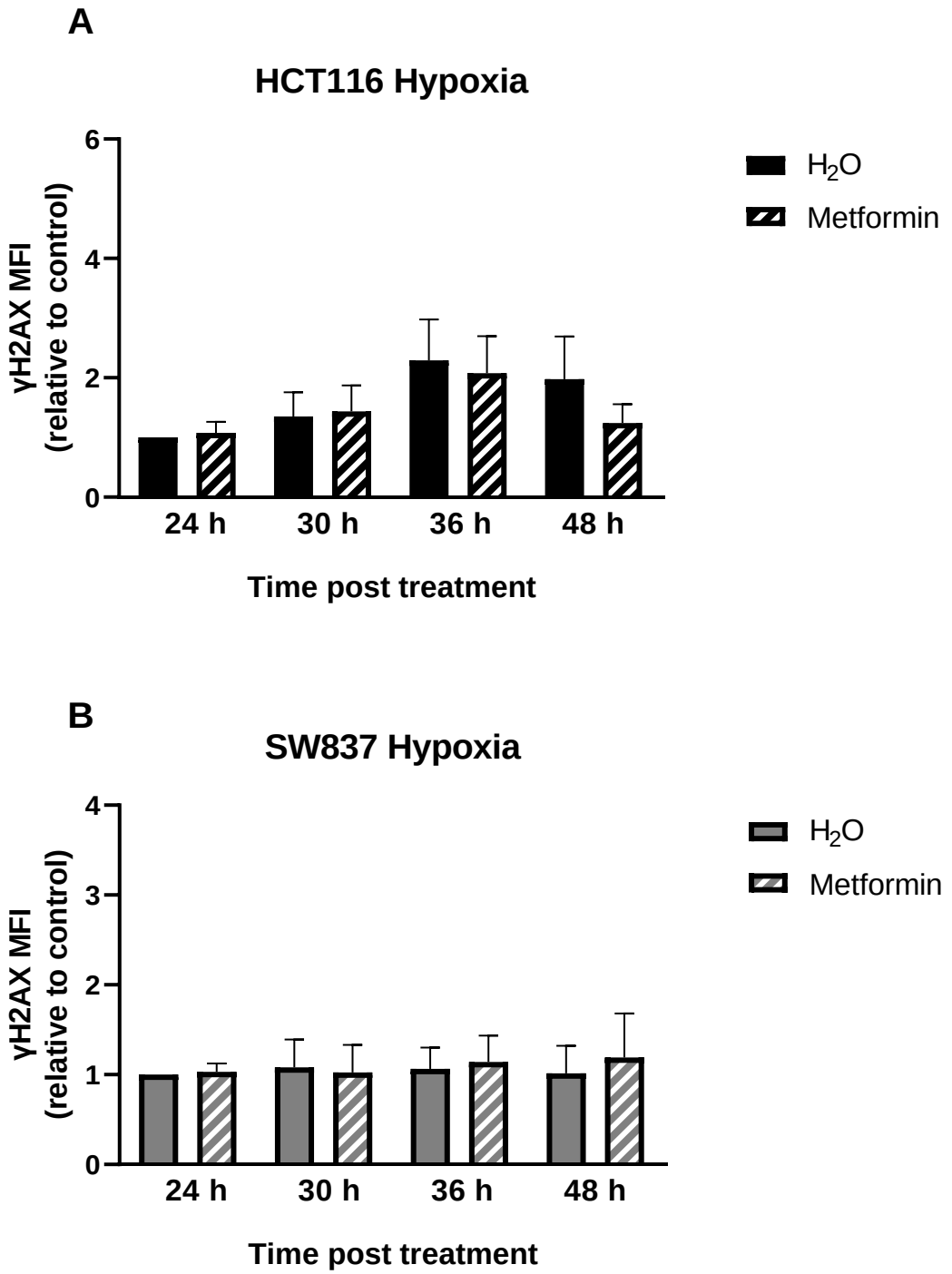

Fig. 5.10: **Metformin treatment does not induce basal DNA damage in HCT116 or SW837 cells under hypoxia.** HCT116 and SW837 cells were treated with metformin (10 mM) or H_2O vehicle control for 24/30/34/38 h under hypoxic (0.5% O_2) conditions, and DNA damage assessed by γH2AX fluorescence on flow cytometry. **A)** DNA damage in HCT116 cells following metformin treatment. **B)** DNA damage in SW837 cells following metformin treatment. Data is presented as mean ± SEM from 4 independent experiments. Statistical analysis was performed by paired *t*-testing. **p*<0.05.

5.4.6. *Metformin treatment inhibits radiation-induced DNA damage repair in HCT116 cells under normoxia*

Having demonstrated that metformin treatment induces DNA damage in HCT116 cells under normoxia, the effect of combined Metformin and X-ray radiation treatment on DNA damage induction and repair was assessed in HCT116 and SW837 cell lines. HCT116 and SW837 cells were treated with metformin (10 mM) or H_2O vehicle control for 24 h under normoxic conditions, exposed to 1.8 Gy radiation or mock irradiated (0 Gy), and γH2AX fluorescence assessed by flow cytometry.

To assess the impact of metformin treatment on radiation-induced DNA damage, γH2AX levels were assessed at 20 min following radiation exposure. In HCT116 cells, at 20 min post radiation, a trend towards enhanced DNA damage induction in cells treated with combination metformin and 1.8 Gy radiation was demonstrated, when compared to irradiated vehicle control, however this did not reach statistical significance (p = 0.075) (**Fig. 5.11A**). In SW837 cells, no significant alteration in DNA damage levels were demonstrated in cells treated with metformin and 1.8 Gy at 20 min post radiation exposure (**Fig. 5.11B**), when compared to irradiated vehicle control**.** The addition of radiation treatment (1.8 Gy) to metformin treated cells resulted in a trend towards enhanced DNA damage, when compared to unirradiated metformin treated cells, however this did not reach statistical significance (p = 0.0501) (Mean relative γH2AX fluorescence ± SEM; SW837 0 Gy metformin 0.98 vs SW837 1.8 Gy Metformin 1.42 ± 0.15) (**Fig. 5.11B**).

To investigate the potential impact of metformin treatment on the repair of radiation-induced DNA damage, γH2AX levels were assessed at 6 h, 10 h and 24 h post irradiation, in both HCT116 and SW837 cells. In HCT116 cells, at 6 h post radiation exposure, a trend towards increased DNA damage levels was demonstrated in HCT116 cells treated with metformin and 1.8 Gy, when compared to irradiated vehicle control, however, this did not reach statistical significance (p = 0.09) (**Fig. 5.11A**). At 10 h post radiation, HCT 116 cells treated with metformin and 1.8 Gy demonstrated significantly elevated γH2AX levels, when compared to irradiated vehicle control cells (p = 0.013) (Mean relative γH2AX fluorescence ± SEM; HCT116 1.8 Gy H_2O 1.78 ± 0.85 vs HCT116 1.8 Gy metformin 2.71 ± 1.05). While a trend towards increased DNA damage was demonstrated in HCT116 cells treated with metformin and 1.8 Gy at 24 h, this did not reach statistical significance.

In SW837 cells, at 10 h post radiation, in metformin treated cells, a significant increase in DNA damage levels was demonstrated following exposure to 1.8 Gy radiation (p = 0.005), when compared to unirradiated metformin treated cells (Mean relative γH2AX fluorescence ± SEM; SW837 0 Gy metformin 1.219 ± 0.28 vs SW837 1.8 Gy metformin 1.64 ± 0.29) (**Fig.5.11B**). However, while a trend towards increased DNA damage was demonstrated in cells treated with metformin and 1.8 Gy, when compared to irradiated vehicle control, this did not reach statistical significance (p = 0.13) (Mean relative γH2AX fluorescence ± SEM; SW837 1.8 Gy H_2O 1.4 ± 0.37 vs SW837 1.8 Gy metformin 1.64 ± 0.29) (**Fig. 5.11B**). By 24 h following radiation exposure, a trend towards increased DNA damage was demonstrated in SW837 cells treated with metformin and 1.8 Gy, when compared to irradiated vehicle control, however, this did not reach statistical significance (p = 0.069, p = 0.13).

These data indicate that in HCT116 cells, radiation-induced DNA damage persists in metformin treated cells, indicating a potential metformin-induced inhibition of DNA repair in these cells.

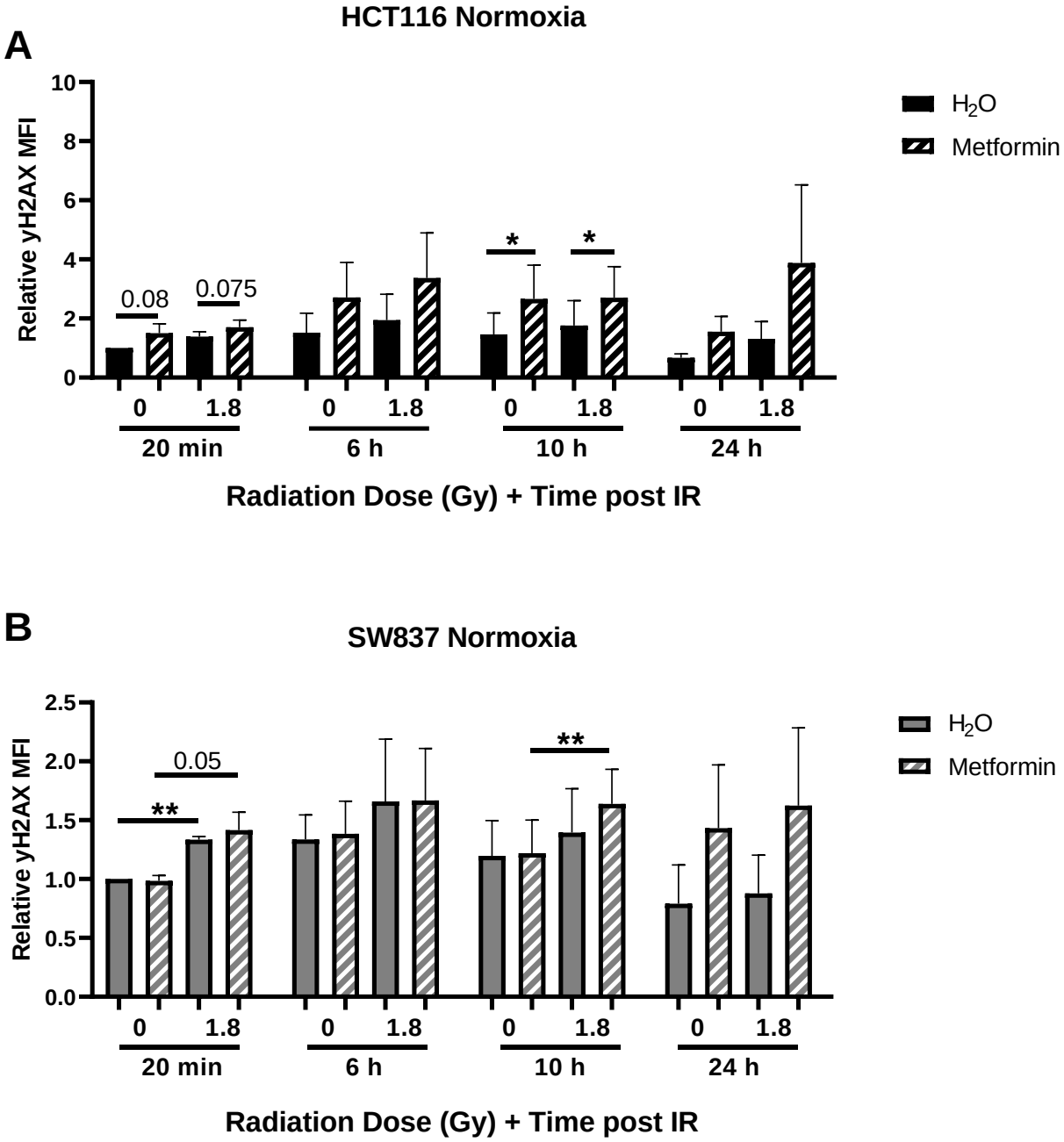

Fig. 5.11: **Metformin treatment inhibits repair of radiation-induced DNA damage in HCT116 cells under normoxia.** HCT116 and SW837 cells were treated with metformin (10 mM) or H_2O vehicle control for 24 h, exposed to 1.8 Gy radiation, and DNA damage assessed by γH2AX fluorescence and flow cytometry. Controls were mock-irradiated **A)** DNA damage in HCT116 cells following metformin and X-ray radiation. **B)** DNA damage in SW837 cells following metformin and X-ray radiation. Data is presented as mean ± SEM from 4 independent experiments. Statistical analysis was performed by paired *t*-testing. *$p < 0.05$, **$p < 0.01$.

5.4.7. *Metformin treatment does not affect induction or repair of radiation-induced DNA damage in HCT116 or SW837 cells under hypoxia (0.5% O_2)*

Given the demonstrated differential effects of metformin on radiosensitivity under hypoxia (**section 4.4.12**), the effect of metformin treatment on radiation-induced DNA damage and repair under hypoxia was assessed in HCT116 and SW837 cells. HCT116 and SW837 cells were treated with metformin (10 mM) or H_2O vehicle control for 24 h under hypoxic conditions and exposed to 1.8 Gy radiation, or mock-irradiated and γH2AX fluorescence assessed by flow cytometry.

To assess the effect of metformin treatment on radiation-induced DNA damage, γH2AX levels were measured at 20 min post radiation exposure. In hypoxic HCT116 cells, exposure to 1.8 Gy radiation induced significant DNA damage in vehicle control treated cells, when compared to unirradiated controls (p = 0.022) (Mean relative γH2AX fluorescence ± SEM; HCT116 0 Gy H_2O 1 vs. HCT116 1.8 Gy H_2O 1.1 ± 0.03) (**Fig. 5.12A**). In contrast, irradiation with 1.8 Gy did not induce DNA Damage in HCT116 metformin treated cells, when compared to unirradiated controls (**Fig. 5.12A)**

In hypoxic SW837 cells, DNA damage was significantly induced in vehicle control treated cells at 20 min post 1.8 Gy radiation, when compared to unirradiated control (p = 0.04) (Mean relative γH2AX fluorescence ± SEM SW837 H_2O 1: SW837 1.8 Gy H_2O 1.4 ± 0.11) (**Fig. 5.12B**). A trend towards increased DNA damage was demonstrated in metformin treated cells following 1.8 Gy radiation, when compared to unirradiated metformin treated cells, however, this did not reach statistical significance (p = 0.066) (**Fig. 5.12B**).

To investigate the impact of metformin treatment on radiation-induced DNA damage repair kinetics under hypoxia, γH2AX was assessed at 6 h, 10 h and 24 h post radiation exposure. No significant differences in DNA damage levels were demonstrated at 6 h, 10 h or 24 h post radiation in either HCT116 or SW837 cells under hypoxia, with all radiation-induced damage resolved by 6 h in both cell lines, regardless of metformin treatment (**Fig. 5.12A-B**).

These data suggest that metformin does not alter radiation-induced DNA damage induction or repair in HCT116 or SW837 cells under hypoxia.

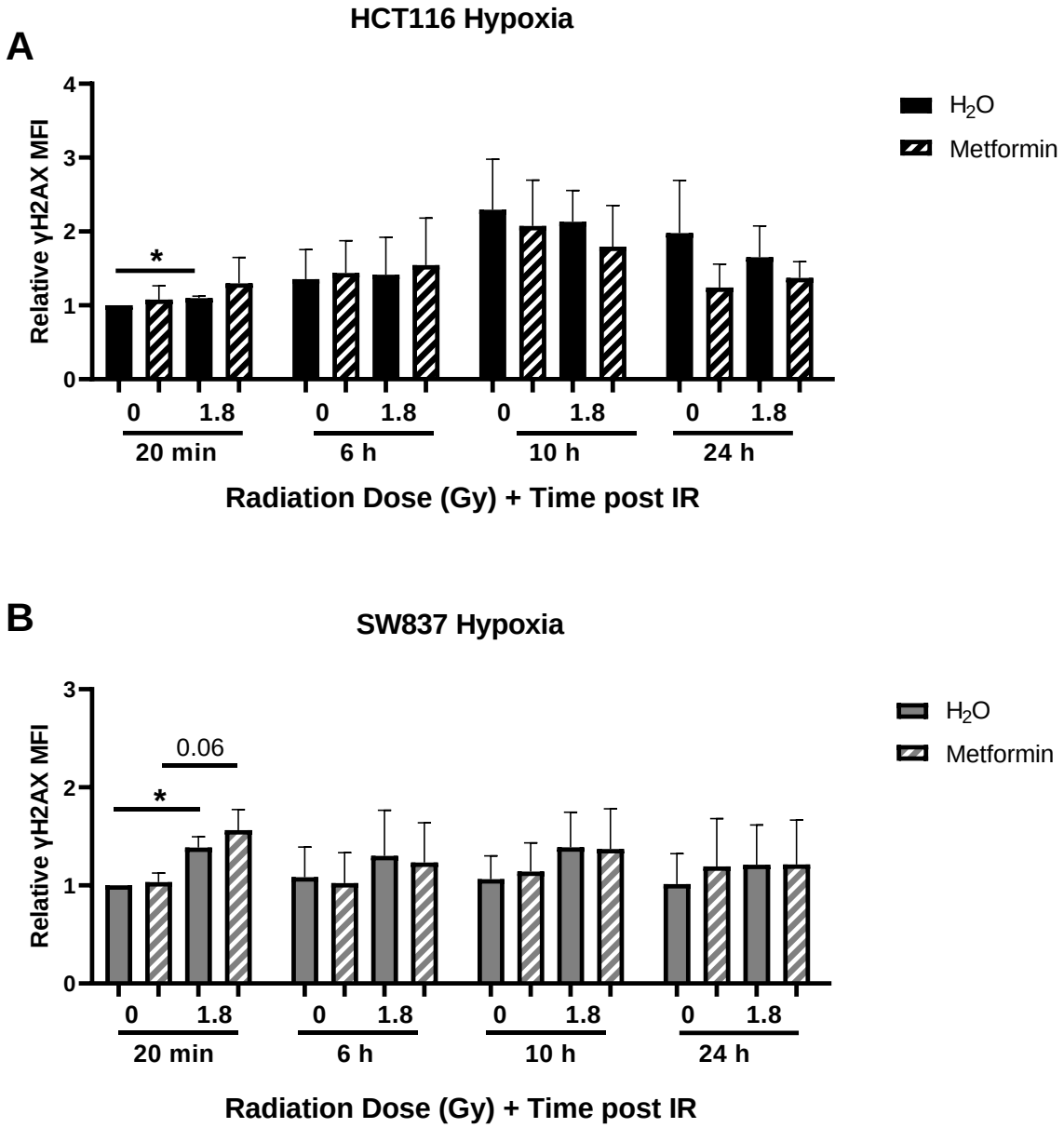

Fig. 5.12: **Metformin treatment does not alter the induction or repair of radiation-induced DNA damage in HCT116 or SW837 cells under hypoxia.** HCT116 and SW837 cells were treated with metformin (10 mM) or H_2O vehicle control for 24 h, exposed to 1.8 Gy radiation in hypoxic conditions (0.5% O_2), and DNA damage was assessed by γH2AX fluorescence and flow cytometry. Controls were mock-irradiated. **A)** DNA damage in HCT116 cells following metformin and X-ray radiation. **B)** DNA damage in SW837 cells following metformin and X-ray radiation. Data is presented as mean ± SEM from 4 independent experiments. Statistical analysis was performed by paired *t*-testing. **p*<0.05.

5.4.8. *Metformin treatment induces cell death in HCT116 and SW837 cells*

To determine the impact of metformin treatment on cell death *in vitro*, HCT116 and SW837 cells were treated with metformin (10 mM), or H_2O control for 24/48/72 h under normoxic (21% O_2) or hypoxic (0.5% O_2) conditions and cell death assessed by Annexin V and PI staining by flow cytometry.

In HCT116 cells, treatment with metformin for 24 h significantly reduced the proportion of live cells, when compared to vehicle control under normoxic conditions (p = 0.011) (Mean % AV-PI- ± SEM; HCT116 H_2O 88.68 ± 1.94, HCT116 metformin 83.8 ± 2.46) (**Fig. 5.13A**). In addition, the proportion of early and late apoptotic cells was significantly elevated following 24 h metformin treatment in HCT116 cells, when compared to vehicle control under normoxia (p = 0.041, p = 0.049) (Mean % AV+PI- ± SEM; HCT116 H_2O 5.11 ± 1.1, HCT116 Metformin 7.05 ± 1.52) (Mean % AV+PI+ ± SEM; HCT116 H_2O 2.22 ± 0.41, HCT116 metformin 4.9 ± 1.09) (**Fig. 5.13B-C**). No significant differences were demonstrated in the proportion of necrotic HCT116 cells under normoxia (**Fig. 5.13D**). Under hypoxic conditions, metformin did not alter the proportion of live, apoptotic or necrotic HCT116 cells (**Fig. 5.13A-D**).

Metformin treatment for 24 h resulted in a trend towards a reduced proportion of live SW837 cells, when compared to H_2O control under normoxia, although this did not reach statistical significance (p = 0.058) (Mean % AV-PI- ± SEM; SW837 H_2O 87.53 ± 1.03, SW837 metformin 82.18 ± 2.19) (**Fig. 5.13E**). Metformin treatment for 24 h significantly increased the proportion of early apoptotic SW847 cells under normoxia, when compared to vehicle control (p = 0.032) (Mean % AV+PI- ± SEM; SW837 H_2O 6.89 ± 1.1, SW837 metformin 8.65 ± 1.18) (**Fig. 5.13F**). No significant differences in the proportion of late apoptotic or necrotic cells were demonstrated following metformin treatment for 24 h, under normoxia, when compared to H_2O (**Fig. 5.13G-H**)**.** Under hypoxia, at 24 h post metformin treatment, a trend towards reduced live SW837 cells was demonstrated, although this did not reach statistical significance (p = 0.077) (**Fig. 5.13E**). Twenty-four-hour metformin treatment significantly increased the proportion of SW837 cells in the early apoptotic stage under hypoxia, when compared to vehicle control (p = 0.026) (Mean % AV+PI- ± SEM; SW837 H_2O 3.31 ± 0.8, SW837 metformin 5.56 ± 1.32) (**Fig. 5.13F**).

At 48 h post metformin treatment, while trends towards reduced live HCT116 cells were demonstrated under both normoxic and hypoxic conditions, no significant differences were demonstrated relative to vehicle control (**Fig. 5.14A**). There were no significant

differences in the percentage of early apoptosis cells in HCT116 following metformin treatment under both normoxic and hypoxic conditions at 48 h post treatment (**Fig. 5.14B**). No significant differences in the proportion of necrotic cells or late apoptotic cells were demonstrated in metformin treated cells under normoxic or hypoxic conditions (**Fig. 5.14C-D**).

In SW837 cells, under hypoxia, there was a significant reduction in the proportion of live cells treated with metformin at 48 h, when compared to vehicle control (p = 0.045) (Mean % AV-PI- ± SEM; SW837 H_2O 91.5 ± 0.79 vs HCT116 metformin 78.52 ± 4.26) (**Fig. 5.14E**). There was a significant increase in early apoptotic cells in metformin treatment under hypoxia, when compared to vehicle control (p = 0.027) (Mean ± SEM; SW837 H_2O 5.3 ± 0.53 vs SW837 metformin 12.05 ± 1.66) (**Fig. 5.14F**). There were no significant differences in necrotic cells or late apoptotic cells following metformin treatment at 48 h, under normoxic or hypoxic conditions (**Fig. 5.14G-H**).

Following 72 h metformin treatment, there was a significant reduction in the number of live HCT116 cells under normoxia, when compared to vehicle control (p = 0.002), with no difference demonstrated under hypoxia (Mean % AV- PI- ±SEM; HCT116 H_2O 88.38 % ± 2.46, HCT116 metformin 53.33 % ± 5.89) (**Fig. 5.15A**). Metformin treatment for 72 h induced a significant increase in early and late apoptotic HCT116 cells, under normoxia, when compared to vehicle control (p = 0.028, p = 0.0076 respectively) (Mean % AV+PI- ±SEM; HCT116 H_2O 5.6 ± 1.15 vs. HCT116 metformin 14.51 ± 2.79) (Mean % AV+PI+ ± SEM; HCT116 H_2O 4.16 ± 1.1 vs. HCT116 metformin 23.65 ± 4.52) (**Fig. 5.15B-C**). Seventy-two-hour treatment with metformin significantly induced necrosis in HCT116 cells under normoxia, when compared to vehicle control (p = 0.008) (Mean % AV-PI+ ± SEM; HCT116 H_2O 1.82 ± 0.49, HCT116 metformin 8.48 ± 1.72) (**Fig. 5.15D**).

In SW837 cells, following 72 h metformin treatment, the number of live cells was significantly reduced under normoxia only, when compared to H_2O vehicle control (p = 0.021) (Mean % AV-PI- ± SEM; SW837 H_2O 86.82 ± 0.77 vs SW837 metformin 80.42 ± 1.31) (**Fig. 5.15E**). While there was a trend towards increased SW837 cells in the early apoptotic stage following 72 h metformin treatment, under normoxia, this did not reach statistical significance (p = 0.058). A significant increase in the percentage of late apoptotic SW837 cells was demonstrated following 72 h metformin treatment under normoxia, when compared to

vehicle control (p = 0.03) (Mean % AV+PI+ ± SEM; SW837 H_2O 2.6 ± 0.09 vs SW837 metformin 6.12 ± 1.09) (**Fig. 5.15G**).

These data demonstrate that metformin treatment (10 mM) induces significant cell death (apoptosis and necrosis) in HCT116 and SW837 CRC cell lines.

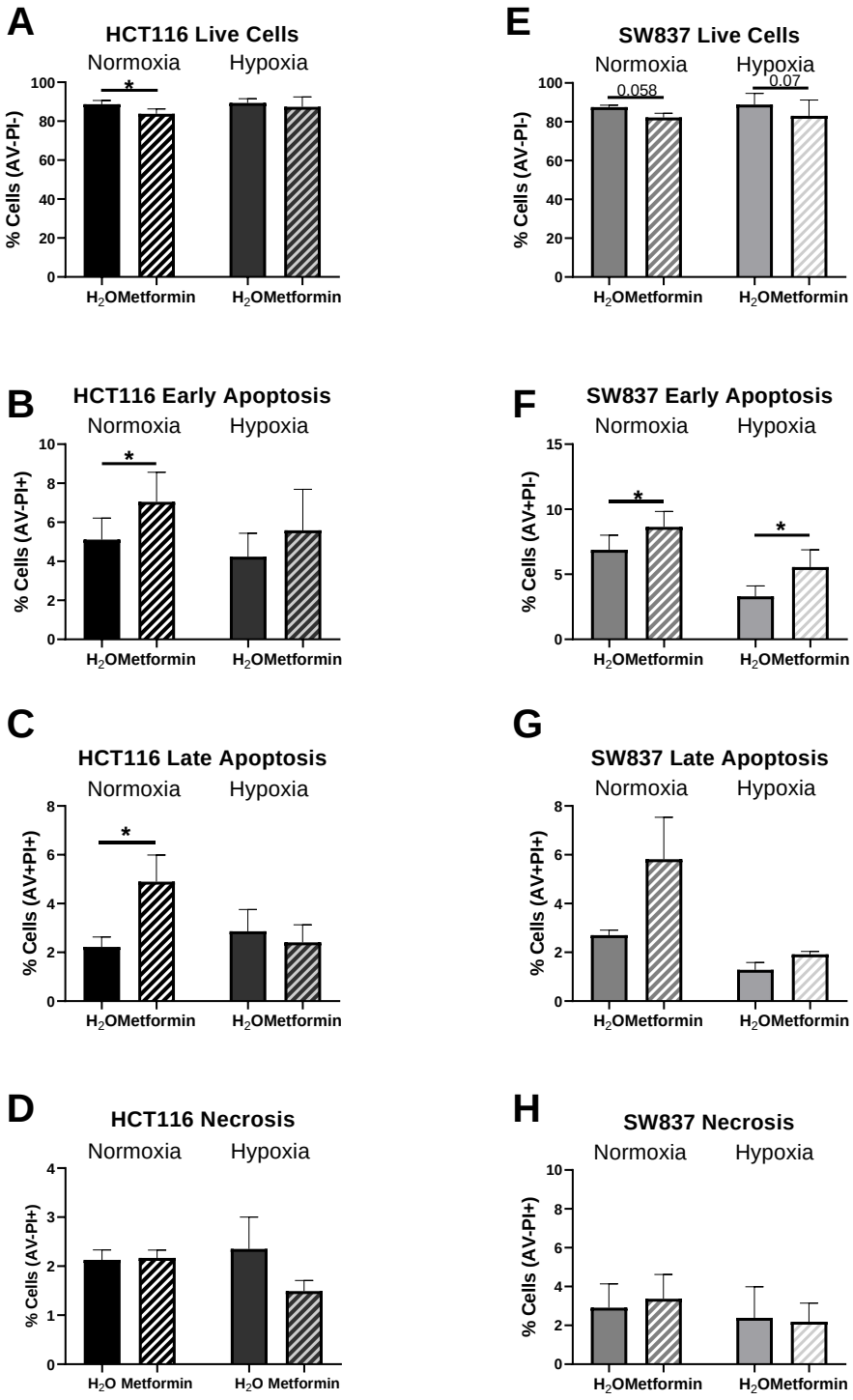

Fig. 5.13: **Effect of metformin treatment for 24 h on cell death under normoxia and hypoxia in HCT116 and SW837 cells.** HCT116 and SW837 cells were treated with either metformin (10 mM) or H_2O vehicle control for 24 h under normoxic or hypoxic (0.5% O_2) conditions, and cell death assessed by concurrent Annexin-V FITC and PI staining and flow cytometry. Impact of metformin on **A)** Live Cells**, B)** Early Apoptosis, **C)** Late Apoptosis and **D)** Necrosis in HCT116 cells. Impact of metformin on **E)** Live Cells, **F)** Early Apoptosis, **G)** Late Apoptosis and **H)** Necrosis in SW837 cells. Data is presented as mean ± SEM for n=6 (normoxia) or *n*=5 (hypoxia) independent experiments. Statistical analysis was performed by paired *t*-testing. **p*<0.05.

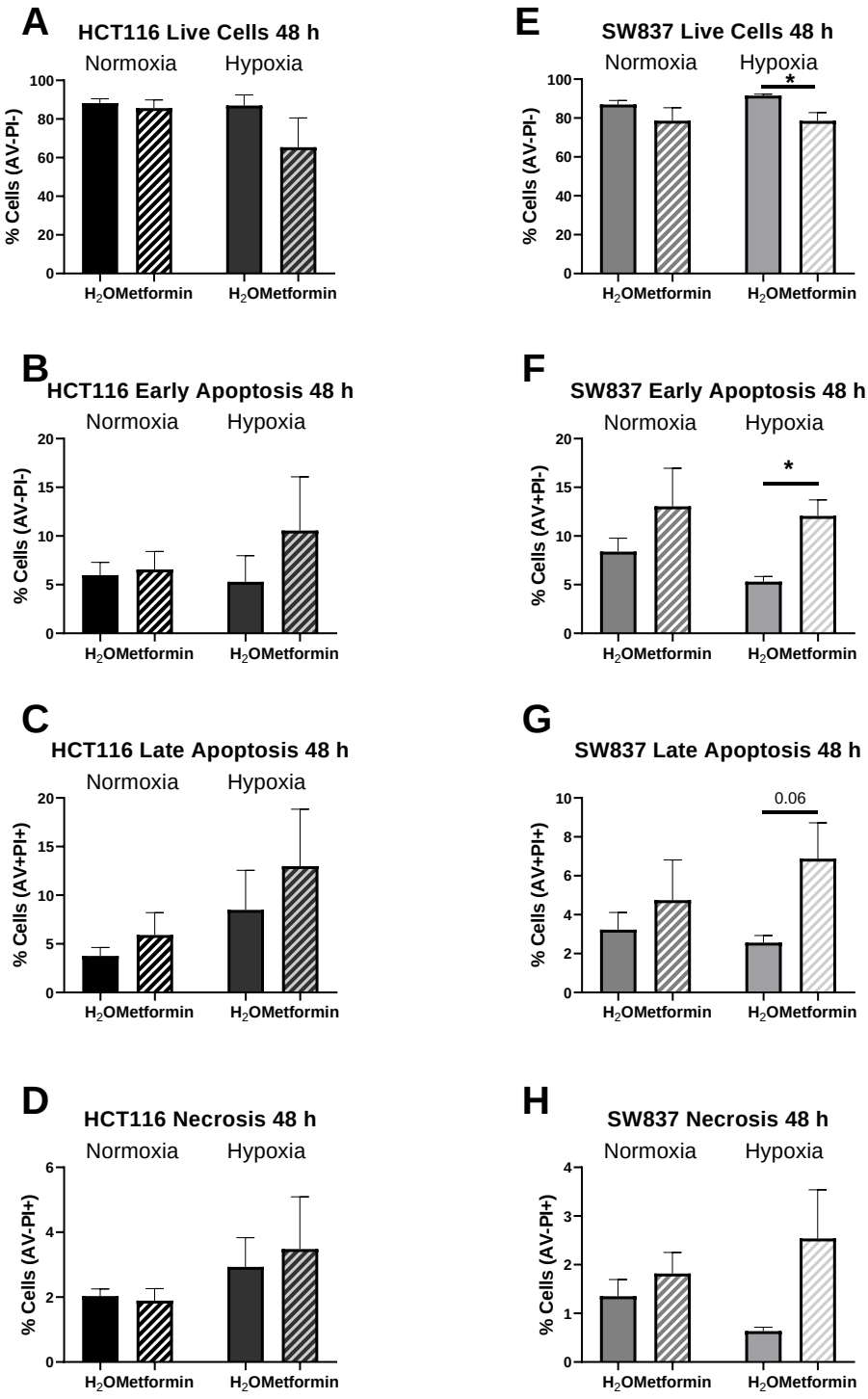

Fig. 5.14: **Effect of metformin treatment for 48 h on cell death under normoxia and hypoxia in HCT116 and SW837 cells.** HCT116 and SW837 cells were treated with either metformin (10 mM) or H_2O vehicle control for 48 h under normoxic or hypoxic (0.5% O_2) conditions, and cell death assessed by concurrent Annexin-V FITC and PI staining and flow cytometry. Impact of metformin on **A)** Live Cells**, B)** Early Apoptosis, **C)** Late Apoptosis and **D)** Necrosis in HCT116 cells. Impact of metformin on **E)** Live Cells**, F)** Early Apoptosis, **G)** Late Apoptosis and **H)** Necrosis in SW837 cells. Data is presented as mean ± SEM for n=6 (normoxia) or *n*=5 (hypoxia) independent experiments. Statistical analysis was performed by paired *t*-testing. **p*<0.05.

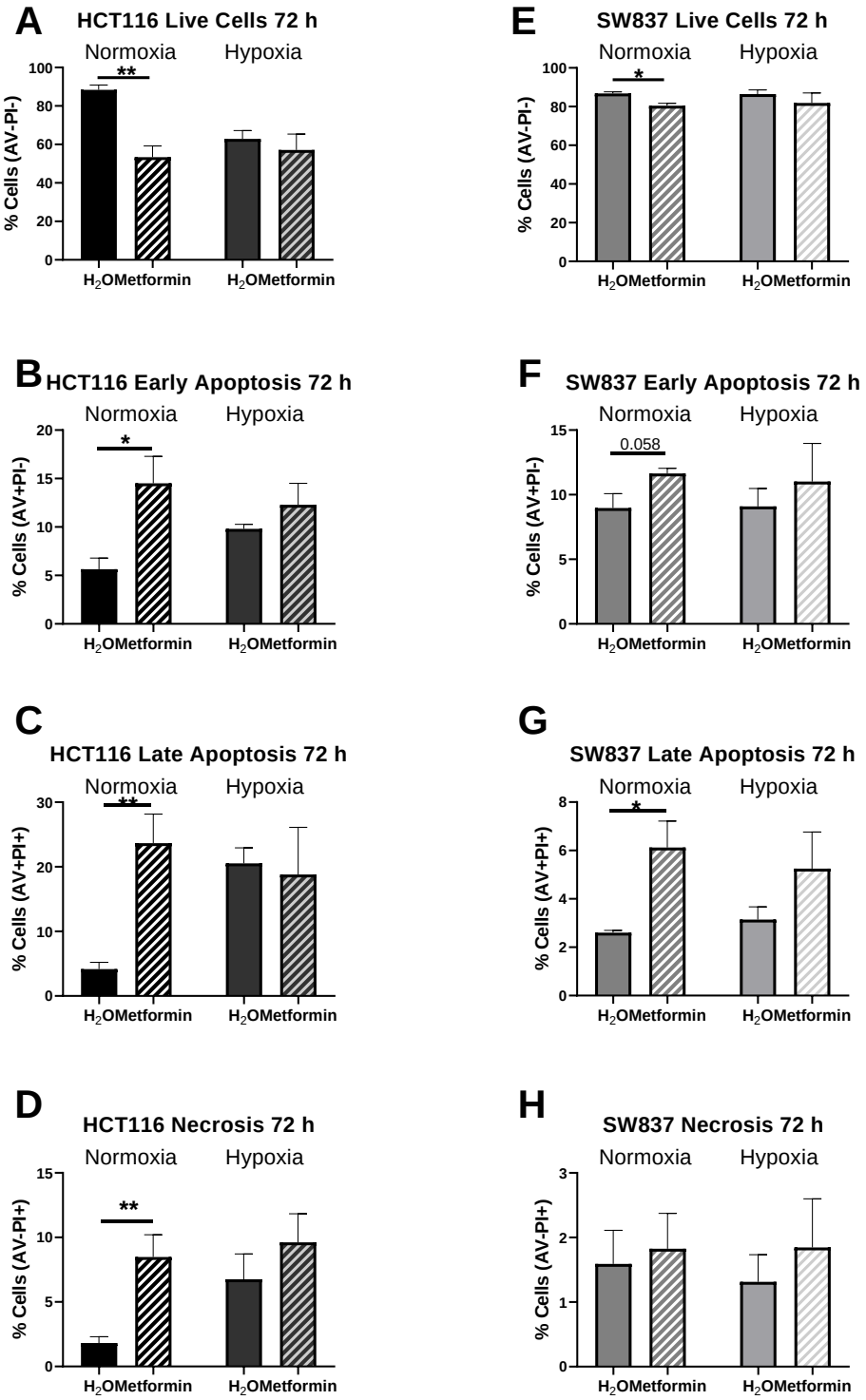

Fig. 5.15: **Effect of metformin treatment for 72 h on cell death under normoxia and hypoxia in HCT116 and SW837 cells.** HCT116 and SW837 cells were treated with either metformin (10 mM) or H_2O vehicle control for 72 h under normoxic or hypoxic (0.5% O_2) conditions, and cell death assessed by concurrent Annexin-V FITC and PI staining and flow cytometry. Impact of metformin on **A)** Live Cells**, B)** Early Apoptosis, **C)** Late Apoptosis and **D)** Necrosis in HCT116 cells. Impact of metformin on **E)** Live Cells, **F)** Early Apoptosis, **G)** Late Apoptosis and **H)** Necrosis in SW837 cells. Data is presented as mean ± SEM for n=6 (normoxia) or *n*=5 (hypoxia) independent experiments. Statistical analysis was performed by paired *t*-testing. **p*<0.05.

5.4.9. *Combined metformin and X-ray radiation treatment induces cell death in HCT116 and SW837 cells*

Having demonstrated that metformin treatment alone induces cell death, the impact of combining metformin and radiation treatment on cell death in HCT116 and SW837 cells in normoxic and hypoxic conditions was assessed by flow cytometry.

In HCT116 cells, while a significant reduction in the percentage of live cells was demonstrated in irradiated vehicle control cells, when compared to unirradiated controls (p = 0.039) (Mean % AV-PI- HCT116 0 Gy H_2O ± 2.26 vs HCT116 1.8 Gy H_2O 84.56 ± 1.35), there were no significant differences to cell death demonstrated in metformin treated cells at 24 h post IR treatment, with or without radiation, when compared to vehicle controls (**Fig. 5.16A**). Under hypoxic conditions, although there was a trend towards reduced proportion of live HCT116 cells with metformin treatment alone, this did not reach statistical significance (**Fig. 5.16A**). In addition, there were no differences to the proportion of early apoptotic, late apoptotic or necrotic cells following combined radiation and metformin treatment in HCT116 cells under hypoxia (**Fig. 5.16B-D**).

Similarly, in SW837 cells, at 24 h post radiation treatment, there were no significant differences in live cells, early apoptosis, late apoptosis or necrosis with metformin and radiation combination under normoxia (**Fig. 5.17A-D**). However, under hypoxia, the percentage of early apoptotic cells was significantly increased in cells treated with metformin and radiation, when compared to irradiated vehicle control (p = 0.044) (Mean % AV+PI- ± SEM; SW837 1.8 Gy H_2O 6.1 ± 0.69 vs SW837 1.8 Gy metformin 14.28 ± 3.01) (**Fig. 5.17B**)**.** A trend towards increased necrotic cells was demonstrated in combined metformin and radiation treated cells, when compared to irradiated vehicle control, however, this did not reach statistical significance (p = 0.0502) (**Fig. 5.17C**).

At 48 h following exposure to radiation, treatment with metformin in combination with 1.8 Gy radiation significantly reduced the percentage of live HCT116 cells, when compared to irradiated vehicle control (p = 0.001) (Mean % AV- PI- ± SEM; HCT116 1.8 Gy H_2O 84.77 ± 4.89 vs HCT116 1.8 Gy metformin 38.9 ± 5.13) (**Fig. 5.18A**). In addition, at 48 h post radiation, metformin treatment in combination with 1.8 Gy radiation significantly increased the number of cells in the early apoptotic stage following 1.8 Gy, when compared to irradiated vehicle controls (p = 0.024) (Mean % AV+PI- ± SEM; HCT116 1.8 Gy H_2O 5.28 ± 0.87 vs HCT116 1.8 Gy Metformin 17.13 ± 3.82) (**Fig. 5.18B**). Forty-eight hours following radiation, the percentage of

late apoptotic cells was also significantly increased in combination metformin and radiation treated cells, when compared to irradiated H_2O vehicle control (p = 0.0034) (Mean % AV+PI+ ± SEM; HCT116 1.8 Gy H_2O 5.75 ± 1.69 vs. HCT116 1.8 Gy metformin 27.42 ± 3.26) (**Fig. 5.18D**). Necrotic cells were also significantly increased at 48 h post radiation in HCT116 cells treated with combination metformin and 1.8 Gy radiation, when compared to irradiated vehicle control (p = 0.01) (Mean % AV+PI- ± SEM; HCT116 1.8 Gy H_2O 1.44 ± 0.23 vs HCT116 1.8 Gy metformin 12.6 ± 2.25) (**Fig.5.18C**). However, while a trend towards increased necrotic cells was demonstrated with the combination metformin and 1.8 Gy radiation treatment, when compared to unirradiated metformin treated cells under normoxia, this did not reach statistical significance.

Under hypoxic conditions, no differences were demonstrated with metformin and 1.8 Gy radiation in HCT116 cells (**Fig. 5.18A**). While a trend towards increased numbers of HCT116 cells in early apoptosis was demonstrated in cells treated with metformin and radiation, when compared to irradiated vehicle control, this did not reach statistical significance (p = 0.09) (**Fig.5.18B**).

At 48 h post radiation, SW837 cells treated metformin and 1.8 Gy radiation, demonstrated a significantly reduced percentage of live cells, when compared to irradiated vehicle control (p = 0.001) (Mean % AV-PI- ± SEM; SW837 1.8 Gy H_2O 82.94 ± 1.6 vs SW837 1.8 Gy Metformin 78.12 ± 1.33) (**Fig.5.19A**). In addition, combination metformin and 1.8 Gy radiation treatment significantly reduced the percentage of live SW837 cells, when compared to unirradiated metformin treated cells (p = 0.009). The percentage of late apoptotic cells was significantly increased in combination metformin and 1.8 Gy treated cells, when compared to irradiated vehicle control (p = 0.0014) (Mean % AV+PI+ ±SEM; SW837 1.8 Gy H_2O 3.92 ± 0.65 vs SW837 1.8 Gy metformin 7.42 ± 0.9) (**Fig. 5.19C**). In addition, combining metformin with 1.8 Gy radiation significantly increased late apoptosis in SW837 cells, when compared to unirradiated metformin treated cells (p = 0.016).

Under hypoxia, no significant differences in the proportion of live, early apoptotic, late apoptotic or necrotic cells were demonstrated in SW837 cells at 48 h post radiation (**Fig. 5.19A-D**).

These data demonstrate that metformin does induce cell death in HCT116 and SW837 alone and in combination with radiation treatment.

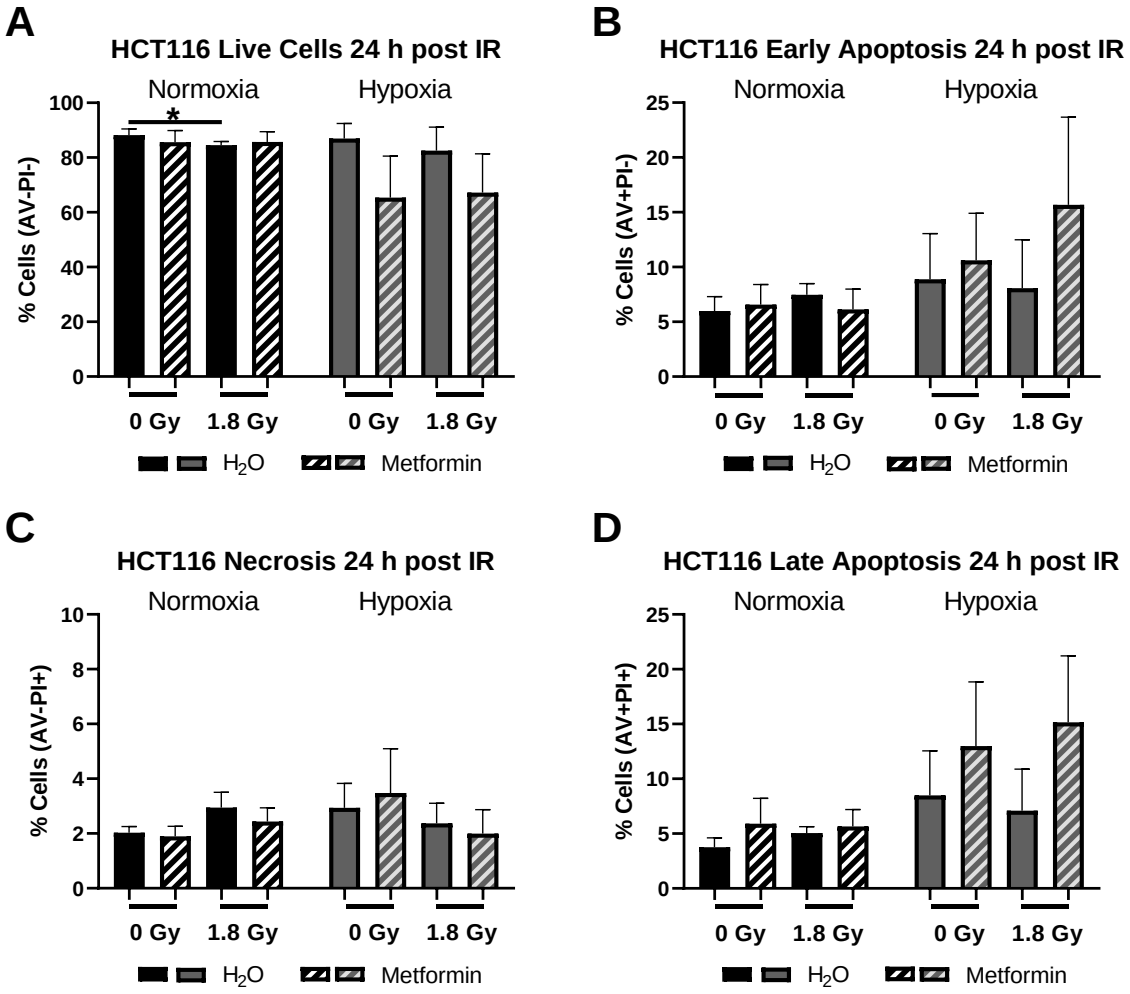

Fig. 5.16: **Effect of metformin treatment on cell death in HCT116 cells at 24 h post irradiation with 1.8 Gy.** HCT116 cells were treated with metformin (10 mM), or H_2O vehicle control for 24 h, either mock-irradiated or exposed to 1.8 Gy radiation, under normoxic or hypoxic conditions and cell death assessed by Annexin V/PI staining and flow cytometry at 24 h post irradiation. **A)** Live cells. **B)** Early apoptotic cells. **C)** Late apoptotic cells. **D)** Necrotic cells**.** Data is presented as mean ± SEM for n=6 (normoxia) or *n*=5 (hypoxia) independent experiments. Statistical analysis was performed by paired *t*-testing. **p*<0.05.

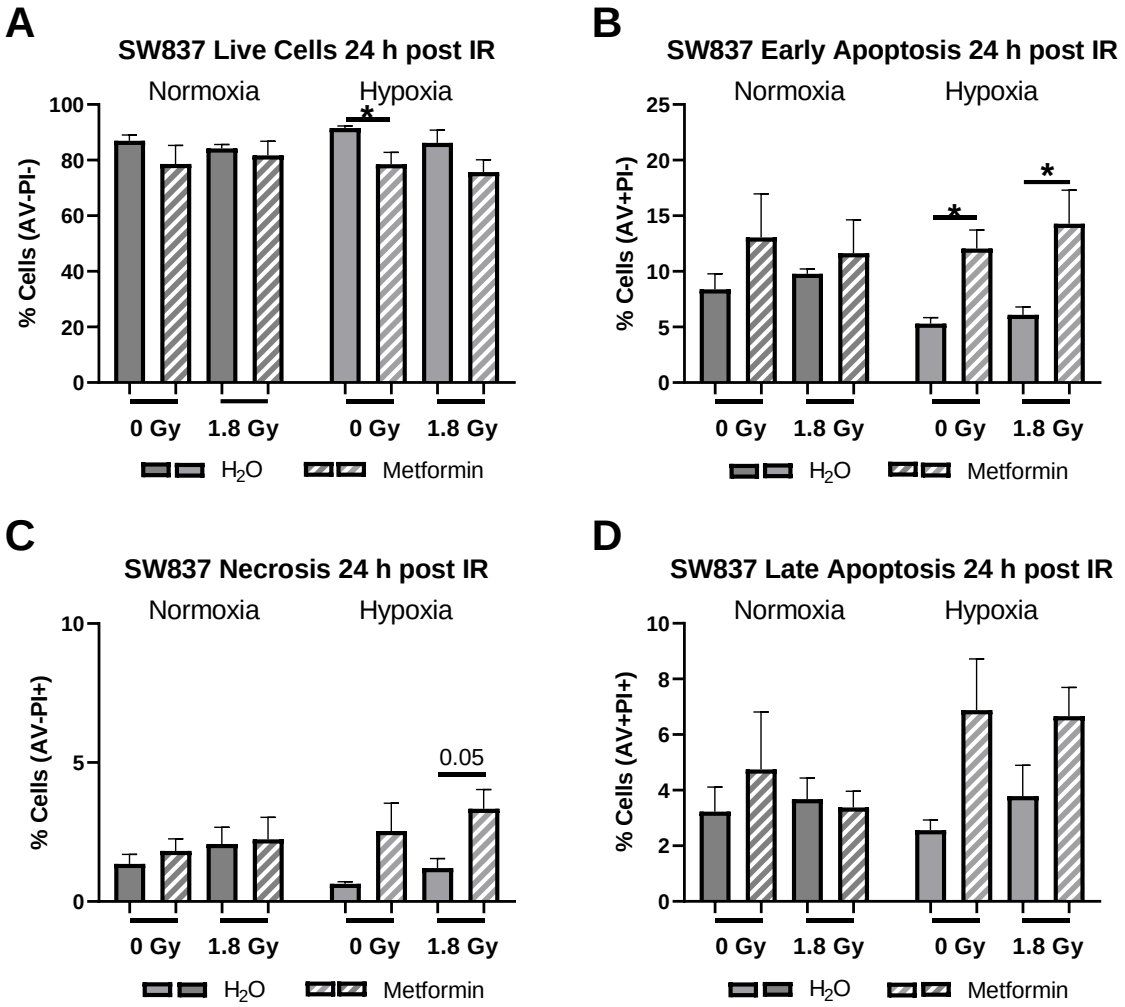

Fig. 5.17: **Metformin treatment significantly induces early apoptosis in SW837 cells under hypoxic conditions, at 24 h post irradiation with 1.8 Gy.** SW837 cells were treated with metformin (10 mM), or H_2O vehicle control for 24 h, either mock-irradiated or exposed to 1.8 Gy radiation, under normoxic or hypoxic conditions and cell death assessed by Annexin V/PI staining and flow cytometry at 24 h post radiation therapy. **A)** Live cells. **B)** Early apoptotic cells. **C)** Late apoptotic cells. **D)** Necrotic cells**.** Data is presented as mean ± SEM for n=6 (normoxia) or *n*=5 (hypoxia) independent experiments. Statistical analysis was performed by paired *t*-testing. **p*<0.05.

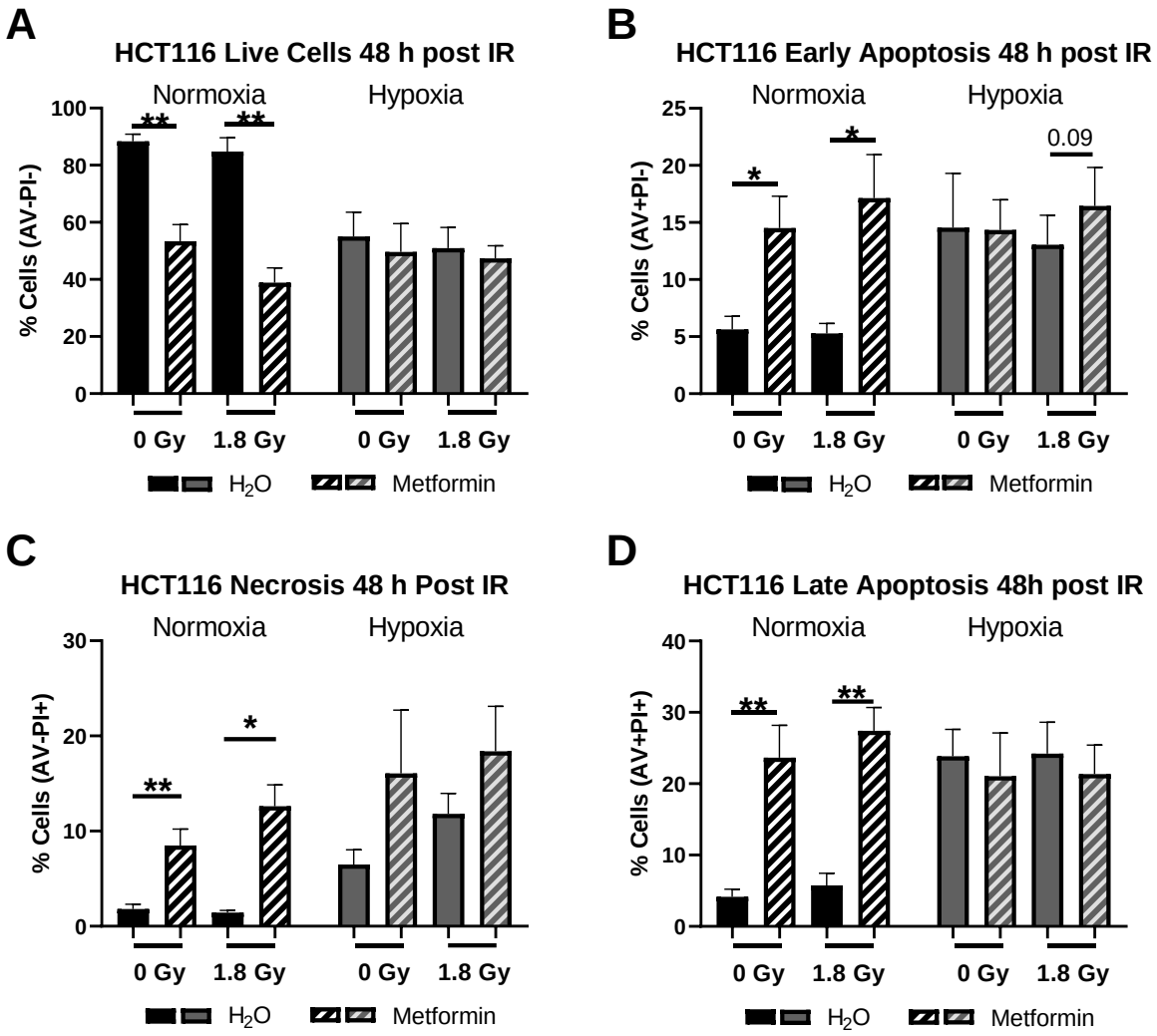

Fig. 5.18: **Metformin treatment significantly induces cell death in HCT116 cells under normoxic conditions, at 48 h post irradiation with 1.8 Gy.** HCT116 cells were treated with metformin (10 mM), or H_2O vehicle control for 24 h, either mock-irradiated or exposed to 1.8 Gy radiation, under normoxic or hypoxic conditions and cell death assessed by Annexin V/PI staining and flow cytometry at 48 h post irradiation. **A)** Live cells. **B)** Early apoptotic cells. **C)** Late apoptotic cells. **D)** Necrotic cells**.** Data is presented as mean ± SEM for n=6 (normoxia) or *n*=5 (hypoxia) independent experiments. Statistical analysis was performed by paired *t*-testing. **p*<0.05, ***p*< 0.01.

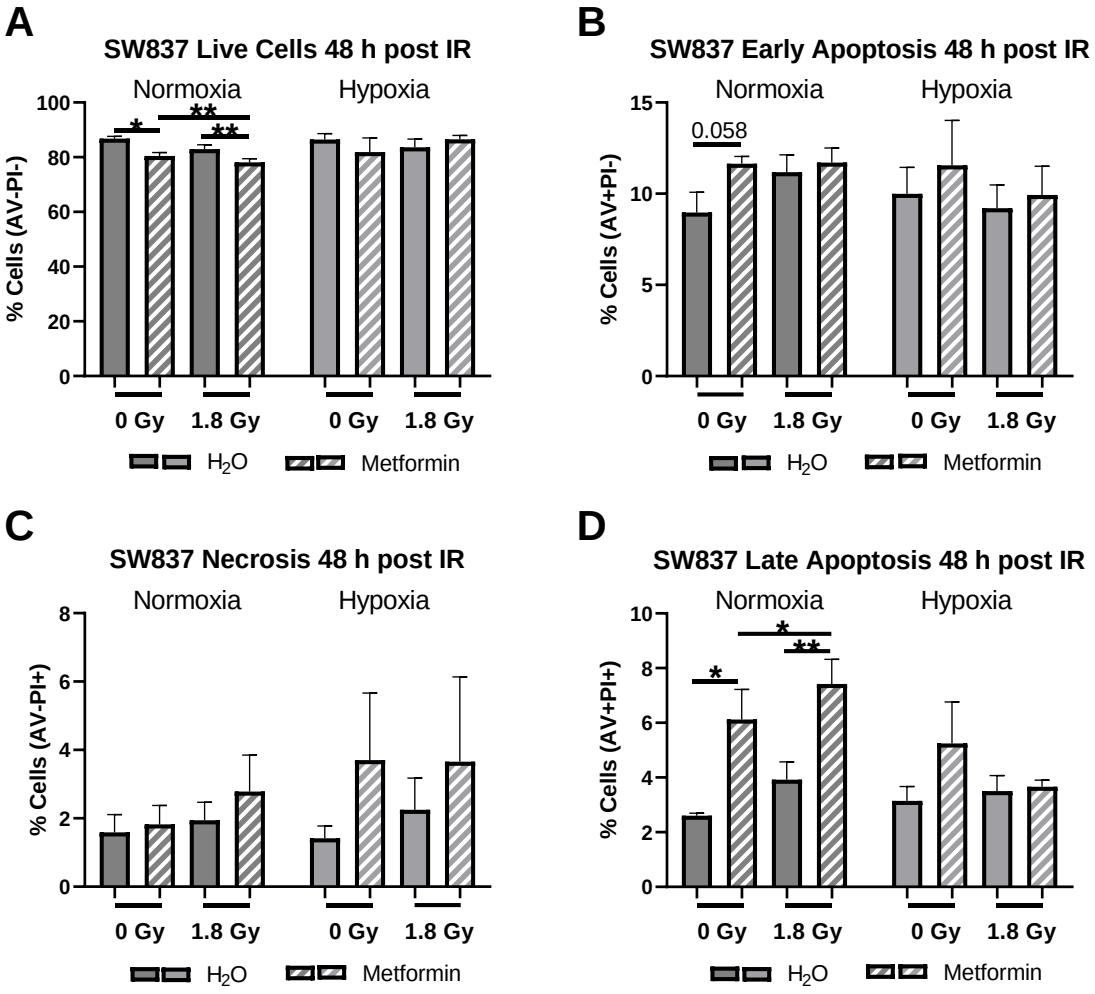

Fig. 5.19: **Metformin treatment significantly induces cell death in SW837 cells under normoxia, but not hypoxic conditions, at 48 h post radiation.** SW837 cells were treated with metformin (10 mM), or H_2O vehicle control for 24 h, either mock-irradiated or exposed to 1.8 Gy radiation, under normoxic or hypoxic conditions and cell death assessed by Annexin V/PI staining and flow cytometry at 48 h post irradiation. **A)** Live cells. **B)** Early apoptotic cells. **C)** Late apoptotic cells. **D)** Necrotic cells**.** Data is presented as mean ± SEM for n=6 (normoxia) or *n*=5 (hypoxia) independent experiments. Statistical analysis was performed by paired *t*-testing. **p*<0.05, ***p*< 0.01.

5.4.10. *Metformin treatment increases total glutathione production in HCT116 and SW837 cells*

Having demonstrated that metformin treatment induces ROS production in HCT116 and SW837 cells (Chapter 4), the impact of metformin treatment on antioxidant capacity was assessed using the GSH/GSSG-Glo™ luminescent assay. This assay permits the detection and quantification of both reduced glutathione (GSH) and oxidised glutathione (GSSG), based on a GSH-dependent conversion of GSH probe Luciferin-NT to luciferin by a glutathione-S-transferase enzyme, coupled to a firefly luciferase reaction.

Treatment with metformin (10 mM) for 24 h resulted in a significant increase in total glutathione (GSH + GSSG) levels in both HCT116 and SW837 cells (p = 0.003, p = 0.038 respectively), when compared to vehicle control (mean total glutathione luminescence ± SEM; HCT116 H_2O 8.2 $x10^6$ ± 9.23 $x10^5$; HCT116 10 mM metformin 9.63$x10^6$ ± 9.04$x10^5$; SW837 H_2O 7.78$X10^6$ ± 3.71$x10^5$; SW837 metformin 8.34$x10^6$ ± 3.35$x10^5$) (**Fig. 5.20A**).

While 24 h metformin treatment (10 mM) did not significantly affect the level of GSSG in SW837 cells, there was a trend towards increased GSSG in HCT116 following metformin treatment, when compared to vehicle control, although this did not reach statistical significance (p = 0.086) (mean GSSG luminescence ±SEM; HCT116 H_2O 4.47$x10^5$ ± 2.37$x10^4$; HCT116 metformin 5.56$x10^6$ ± 5.29$x10^4$) (**Fig. 5.20B**).

These data demonstrate that metformin treatment significantly increases total GSH production, while not affecting GSSG levels in both HCT116 and SW837 CRC cells.

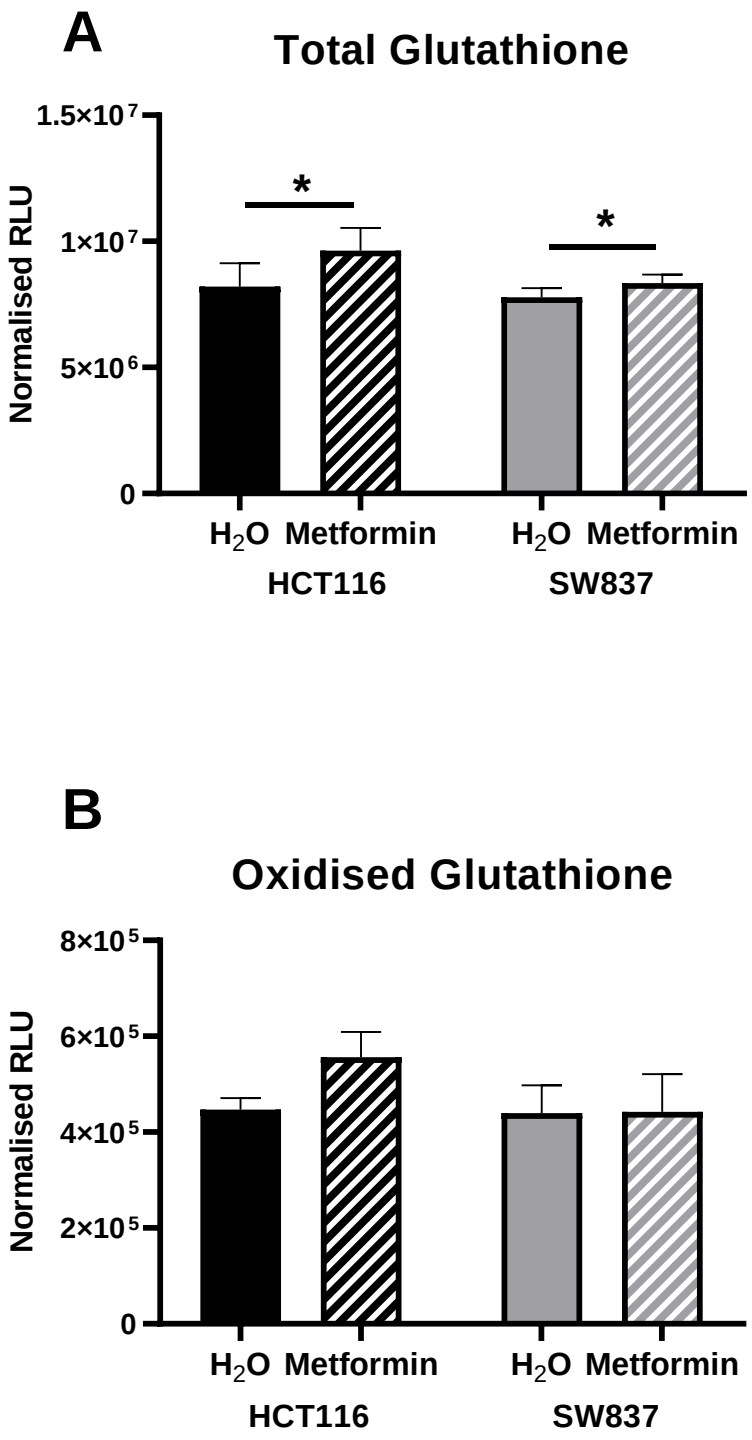

Fig. 5.20: **Metformin treatment significantly increases GSH levels in HCT116 and SW837 cells.** GSH and GSSG levels were assessed by GSSG/GSH-Glo™ luminescent assay in HCT116 and SW837 cells at 24 h post treatment with either metformin (10mM) or H_2O vehicle control. **A)** Total GSH levels in HCT116 and SW837 cells. **B)** GSSG levels in HCT116 and SW837 cells. Data is presented as mean ± SEM for *n*=5 (HCT116) or *n*=6 (SW837) independent experiments. Statistical analysis was performed by paired t-testing *$p < 0.05$.

5.4.11. *Metformin treatment significantly alters the transcriptome of radioresistant SW837 cells*

To further interrogate the potential mechanisms of metformin-mediated radiosensitisation, HCT116 and SW837 cells were treated with metformin (10 mM) or H_2O vehicle control for 24 h, RNA was isolated, and transcriptomic profiling performed using the Lexogen QuantSeq 3' mRNA FWD sequencing kit. Differential expression analysis was performed using BlueBee™ software and the DESeq2 script extension.

In HCT116 cells, a total of 22,804 genes were expressed across metformin and vehicle control treated HCT116 cells. Differential expression analysis demonstrated no significant differences to the gene expression in HCT116 cells treated with metformin, when compared to vehicle control, due to variation within samples.

A total of 24,391 genes were expressed across metformin and vehicle control treated SW837 cells. Principal component analysis (PCA) demonstrated moderate separation between metformin treated and vehicle control SW837 cells (**Fig. 5.21**). Principal component 1 (PC1) accounted for 67% of variance in the dataset, with PC2 accounting for 13% of variance. Differential expression analysis demonstrated a total of 417 genes were significantly altered between SW837 cells treated with metformin and H_2O vehicle control, based on adjusted *p*-value (*p*-adj) < 0.05 (**Fig. 5.22A**).

In total, 200 genes were significantly downregulated, and 217 genes were significantly upregulated in metformin treated SW837 cells, when compared to H_2O vehicle control (*p*-adj < 0.05) (**Fig. 5.22A**). Of the significantly altered genes, the top 25 downregulated and upregulated genes in metformin treated SW837 cells are demonstrated in **Fig. 5.22B-C**. SP5, a transcription factor primarily involved in WNT-β-catenin signalling, was the most downregulated gene (as determined by fold change, Log2 Fold Change = -2.25) in metformin treated SW837 cells, when compared to H_2O vehicle control. RRAGC (ras-related GTP binding C), which is involved in the cellular response to amino acid availability and regulation of mTORC1 signalling, was the most upregulated gene (as determined by fold change, Log_2 Fold Change = 2.23) in metformin treated SW837 cells, when compared to H_2O vehicle control.

The top 25 genes most significantly altered by metformin treatment in SW837 cells are displayed in **Table 5.1**. PLA2G16 (Group XVI phospholipase A2, also known as PLAAT3 (phospholipase A and acyltransferase 3), which acts as an oncogene and has a role in fat metabolism, was the most significantly downregulated gene (as determined by *p*-adj, *p*-adj =

3.46 x 10^{-6}) in metformin treated SW837 cells, when compared to H_2O vehicle control. SLFN5 (Schlafen family member 5), which is involved in interferon signalling, was the most significantly upregulated gene (*p*-adj = 1.63 x 10^{-12}) in metformin treated cells, when compared to H_2O vehicle control.

These data demonstrate that metformin treatment significantly alters the transcriptome of radioresistant SW837 cells.

5.4.12. *Metformin treatment alters biological functions in radioresistant SW837 cells*

Having demonstrated significant alterations to the transcriptome of metformin treated SW837 cells, biostatistical analysis was performed on the differentially expressed genes to identify biological functions affected by metformin treatment in radioresistant SW837 cells. IPA analysis was utilised to identify pathways altered based on transcriptomic data.

The cellular functions significantly altered in metformin treated SW837 cells are displayed in **Table 5.2** The *p*-values represent the statistical probability that selecting genes associated with each function is due to chance alone. As each biological function is comprised of multiple functional pathways, significance is represented as *p*-value range.

The cellular function most significantly altered in metformin treated SW837 cells was 'cellular assembly and organisation' (*p* value range 9.26 x 10^{-7} – 6.84 x 10^{-4}). Other molecular and cellular functions demonstrated to be significantly altered between metformin treatment and vehicle control include 'cellular function and maintenance', 'cell cycle' and 'DNA replication, recombination and repair' (**Table 5.2**).

These data demonstrate significant alterations to molecular and cellular functions in SW837 cells treated with metformin, when compared to H_2O vehicle control, including functions which are associated with radioresponse.

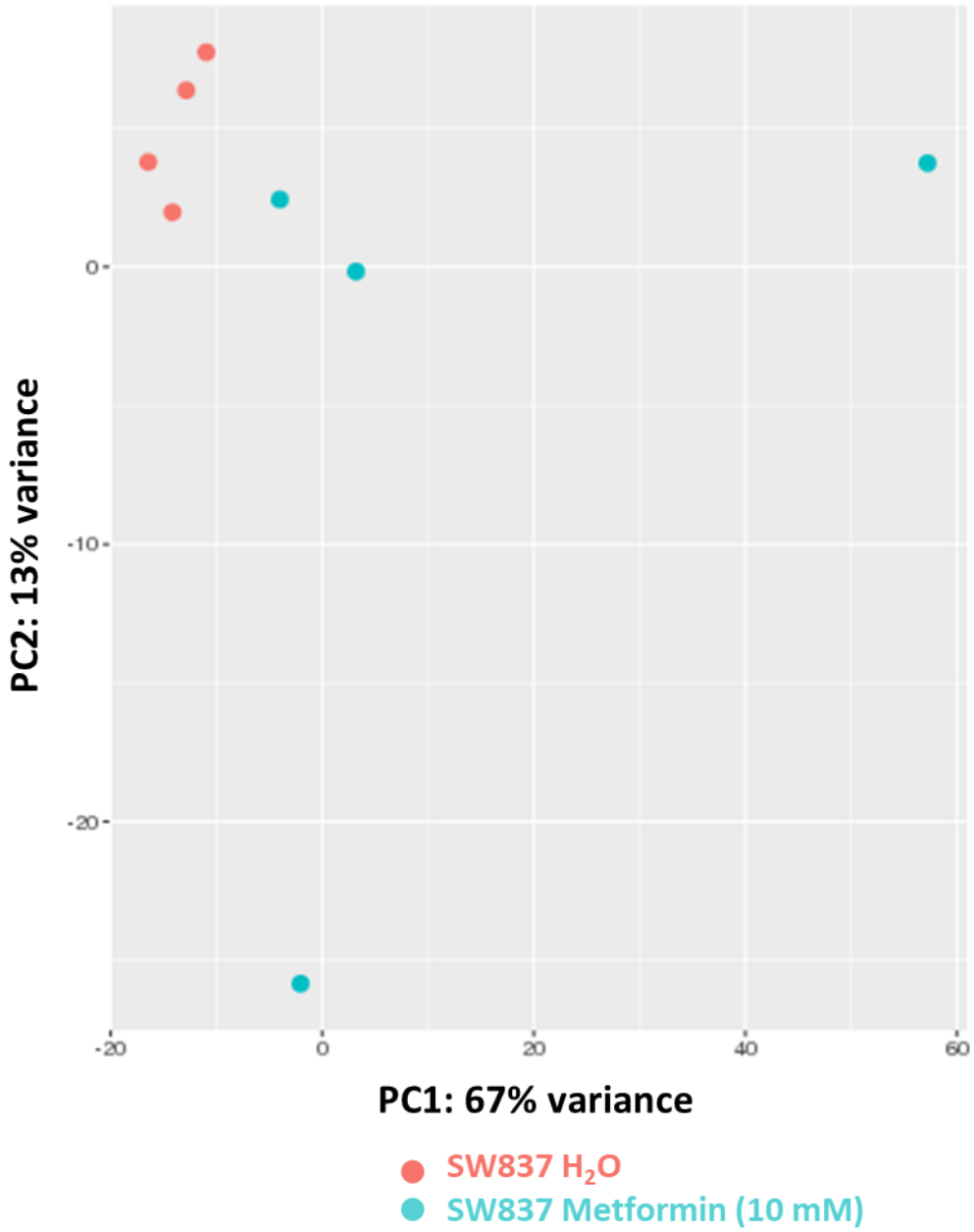

Fig. 5.21: **Principal component analysis of RNA Seq data for radioresistant SW837 cells treated with metformin.** PCA was performed on normalised read counts from SW837 replicates treated with metformin (10 mM) or H_2O vehicle control for 24 h using BlueBee software. PC-1 (x-axis) accounts or 67% of variation between groups, while PC2 (y-axis) accounts for 13%. Red dots indicate replicates of vehicle control SW837 cells (*n*=4). Blue dots indicate replicates of SW837 cells treated with metformin (10mM) (*n*=4).

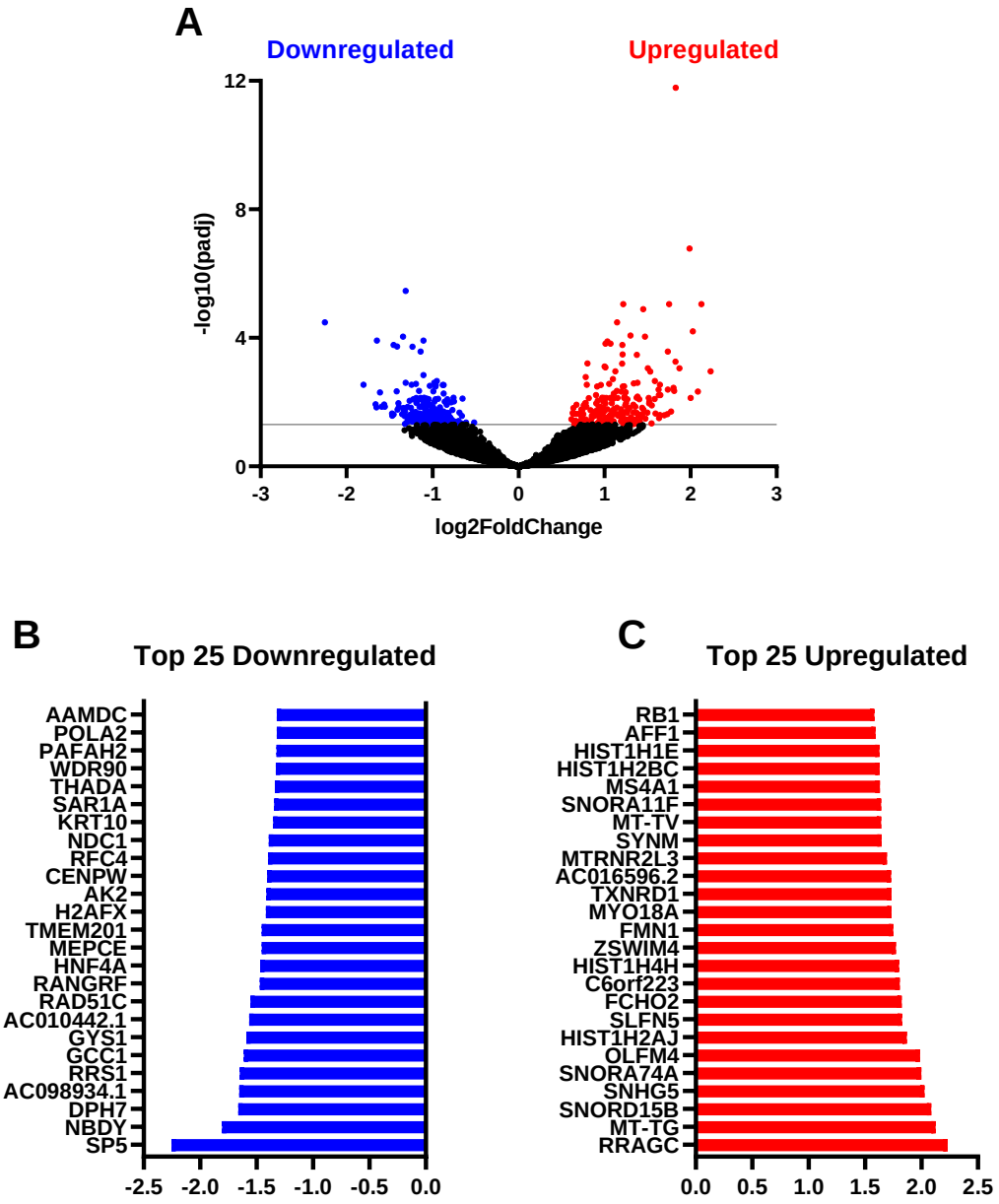

Fig. 5.22: **Metformin treatment significantly alters the transcriptome of radioresistant SW837 cells.** Transcriptomic profiling was performed on SW837 cells treated with metformin (10 mM) or H_2O vehicle control for 24 h. Differential expression analysis was performed using BlueBee™ software, and the DESeq2 R extension. **A**) Volcano plot demonstrating 407 genes significantly altered in SW837 cells treated with metformin, when compared to H_2O vehicle control. The y-axis corresponds to the -log10(*p*-adj), and the x-axis represents the Log2 (Fold Change). Dots in blue and red represent the significantly downregulated/upregulated genes in metformin treated SW837 cells. Dots in black represent the genes that did not reach statistical significance (*p*-adj > 0.05). **B**) The top 25 downregulated genes (by fold change) in SW837 cells treated with metformin, when compared to H_2O vehicle control. **C)** The top 25 upregulated genes (by fold change) in metformin treated SW837 cells, when compared to H_2O vehicle control. Data is presented for 4 independent experiments. Statistical analysis was performed using the Wald test, with corrections for multiple comparisons performed by the Benjamini-Hochberg correction (FDR).

Table 5.1: **Top 25 most significantly altered genes in metformin treated SW837 cells, when compared to H_2O vehicle control**

Gene name	Up/Down-regulated in metformin treated SW837 cells	Log_2 Fold Change	*p*-adj
SLFN5	Up	1.826852	1.63E-12
OLFM4	Up	1.988595	1.66E-07
PLA2G16	Down	-1.31396	3.46E-06
LIMA1	Up	1.215998	8.87E-06
FMN1	Up	1.749753	8.87E-06
MT-TG	Up	2.124481	8.87E-06
KIF2A	Up	1.448065	1.28E-05
SP5	Down	-2.25402	3.28E-05
CDC42BPB	Up	1.144061	3.28E-05
SNHG5	Up	2.025787	6.25E-05
MYOF	Up	1.301215	8.43E-05
SAR1A	Down	-1.34533	9.10E-05
SMG7	Up	1.469891	9.10E-05
RRS1	Down	-1.64876	0.000122
POLE3	Down	-1.10599	0.000122
MUC13	Up	1.03403	0.000129
HSP90B1	Up	1.008634	0.000151
CCDC186	Up	1.069594	0.000151
ARFGEF2	Up	1.206228	0.000166
MEPCE	Down	-1.45335	0.000166
AK2	Down	-1.41231	0.000187
TIMM8B	Down	-1.23322	0.000189
BCAP31	Down	-1.13892	0.000268
TXNRD1	Up	1.733972	0.000268
MT-RNR2	Up	1.207826	0.000326

Log2 Fold Change indicated the differential expression of each gene in metformin treated SW837 cells, when compared to H_2O vehicle control SW837 cells, with negative values indicating genes downregulated in metformin treated cells, and positive values indicating genes upregulated in metformin treated cells, when compared to H_2O vehicle control. The *p*-adj values indicate the statistical significance of the differential expression of each gene between metformin and H_2O-treated SW837 cells. Statistical analysis performed using the Wald test, with corrections for multiple comparisons performed by the Benjamini-Hochberg correction (FDR).

***Table 5.2*: The significantly altered biological functions in metformin treated SW837 cells.**

Category	***p*-value range**
Cellular Assembly and Organization	9.26E-07-6.84E-04
Cellular Function and Maintenance	9.26E-07-7.22E-04
Cell Cycle	6.64E-06-4.98E-04
DNA Replication, Recombination, and Repair	6.64E-06-8.3E-05
Protein Synthesis	7.08E-05-7.29E-04
Cell Death and Survival	2.81E-04-5.56E-04
Cellular Movement	2.83E-04-3.54E-04
Cell Signalling	4.68E-04-4.68E-04
Post-Translational Modification	4.68E-04-4.68E-04
Molecular Transport	5.76E-04-5.76E-04
RNA Trafficking	5.76E-04-5.76E-04
Gene Expression	6.37E-04-6.37E-04
Cell-To-Cell Signalling and Interaction	7.22E-04-7.22E-04
Cellular Compromise	7.22E-04-7.22E-04

Biostatistical analysis was performed on significantly altered genes in metformin treated SW837 cells, when compared to H_2O-treated SW837 cells by IPA analysis to identify projected altered biological functions between the two cell lines. Statistical analysis performed by right-tailed Fisher's exact test using IPA analysis.

5.4.13. *Metformin treatment significantly alters cellular mechanisms associated with radioresistance, including energy metabolism, cell cycle and DNA damage repair in SW837 cells*

Having demonstrated altered biological functions in metformin treated SW837 cells, the specific pathways involved in these functional processes were investigated. Transcriptomic data was analysed using IPA Canonical Pathway Analysis, which predicts the activation/inhibition of molecular pathways on input data and the Ingenuity Knowledge Base.

The most significantly altered pathways in metformin treated SW837 cells are demonstrated in **Table 5.3.** The *p*-value represents the significance between the overlap of input experimental data and the Ingenuity Knowledge Base, indicating confidence in pathway involvement. The Z-score refers to software prediction of the activation or inhibition of each affected canonical pathway, with a Z-score ≥ 2, or ≤ -2 indicating significant activation or inhibition of each pathway, respectively.

The sirtuin signalling pathway was demonstrated to be significantly altered in metformin treated SW837 cells, with predicted activation (Z-score = 1.069) (**Table 5.3**). In total 18 of the 284 genes in the knowledge base for the sirtuin signalling pathway were significantly altered in metformin treated SW837 cells.

Oxidative phosphorylation was also significantly altered, with IPA software predicting inhibition of oxidative phosphorylation in metformin treated cells (Z-score -1.897) (**Table 5.3**) (**Fig. 5.23)**. In total, 10 of 106 genes related to oxidative phosphorylation were significantly altered in metformin treated cells. 'Mitochondrial dysfunction' was also significantly altered in SW837 cells following metformin treatment. However, the software was unable to predict activation/inhibition status.

Numerous canonical pathways significantly altered in metformin treated SW837 cells are associated with mechanisms involved in radioresponse. A number of these pathways, and the specific genes altered in the dataset are demonstrated in **Table 5.3.** 'NER enhanced pathway', a DNA damage repair mechanism was predicted to be significantly inhibited in metformin treated SW837 cells (Z-score -2.449). Furthermore, genes associated with the 'role of BRCA1 in DNA damage response' were also significantly altered in metformin treated SW837 cells. 'HIF-1α signalling' was also demonstrated to be significantly altered in SW837 cell treated with metformin.

Table 5.3: **Canonical pathways altered in SW837 cells treated with metformin**

Ingenuity Canonical Pathways	-log(p-value)
Sirtuin Signalling Pathway	5.08
Oxidative Phosphorylation	4.49
Mitochondrial Dysfunction	4.14
Huntington's Disease Signalling	4.08
Remodelling of Epithelial Adherens Junctions	3.62
Germ Cell-Sertoli Cell Junction Signalling	3.49
Hypoxia Signalling in the Cardiovascular System	3.31
FAT10 Signalling Pathway	3.29
Oestrogen Receptor Signalling	3.19
Unfolded protein response	2.84
Sertoli Cell-Sertoli Cell Junction Signalling	2.79
Protein Ubiquitination Pathway	2.71
NER (Nucleotide Excision Repair, Enhanced Pathway)	2.5
Arsenate Detoxification I (Glutaredoxin)	2.47
BAG2 Signalling Pathway	2.37
GDP-mannose Biosynthesis	2.3
Coronavirus Replication Pathway	2.1
Sphingomyelin Metabolism	2.04
Ferroptosis Signalling Pathway	1.98
Ephrin Receptor Signalling	1.84
Superpathway of Cholesterol Biosynthesis	1.82
Xenobiotic Metabolism AHR Signalling Pathway	1.78
Role of BRCA1 in DNA Damage Response	1.75
Transcriptional Regulatory Network in Embryonic Stem Cells	1.73
NRF2-mediated Oxidative Stress Response	1.72
EIF2 Signalling	1.71
Autophagy	1.7
Endocannabinoid Cancer Inhibition Pathway	1.68
Cholesterol Biosynthesis I	1.62
Cholesterol Biosynthesis II (via 24,25-dihydrolanosterol)	1.62
Cholesterol Biosynthesis III (via Desmosterol)	1.62
HER-2 Signalling in Breast Cancer	1.59
Chondroitin Sulfate Degradation (Metazoa)	1.56
Colanic Acid Building Blocks Biosynthesis	1.56
Oxytocin In Brain Signalling Pathway	1.52
Mitotic Roles of Polo-Like Kinase	1.51
Gap Junction Signalling	1.51
ILK Signalling	1.5
14-3-3-mediated Signalling	1.49
Epoxysqualene Biosynthesis	1.43
CXCR4 Signalling	1.42
Molecular Mechanisms of Cancer	1.4
HIF1α Signalling	1.4
Androgen Signalling	1.39
Axonal Guidance Signalling	1.34
PPAR Signalling	1.33
Hereditary Breast Cancer Signalling	1.32
α-Adrenergic Signalling	1.3

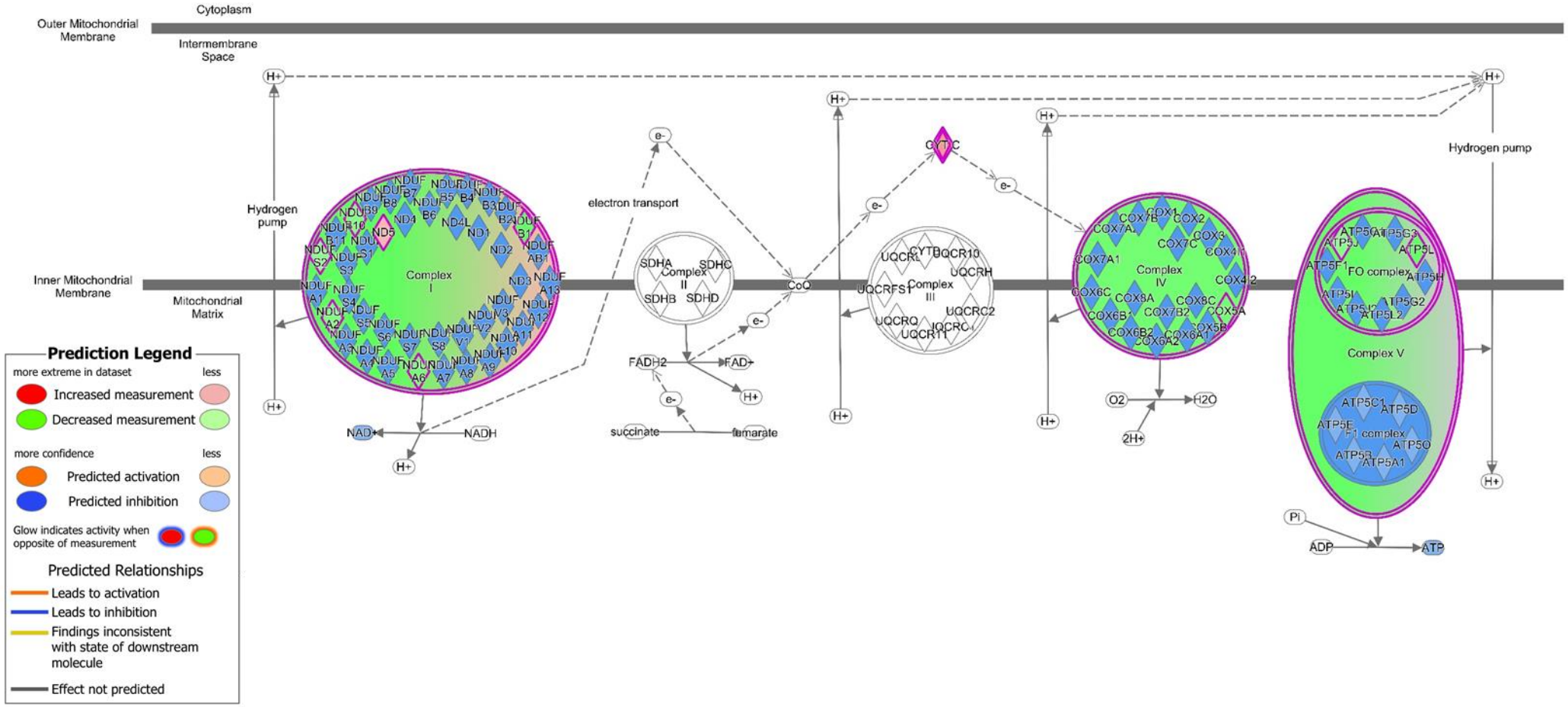

Fig. 5.23: **Metformin treatment significantly inhibits oxidative phosphorylation at the transcriptome level in radioresistant SW837 cells, when compared to vehicle control.** MAP software analysis was performed on significantly altered genes in metformin treated SW837 cells, when compared to H_2O vehicle control. Oxidative phosphorylation was demonstrated to be significantly inhibited in metformin treated SW837 cells, when compared to vehicle control. An increasing red colour indicates an increasing measurement in the uploaded dataset, while an increasing green colour indicates a decreasing measurement in the uploaded dataset. Orange colour denotes predicted activation of enzymes, and blue colour indicated predicted inhibition of enzymes, based on IPA Knowledge base, and the uploaded dataset.

5.4.14. *Metformin significantly inhibits oxidative phosphorylation and glycolysis in pre-treatment rectal adenocarcinoma biopsies*

Having demonstrated in Chapter 4 that metformin treatment significantly inhibits oxidative phosphorylation in an *in vitro* model of radiosensitive/radioresistant CRC, the effect of metformin treatment on pre-treatment *ex vivo* biopsies of rectal adenocarcinoma was assessed in real-time using the Seahorse XFe analyser. Rectal tumour biopsies were collected from the clinic, a baseline measurement of metabolic rate was recorded, biopsies were treated for 24 h with metformin (10 mM) or H_2O vehicle control and metabolism was assessed at 24 h post treatment.

The patient characteristics of this cohort of cancer patients is demonstrated in **Table 5.4.** Treatment with the vehicle control, H_2O, did not significantly impact the OCR of pre-treatment rectal cancer biopsies (**Fig. 5.24A**). Metformin treatment (10 mM) significantly inhibited OCR, a surrogate marker of oxidative phosphorylation, in pre-treatment rectal adenocarcinoma biopsies, when compared to baseline measurements (p = 0.014) (OCR % of baseline, metformin 52.98 ± 13.61) (**Fig. 5.24A**). Metformin treatment reduced OCR by 47% in rectal cancer biopsies.

While treatment with H_2O vehicle control did not significantly affect ECAR, a surrogate marker of glycolysis in pre-treatment rectal cancer biopsies, treatment with metformin significantly reduced ECAR in these biopsies, when compared to baseline (p= 0.0488) (ECAR % of baseline, metformin 64.42 ± 12.87) (**Fig. 5.24B**). Metformin treatment reduced ECAR by 35.58% in rectal cancer biopsies.

To determine whether the reductions in OCR and ECAR demonstrated following metformin treatment was dependant on clinical characteristics, the percentage reduction in OCR following metformin treatment was assessed according to clinical characteristics; clinical tumour (T) stage and body mass index (BMI) (broken into three groups according to Weir *et al*. (409))(**Fig. 5.25**). No significant differences were demonstrated between OCR or ECAR readings dependent on any clinical parameter examined (**Fig. 5.25**).

These data demonstrate that metformin treatment significantly inhibits oxidative phosphorylation and glycolysis in treatment-naïve rectal cancer biopsies, and that these metabolic alterations are independent of examined clinical parameters.

Table 5.4: **Patient characteristics of patient cohort used in *ex vivo* real-time metabolism study.**

		Cancers (*n*=10)
Gender	**Male (*n*)**	5
	Female (*n*)	5
Age at diagnosis	**Median (range)**	69 (47-78)
BMI at Diagnosis*	**Median**	27.5
	Normal (18.5-24.9) (*n*)	3
	Overweight (25-29.9) (*n*)	3
	Obese (≥30) (*n*)	3
Clinical T stage*	**2 (*n*)**	3
	3 (*n*)	5
	4 (*n*)	1
Clinical N stage*	**0 (*n*)**	6
	2 (*n*)	2
	3 (*n*)	1
Differentiation Stage	**Moderate-poor (*n*)**	1
	Moderate (*n*)	5
	Well (*n*)	1
	Awaiting (*n*)	3
Treatment received	**NeoCRT (*n*)**	4
	Surgery only (*n*)	3
	CT only (*n*)	1
	Awaiting (*n*)	2
TRS (of neoCRT patients)	**0 (*n*)**	1
	1 (*n*)	1
	2 (*n*)	2

*BMI at diagnosis, clinical tumour stage, clinical nodal stage only available for *n*=9 patients. Abbreviations; BMI, body mass index; Clinical T stage, clinical tumour stage, clinical N stage, clinical nodal stage; TRS, tumour regression score; neoCRT, Neoadjuvant chemoradiation therapy; CT, chemotherapy

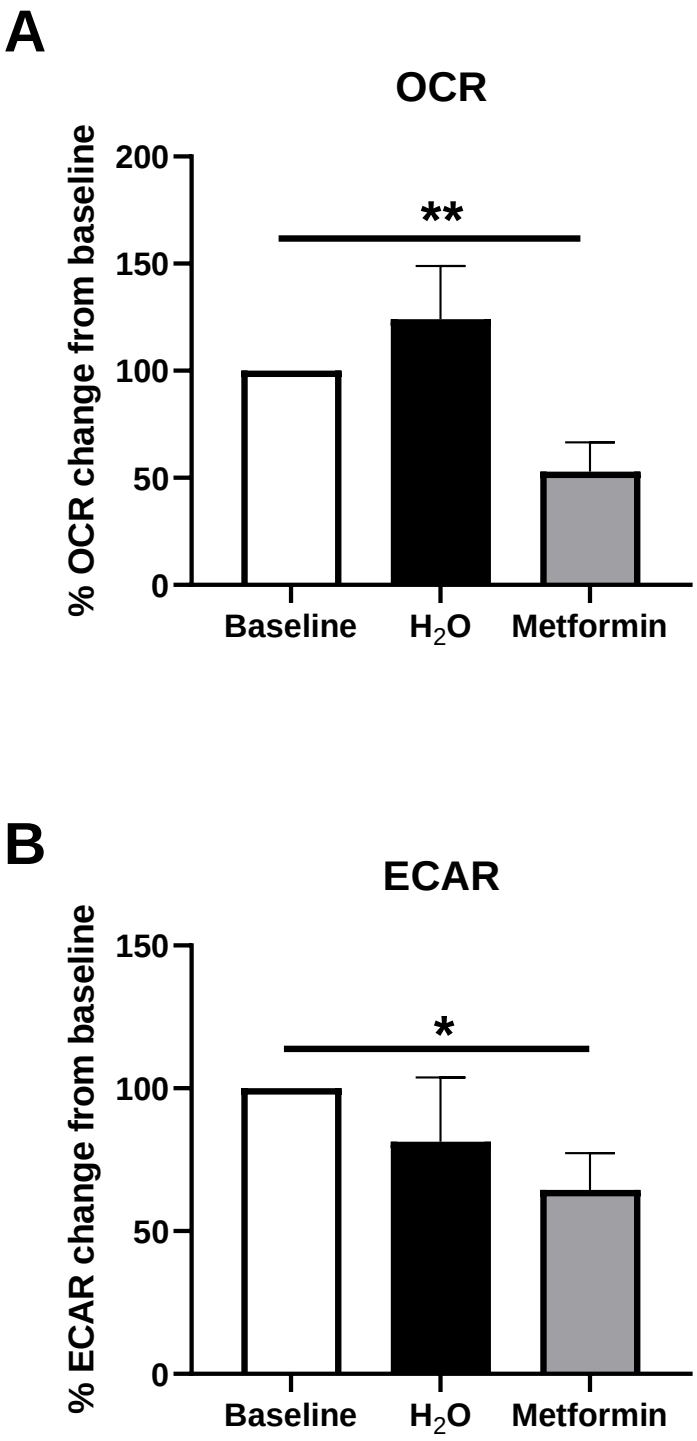

***Fig. 5.24*: Metformin treatment significantly reduces OCR and ECAR in treatment-naïve rectal adenocarcinoma biopsies.** OCR and ECAR were measured in pre-treatment rectal cancer biopsies prior to and 24 h post treatment with metformin (10 mM) or H_2O vehicle control using the Seahorse XFe24 analyser. **A)** OCR percentage change from baseline following treatment with metformin or H_2O vehicle control. **B)** ECAR percentage change from baseline following treatment with metformin or H_2O vehicle control. Data is presented as mean ± SEM for 10 independent experiments. Statistical analysis was performed using Wilcoxon matched pairs signed rank test. $*p < 0.05$, $**p < 0.01$.

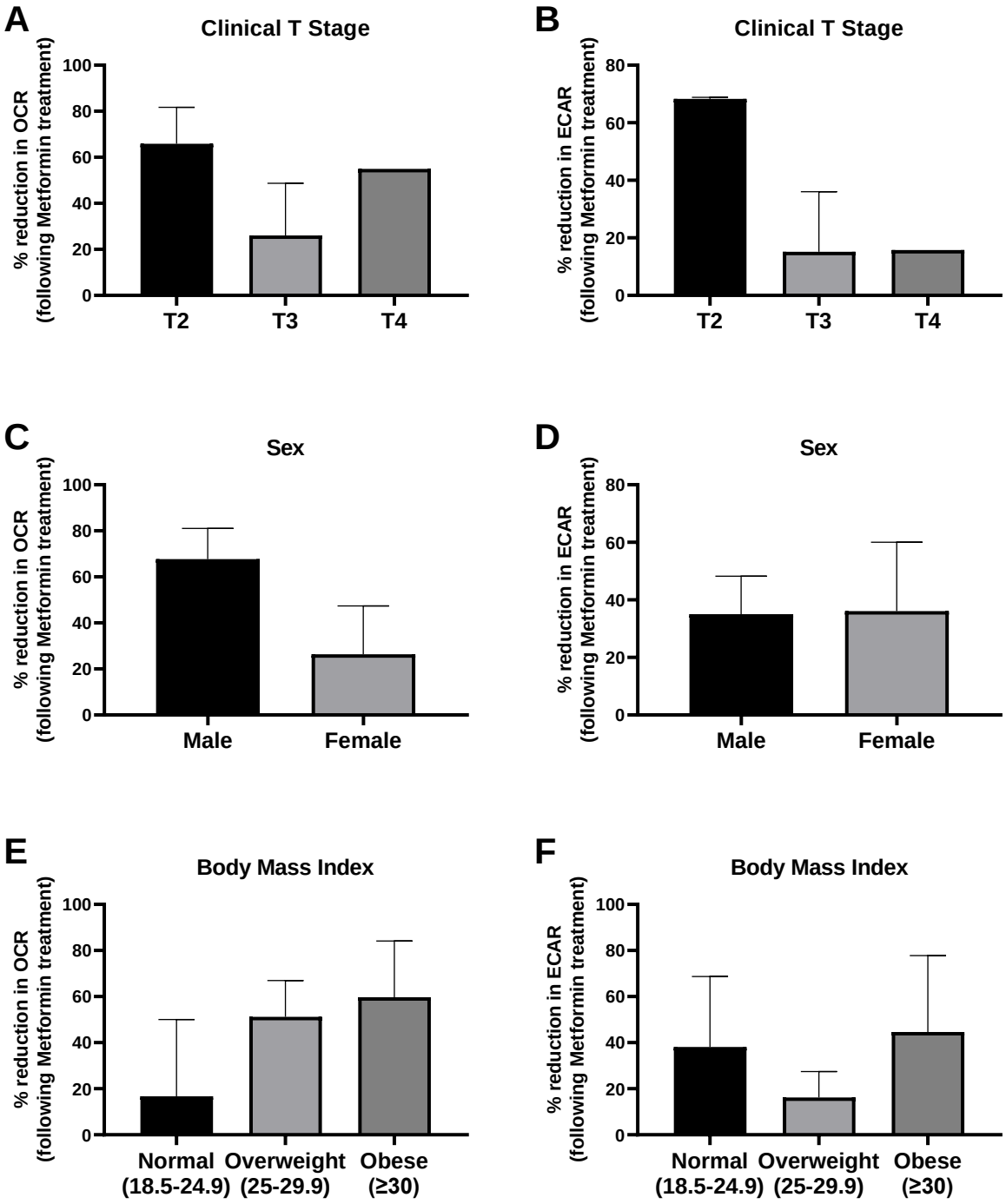

Fig. 5.25: **Metformin-induced reduction in OCR and ECAR in pre-treatment rectal cancer biopsies is not dependant on clinical patient characteristics.** OCR and ECAR were measured in metformin treated rectal cancer biopsies using the Seahorse XFe24 analyser. Percentage reduction of OCR in biopsies treated with metformin (24 h) was sub-divided according to **A)** clinical T stage (*n*=9), **C)** Sex (*n*=10) and **E)** Body Mass Index. Percentage reduction of ECAR in biopsies treated with metformin (24 h) was sub-divided according to **B)** clinical T stage (*n*=9), **D)** Sex (*n*=10) and **F)** Body Mass Index. Data is presented as mean ± SEM. Statistical analysis was performed by un-paired Mann-Whitney U or Kruskal-Wallis testing with post-hoc multiple comparisons, as appropriate.

5.4.15. *Metformin treatment does not significantly alter real-time metabolic phenotype of non-cancer rectal tissue biopsies*

Having demonstrated in that metformin treatment significantly inhibits oxidative phosphorylation in both *in vitro* and *ex vivo* models of rectal cancer, the effect of metformin treatment on non-cancer rectal tissue was assessed in real-time using the Seahorse XFe analyser. Non-cancer rectal tissue biopsies were collected from the clinic, a baseline measurement of metabolic rate was recorded, biopsies were treated for 24 h with metformin (10 mM) or H_2O vehicle control and metabolism was assessed at 24 h post treatment.

Twelve non-cancer rectal tissue samples were utilised in this study, with a median age of 41.5 years, and an even gender breakdown (*n* = 6 female, and *n* = 6 males). While OCR was demonstrated to increase in non-cancer tissue in H_2O vehicle control biopsies from baseline ($p = 0.002$), no significant alteration in OCR was demonstrated in metformin treated non-cancer rectal tissue, when compared to baseline (**Fig. 5.26A**). In addition, a significant increase in ECAR was demonstrated in H_2O vehicle control treated non-cancer rectal tissue biopsies ($p = 0.024$), however, no alterations to ECAR were demonstrated in metformin treated non-cancer rectal tissue biopsies, when compared to baseline measurements (**Fig. 5.26B**).

This suggests that metformin treatment does not significantly alter metabolism in non-cancer rectal tissue biopsies.

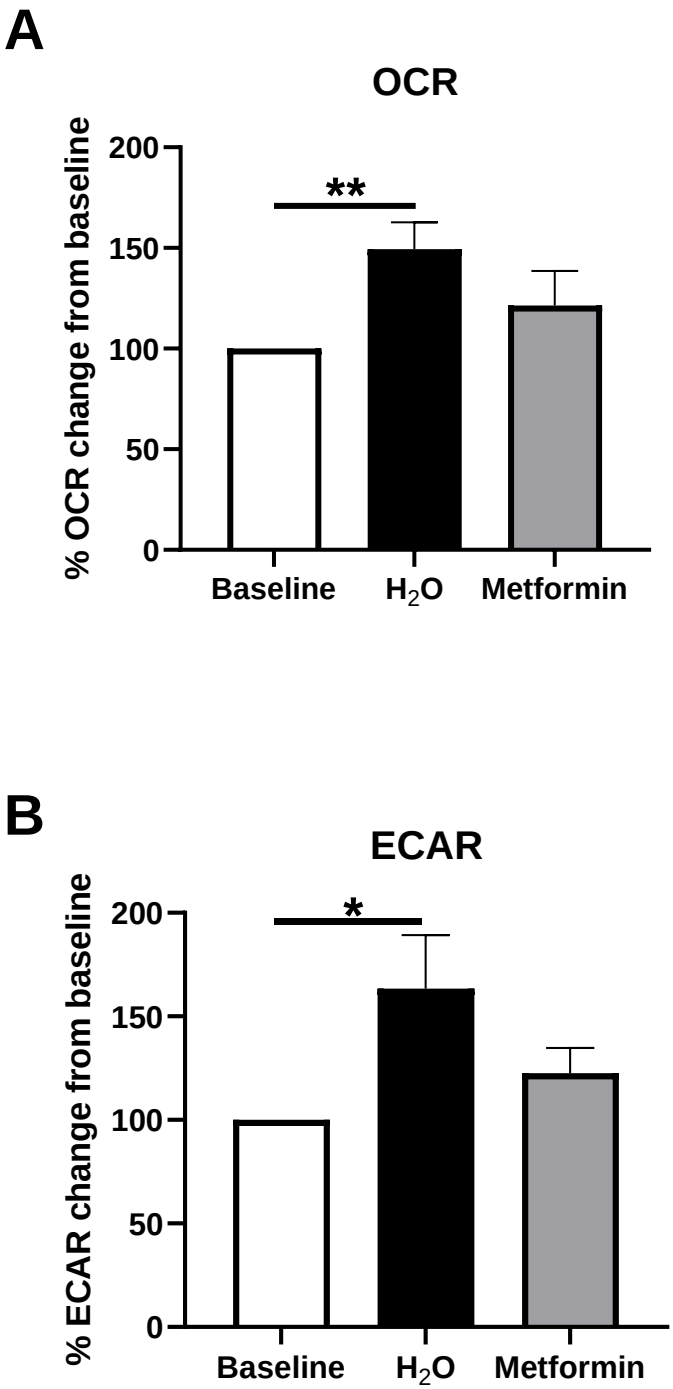

Fig. 5.26: **Metformin treatment does not alter OCR or ECAR in non-cancer rectal tissue biopsies.** OCR and ECAR were measured in non-cancer rectal tissue biopsies prior to and 24 h post treatment with metformin or H_2O vehicle control. **A)** Percentage change from baseline of OCR following treatment with metformin or H_2O vehicle control. **B)** Percentage change from baseline of ECAR following treatment with metformin or H_2O vehicle control. Data is presented as mean ± SEM for 12 independent experiments. Statistical analysis was performed using Wilcoxon matched pairs signed rank test. $*p < 0.05$.

5.4.16. *Metformin treatment alters the secretome of pre-treatment rectal cancer biopsies*

Having demonstrated that metformin significantly alters OCR and ECAR in pre-treatment rectal cancer biopsies, the effect of metformin treatment on the protein secretome of pre-treatment rectal tumour biopsies was assessed. TCM samples from biopsies treated with either metformin or H_2O vehicle control were profiled for inflammatory, angiogenic, chemokine and cytokine secretions using the MSD 54 multiplex ELISA.

The characteristics of the patient cohort utilised in this study are demonstrated in **Table 5.5.** In TCM samples, 7 proteins were demonstrated to be significantly altered in metformin treated samples, when compared to vehicle control (**Fig. 5.27**). Of these, five proteins were cytokines. Interleukin (IL)-1α was significantly increased in TCM of metformin treated rectal cancer biopsies, when compared to vehicle control (p = 0.021) (Mean concentration (pg/mL) per µg of protein ± SEM; H_2O 54.03 ± 20.69 vs metformin 92.15 ± 39.45) (**Fig. 5.27A**). In addition, IL-5 levels were significantly increased in the TCM of metformin treated rectal cancer biopsies, when compared to vehicle control (p = 0.012) (H_2O 19.28 ± 3.78 vs metformin 29.11 ± 5) (**Fig. 5.27B)**. The levels of IL-15 and IL-16 were also significantly increased in metformin treated TCM, when compared to vehicle control (p = 0.043, p = 0.043 respectively) (IL-15; H_2O 3.2 ± 0.68 vs metformin 4.24 ± 0.97, IL-16; H_2O 1125 ± 301 vs Metformin 1484 ± 344) (**Fig. 5.27C** and **5.27D**). IL-17B was significantly increased in the secretome of metformin treated cancer biopsies, when compared to vehicle control (p = 0.042) (H_2O 4.4 ± 0.96 vs metformin 6.1 ± 1.32) (**Fig. 5.27E**).

Levels of C-reactive protein (CRP) were significantly increased in the secretome of metformin treated biopsies (p = 0.02) (H_2O 168,946 ± 109,816 vs metformin 255,945 ± 130,108) (**Fig. 5.27F).** Macrophage inflammatory protein 1α (MIP-1α), a chemokine, was significantly decreased in metformin treated TCM, when compared to vehicle control (p = 0.037) (H_2O 637.1 ± 212.1 vs metformin 111.6 ± 20.93) (**Fig. 5.27G**).

These data demonstrate that the inflammatory secretome of rectal cancer is significantly altered following metformin treatment.

Table 5.5: **Patient characteristics of patient cohort used in multiplex ELISA secretome study.**

		Cancers (n=12)
Gender	**Male (*n*)**	6
	Female (*n*)	6
Age at diagnosis	**Median (range)**	69 (47-78)
BMI at diagnosis*	**Median**	27.7
	Normal (18.5-24.9) (*n*)	3
	Overweight (25-29.9) (*n*)	4
	Obese (≥30) (*n*)	4
Clinical T stage*	**1/2 (*n*)**	1
	2 (*n*)	3
	3 (*n*)	6
	4 (*n*)	1
Clinical N stage*	**0 (*n*)**	7
	2 (*n*)	3
	3 (*n*)	1
Differentiation stage	**Moderate-poor (*n*)**	2
	Moderate (*n*)	6
	Well (*n*)	1
	Awaiting (*n*)	3
Treatment received	**NeoCRT (*n*)**	5
	Surgery only (*n*)	4
	CT only (*n*)	1
	Awaiting (*n*)	2
TRS (of neoCRT patients)	**0 (*n*)**	2
	1 (*n*)	1
	2 (*n*)	2

*BMI at diagnosis, clinical tumour stage, clinical nodal stage only available for *n* = 11 patients. Abbreviations; BMI, body mass index; Clinical T stage, clinical tumour stage, clinical N stage, clinical nodal stage; TRS, tumour regression score; neoCRT, neoadjuvant chemoradiation therapy; CT, chemotherapy

5.4.17. *Metformin treatment alters the secretome of non-cancer rectal tissue biopsies*

Having demonstrated that metformin treatment significantly alters secretion of inflammatory factors from rectal cancer biopsies, the protein secretome of rectal tissue biopsies from non-cancer patients was assessed following metformin treatment. NCM samples from biopsies treated with metformin or H_2O vehicle control were profiled for inflammatory, angiogenic, chemokine and cytokine secretions using the MSD 54 multiplex ELISA.

In total, non-cancer histologically normal rectal tissue biopsies from 12 patients were utilised in this study. The median age of this cohort was 41.5 years, and there was an even gender distribution (*n*=6 female, *n*=6 male).

In total, three inflammatory factors were significantly altered in rectal tissue treated with metformin, when compared to vehicle control. All three significantly altered factors were inflammatory cytokines belonging to the IL-17 family. Levels of IL-17A were significantly increased in NCM from metformin treated biopsies, when compared to vehicle control (p = 0.034) (Mean concentration (pg/mL) per µg of protein ± SEM; H_2O 37.08 ± 9.16 vs metformin 84.58 ± 28.48) (**Fig. 5.28A**). IL-17B levels were significantly increased in NCM from metformin treated non-cancer biopsies, when compared to vehicle control treated NCM samples (p = 0.031) (H_2O 3.71 ± 1.15 vs metformin 6.85 ± 2.04) (**Fig. 5.28B**). In addition, IL-17D levels were significantly increased in the NCM of metformin treated biopsies, when compared to vehicle control (p= 0.037) (H_2O 50.9 ± 19.37 vs metformin 96.37 ± 27.72) (**Fig. 5.28C**). A trend towards significantly decreased levels of secreted IL-6 was demonstrated in metformin treated NCM, when compared to vehicle control, however this did not reach statistical significance (p = 0.052) (**Fig. 2.28D**). In addition, a trend towards increased levels of IL-5 secretion in metformin treated NCM, when compared to vehicle control was demonstrated, but did not reach statistical significance (p= 0.077) (**Fig. 5.28E**).

These data demonstrate that metformin treatment alters the inflammatory secretome of non-cancer rectal tissue, particularly through IL-17-related proteins.

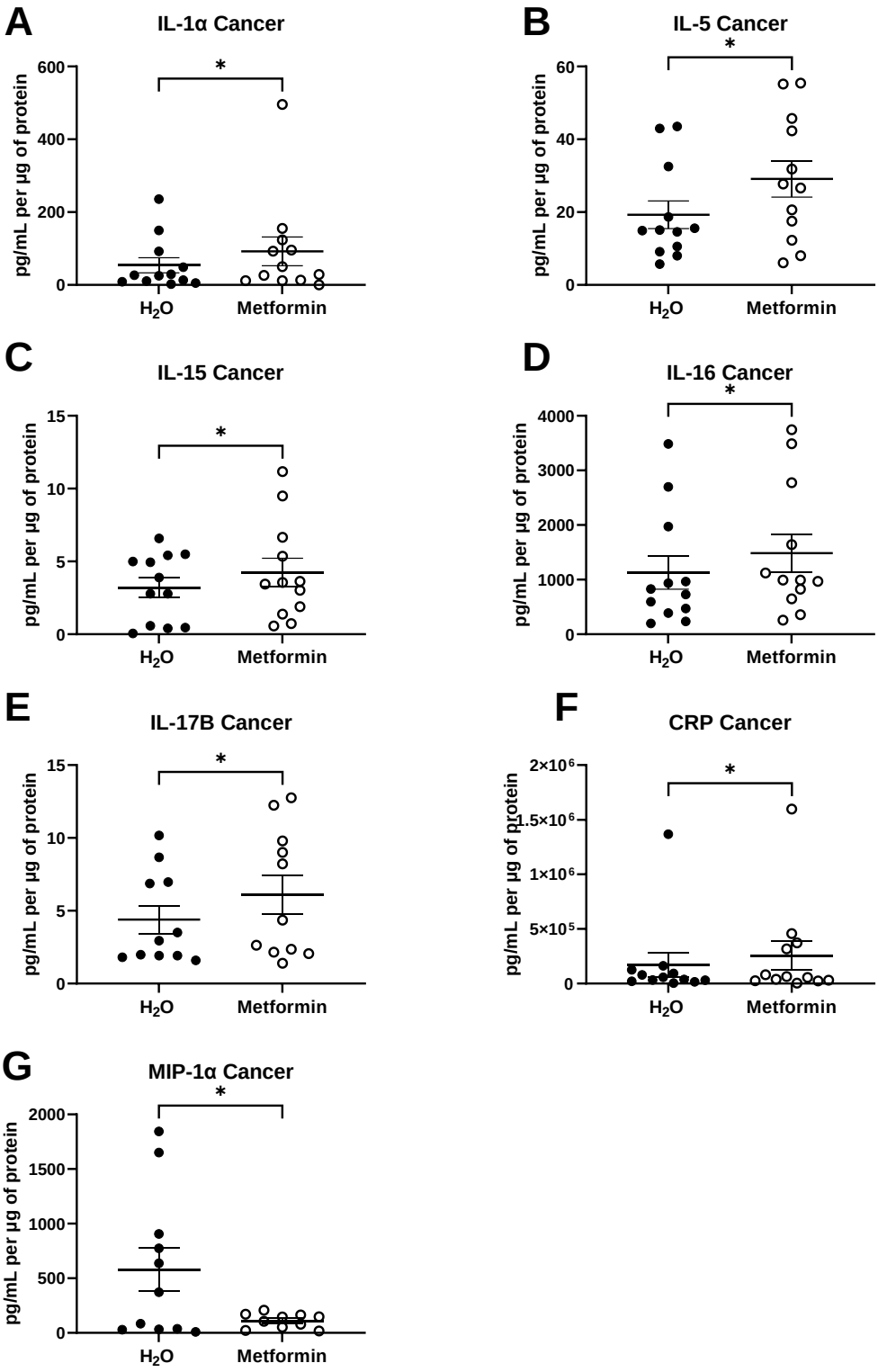

Fig. 5.27: **Metformin treatment significantly increases secretion of IL-1α, IL-5, IL-15, IL-16 and IL-17B from rectal cancer biopsies, when compared to H2O vehicle control.** The effect of 24 h treatment of rectal cancer tissue biopsies with metformin (10 mM) or H_2O vehicle control on protein secretion was assessed by multiplex ELISA. The effect of metformin treatment on the secretion of **A)** IL-1α **B)** IL-5 from **C)** IL-15 **D)** IL-16, **E)** IL-17B **F)** CRP and **G)** MIP-1α from rectal cancer tissue. Data is presented from n=12 patient samples. Statistical analysis was performed by Wilcoxon signed rank t-test. *$p < 0.05$.

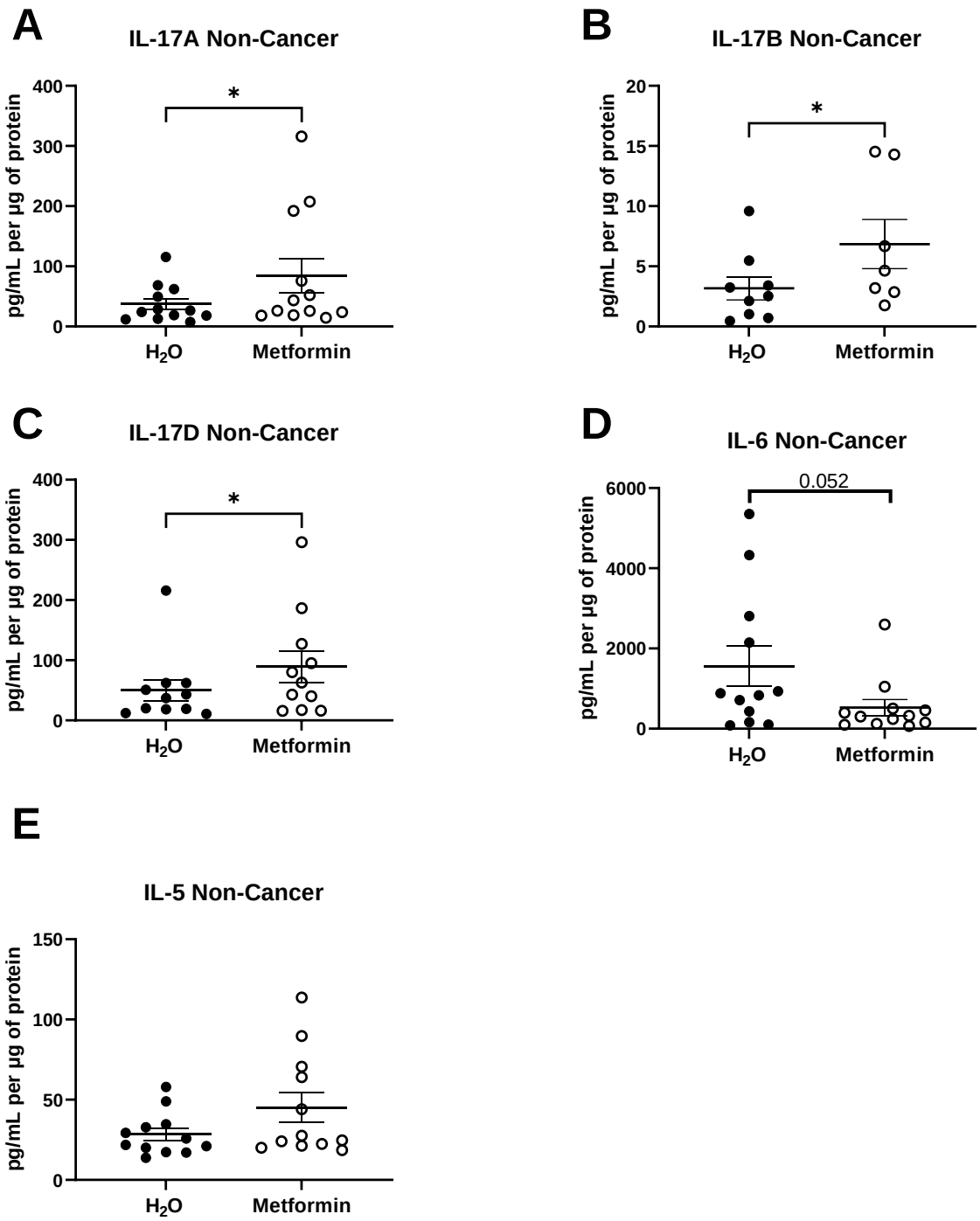

Fig. 5.28: **Metformin treatment significantly increases secretion of IL-17A, IL-17B and IL-17D from non-cancer rectal tissue, when compared to vehicle control.** The effect of 24 h treatment of non-cancer rectal tissue biopsies with metformin (10 mM) or H_2O vehicle control on protein secretion was assessed by multiplex ELISA. The effect of metformin treatment on the secretion of **A)** IL-17A, **B)** IL-17B, **C)** IL-17D, **D)** IL-6 and **E)** and IL-5 from non-cancer rectal tissue. Data is presented from *n*=12 patient samples. Statistical analysis was performed by Wilcoxon signed rank *t*-test. **p* < 0.05.

5.5. Summary of Results of Chapter 5

- Metformin treatment affects basal cell cycle distribution under normoxia and hypoxia in HCT116 and SW837 cells.
- Metformin treatment affects cell cycle progression following radiation treatment in HCT116 and SW837 cells.
- Metformin induces DNA damage in HCT116 cells under normoxia but not hypoxia.
- Metformin treatment inhibits repair of radiation-induced DNA damage in HCT116 cells under normoxia.
- Metformin treatment significantly induces cell death in HCT116 and SW837 cells under normoxia.
- Metformin treatment significantly increases total GSH levels in both HCT116 and SW837.
- Metformin treatment significantly alters the transcriptome of radioresistant SW837 rectal cancer cells.
- IPA analysis revealed significant alterations in pathways commonly associated with radioresponse in metformin treated SW837 cells including metabolism, DNA damage repair, oxidative stress and hypoxia signalling.
- Metformin treatment significantly inhibited OCR, a measure of oxidative phosphorylation, and ECAR, a measure of glycolysis in *ex vivo* rectal cancer biopsies.
- Metformin treatment did not alter OCR and ECAR in non-cancer rectal tissue.
- Metformin treatment significantly increased 7 inflammatory mediators in the secretome of rectal tumour biopsies.
- Metformin treatment increased 3 IL-17-related inflammatory mediators in the secretome of non-cancer rectal tissue.

5.6. Discussion

Having demonstrated in chapter 4 that metformin acts as a metabolic modulator and radiosensitising drug in HCT116 and SW837 CRC cells, this chapter aimed to investigate the potential underlying mechanisms of this metformin-induced radiosensitisation, and to further profile the effect of metformin on CRC. Th effect of metformin on cell cycle, DNA damage repair, apoptosis and metabolism were assessed as these are processes frequently implicated in radioresistance, and were also demonstrated to be altered basally between radiosensitive HCT116 and radioresistant SW837 cells in Chapter 2.

A potential mechanism of metformin-induced radiosensitisation is alteration of basal cell cycle distribution. To investigate this, HCT116 and SW837 cells were treated with metformin (10 mM) for 24/30/34 or 48 h and cell cycle distribution assessed under normoxic (21% O_2) and hypoxic (0.5% O_2) conditions.

At 24 h following metformin treatment, no significant alterations were demonstrated to basal cell cycle distribution in HCT116 or SW837 cells under normoxia, suggesting that altered basal cell cycle distribution is not a mechanism underlying the metformin-induced radiosensitisation demonstrated in these cells in Chapter 4.

In hypoxia, a small but significant increase in S phase and reduction in G2/M phase cells was observed in radioresistant SW837 cells. Importantly, in the radiosensitisation experiments (Chapter 4), this timepoint (24 h) was the time at which cells were irradiated following metformin treatment to investigate the impact of metformin treatment on radiosensitivity. The one condition investigated in which metformin did not radiosensitise at 1.8 Gy radiation was in radioresistant SW837 rectal cancer cells under hypoxia, and this is also the one condition in which cell cycle distribution was altered at the point of radiation exposure. The G2/M phase of the cell cycle is the most radiosensitive phase of the cell cycle, with cells in the S phase being the most radioresistant phase (52). This more radioresistant basal cell cycle distribution of SW837 cells under hypoxia when treated with metformin may contribute to the inability of metformin to radiosensitise under these conditions.

However, at later timepoints, a significant reduction in the proportion of G0/G1 phase cells and increase to the percentage of S phase cells was demonstrated in HCT116 cells following metformin treatment under normoxia. While a slight but significant increase in the proportion of G0/G1 phase cells was observed in SW837 cells under normoxia at later timepoints.

In addition, cell cycle progression and checkpoint activation are frequently implicated in the cellular radioresponse (66, 344). In cancer cells, G2/M arrest is a common response following exposure to ionising radiation, to permit the repair of DSBs. This G2/M checkpoint has been proposed as a target for drugs to enhance the efficacy of radiation therapy, as many cancer cells have a deficient G1 checkpoint (96, 97). In this chapter, it was demonstrated that metformin treatment combined with radiation treatment significantly reduced the proportion of cells in the G2/M phase, thereby overcoming this radiation-induced G2/M blockade in HCT116 and SW837 cells in normoxia, and HCT116 cells under hypoxia. Interestingly, the one condition in which metformin treatment increased the proportion of cells in the G2/M phase following radiation was in the SW837 cells under hypoxic conditions. Importantly, as demonstrated in Chapter 4, this was the one condition tested in which metformin failed to sensitise SW837 cells to 1.8 Gy radiation. Elimination of the G2/M checkpoint has been demonstrated to be an effective strategy to enhance radioresponse in cancer cells (97, 407), and has been proposed as a mechanism of metformin-induced radiosensitisation in pancreatic cancer (307). In rectal cancer, a CHK1 and CHK2 inhibitor, has been demonstrated to radiosensitise rectal cancer cells, while inhibiting radiation-induced G2/M arrest and enhancing apoptosis and DNA damage. These data may indicate a similar metformin-induced elimination of G2/M blockade in HCT116 and SW837 under normoxia, and HCT116 under hypoxia, contributing to radiosensitisation under these conditions.

Increase in G0/G1 cells was demonstrated at 20 min, 6 h and 10 h post radiation exposure in SW837 cells under normoxia and in HCT116 cells under hypoxic conditions, while the proportion of G0/G1 phase cells was decreased in SW837 cells under hypoxia. G0/G1 arrest is a common feature of metformin treated cancer cells (308-310). Exposure to radiation, typically induces a reduction in G0/G1 phase cells, and elevated G2/M phase cells. Metformin treatment in these conditions, seemed to counteract the effects of radiation on G0/G1 phase. Interestingly, an accumulation of cells in the G0/G1 phase of the cell cycle may indicate the induction of cellular senescence (410). These data may suggest that metformin-induced alterations to cell cycle distribution impact the radioresponse in radiosensitive and radioresistant CRC cells.

The impact of metformin treatment on DNA damage induction and repair was also investigated. The only condition in which metformin induced basal damage to DNA was in HCT116 cells at 36 h treatment. The effect of combined metformin and radiation treatment

on DNA damage induction and repair was also assessed. At 10 h following radiation exposure, DNA damage persisted in radiosensitive HCT116 cells treated with metformin under normoxic conditions. In addition, there was a significant increase in γH2AX in SW837 cells treated with metformin and 1.8 Gy radiation, at 10 h post radiation exposure while γH2AX levels in cells treated with radiation alone had returned to baseline levels at this timepoint. This may indicate that metformin treatment impairs repair of radiation-induced DNA damage repair in SW837 cells under normoxic conditions. This is supported by previous studies, which have demonstrated metformin-induced radiosensitisation and inhibition of DNA damage repair, as indicated by persistent γH2AX in nasopharyngeal cancer (306) and pancreatic cancer (307).

Cell cycle checkpoints and progression through the cell cycle are intrinsically linked to DNA damage repair (360). Interestingly, abrogation of the G2/M checkpoint, as demonstrated with metformin treatment under normoxia in HCT116 and SW837 cells, has been proposed to induce mitotic catastrophe and ultimately cell death and senescence, when combined with DNA targeting therapies, such as radiation therapy (411, 412). These data indicate that metformin treatment, and inhibition of G2/M arrest and impaired DNA damage repair may be contributing to radiosensitisation in this CRC cell line model under normoxia. Furthermore, research has indicated that oxidative stress-induced DNA damage may be a mechanism of metformin-induced radiosensitisation in breast cancer (313). As ROS production is demonstrated to be significantly induced with metformin treatment in HCT116 and SW837 cells, this may be contributing to the metformin-induced DNA damage demonstrated in this chapter, and associated radiosensitisation.

To investigate the impact of metformin on apoptosis, HCT116 and SW837 cells were treated with metformin for 24/48/72 h and cell death assessed by flow cytometry. Metformin treatment was demonstrated to induce significant early and late apoptosis and necrosis in HCT116 and SW837 cells, particularly under normoxic conditions. Metformin treatment has been demonstrated to induce apoptosis in various cancer types (311-313, 405, 408). Research has recently demonstrated that treatment with metformin induces apoptosis in CRC cell lines, including HCT116 and SW837 cells (405, 413). This study demonstrates that HCT116 cells are more sensitive to Metformin treatment by assessment of apoptosis, crystal violet assay, and clonogenic assay, the gold-standard method of assessing cytotoxicity. In addition, in a study conducted by Park *et al.,* 72 h treatment with metformin was also demonstrated to inhibit proliferation, as assessed by MTT assay in both HCT116 and SW837 cells, supporting the

demonstrated increased apoptosis and necrosis and reduced reproductive integrity in these cell lines (405). When metformin treatment was combined with radiation, there was no additive effect on cell death, demonstrating that while metformin treatment alone induces cells death, it may not be enhancing radiation-induced cell death at these timepoints.

Alterations to oxidative stress and antioxidant capacity have been demonstrated to contribute to radioresistance in various cancer types (345, 346). In chapter 3, it was demonstrated that metformin significantly induces ROS production in HCT116 and SW837 cells under normoxic conditions (**Fig. 4.16)**. Subsequently, the impact of metformin treatment on HCT116 and SW837 cells on the antioxidant glutathione, in both reduced (GSH) and oxidised (GSSG) forms were assessed, to further investigate the role of oxidative stress in metformin-induced radiosensitisation.

Metformin treatment for 24 h was demonstrated to significantly upregulate the production of GSH, while no significant differences were demonstrated to GSSG levels in both HCT116 and SW837 cells. GSH is the most abundant antioxidant, significantly increased in both colon and rectal cancer (130, 131) and is associated with therapeutic resistance in cancer (347). This association with radioresistance is due in part to the neutralising of oxygen free radicals, which cause indirect IR-induced DNA damage. The observation that metformin enhances GSH levels may be initially counterintuitive to its radiosensitising ability in these cells. However, it is important to note that GSSG levels remained unaffected at 24 h following metformin treatment in HCT116 and SW837 cells. These data would suggest that while GSH levels are elevated, this may not translate to enhanced ROS detoxification in these cell lines. As previously demonstrated, enhanced ROS production demonstrated in these cells following metformin treatment, may be inducing elevated GSH production, but the balance between antioxidant capacity and oxidative stress seems to tip towards elevated oxidative stress following metformin treatment in this model, as oxidised GSSG levels remain steady. In addition, these data may suggest that metformin treatment could be affecting the expression or activity of the enzyme glutathione peroxidase (GPx), which catalyses GSH to GSSG conversion. Metformin has been previously demonstrated to decrease GPx activity and enhance GSH levels in the brain (414). Further investigation of this impact of metformin on antioxidant capacity is warranted.

Despite being used clinically, the precise mechanism of action and biological targets of metformin are largely unknown (278). One approach to further elucidate potential

mechanisms of action of metformin, both as an anti-neoplastic and radiosensitising agent is transcriptomic profiling, giving a high-level overview of molecular pathways and processes altered by metformin. Transcriptomic profiling demonstrated significant alterations in the transcriptome of radioresistant SW837 cells treated with metformin, when compared to vehicle control. IPA pathway analysis demonstrated alteration of multiple biological functions following metformin treatment, these included multiple mechanisms implicated in the radioresponse, such as cell cycle, cell death and survival and DNA damage repair. Furthermore, IPA canonical pathway analysis demonstrated specific predictions on biological pathways altered by metformin treatment. For example. NER, a DNA damage repair pathway was predicted to be significantly inhibited in SW837 cells treated with metformin, which supports data from functional experiments in this chapter. In addition, pathways related to oxidative stress were predicted by IPA software to be significantly altered in metformin treated SW837 cells, supporting experimental findings in this chapter. Transcriptomic profiling of metformin treated CRC cells has previously been performed in LoVo colon cancer cells, treated with metformin (415). This study demonstrated significant alterations to the transcriptome of LoVo cells following treatment with metformin, including alterations to pathways also demonstrated in this study to be affected by metformin treatment in SW837 rectal cancer cells. Transcriptomic analysis in this study demonstrated significant alterations to reactive oxygen species, cell cycle and programmed cell death pathways in metformin treated LoVo cells (415), supporting both functional and transcriptomic data demonstrated in this chapter which highlight the effects of metformin on these mechanisms of radioresistance in SW837 cells. Furthermore, this study by He *et al.* also demonstrated significant alterations to energy metabolism pathways in metformin treated LoVo cells, including alterations to the metabolism of carbohydrates, cholesterol, lipids, amino acids and nucleotides (415). This supports data from this chapter demonstrating significant alterations in lipid metabolism, cholesterol synthesis and metabolism, and inhibition of oxidative phosphorylation demonstrated in the transcriptome of metformin treated SW837 rectal cancer cells. Together these data support metformin induced alterations to hallmarks of cancer radioresistance in CRC.

Having demonstrated significant metabolic modulation by metformin treatment *in vitro* in CRC, the effect of metformin on the metabolic phenotype of *ex vivo* rectal cancer biopsies was assessed. This *ex vivo* explant model of CRC more accurately reflects the tumour

microenvironment than *in vitro* models, as these pre-treatment tissue samples mimic the 3D architecture and diverse microenvironment in tumours, containing cancer cells, stromal cells and immune cells. In addition, the crosstalk between cancer and stromal cells has implications for the development, progression and therapeutic response of cancer, highlighting the utility of explant models in drug discovery (416). Furthermore, these *ex vivo* explants also reflect the inherent genetic diversity between patients, aiding the identification of biomarkers of inherent radioresistance, and the development of novel radiosensitising drugs.

Metformin treatment was demonstrated to significantly inhibit OCR, a marker of oxidative phosphorylation in pre-treatment rectal cancer biopsies, supporting metformin as an inhibitor of oxidative phosphorylation in rectal cancer. In addition, metformin treatment was demonstrated to significantly inhibit ECAR, a marker of glycolysis in rectal cancer biopsies, in contrast to *in vitro* data. While compensatory upregulation of glycolysis in cells treated with metformin has been demonstrated as a mechanism to preserve some ATP production following oxidative phosphorylation inhibition, it has also been demonstrated that metformin inhibits HK2 in cancer, and subsequently can impair glycolysis (274, 417). It has also been proposed that tumours which are not metabolically flexible, and cannot meet energy demands following inhibition of oxidative phosphorylation, are more sensitive to metformin treatment, and that the metabolic phenotype may act as a marker predicting response to metformin in cancer (274). This suggests that the patient samples assessed in this study may display reduced metabolic flexibility capacity and be susceptible to metformin treatment.

Importantly, one of the main considerations in designing a novel radiosensitising agent is the effect on normal, non-malignant tissue. The ideal radiosensitiser will have a wide therapeutic index, which targets cancer cells, while sparing non-cancer normal tissue, to reduce therapeutic toxicity (418). In addition to investigating the effect of metformin treatment on rectal cancer biopsies, the metabolic phenotype of non-cancer rectal tissue treated with metformin was also investigated. No significant alterations in the metabolic phenotype of non-cancer rectal tissue were demonstrated following metformin treatment. These data support the potential of metformin as a radiosensitising drug, with no impact on the energy metabolism of non-cancer tissue demonstrated and warrants further research.

Profiling of the secretome of rectal cancer and non-cancer rectal biopsies also demonstrated significant alterations following metformin treatment. However, while 7 inflammatory mediators were significantly altered in cancer biopsies treated with metformin,

only three TH17-related cytokines were significantly altered in non-cancer rectal tissue. The secretion of IL-15 was demonstrated to be significantly increased from rectal tumour biopsies, treated with metformin. IL-15 in the tumour microenvironment promotes the maturation and durable activation of anti-tumour T cells, including CD8+ T cells and natural killer (NK) cells (419). In fact, IL-15 as a potential anti-tumour immunotherapy is under investigation in multiple clinical trials (419). In a recent study by Pilones *et al.,* it was demonstrated that combination treatment of radiation therapy and IL-15 resulted in enhanced response to radiation, improved survival and enhanced infiltration of CD8+ effector T cells in a mouse model of breast cancer (420). This study demonstrates that IL-15 enhances immune infiltration to overcome immunosuppression in the tumour microenvironment. The metformin mediated increase in IL-15 secretion in rectal tumour may therefore contribute to enhanced response to radiation.

Of the seven inflammatory mediators significantly increased by metformin treatment in cancer TCM only one, IL-17B, was also demonstrated to be significantly increased in non-cancer NCM. In addition, IL-17A and IL-17D were significantly increased following metformin treatment in the secretome of non-cancer rectal tissue only, not in rectal cancer tissue. Metformin treatment

A trend towards decreased secretion of IL-6 was demonstrated in metformin treated non-cancer tissue. In the sera of patients with T2DM, the concentration of inflammatory cytokines, including IL-6 are demonstrated to increase. It has been demonstrated that metformin treatment significantly reduces the concentration of inflammatory cytokines in the sera of patients with T2DM, including reducing IL-6, normalising the inflammatory cytokine index in these patients (421). These data demonstrate that metformin treatment does not contribute to an extensive pro-inflammatory phenotype in non-cancer patients.

An important consideration in the development or discovery of novel radiosensitiser drugs is the impact of the radiosensitiser on normal tissue toxicity (422). As mentioned, ideal radiosensitisers enhance the radiosensitivity of tumour cells, while sparing non-cancer tissue, to limit patient side effects and increase the therapeutic index. These data demonstrate that metformin treatment does not alter the inflammatory secretome of non-cancer tissue to the same extent as in rectal tissue, indicating that metformin may be less toxic to normal tissue. Furthermore, in a recent study, it was demonstrated that while metformin treatment significantly induced cell death, DNA damage and ROS production in an *in vitro* model of

pancreatic cancer, minimal negative impact was demonstrated in human primary dermal fibroblasts following metformin treatment, further supporting that metformin may be less toxic in non-cancer tissue, and strengthening its potential as a novel radiosensitiser (399).

This chapter demonstrated that metformin-induced radiosensitisation may be mediated through induction of oxidative stress, cell cycle alterations and altered DNA damage repair in HCT116 and SW837 cells. Importantly, metformin was demonstrated to exert anti-metabolic effects in rectal cancer biopsies, supporting the potential of metformin as a novel anti-metabolic radiosensitiser *in vivo.*

In Chapter 6, multi-omic profiling of sera and tissue from rectal cancer and non-cancer patients is performed to further investigate pathways associated with therapeutic response in rectal cancer.

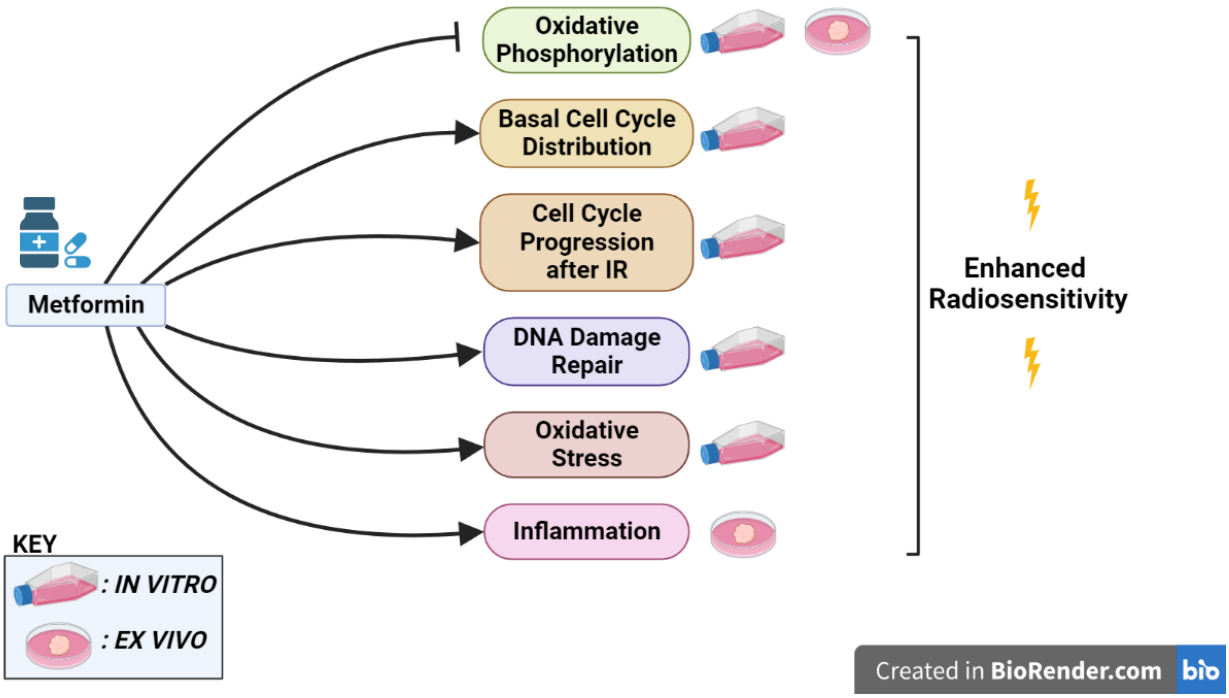

Fig. 5.29: **Summary of main findings of chapter 5.** The effect of metformin treatment on common mechanisms of radioresistance was assessed in *in vitro* and *ex vivo* models of rectal cancer. Metformin was demonstrated to significantly inhibit oxidative phosphorylation *in vitro* and *ex vivo*. Metformin treatment altered basal cell cycle distribution and progression following ionising radiation (IR) exposure, and affect DNA damage repair *in vitro*. Metformin treatment altered oxidative stress *in vitro* and induced the secretion of inflammatory mediators *ex vivo*. Figure created using BioRender.com.